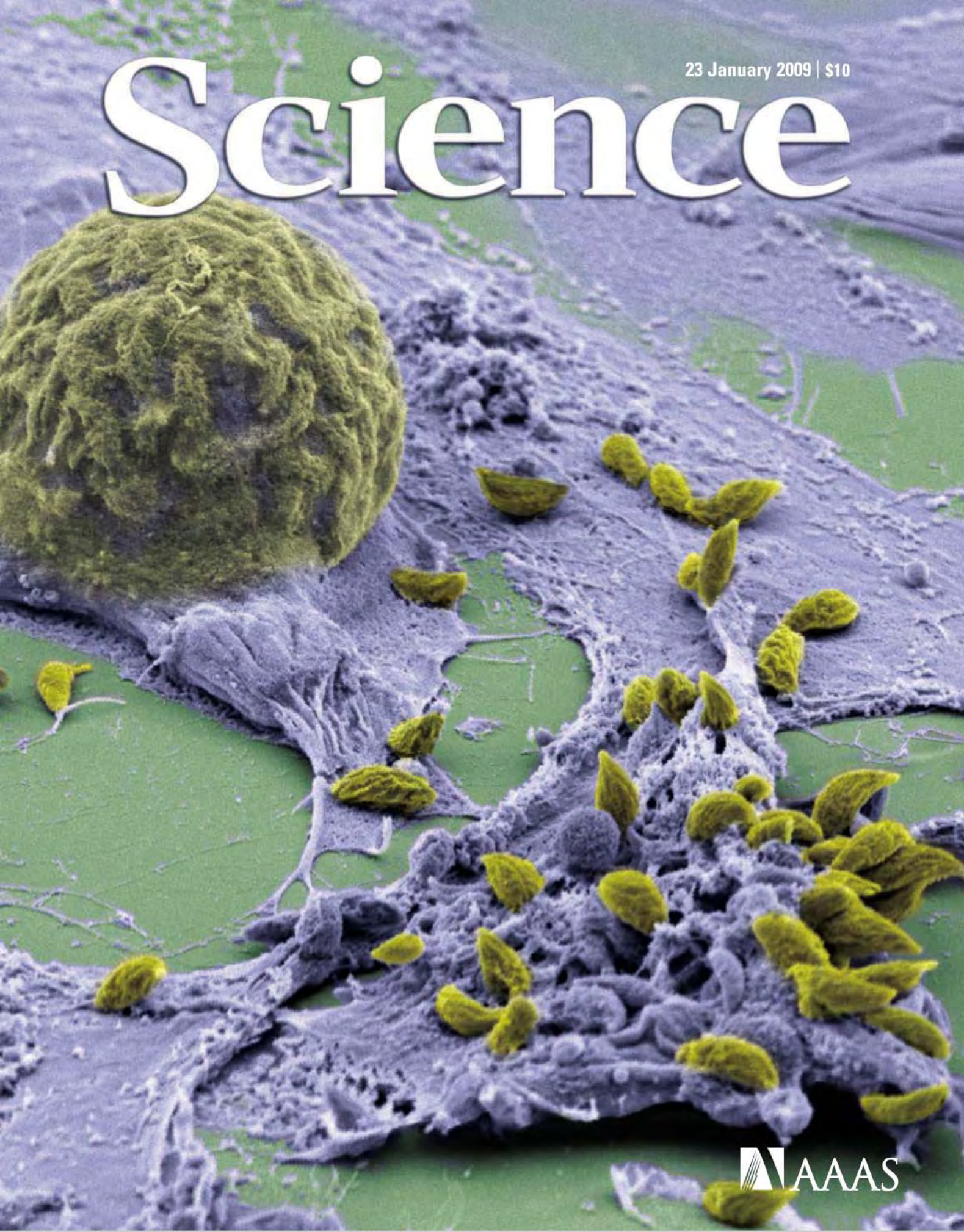


23 January 2009 | \$10

Science



collaboratory.

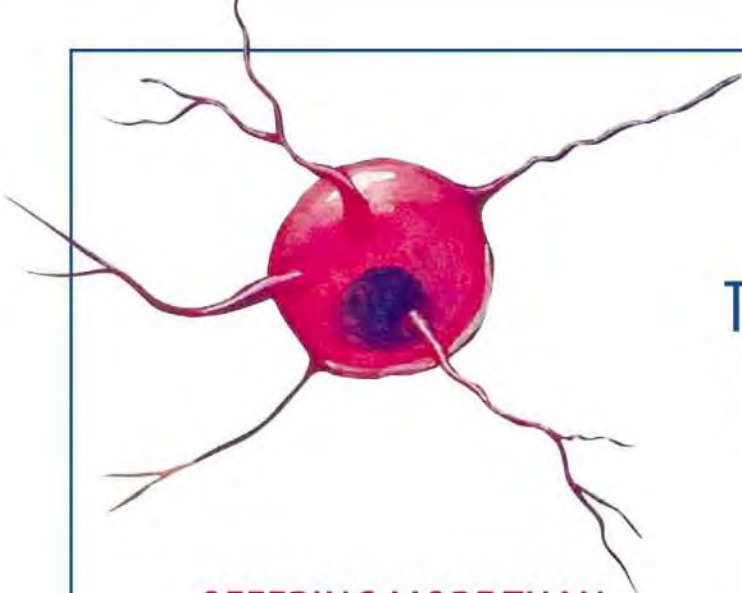
RESEARCH. TOGETHER.

Research is a collaborative process.

We understand and embrace that. For more than 50 years we've worked with our customers to deliver the best quality products backed by the best service and support at a responsible price. Because what we do together is too important for anything less, and we think there should be a word for that.

Let's research, together.

Learn more at www.bio-rad.com/researchtogether/



R&D Systems

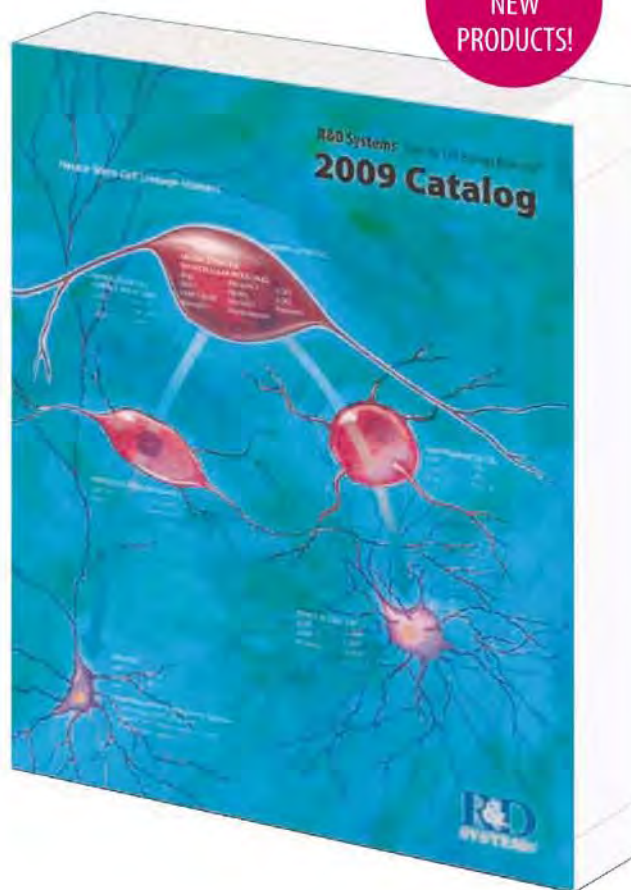
Tools for Cell Biology Research™

2009 Catalog Available Now!

**OFFERING MORE THAN
15,000
QUALITY PRODUCTS
for Cell Biology Research.**

R&D Systems is a leading supplier of cell biology reagents with over 20 years of experience serving the research community. More than 97% of the products supplied by R&D Systems are developed and manufactured at our own facilities. This enables us to maintain strict manufacturing and quality control standards, ensuring that our reagents meet the high levels of performance and consistency expected by our customers.

Request a catalog online:
www.RnDSystems.com/go/Catalog



Cancer • Endocrinology • Immunology • Proteases • Neuroscience
Development • Stem Cells • Signal Transduction • Glycobiology

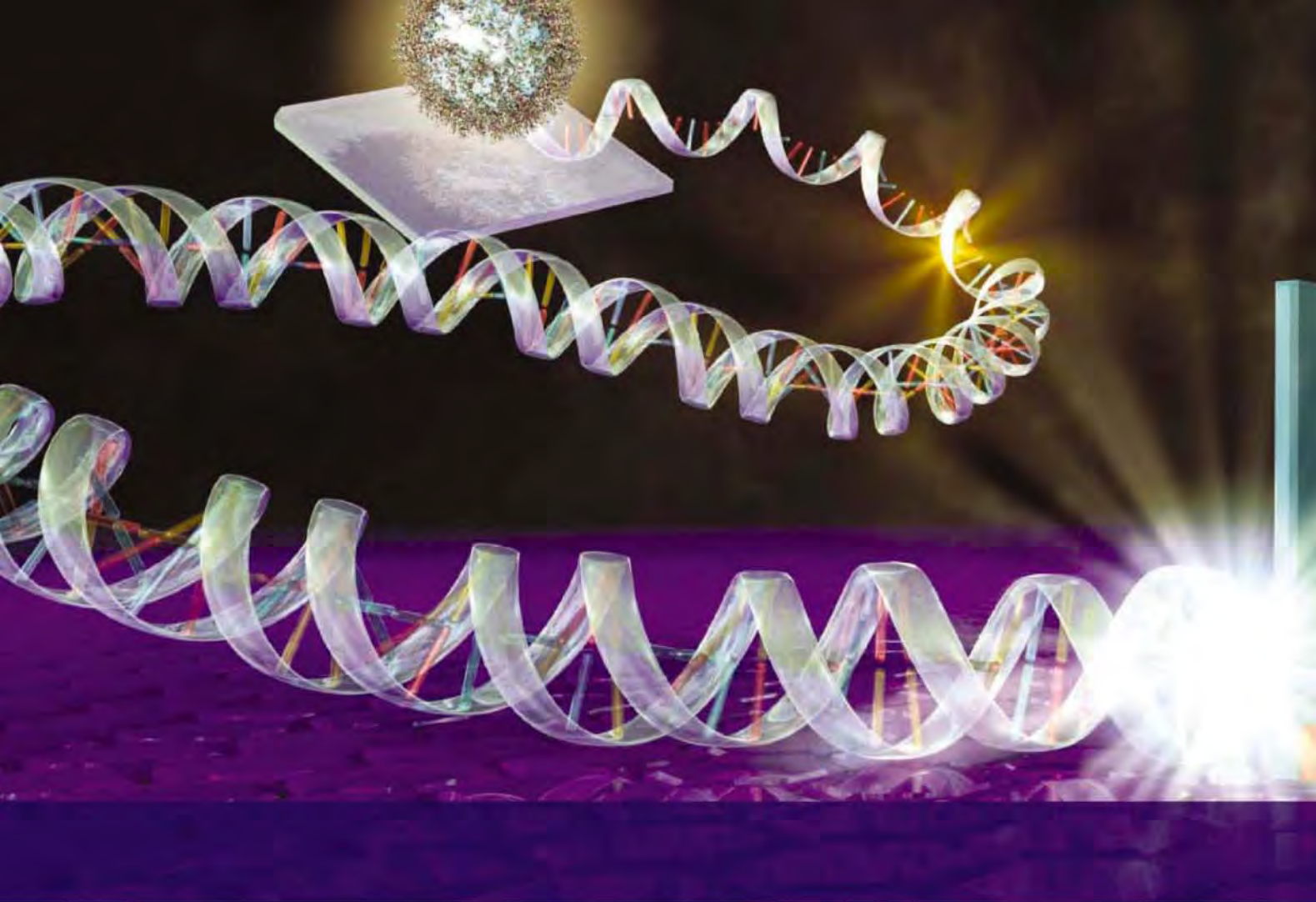
R&D Systems Tools for Cell Biology Research™

USA & Canada R&D Systems, Inc. Tel: (800) 343-7475 info@RnDSystems.com

Europe R&D Systems Europe, Ltd. Tel: +44 (0)1235 529449 info@RnDSystems.co.uk

Selection expanding weekly—visit www.RnDSystems.com/go/request to sign up for weekly new product updates.

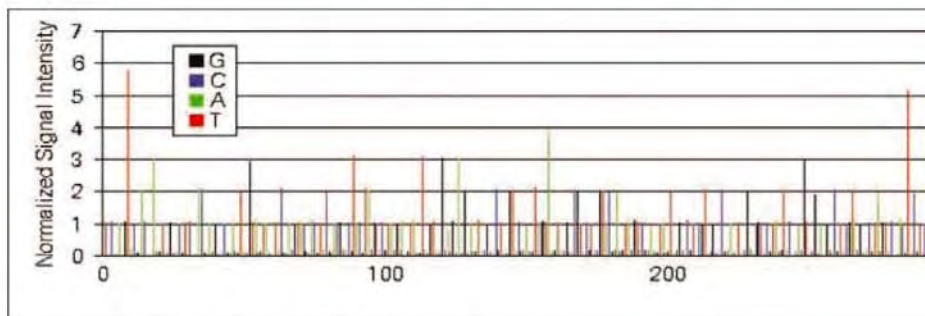




Genome Sequencer FLX System

454
SEQUENCING

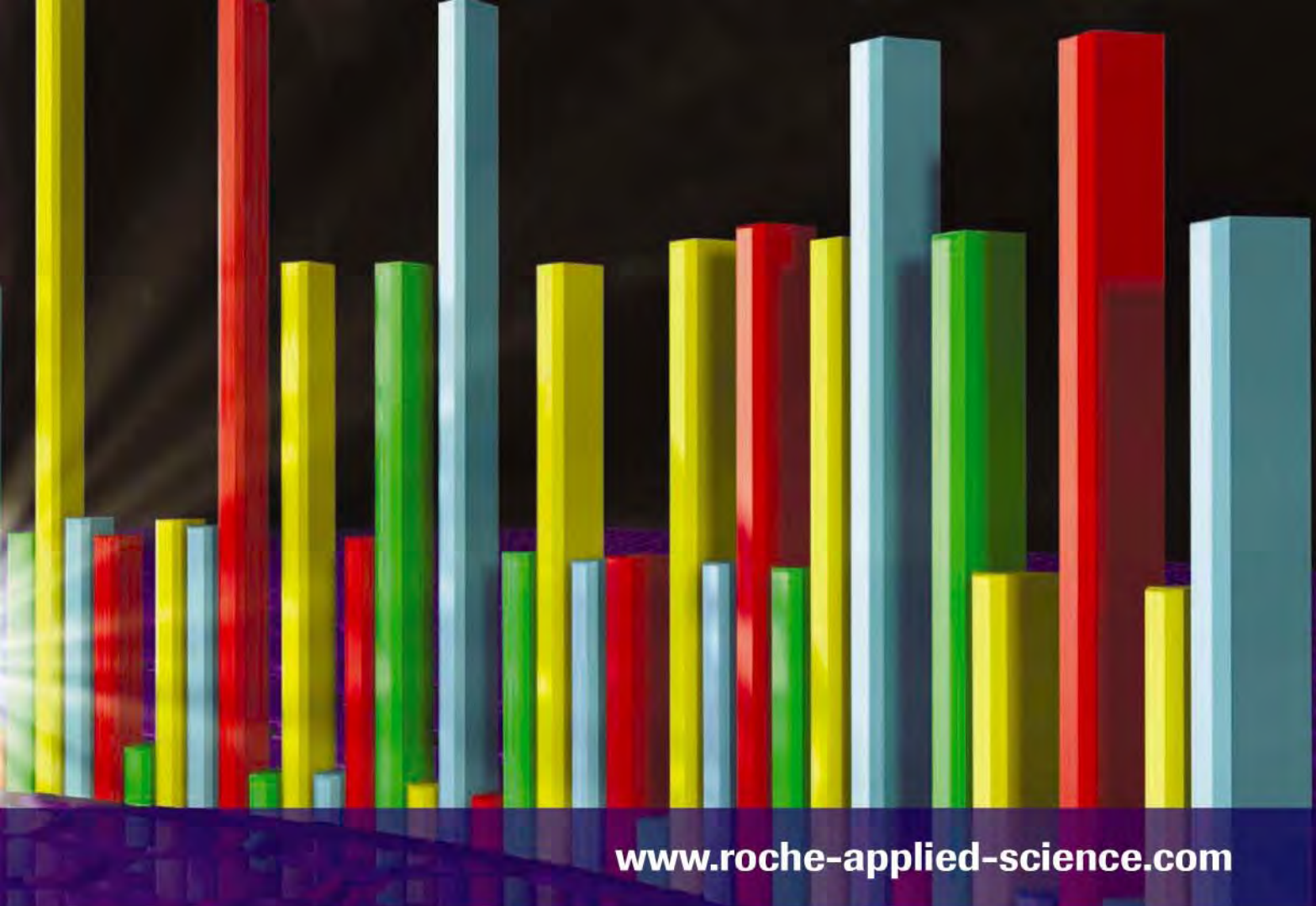
Really Length Matters



DNA Sequencing Flowgram: Each bar within the flowgram represents a discrete nucleotide (A, T, C, or G) and the height of the bar corresponds to the number of nucleotides detected. Although the majority of sequencing reads are 400 to 500 bases, the above flowgram represents a sequencing read of 543 bases.

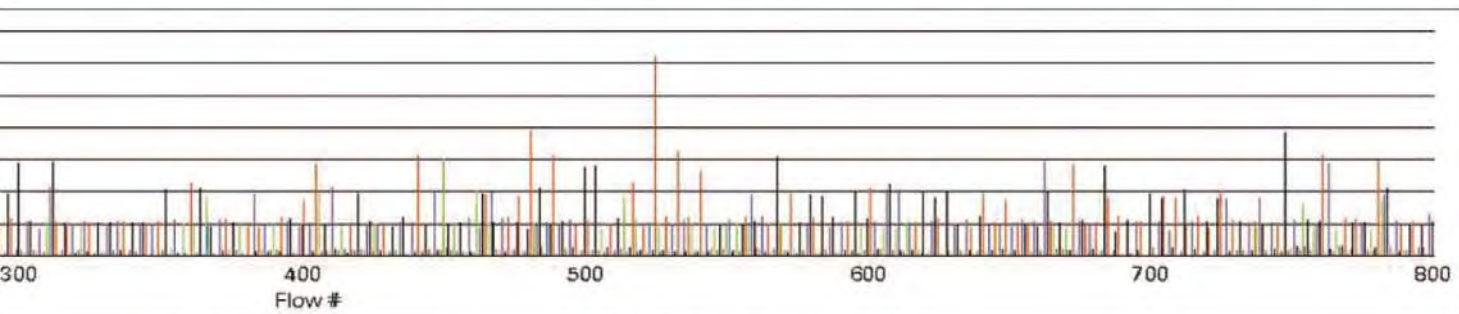
For life science research only. Not for use in diagnostic procedures.

454, 454 LIFE SCIENCES, 454 SEQUENCING, and GS FLX TITANIUM are trademarks of Roche. Other brands or product names are trademarks of their respective holders. © 2009 Roche Diagnostics. All rights reserved.



www.roche-applied-science.com

Introducing the GS FLX Titanium Reagents



- Obtain sequencing read lengths of 400 to 500 bases.
- Generate more than 1 million sequencing reads per 10-hour instrument run.

Learn more at www.454.com

Roche Diagnostics
Roche Applied Science
Indianapolis, Indiana



Biacore systems



from inspiration
...to publication

Highest quality, information-rich interaction data from Biacore™ systems deepen your understanding of molecular mechanisms and interaction pathways and enable you to add function to structure.

Select the perfect solution for your application and draw conclusions with confidence – from the company that continues to set the standard for label-free protein interaction analysis.



Biacore T100
unmatched performance



Biacore X100
ready to run research system



Biacore Flexchip
array-based comparative profiling



www.biacore.com



imagination at work

EDITORIAL

- 437 Redefining Science Education
Bruce Alberts

NEWS OF THE WEEK

- 446 Acquittals in CJD Trial Divide French Scientists
- 447 Western U.S. Forests Suffer Death by Degrees
>> Report p. 521
- 448 Debate Continues Over Rainforest Fate—With a Climate Twist
- 449 Confused Pelicans May Have Lingered Too Long Up North
- 449 Two Americans Win Japan Prize
- 450 European Pesticide Rules Promote Resistance, Researchers Warn
- 451 Scientists Puzzle Over Ebola-Reston Virus in Pigs
- 451 Educators Decry New Louisiana Policy
- 452 Proposed Regulatory Czar Has Long and Perplexing Track Record
- 452 U.S. Appellate Court Weighs 'Obvious' Patents
- 453 Photon Sieve Lights a Smooth Path to Entangled Quantum Weirdness
>> Report p. 483

NEWS FOCUS

- 454 Friendship as a Health Factor
With Isolation Comes Ill Health
>> Science Podcast
- 458 American Geophysical Union Meeting
Galloping Glaciers of Greenland Have Reined Themselves In
Tang Hints of a Watery Interior for Enceladus
The Many Dangers of Greenhouse Acid
Snapshots From the Meeting

LETTERS

- 460 Bailing Out Creatures Great and Small
J. Ghazoul
Proposed French Reforms Miss the Mark
D. Job
Ban Impact Factor Manipulation
C. Wallner
GOP Must Embrace Science Again
R. White
A Word of Caution on the Coca-Cola Way
G. Satchwell

BOOKS ET AL.

- 462 Dead Pool
J. L. Powell, reviewed by J. Farmer
- 463 Don't Sleep, There Are Snakes
D. L. Everett, reviewed by A. S. Calude

POLICY FORUM

- 464 Could Access Requirements Stifle Your Research?
S. Jinnah and S. Jungcurt

PERSPECTIVES

- 466 Ex Uno Plura
S. Feau and S. P. Schoenberger
>> Reports pp. 502 and 505
- 467 Where Bacteria and Languages Concur
C. Renfrew
>> Research Article p. 479; Report p. 527; Science Podcast
- 469 Teleporting a Quantum State to Distant Matter
M. S. Kim and J. Cho >> Report p. 486
- 470 Sources of Asian Haze
S. Szidat >> Report p. 495
- 471 Life on an Anaerobic Planet
F. Westall
- 472 Protein Filaments Caught in the Act
G. J. Jensen >> Report p. 509



page 454



page 462

REVIEW

- 474 Membrane Fusion: Grappling with SNARE and SM Proteins
T. C. Südhof and J. E. Rothman
>> Reports pp. 512 and 516

CONTENTS continued >>



COVER

Human cells infected with the protozoan parasite *Toxoplasma gondii* visualized by scanning electron microscopy. In the foreground are parasites (yellow-green) rupturing out of a dying host cell (blue); in the background is an intact host cell containing a large parasite-filled vacuole. See page 530.

Image: Sasha Meshinchi, Michael Robinson, Bjorn Kafsack, and Vern Carruthers

DEPARTMENTS

- 433 This Week in *Science*
- 438 Editors' Choice
- 440 *Science* Staff
- 443 Random Samples
- 445 Newsmakers
- 534 New Products
- 535 *Science* Careers

Automated sample and assay technologies by QIAGEN

Free up your time



Automated solutions from sample to result:

- The widest choice of sample processing protocols
- Low-, medium-, and high-throughput automation
- Leading solutions for molecular diagnostics
- Plug-and-play automated sample preparation
- Quantitative, real-time PCR detection
- Automated analysis of DNA fragments and RNA
- High-resolution sequence-based DNA detection and quantification
- HPV testing

Making improvements in life possible — www.qiagen.com



Sample & Assay Technologies

BREVIA

478 Earth's Degassing: A Missing Ethane and Propane Source

G. Etiope and P. Ciccioli

Natural gas seepage contributes far more methane, ethane, and propane to the atmosphere than formerly realized.

RESEARCH ARTICLE

479 Language Phylogenies Reveal Expansion Pulses and Pauses in Pacific Settlement

R. D. Gray et al.

Geographical distribution of Austronesian languages reveals the rate and direction of migrations from Taiwan 5200 years ago.

>> Perspective p. 467

REPORTS

483 An Entanglement Filter

R. Okamoto et al.

A useful tool for quantum information processing transmits entangled photons only when they have the same polarization.

>> News story p. 453

486 Quantum Teleportation Between Distant Matter Qubits

S. Olmschenk et al.

Transporting quantum states between trapped ions one meter apart may enable local storage of information in quantum memories.

>> Perspective p. 469

489 Femtosecond XANES Study of the Light-Induced Spin Crossover Dynamics in an Iron(II) Complex

Ch. Bressler et al.

X-ray absorption spectroscopy resolves the dynamics of spin-state interconversions, which take place in less than a picosecond, in a well-studied class of iron compounds.

492 Complementary Active Sites Cause Size-Selective Reactivity of Aluminum Cluster Anions with Water

P. J. Roach et al.

Water dissociates at similar active sites on anionic aluminum clusters that have different sizes and electronic structure.

495 Brown Clouds over South Asia: Biomass or Fossil Fuel Combustion?

Ö. Gustafsson et al.

Biomass burning accounts for at least one-half of carbon-rich aerosols in the Asian atmospheric brown cloud that forms each winter.

>> Perspective p. 470

498 Genetic Interactions Between Transcription Factors Cause Natural Variation in Yeast

J. Gerke et al.

Adaptive differences in yeast sporulation arise from single-nucleotide mutations in transcription factors regulating sex.

502 Different T Cell Receptor Signals Determine CD8⁺ Memory Versus Effector Development

E. Teixeira et al.

Point mutations in the T cell receptor decide the fate of killer T cells and the development of immunological memory.

>> Perspective p. 466

505 Secondary Replicative Function of CD8⁺ T Cells That Had Developed an Effector Phenotype

O. Bannard et al.

Killer T cells that developed during a primary antiviral response can become memory T cells in secondary infections.

>> Perspective p. 466

509 Electron Cryomicroscopy of *E. coli* Reveals Filament Bundles Involved in Plasmid DNA Segregation

J. Salje et al.

The actin-like filaments that power movement of DNA during bacterial cell division form small bundles of three to five filaments near the nucleoid.

>> Perspective p. 472

512 Alternative Zippering as an On-Off Switch for SNARE-Mediated Fusion

C. G. Giraudo et al.

A structural motif in the protein complexin may act as a switch during membrane fusion.

>> Review p. 474

516 Complexin Controls the Force Transfer from SNARE Complexes to Membranes in Fusion

A. Maximov et al.

The protein complexin may act as a force-transferring switch during membrane fusion.

>> Review p. 474

521 Widespread Increase of Tree Mortality Rates in the Western United States

P. J. van Mantgem et al.

Regional warming is contributing to the recent acceleration of tree deaths seen in undisturbed forests of the western U.S.

>> News story p. 447; Science Podcast

524 The Sphingolipid Transporter Spns2 Functions in Migration of Zebrafish Myocardial Precursors

A. Kawahara et al.

Normal heart development in zebrafish requires the function of a lipid transporter in a membrane surrounding the yolk, a tissue outside of the embryo proper.

527 The Peopling of the Pacific from a Bacterial Perspective

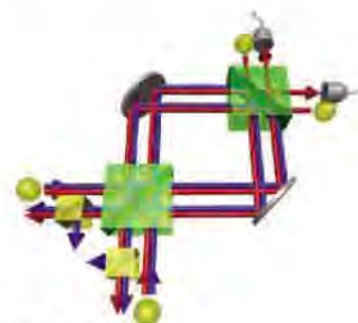
Y. Moodley et al.

The geographical distribution of strains of a specific human pathogen helps to define patterns of colonization out of Taiwan.

>> Perspective p. 467



page 463



page 453 & 483



pages 469 & 486

530 Rapid Membrane Disruption by a Perforin-Like Protein Facilitates Parasite Exit from Host Cells

B. F. C. Kafsack et al.

The human and animal parasite that causes toxoplasmosis escapes from host cells by using a perforin-like protein to make holes in the intracellular vacuole in which it resides.

CONTENTS continued >>

Cell-free protein expression delivers data faster

Now, Get the Most Reliable System for Your Specific Needs

Express proteins in hours instead of days. Referenced in thousands of citations, Promega is the choice for cell-free expression. Select your system from the most comprehensive product portfolio commercially available. Whether you require eukaryotic- or prokaryotic-based expression from either DNA or RNA templates, Promega has the right system for you.

E. coli expression

Transform and overnight growth

DAY 1

Induction and protein expression

DAY 2-3

Purification/dialysis

DAY 4

Use in application

DAY 5

Total: 4-5 DAYS

TnT® Quick System

Add DNA directly to TnT® Master Mix, express protein

1 Hour

Use directly in application

Total: 1 Hour

08931MD

To select the best system
for your needs visit:
www.promega.com/selectors/tnt/

TODAY COULD
BE THE DAY.


Promega

SCIENCEONLINE

SCIENCEXPRESS

www.sciencexpres.org

Coherence Factors in a High- T_c Cuprate Probed by Quasi-Particle Scattering off Vortices

T. Hanaguri et al.

The momentum-dependent coherence factors in a high-temperature superconductor are revealed by introducing magnetic vortices.

10.1126/science.1166138

The Formation of Warm Dense Matter: Experimental Evidence for Electronic Bond Hardening in Gold

R. Ernstorfer et al.

Injecting energy into a gold film can create a transient excited state with stronger bonds prior to melting.

10.1126/science.1162697

Analysis of the *Drosophila* Segmentation Network Identifies a JNK Pathway Factor Overexpressed in Kidney Cancer

J. Liu et al.

A developmental marker in fruit flies also acts as a marker of renal cell cancer in humans.

10.1126/science.1157669

Axon Regeneration Requires a Conserved MAP Kinase Pathway

M. Hammarlund et al.

Axon regeneration in adult nematode worms has distinct signals that are independent of earlier developmental programs.

10.1126/science.1165527

SCIENCENOW

www.sciencenow.org

Highlights From Our Daily News Coverage

Extinct Tiger Lives On in Close Relative

Caspian tiger is essentially the same subspecies as Siberian tiger.

The Brain's Pied Piper

Researchers identify neural system that prods us to conform.

Care for a Silkworm With Your Tang?

Caterpillars may be on the menu for future space expeditions.

SCIENTESIGNALING

www.sciencesignaling.org

The Signal Transduction Knowledge Environment

PERSPECTIVE: Protein Kinase Activation Loop Autophosphorylation in Cis—Overcoming a Catch-22 Situation

P. A. Lochhead

The mechanisms by which kinases activate themselves are still emerging.

PROTOCOL: Genome to Kinome—Species-Specific Peptide Arrays for Kinome Analysis

S. Jalal et al.

Marrying bioinformatics and phosphorylation assays enables the empirical analysis of kinomes of multiple species.

CONNECTIONS MAP: Neuro2A Differentiation by $G\alpha_{i/o}$ Pathway

A. Ma'ayan et al.

Neurite outgrowth can be stimulated by G protein-coupled receptors that signal through $G\alpha_i$ and $G\alpha_o$ proteins.

GLOSSARY

Find out what IRAP, Spred, and DOPA mean in the world of cell signaling.

SCIENCECAREERS

www.sciencereers.org/career_magazine

Free Career Resources for Scientists

Mind Matters: Stress, an Uninvited Lab Visitor

I. Levine

Work-related stress is an insidious health hazard.

Lost in Translation

C. Rey

America needs more science writers of color, just as it needs more scientists of color.

Consulting Experience for Doctoral Students in France

E. Pain

A program launched by the French government allows Ph.D. students to sell their skills to nonacademic clients.

SCIENCEPODCAST

www.sciencemag.org/multimedia/podcast

Free Weekly Show

Download the 23 January *Science* Podcast to hear about increased tree mortality in the western U.S., human population history in the Pacific, how social networks influence health, and more.

ORIGINSBLOG

blogs.sciencemag.org/origins

A History of Beginnings

SCIENCEINSIDER

blogs.sciencemag.org/scienceinsider

Science Policy News and Analysis



SCIENCENOW

Not gone after all.



SCIENTESIGNALING

An active kinase.

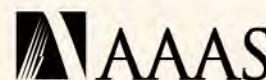


SCIENCECAREERS

A hazard in the lab.

SCIENCE (ISSN 0036-8075) is published weekly on Friday, except the last week in December, by the American Association for the Advancement of Science, 1200 New York Avenue, NW, Washington, DC 20005. Periodicals Mail postage (publication No. 484460) paid at Washington, DC, and additional mailing offices. Copyright © 2009 by the American Association for the Advancement of Science. The title **SCIENCE** is a registered trademark of the AAAS. Domestic individual membership and subscription (51 issues): \$146 (\$74 allocated to subscription). Domestic institutional subscription (51 issues): \$835; Foreign postage extra: Mexico, Caribbean (surface mail) \$55; other countries (air assist delivery) \$85. First class, airmail, student, and emeritus rates on request. Canadian rates with GST available upon request, GST #1254 88122. Publications Mail Agreement Number 1069624. **Printed in the U.S.A.**

Change of address: Allow 4 weeks, giving old and new addresses and 8-digit account number. **Postmaster:** Send change of address to AAAS, P.O. Box 96178, Washington, DC 20090-6178. **Single-copy sales:** \$10.00 current issue, \$15.00 back issue prepaid includes surface postage; bulk rates on request. **Authorization to photocopy** material for internal or personal use under circumstances not falling within the fair use provisions of the Copyright Act is granted by AAAS to libraries and other users registered with the Copyright Clearance Center (CCC) Transactional Reporting Service, provided that \$20.00 per article is paid directly to CCC, 222 Rosewood Drive, Danvers, MA 01923. The identification code for *Science* is 0036-8075. *Science* is indexed in the *Reader's Guide to Periodical Literature* and in several specialized indexes.

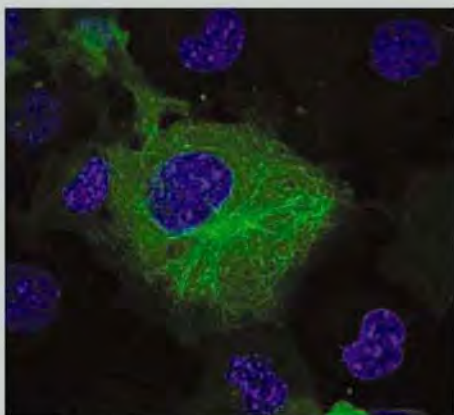


ADVANCING SCIENCE. SERVING SOCIETY

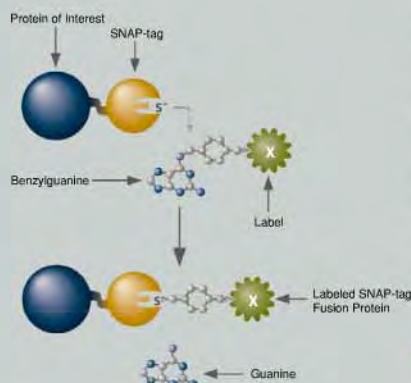
INFINITE POSSIBILITIES

Cellular Imaging & Analysis

NEB introduces SNAP-tag™ and CLIP-tag™ protein labeling systems. These innovative technologies provide simplicity and extraordinary versatility to the imaging of mammalian proteins *in vivo*, and to protein capture experiments *in vitro*. The creation of a single genetic construct generates a fusion protein which, when covalently attached to a variety of fluorophores, biotin, or beads provides a powerful tool for studying the role of proteins in living and fixed cells.



Live COS-7 cells transiently transfected with pSNAPm-Tubulinβ. Cells were labeled with SNAP-Cell TMR-Star (green pseudocolor) for 30 minutes and counterstained with Hoechst 33342 (blue) for nuclei.



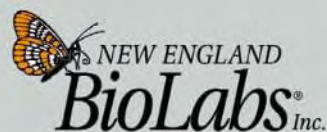
SNAP-tag Technology: SNAP-tag (gold) fused to the protein of interest (blue) self labels releasing guanine.

Advantages:

Versatile - Compatible systems enable dual labeling

Flexible - Multiple fluorophores allow for choice & flexibility

Innovative - A range of applications is possible with a single construct



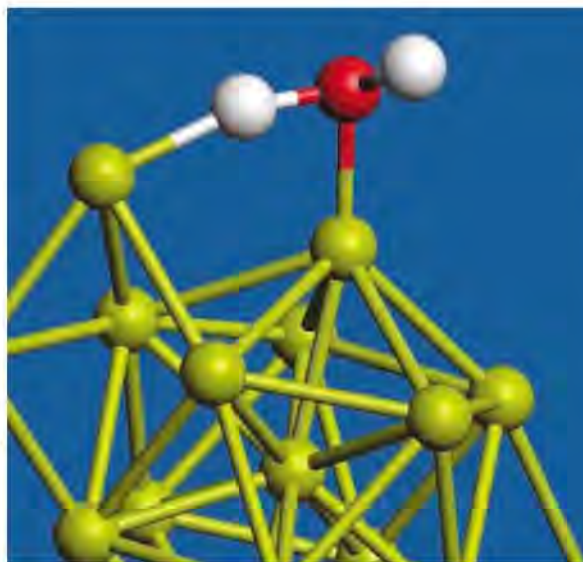
CLONING & MAPPING

DNA AMPLIFICATION
& PCR

RNA ANALYSIS

PROTEIN EXPRESSION
& ANALYSIS

GENE EXPRESSION
& CELLULAR ANALYSIS



<< Active Sites on Aluminum Clusters

The reactivity of electrons of metal clusters formed in the gas phase can be dominated by shell-filling rules that arise from quantum confinement of the valence electrons and that mirror the shell-filling rules of atoms. For aluminum clusters, these rules can account for their reactivity with O_2 . Roach *et al.* (p. 492) show that reactions of these clusters with water represent a different case and that its propensity for dissociative chemisorption on Al_{16}^- , Al_{17}^- , and Al_{18}^- clusters depends more on the presence of particular geometric sites than on filling electronic shells.

Teleporting Quantum Matter

Quantum teleportation is the faithful transfer of the quantum state of one system onto another, and is at the heart of quantum information processing. While photons are ideal for teleportation over long distances, there is also the requirement to store the information locally in quantum memories. Here, trapped ions are ideal candidates because of their long memory times. Olmschenk *et al.* (p. 486; see the Perspective by Kim and Cho) combine the benefits of photons and trapped ions by demonstrating the ability to teleport the quantum state of one trapped ion onto another trapped ion about 1 meter away. The technique may eventually be scalable to larger quantum networks.

Monitoring Human Migrations

Among the most dramatic of human expansions is the prehistoric colonization of the islands scattered across the Pacific Ocean (see the Perspective by Renfrew). Two competing scenarios attempt to explain this astonishing migration: The pulse-pause scenario posits a Taiwanese origin of the Austronesian language complex between 5000 to 6000 years ago, while the slow boat scenario suggests an origin in Island South/East Asia 13,000 to 17,000 years ago. Gray *et al.* (p. 479) apply phylogenetic techniques to 210 basic vocabulary words (animals, kinship terms, simple verbs, colors, and numbers) from 400 Austronesian languages to show that the language family has a root in Taiwan, some ~5000 years ago, followed by languages of the Philippines, Borneo/Sulawesi, Central Malayo-Polynesia, and South Halmahera/West New Guinea, and reflects the origin and path

of the migration predicted under the pulse-pause scenario. In a separate approach to migration research, Moodley *et al.* (p. 527) turned the ubiquitous occurrence of a human pathogen to good use. *Helicobacter pylori* is a bacterium that specifically colonizes the human stomach, where it occurs in about half the population who do not have access to modern medicines. Because *H. pylori* is so specific to humans, it has spread around the world and diverged genetically alongside its host since people emerged from Africa. The discovery of the Sahul strain of the bacterium indicates that humans spread from Taiwan in two waves. The first wave spread across the exposed land bridges of what is now the Indonesian Archipelago into New Guinea and Australia. A second wave carrying the Maori strain of the bacterium traveled within humans via the Philippines into Polynesia and New Zealand.

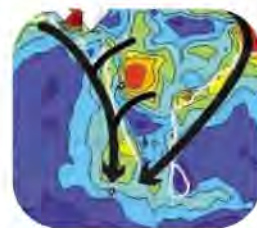
Separating Immune Cell Fate

The adaptive immune response is mediated in part by $CD8^+$ T cells, which protect against intracellular infection by pathogens and against some tumors. This T cell population fulfills a dual function by providing immediate protection via effector cells and retaining this protective immunity long-term, via memory cells. On infection, naïve T cells carrying pathogen-specific T cell receptors (TCR) differentiate into short-lived effector cells and long-lived memory cells. However, it is unclear how this is regulated, and whether memory cells are formed from the effector cells or differentiate separately (see the Perspective by Feau and Schoenberger). Teixeira *et al.* (p. 502) have now shown a direct role for the TCR specifically in $CD8^+$

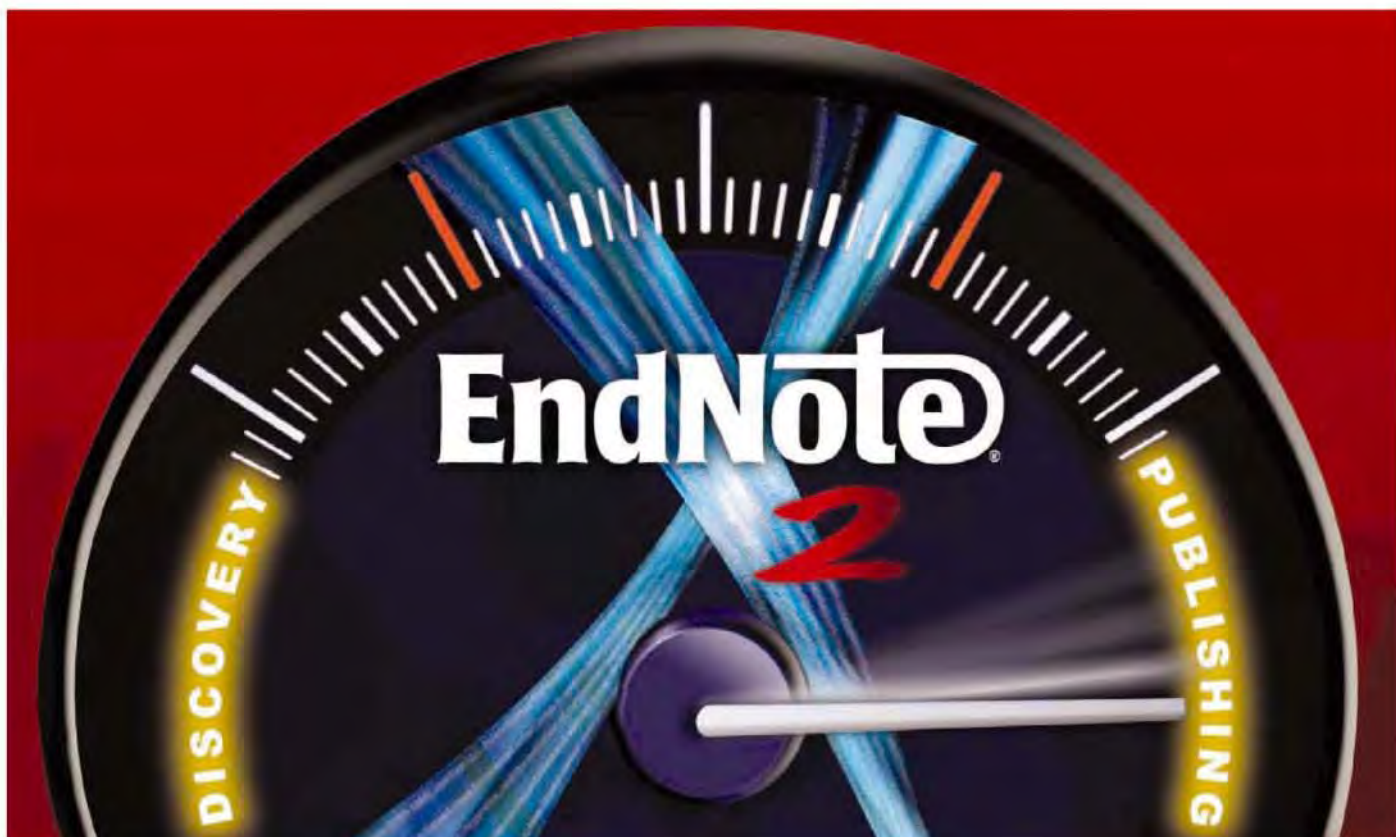
memory T cell differentiation. Upon bacterial infection of mice harboring defective TCRs, mutant T cells were still able to generate effector T cells and a robust primary immune response, but were specifically impaired in developing memory T cells. Thus, the differentiation of effector and memory $CD8^+$ T cells are separable, and determined by the induction of a distinct set of TCR signals. However, Bannard *et al.* (p. 505) used a transgenic mouse line to closely map the cell fate of a subset of effector T cells that were generated during the primary response to infection by influenza. These effector cells were found to survive and become memory cells that could replicate and expand during secondary infection.

Cooking and Burning

A huge plume of air pollution, called the Asian Atmospheric Brown Cloud (ABC), emanates from Southern Asia and persists over much of the Indian continent and the Indian Ocean during the winter. It is so large and dense that its cooling effect may balance, or even surpass, the warming effect of greenhouse gases in the region. In order to know how to mitigate this scourge, its origin must be known. There are two major sources that contribute to the ABC—biomass burning and fossil fuel combustion—whose relative importance is unclear. Gustafsson *et al.* (p. 495; see the Perspective by Szidat) measured radiocarbon in particles from the cloud, and between one-half and two-thirds of the



Continued on page 435



FROM DISCOVERY TO PUBLISHING ENDNOTE X2 GETS YOU THERE FASTER.

Don't waste time in the slow to publish lane. Let EndNote X2 take you there, faster. Revered by millions for its blazing online search speeds, instantaneous Cite While You Write™ technology and organizing references in a snap, EndNote X2 has all the high performance features you could possibly want in an easy-to-use bibliography software, and more.

Now, EndNote X2 can locate full text and connect it with references while you move on down the research road. Within a single window you can group references automatically, search your favorite online databases and transfer to and from your EndNote Web account, all in record time.



So now that you're up to speed on what EndNote X2 has to offer, it's easy to see how EndNote makes you the leader of the pack.

Download your free demo or buy online today
www.endnote.com

800-722-1227 • 760-438-5526 • rs.info@thomson.com



Continued from page 433

carbonaceous aerosols were from biomass burning. Thus, controlling biomass combustion, particularly residential cooking and agricultural burning, will be important to mitigate climate effects and to improve air quality in the region.

Bacterial Cytoskeleton Revealed

The ParMRC DNA-segregation system of bacteria is the simplest known "mitosis-like" DNA partitioning machinery, which uses filament polymerization to move DNA through the cell. Recent studies have demonstrated the similarity of the filaments to actin filaments, uncovered the dynamic properties of the filaments, reconstituted the system *in vitro*, and determined the structure and function of the filament-polymerizing protein ParR. **Salje *et al.*** (p. 509, published online 18 December; see the Perspective by **Jensen**) observed the ParMRC directly in natively cryoimmobilized cells using a combination of vitreous sectioning and cryoelectron tomography. Small bundles of three to five filaments that may represent the actively segregating filaments were observed close to the surface of the bacterial nucleoid.



Grappling with Membrane Fusion

The process of membrane fusion is fundamental to cellular organization and has been the focus of a vast literature. **Südhof and Rothman** (p. 474) review the role of so-called SNARE and SM proteins in membrane fusion and present a hypothesis for how they are regulated by other proteins, termed grapples, exemplified by complexin. Two further papers also shed light on complexin's role

in regulating SNARE-mediated membrane fusion. **Giraud *et al.*** (p. 512) show that a structural motif within complexin appears to act as a molecular switch directly interacting with SNAREs during membrane fusion. **Maximov *et al.*** (p. 516) confirm that, in neuronal systems, complexin can play a negative or positive role in SNARE-mediated membrane fusion during neurotransmitter release, potentially either clamping SNAREs to prevent spontaneous fusion, or promoting fusion when appropriate.

Dying Trees

Tree mortality rates have more than doubled in recent decades in otherwise undisturbed forests of the western United States, possibly as a consequence of ongoing regional warming. **Van Mantgem *et al.*** (p. 521; see the news story by **Pennisi**) use a long-term set of demographic data to reveal a pervasive increase in background mortality rates for trees in seemingly healthy forest. The increases occur regardless of elevations, tree size, taxon, or fire history and cannot be attributed to processes such as increasing competition or aging of large trees. The increases in mortality are likely to have been driven by environmental changes, with ongoing regional warming and its widespread effects on the western U.S. hydrologic cycle being the most probable contributors. Changes in tree mortality rates can affect future forest structure and composition, which in turn affect ecosystem services such as carbon sequestration, and thereby biological contributions and responses to climatic changes.

Taking a S1P

Lipid mediators derived from the cell membrane have important signaling functions. Among them, sphingosine-1-phosphate (S1P) activates its cell surface receptor to control immunity, vascular tone, cell migration, and cancer. The amount of extracellular S1P depends upon the conversion of sphingosine to S1P and upon the release mediated by S1P transporters. **Kawahara *et al.*** (p. 524, published online 11 December) have identified the S1P transporter, Spns1, by zebrafish forward genetics and show that Spns1 interacts genetically with the S1P receptor-2 (S1P2). S1P released from the yolk syncytial layer by Spns1 activates S1P2 expressed in the mesoderm, thereby regulating heart development.

Let Me Out

Perforin-like proteins are expressed by many bacterial and protozoan pathogens, but little is known about their mode of action or role in pathogenesis. **Kafsack *et al.*** (p. 530, published online 18 December; see the cover) reveal the function of a perforin-like protein, TgPLP1, expressed by the human and animal pathogen *Toxoplasma gondii*, in the exit of vacuole-enclosed parasites from host cells. TgPLP1 appears to permeabilize the host cell membranes within which the parasite resides and divides and is an essential virulence factor of *Toxoplasma* *in vivo* in mice.

2009

SARDINIA

for Plant Enthusiasts!

April 17-29, 2009

Explore Capo Caccia, a hotspot for endemic plants and the Gallura region. Cross to the unspoiled island of Caprera, and explore the island's prehistoric Nuragic culture. Visit the Sinis peninsula, the remarkable Phoenician and Roman site of Tharros, and the basalt plateau of Giara di Gesturi. \$3,850 + air.



AEGEAN HERITAGE

by Yacht

May 1-9, 2009

Explore the heritage of the Aegean, including the Cyclades Islands and the Aegean Coast of Turkey, on board the 170-passenger sailing yacht, *Star Clipper*. See Rhodes, Bodrum Castle, Caunos, Santorini, and Hydra. From \$3,295 + air.

Wild & Prehistoric FRANCE

May 22-June 4, 2009

Join **Mark Walters** and discover wild areas and prehistoric sites in Haute Provence, the Massif Central, and the Dordogne. See images of the greatest cave paintings in Europe at Lascaux II. See the cave art by train at Rouffignac. Visit the Vézère Valley, Font de Gaume, Arles, and Les Baux. \$3,895 + air.

ALASKA

May 31-June 7, 2009

Explore Southeast Alaska's coastal wilderness aboard the *National Geographic Sea Lion*. From \$5,390 plus free air from Seattle.

For a detailed brochure,
please call (800) 252-4910

AAAS Travels

17050 Montebello Road
Cupertino, California 95014
Email: AAASInfo@betchartexpeditions.com



Genomics of Energy & Environment is the topic of the 2009 Department of Energy Joint Genome Institute (DOE JGI) User Meeting, which will be held March 25-27 in Walnut Creek, California. This year's meeting will specifically emphasize the **genomics of renewable energy strategies, biomass conversion to biofuels, environmental gene discovery, and engineering of fuel-producing organisms**. The meeting will feature presentations by leading scientists advancing these topics. The meeting will also include informatics workshops and tutorials for the analysis of prokaryotic and eukaryotic genomes, and the evaluation of new sequencing platforms and their applications. Poster submissions are encouraged. Pre-registration is required as interest is expected to exceed meeting capacity again this year. Registration and a preliminary agenda can be found at: www.jgi.doe.gov.

FREE
with registration

Science Alerts in Your Inbox

Get daily and weekly E-alerts on the latest news and research! Sign up for our e-alert services and you can know when the latest issue of *Science* or *Science Express* has been posted, peruse the latest table of contents for *Science* or *Science Signaling*, and read summaries of the journal's research, news content, or Editors' Choice column, all from your e-mail inbox. To start receiving e-mail updates, go to:

sciencemag.org/ema

Science Posting Notification
Alert when weekly issue is posted

ScienceNOW Weekly Alert
Weekly headline summary

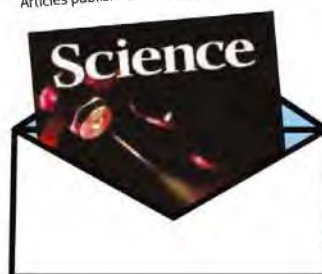
Science News This Week
Brief summaries of the journal's news content

ScienceNOW Daily Alert
Daily headline summary

Science Magazine TOC
Weekly table of contents

Science Express Notification
Articles published in advance of print

Science Signaling TOC
Weekly table of contents

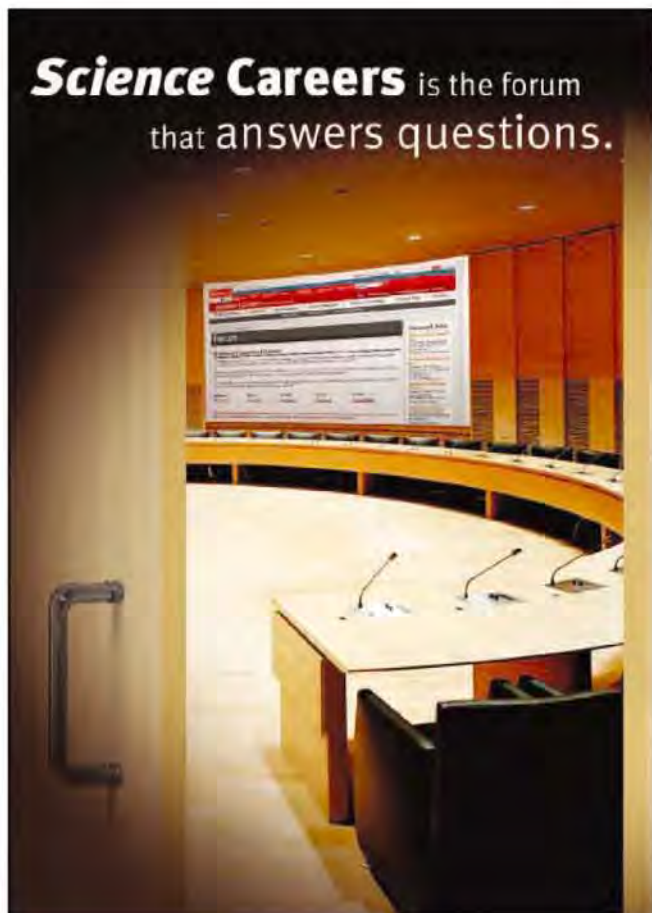


Editors' Choice
Highlights of the recent literature

This Week in Science
Summaries of research content



Science Careers is the forum that answers questions.



Science Careers is dedicated to opening new doors and answering questions on career topics that matter to you. With timely feedback and a community atmosphere, our careers forum allows you to connect with colleagues and experts to get the advice and guidance you seek as you pursue your career goals.

Science Careers Forum:

- » Relevant Career Topics
- » Timely Advice and Answers
- » Community, Connections, and More!

Visit the forum and join the conversation today!



Your Future Awaits.



ScienceCareers.org



Bruce Alberts is Editor-in-Chief of *Science*.

Redefining Science Education

THERE IS A MAJOR MISMATCH BETWEEN OPPORTUNITY AND ACTION IN MOST EDUCATION SYSTEMS today. It revolves around what is meant by “science education,” a term that is incorrectly defined in current usage. Rather than learning how to think scientifically, students are generally being told about science and asked to remember facts. This disturbing situation must be corrected if science education is to have any hope of taking its proper place as an essential part of the education of students everywhere.

Scientists may tend to blame others for the problem, but—strange as it may seem—we have done more than anyone else to create it. Any objective analysis of a typical introductory science course taught today in colleges and universities around the world, whether it be biology, chemistry, physics, or earth sciences, would probably conclude that its purpose is to prepare students to “know, use, and interpret scientific explanations of the natural world” (strongly emphasizing the “know”). This is but one of four goals recommended for science education by the distinguished committee of scientists and science education experts convened by the U.S. National Academies that produced *Taking Science to School: Learning and Teaching Science in Grades K-8*. And yet college courses set the model for the teaching of science in earlier years.

The three other goals of equal merit and importance are to prepare students to generate and evaluate scientific evidence and explanations, to understand the nature and development of scientific knowledge, and to participate productively in scientific practices and discourse (summarized in the Academies’ *Ready, Set, Science!*). Scientists would generally agree that all four types of science understanding are critical not only to a good science education but also to the basic education of everyone in the modern world. Why then do most science professors teach only the first one?

As the scientist and educator John A. Moore emphasized in his prolific writings, science provides a special way of knowing about the world.* The failure of most students and adults to understand this fact, despite having taken science courses, reveals a serious deficiency in our education systems. And the failure of students to acquire the logical problem-solving skills of scientists, with their emphasis on evidence, goes a long way to explain why business and industry are so distressed by the quality of our average high-school and college graduates, finding them unable to function effectively in the workforce.

Vast numbers of adults fail to take a scientific approach to solving problems or making judgments based on evidence. Instead, they readily accept simplistic answers to complicated problems that are confidently espoused by popular talk-show hosts or political leaders, counter to all evidence and logic. Most shocking to me is the finding that many college-educated adults in the United States see no difference between scientific and nonscientific explanations of natural phenomena such as evolution. Their science teachers failed to make it clear that science fundamentally depends on evidence that can be logically and independently verified; instead, they taught science as if it were a form of revealed truth from scientists.

Teaching the missing three strands requires that students at all levels engage in active inquiry and in-depth discussion in classrooms. What would it take to get scientists to teach their college courses this way? I suggest that we start with new assessments. It is much easier to test for the facts of science than it is to test for the other critical types of science understanding, such as whether students can participate productively in scientific discourse. For the United States, I therefore propose an intense, high-profile national project to develop quality assessments that explicitly measure all four strands of science learning that were defined by the National Academies.† Designing such assessments for students at all levels (from fourth grade through college), energetically advertising and explaining them to the public, and making them widely available at low cost to states and universities would greatly accelerate the redefinition of science education that the world so urgently needs.

— Bruce Alberts

10.1126/science.1170933

*See *Science as a Way of Knowing* (Harvard Univ. Press, Cambridge, MA, 1999).

†E. S. Quellmatz, J. W. Pellegrino, *Science* 323, 75 (2009).

CHEMISTRY

Filming Chalcogenides

In atomic layer deposition (ALD), thin films are deposited with two alternating chemical reactions. Because both reactions stop once they have exhausted the reactive groups on the surface, growth rates are highly controlled. Extending ALD growth to new materials systems requires the identification of fast reactions that saturate and that avoid the use of highly toxic reagents. Pore *et al.* report an ALD route for the growth of metal tellurides and selenides, which include germanium antimony telluride (GST), a material used in phase-change memories; and copper indium selenide, a photovoltaic material. Bis(trialkylsilyl) compounds of Te and Se can be used with metal salts of Ge, Sb, and Cu, as well as other metals, to grow films in a controlled manner. GST films could be grown by mixing the precursor metal chlorides, and in the case of copper, the use of copper(II) pivalate allowed for temperature-controlled tuning of the film stoichiometry. — PDS

J. Am. Chem. Soc. **131**, 10.1021/ja8090388 (2009).

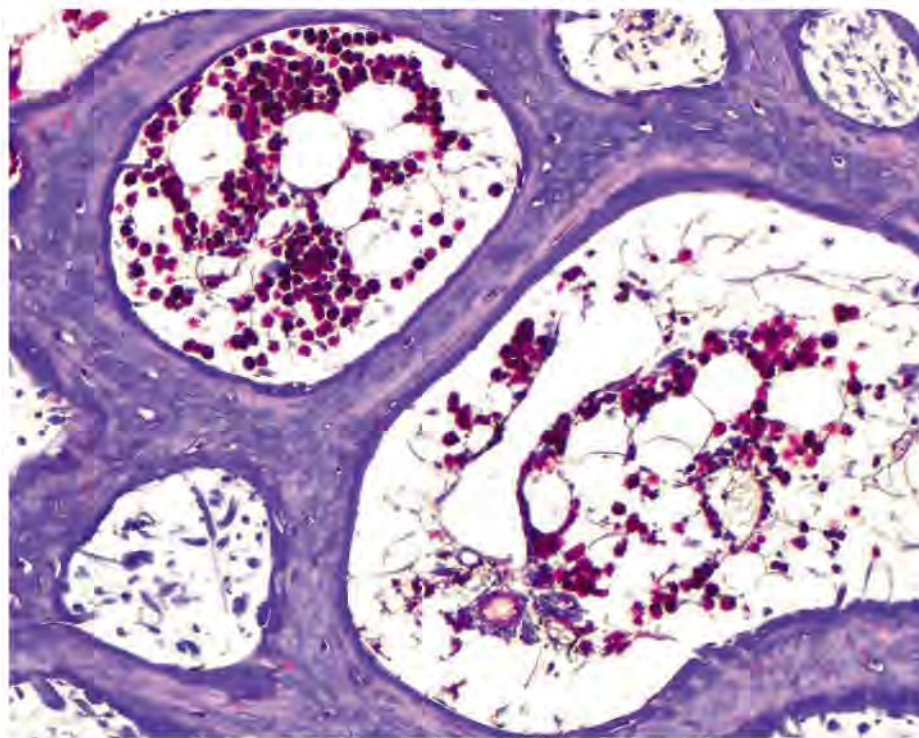
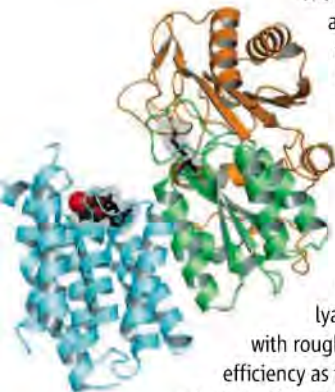
BIOCHEMISTRY

Creating a Spinoff

How might one acquire a new catalytic ability? Other than by stealing an enzyme (akin to lateral gene transfer), one could take advantage of an existing but suboptimal active site. Sánchez-Moreno *et al.* describe the promiscuous behavior of the decidedly un-sexy protein dihydroxyacetone kinase (DHAK), whose generally accepted role is to use ATP to phosphorylate the metabolite dihydroxyacetone; the product, dihydroxyacetone phosphate, can be used in lipid and carbohydrate biosynthesis, whereas the unphosphorylated substrate is toxic. What these

authors document is that DHAK (shown at left) also catalyzes the FAD-AMP lyase reaction, in which the cofactor FAD is split into AMP and a molecule of riboflavin 4',5'-phosphate. A key point is that the lyase reaction proceeds with roughly the same catalytic efficiency as the kinase reaction, albeit significantly more slowly and with a requirement for Mn^{2+} instead of Mg^{2+} .

Intriguingly, the intracellular concentration of Mn is much lower than that of Mg, yet several other



BIOMATERIALS

One Shell Fits All

Nature has evolved remarkably complex structures from a limited number of materials in order to obtain multifunctionality. For example, the shell of a turtle needs to be stiff in order to protect the internal organs from trauma. However, it also needs to be sufficiently flexible to enable efficient respiration and locomotion. As such, the shell needs to be compliant at low cyclical loads but simultaneously stiff and tough to resist sudden large impacts. Krauss *et al.* show that turtle shells contain densely packed inner and outer cortical sheets, and these two layers in turn sandwich sparsely located porous trabecular bone tissue. Attached to the spinal column are rigid ribs, which are separated by regions of suture (shown above). The suture has a seesaw or wavy geometry and is not mineralized, but instead is composed of aligned collagen fibers that are angled relative to the direction of the suture. This arrangement allows the fibers to remain in tension when the shell is loaded in either tension or compression. At low loading, the suture compresses only slightly, allowing flexibility in the movement of neighboring bones, but at high loading, the bones can lock together to strongly resist deformation. — MSL

Adv. Mater. **10.1002/adma.200801256** (2008).

carbohydrate-handling enzymes, such as pyruvate kinase, are also manganese-dependent. — GJC

ChemBioChem **10**, 10.1002/cbic.200800573 (2009).

CLIMATE SCIENCE

Methane Mystery

Methane is a powerful greenhouse gas, implicated as a cause of many episodes of climate change in the past and also as a major factor in Earth's contemporary radiative balance. Nonetheless, we still lack an adequate understanding of the global

atmospheric methane budget, and in particular the strength of its sources. Recent research suggested that plants were a major source of methane, supplying as much as almost half of the methane released to the atmosphere; the results implied an unknown biochemical pathway for methane production in plants. Nisbet *et al.* have performed additional experiments, in chambers that allow careful control of the growing environment, which show that plants do not produce appreciable quantities of methane; genetic analyses moreover revealed no genes that would indicate the presence of any known methane biosyn-

thesis pathway. Instead, the authors suggest that previous observations of methane production may have been reflecting the spontaneous breakdown of plant material under high ultraviolet stress conditions or the transpiration of water containing dissolved methane. They conclude that plants are not a major source of global methane production. — HJS

Proc. R. Soc. London Ser. B 10.1098/rspb.2008.1731 (2009).

NEUROSCIENCE

Sophisticated Movements

The ability of human beings to exert fine motor control is astonishing. Just think of the precision movements executed by a brain surgeon or a concert pianist or even a top-flight tennis player. What enables us to control the muscles of our upper extremities to such an unmatched degree?

To establish the anatomical underpinnings of these abilities, Rathelot and Strick injected a strain of rabies virus into single shoulder and arm muscles of monkeys and also reanalyzed previously published results from similar injections into finger muscles. Retrograde transneuronal transport of the virus demonstrated that the primary motor cortex (area M1 in the brain) contains two subdivisions. A rostral region of M1 contains corticospinal cells that project to spinal interneurons; these cells do not make direct connections onto motoneurons and represent a phylogenetically old part of M1 that is standard for most mammals. In contrast, a caudal region of M1 contains neurons that do synapse directly onto motoneurons; this region represents a phylogenetically younger part of M1 that is present only in some higher primates and in humans. The direct access to motoneurons afforded by corticospinal cells enables this younger part of M1 to bypass spinal cord mechanisms and to sculpt idiosyncratic patterns of motor output that are revealed as highly skilled movements. — PRS

Proc. Natl. Acad. Sci. U.S.A. 106, 918 (2009).



MOLECULAR BIOLOGY

Controlling the Masses

The regulation of gene transcription is complex and occurs at many different stages, of which one is the transformation of chromatin from an open

and more active structure to a closed and inactive state. This regulatory challenge is amplified when the target genes are present in hundreds of copies on several different chromosomes. Ribosomes are composed of proteins and RNAs, and the number of genes encoding ribosomal RNAs (rRNAs) ranges from several hundred in mammals to several thousand in plants. They are organized in tandem repeats that reside in nucleolar organizing regions on chromatin, and the activity of these rRNA genes is finely tuned to support cell growth. However, not all rRNA genes are actively transcribed at the same time, and Sanij *et al.* show that decreasing the amount of upstream binding factor (UBF) causes methylation-independent and reversible silencing of rRNA genes. UBF depletion led to chromatin remodeling, although total rRNA production was only partially reduced, as there was an increase in transcription from the remaining active genes. The authors found that during differentiation, the active pool of rRNA genes actually decreases, along with the levels of UBF, suggesting that UBF may regulate the ratio of active versus inactive rRNA genes during development. — HP*

J. Cell Biol. 183, 1259 (2008).

DEVELOPMENT

Fly Fishing with a Hedgehog

The complexity of gene regulation mechanisms is also evident in the analysis by Amano *et al.* of the temporal and spatial patterns of *Sonic hedgehog* (*Shh*) expression. *Shh* is required for proper limb formation in mice. In the limb bud, it is expressed exclusively in a group of posterior mesenchymal cells called the zone of polarizing activity (ZPA). The authors found that colocalization of the *Shh* coding region and the long-range enhancer of its expression in limb bud, MFCS1, frequently occurs in the ZPA of day-10.5 limb buds but not by day 12.5, when *Shh* has been turned off. Chromosome conformation capture assays confirmed that MFCS1 and *Shh* interact directly in the limb bud. This interaction appears to indicate transcriptional competence; for active transcription to occur, a chromosome loop involving *Shh* needs to form, and evidence of loop formation was seen only in the ZPA. Such loops have been observed in other systems, and the authors propose that the interaction of MFCS1 and *Shh* promotes a looping-out of the chromosome that renders *Shh* accessible to transcription factors. This change in chromosomal configuration was observed in only a fraction of the ZPA cells at any one time; the resultant intermittent exposure of *Shh* may ensure proper control of levels of *Shh* needed for limb morphogenesis. — BJ

Dev. Cell 16, 10.1016/j.devcel.2008.11.011 (2009).

TIBET

& Total Solar Eclipse

July 8-24, 2009



Centerline of totality for this Eclipse arcs from India across Bhutan and China. See the eclipse south of Shanghai, near **Hangzhou**, reputedly Marco Polo's favorite city in China. This will be an excellent location for getting the best view of the Total Solar Eclipse.

Start in **Chengdu**, vibrant capital city of Sichuan, and then fly west to explore the cultural heart of Tibet. The Tibetan Plateau has long been a place of fascination for Western naturalists and explorers.

Our first destination in Tibet is **Tsedang** near some of the oldest villages and sacred sites in Tibet. They pre-date Buddhism in this area by more than 1,000 years.

From Tsedang, follow the Yarlung Tsangpo & Kyichu rivers upstream to **Lhasa**, historic center of the Tibetan world renowned for its sacred sites, each with distinctive esoteric rituals, colorful iconography, and profound spiritual



significance to the Tibetan people. These include the **Jorkang Temple**, the **Potala** and **Norbulinka Palace**, the winter and summer residences of the Dalai Lama, and **Ganden Monastery**, poised dramatically on a ridge above the Lhasa Valley.

Although the Tibetan Plateau is quite high, we will spend most of our time at moderate elevations. After a few days, most visitors acclimatize and do fine at these elevations. \$4,195 + air

For a detailed brochure, please call (800) 252-4910

AAAS Travels

17050 Montebello Road
Cupertino, California 95014
Email: AAASInfo@betchartexpeditions.com

*Helen Pickersgill is a locum editor in *Science's* editorial department.

1200 New York Avenue, NW
Washington, DC 20005

Editorial: 202-326-6550, FAX 202-379-7562

News: 202-326-6581, FAX 202-371-9227

Bateman House, 82-88 Hills Road
Cambridge, UK CB2 1LQ

+44 (0) 1223 326500, FAX +44 (0) 1223 326501

SUBSCRIPTION SERVICES For change of address, missing issues, new orders and renewals, and payment questions: 866-434-AAAS (2227) or 202-326-6417, FAX 202-842-1065. Mailing addresses: AAAS, P.O. Box 96178, Washington, DC 20090-6178 or AAAS Member Services, 1200 New York Avenue, NW, Washington, DC 20005

INSTITUTIONAL SITE LICENSES please call 202-326-6755 for any questions or information

REPRINTS: Author Inquiries 800-635-7181

Commercial Inquiries 803-359-4578

PERMISSIONS 202-326-7074, FAX 202-682-0816

MEMBER BENEFITS AAAS/Barnes&Noble.com bookstore www.aaas.org/bn; AAAS Online Store www.apisource.com/aaas/ code MKB6; AAAS Travels: Betchart Expeditions 800-252-4910; Apple Store www.apple.com/store/aaas; Bank of America MasterCard 1-800-833-6262 priority code FAA3YU; Cold Spring Harbor Laboratory Press Publications www.cshlpress.com/affiliates/aaas.htm; GEICO Auto Insurance www.geico.com/landingpage/go51.htm?logo=17624; Hertz 800-654-2200 CDP#343457; Office Depot https://bsd.officedepot.com/portalLogin.do; Seabury & Smith Life Insurance 800-424-9883; Subaru VIP Program 202-326-6417; VIP Moving Services www.vipmayflower.com/domestic/index.html; Other Benefits: AAAS Member Services 202-326-6417 or www.aaasmember.org.

science_editors@aaas.org (for general editorial queries)

science_letters@aaas.org (for queries about letters)

science_reviews@aaas.org (for returning manuscript reviews)

science_bookrevs@aaas.org (for book review queries)

Published by the American Association for the Advancement of Science (AAAS), *Science* serves its readers as a forum for the presentation and discussion of important issues related to the advancement of science, including the presentation of minority or conflicting points of view, rather than by publishing only material on which a consensus has been reached. Accordingly, all articles published in *Science*—including editorials, news and comment, and book reviews—are signed and reflect the individual views of the authors and not official points of view adopted by AAAS or the institutions with which the authors are affiliated.

AAAS was founded in 1848 and incorporated in 1874. Its mission is to advance science, engineering, and innovation throughout the world for the benefit of all people. The goals of the association are to: enhance communication among scientists, engineers, and the public; promote and defend the integrity of science and its use; strengthen support for the science and technology enterprise; provide a voice for science on societal issues; promote the responsible use of science in public policy; strengthen and diversify the science and technology workforce; foster education in science and technology for everyone; increase public engagement with science and technology; and advance international cooperation in science.

INFORMATION FOR AUTHORS

See pages 634 and 635 of the 1 February 2008 issue or access www.sciencemag.org/about/authors

EDITOR-IN-CHIEF **Bruce Alberts**

EXECUTIVE EDITOR **Monica M. Bradford**

DEPUTY EDITORS

NEWS EDITOR

R. Brooks Hanson, Barbara R. Jasny, Colin Norman

Katrina L. Kelnor

EDITORIAL SUPERVISORY SENIOR EDITOR Phillip D. Szuroni; **SENIOR EDITOR/PERSPECTIVES** Lisa D. Chong; **SENIOR EDITORS** Gilbert J. Chin, Pamela J. Hines, Paula A. Kiberstis (Boston), Marc S. Lavine (Toronto), Beverly A. Purnell, L. Bryan Ray, Guy Riddihough, H. Jesse Smith, Valda Vinson; **ASSOCIATE EDITORS** Kristen L. Mueller, Jake S. Yeston, Laura M. Zahn; **ONLINE EDITOR** Stewart Wills; **ASSOCIATE ONLINE EDITORS** Robert Frederick, Tara S. Marathe; **WEB CONTENT DEVELOPER** Martin Green; **BOOK REVIEW EDITOR** Sherman J. Suter; **ASSOCIATE LETTERS EDITOR** Jennifer Sills; **EDITORIAL MANAGER** Cara Tate; **SENIOR COPY EDITORS** Jeffrey E. Cook, Cynthia Howe, Harry Jach, Barbara P. Ordway, Trista Wagoner; **COPY EDITORS** Chris Filiateau, Lauren Kmeck; **EDITORIAL COORDINATORS** Carolyn Kyle, Beverly Shields; **PUBLICATIONS ASSISTANTS** Ramatoulaye Diop, Joi S. Granger, Jeffrey Hearn, Lisa Johnson, Scott Miller, Jerry Richardson, Jennifer A. Seibert, Brian White, Anita Wynn; **EDITORIAL ASSISTANTS** Carlos L. Durham, Emily Guise, Patricia M. Moore; **EXECUTIVE ASSISTANT** Sylvia S. Kihara; **ADMINISTRATIVE SUPPORT** Maryrose Madrid

NEWS DEPUTY NEWS EDITORS Robert Coontz, Eliot Marshall, Jeffrey Mervis, Leslie Roberts; **CONTRIBUTING EDITORS** Elizabeth Culotta, Polly Shulman; **NEWS WRITERS** Yudhijit Bhattacharjee, Adrian Cho, Jennifer Couzin, David Grimm, Constance Holden, Jocelyn Kaiser, Richard A. Kerr, Eli Kintisch, Andrew Lawler (New England), Greg Miller, Elizabeth Pennisi, Robert F. Service (Pacific NW), Erik Stokstad; **INTERN** Jackie D. Grom; **CONTRIBUTING CORRESPONDENTS** Jon Cohen (San Diego, CA), Daniel Ferber, Ann Gibbons, Robert Koenig, Mitch Leslie, Charles C. Mann, Virginia Morell, Evelyn Strauss, Gary Taubes; **COPY EDITORS** Linda B. Felaco, Melvin Gatling, Melissa Raimond; **ADMINISTRATIVE SUPPORT** Scherraine Mack, Fannie Groom; **BUREAU NEW ENGLAND:** 207-549-7755, San Diego, CA: 760-942-3252, FAX 760-942-4979, Pacific Northwest: 503-963-1940

PRODUCTION DIRECTOR James Landry; **SENIOR MANAGER** Wendy K. Shank; **ASSISTANT MANAGER** Rebecca Doshi; **SENIOR SPECIALISTS** Steve Forrester, Chris Redwood; **SPECIALIST** Anthony Rosen; **PREFLIGHT DIRECTOR** David M. Tompkins; **MANAGER** Marcus Spiegler

ART DIRECTOR Yael Kats; **ASSOCIATE ART DIRECTOR** Laura Creveling;

ILLUSTRATORS Chris Bickel, Katharine Suttill; **SENIOR ART ASSOCIATES** Holly Bishop, Preston Huey, Nayomi Kevitigagala; **ART ASSOCIATE** Jessica Newfield; **PHOTO EDITOR** Leslie Blizard

SCIENCE INTERNATIONAL

EUROPE (science@science-int.co.uk) **EDITORIAL: INTERNATIONAL MANAGING EDITOR** Andrew M. Sugden; **SENIOR EDITOR/PERSPECTIVES** Julia Fahrenkamp-Uppenbrink; **SENIOR EDITORS** Caroline Ash, Stella M. Hurtle, Ian S. Osborne, Peter Stern; **ASSOCIATE EDITOR** Maria Cruz; **EDITORIAL SUPPORT** Deborah Dennison, Rachel Roberts, Alice Whaley; **ADMINISTRATIVE SUPPORT** John Cannell, Janet Clements; **NEWS: EUROPE NEWS EDITOR** John Travis; **DEPUTY NEWS EDITOR** Daniel Cleary; **CONTRIBUTING CORRESPONDENTS** Michael Balter (Paris), John Bohannon (Vienna), Martin Enserink (Amsterdam and Paris), Gretchen Vogel (Berlin); **INTERN** Sara Coelho

ASIA Japan Office: Asca Corporation, Eiko Ishioka, Fusako Tamura, 1-8-13, Hirano-cho, Chuo-ku, Osaka-shi, Osaka, 541-0046 Japan; +81 (0) 6 6202 6272, FAX +81 (0) 6 6202 6271; asca@os.gulf.or.jp; **ASIA NEWS EDITOR** Richard Stone (Beijing: rstone@aaas.org); **CONTRIBUTING CORRESPONDENTS** Dennis Normile (Japan: +81 (0) 3 3391 0630, FAX +81 (0) 3 5936 3531; dnormile@gol.com); Hao Xin (China: +86 (0) 10 6307 4439 or 6307 3676, FAX +86 (0) 10 6307 4358; cindyhao@gmail.com); Pallava Bagla (South Asia: +91 (0) 11 2271 2896; pbagla@vsnl.com)

EXECUTIVE PUBLISHER **Alan I. Leshner**

PUBLISHER **Beth Rosner**

FULFILLMENT SYSTEMS AND OPERATIONS (membership@aaas.org); **DIRECTOR** Waylon Butler; **SENIOR SYSTEMS ANALYST** Jonny Blaker; **CUSTOMER SERVICE SUPERVISOR** Pat Butler; **SPECIALISTS** Latoya Casteel, LaVonda Crawford, Vicki Linton, April Marshall; **DATA ENTRY SUPERVISOR** Cynthia Johnson; **SPECIALISTS** Eintou Bowden, Tarrika Hill, William Jones

BUSINESS OPERATIONS AND ADMINISTRATION DIRECTOR Deborah Rivera-Wienhold; **ASSISTANT DIRECTOR, BUSINESS OPERATIONS** Randy Yi; **MANAGER, BUSINESS ANALYSIS** Michael LoBue; **MANAGER, BUSINESS OPERATIONS** Jessica Tierney; **FINANCIAL ANALYSTS** Priti Pannani, Celeste Troxler; **RIGHTS AND PERMISSIONS: ADMINISTRATOR** Emilie David; **ASSOCIATE** Elizabeth Sandler; **MARKETING DIRECTOR** Ian King; **MARKETING MANAGER** Allison Pritchard; **MARKETING ASSOCIATES** Aimee Aponte, Alison Chandler, Mary Ellen Crowley, Julianne Wielga, Wendy Wise; **INTERNATIONAL MARKETING MANAGER** Wendy Sturley; **MARKETING EXECUTIVE** Jennifer Reeves; **MARKETING/MEMBER SERVICES EXECUTIVE** Linda Rusk; **DIRECTOR, SITE LICENSING** Tom Ryan; **DIRECTOR, CORPORATE RELATIONS** Eileen Bernadette Moran; **PUBLISHER RELATIONS, eResources SPECIALIST** Kiki Forsythe; **SENIOR PUBLISHER RELATIONS SPECIALIST** Catherine Holland; **PUBLISHER RELATIONS, EAST COAST** Phillip Smith; **PUBLISHER RELATIONS, WEST COAST** Philip Tsolakis; **FULFILLMENT SUPERVISOR** Iquo Edim; **FULFILLMENT COORDINATOR** Laura Clemens; **ELECTRONIC MEDIA: MANAGER** Elizabeth Harman; **PROJECT MANAGER** Trista Snyder; **ASSISTANT MANAGER** Lisa Stanford; **SENIOR PRODUCTION SPECIALISTS** Christopher Coleman, Walter Jones; **PRODUCTION SPECIALISTS** Nichole Johnston, Kimberly Oster

ADVERTISING DIRECTOR, WORLDWIDE AD SALES Bill Moran

PRODUCT (science_advertising@aaas.org); **MIDWEST/WEST COAST/W. CANADA** Rick Bongiovanni: 330-405-7080, FAX 330-405-7081; **EAST COAST/E. CANADA** Laurie Faraday: 508-747-9395, FAX 617-507-8189; **UK/EUROPE/ASIA** Roger Goncalves: TEL/FAX +41 43 243 1358; **JAPAN** Masahiko Yoshikawa: +81 (0) 3 3235 5961, FAX +81 (0) 3 3235 5852; **SENIOR TRAFFIC ASSOCIATE** Delandra Simms

COMMERCIAL EDITOR Sean Sanders: 202-326-6430

PROJECT DIRECTOR, OUTREACH Brianna Blaser

CLASSIFIED (advertise@sciencecareers.org); **INSIDE SALES MANAGER: MIDWEST/CANADA** Daryl Anderson: 202-326-6543; **INSIDE SALES REPRESENTATIVE** Karen Foote: 202-326-6740; **KEY ACCOUNT MANAGER** Jorihab Able; **NORTHEAST** Alexis Fleming: 202-326-6578; **SOUTHEAST** Tina Burks: 202-326-6577; **WEST** Nicholas Hintibidze: 202-326-6533; **SALES COORDINATORS** Rohan Edmonson, Shirley Young; **INTERNATIONAL SALES MANAGER** Tracy Holmes: +44 (0) 1223 326525, FAX +44 (0) 1223 326532; **Sales** Susanne Kharraz, Dan Pennington, Alex Palmer; **SALES ASSISTANT** Louise Moore; **JAPAN** Masahiko Yoshikawa: +81 (0) 3 3235 5961, FAX +81 (0) 3 3235 5852; **ADVERTISING PRODUCTION OPERATIONS MANAGER** Deborah Tompkins; **SENIOR PRODUCTION SPECIALIST/GRAPHIC DESIGNER** Amy Hardcastle; **SENIOR PRODUCTION SPECIALIST** Robert Buck; **SENIOR TRAFFIC ASSOCIATE** Christine Hall; **PUBLICATIONS ASSISTANT** Mary Lagnaoui

AAAS BOARD OF DIRECTORS **RETIRED PRESIDENT, CHAIR** David Baltimore; **PRESIDENT** James J. McCarthy; **PRESIDENT-ELECT** Peter C. Agre; **TREASURER** David E. Shaw; **CHIEF EXECUTIVE OFFICER** Alan I. Leshner; **BOARD** Lynn W. Enquist, Susan M. Fitzpatrick, Alice Gast, Linda P. B. Katehi, Nancy Knowlton, Cherry A. Murray, Thomas D. Pollard, Thomas A. Woolsey



ADVANCING SCIENCE, SERVING SOCIETY

SENIOR EDITORIAL BOARD

John I. Brauman, Chair, Stanford Univ.
Richard Losick, Harvard Univ.
Robert May, Univ. of Oxford
Marcia McNitt, Monterey Bay Aquarium Research Inst.
Linda Partridge, Univ. College London
Vera C. Rubin, Carnegie Institution
Christopher R. Somerville, Univ. of California, Berkeley

BOARD OF REVIEWING EDITORS

Joanna Aizenberg, Harvard Univ.
David Altshuler, Broad Institute
Arturo Alvarez-Buylla, Univ. of California, San Francisco
Richard Amasino, Univ. of Wisconsin, Madison
Angelika Amon, MIT
Meinrat O. Andreae, Max Planck Inst., Mainz
Kristi S. Anseth, Univ. of Colorado
John A. Bargh, Yale Univ.
Cornelia I. Bargmann, Rockefeller Univ.
Ben Barnes, Stanford Medical School
Marisa Bartolomei, Univ. of Penn. School of Med.
Facundo Batista, London Research Inst.
Ray H. Baughman, Univ. of Texas, Dallas
Stephen J. Benkovic, Penn State Univ.
Ton Bisseling, Wageningen Univ.
Mina Bissell, Lawrence Berkeley National Lab
Peer Bork, EMBL
Robert W. Boyd, Univ. of Rochester
Paul M. Brakenfeld, Leiden Univ.
Dennis Bray, Univ. of Cambridge
Stephen Burdowski, Harvard Medical School
Joseph A. Burns, Cornell Univ.
William P. Butz, Population Reference Bureau
Mats Carlsson, Univ. of Oslo
Peter Carmeliet, Univ. of Leuven, VIB
Mildred Cho, Stanford Univ.
David Clapham, Children's Hospital, Boston
David Clary, Oxford University
J. M. Claverie, CNRS, Marseille
Jonathan D. Cohen, Princeton Univ.

Andrew Cossins, Univ. of Liverpool
Robert H. Crabtree, Yale Univ.
Wolfgang Cramer, Potsdam Inst. for Climate Impact Research
F. Fleming Crim, Univ. of Wisconsin
William Cumberland, Univ. of California, Los Angeles
Jeff L. Dangl, Univ. of North Carolina
Stanislas Dehaene, Collège de France
Edward DeLong, MIT
Emmanouil T. Dermatzakis, Wellcome Trust Sanger Inst.
Robert Desimone, MIT
Dennis Discher, Univ. of Pennsylvania
Scott Doney, Woods Hole Oceanographic Inst.
W. Ford Doolittle, Dalhousie Univ.
Jennifer A. Doudna, Univ. of California, Berkeley
Julian Downward, Cancer Research UK
Denis Duboule, Univ. of Geneva/EPFL Lausanne
Christopher Dye, WHO
Gerhard Ertl, Fritz-Haber-Institut, Berlin
Mark Estelle, Indiana Univ.
Barry Everitt, Univ. of Cambridge
Paul G. Falkowski, Rutgers Univ.
Ernst Fehr, Univ. of Zurich
Toni Fenchel, Univ. of Copenhagen
Alain Fischer, INSERM
Scott E. Fraser, Cal Tech
Chris D. Frith, Univ. College London
Wulfraam Gerstner, EPFL Lausanne
Charles Godfrey, Univ. of Oxford
Diane Griffin, Johns Hopkins Bloomberg School of Public Health
Christian Haass, Ludwig Maximilians Univ.
Niels Hansen, Technical Univ. of Denmark
Dennis L. Hartmann, Univ. of Washington
Chris Hawkesworth, Univ. of Bristol
Martin Heimann, Max Planck Inst., Jena
James A. Hendler, Rensselaer Polytechnic Inst.
Roy Hilborn, Univ. of Washington
Ove Hoegh-Guldberg, Univ. of Queensland
Bridget L. M. Hogan, Duke Univ. Medical Center
Ronald R. Hoy, Cornell Univ.
Orli Ikkala, Helsinki Univ. of Technology
Meyer B. Jackson, Univ. of Wisconsin Med. School
Stephen Jackson, Univ. of Cambridge
Steven Jacobsen, Univ. of California, Los Angeles

Peter Jonas, Universität Freiburg
Barbara B. Kahn, Harvard Medical School
Daniel Kahne, Harvard Univ.
Gerard Karsenty, Columbia Univ. College of P&S
Bernhard Keimer, Max Planck Inst., Stuttgart
Elizabeth A. Kellog, Univ. of Missouri, St. Louis
Alan B. Krueger, Princeton Univ.
Lee Kump, Penn State Univ.
Mitchell A. Lazar, Univ. of Pennsylvania
Virginia Lee, Univ. of Pennsylvania
Olle Lindvall, Univ. Hospital, Lund
Marcia C. Lin, Univ. of California, Berkeley
John Lis, Cornell Univ.
Richard Losick, Harvard Univ.
Ke Lu, Chinese Acad. of Sciences
Andrew P. MacKenzie, Univ. of St Andrews
Raul Madariaga, Ecole Normale Supérieure, Paris
Anne Magurran, Univ. of St Andrews
Charles Marshall, Harvard Univ.
Virginia Miller, Washington Univ.
Yasushi Miyashita, Univ. of Tokyo
Richard Morris, Univ. of Edinburgh
Edward Moser, Norwegian Univ. of Science and Technology
Naoto Nagaosa, Univ. of Tokyo
James Nelson, Stanford Univ. School of Med.
Timothy W. Nilsen, Case Western Reserve Univ.
Roeland Nolte, Univ. of Nijmegen
Helga Nowotny, European Research Advisory Board
Eric N. Olson, Univ. of Texas, SW
Stuart H. Orkin, Dana-Farber Cancer Inst.
Erin O'Shea, Harvard Univ.
Elinor Ostrom, Indiana Univ.
Jonathan T. Overpeck, Univ. of Arizona
John Penney, Imperial College
Simon Philpot, Univ. of Florida
Philippe Poulin, CNRS
Molly Power, Univ. of California, Berkeley
Molly Przeworski, Univ. of Chicago
Colin Renfrew, Univ. of Cambridge
Trevor Robbins, Univ. of Cambridge
Barbara A. Romanowicz, Univ. of California, Berkeley
William M. Rubin, Lawrence Berkeley National Lab
Shimon Sakaguchi, Kyoto Univ.
Jürgen Sandkühner, Medical Univ. of Vienna

David W. Schindler, Univ. of Alberta
Georg Schulz, Albert-Ludwigs-Universität
Paul Schulze-Lefert, Max Planck Inst., Cologne
Christine Seidman, Harvard Medical School
Terrence J. Sejnowski, The Salk Institute
David Sibley, Washington Univ.
Joseph Silk, Univ. of Oxford
Montgomery Slatkin, Univ. of California, Berkeley
Davor Solter, Inst. of Medical Biology, Singapore
Joan Steitz, Yale Univ.
Elisbeth Stern, ETH Zürich
Jerome Strauss, Virginia Commonwealth Univ.
Jörg Tschopp, Univ. of Lausanne
Derek van der Kooy, Univ. of Toronto
Bert Vogelstein, Johns Hopkins Univ.
Ulrich H. von Andrian, Harvard Medical School
Bruce D. Walker, Harvard Medical School
Christopher A. Walsh, Harvard Medical School
Graham Warren, Yale Univ. School of Med.
Colin Watts, Univ. of Dundee
Detlef Weigel, Max Planck Inst., Tübingen
Jonathan Weissman, Univ. of California, San Francisco
Ellen D. Williams, Univ. of Maryland
Ian A. Wilson, The Scripps Res. Inst.
Jerry Workman, Stowers Inst. for Medical Research
Xiaoliang Sunney Xie, Harvard Univ.
John R. Yates III, The Scripps Res. Inst.
Jan Zaenen, Leiden Univ.
Huda Zoghbi, Baylor College of Medicine
Maria Zuber, MIT

BOOK REVIEW BOARD

John Aldrich, Duke Univ.
David Bloom, Harvard Univ.
Angela Creager, Princeton Univ.
Richard Sweder, Univ. of Chicago
Ed Wasserman, DuPont
Lewis Wolpert, Univ. College London

Small RNA
Quantification

HRM

Biomarker
Validation

Gene
Expression

miRNA
Profiling

Pathway
Analysis

SNP
Genotyping



A Portfolio of Real-Time Possibilities. Just for Me.

Only Applied Biosystems delivers superior end-to-end workflow solutions for all your real-time PCR applications.

Finding a line of real-time PCR solutions to advance your experiments from start to finish is all about knowing where to look. Applied Biosystems offers a range of quality real-time PCR instruments, reagents, assays, service, and support to help accelerate your research at every step—saving you time and money along the way. When you want a real-time portfolio that can take you from sample prep to proven results, talk to us. We have a growing range of affordable real-time PCR solutions optimized just for you!



As Flexible as You Want to Be.

AB Applied
Biosystems

Real-time PCR solutions optimized just for you at
www.appliedbiosystems.com/realsystems

©2009 Applied Biosystems Inc. All rights reserved. Applied Biosystems and AB (Design) are registered trademarks of Applied Biosystems Inc. or its subsidiaries in the US and/or certain other countries.

Call for Papers

*Science
Signaling*

Now accepting
original research
submissions



ISSN: 1937-9145

Announcing Chief Scientific
Editor for *Science Signaling* –

Michael B. Yaffe, M.D., Ph.D.

Associate Professor, Department of Biology
Massachusetts Institute of Technology

Submit your paper to:
sciencesignaling.org/about/help/research.dtl

From the publishers of *Science*, *Science Signaling*, formerly known as *Science's* STKE, now features top-notch, peer reviewed, original research. Each week the journal will publish leading-edge findings in addition to the current features, including Perspectives, Reviews, Protocols, Meeting Reports, Book Reviews, Teaching Resources, and the Database of Cell Signaling.

Science Signaling showcases high-impact research in cellular regulation in such fields as molecular biology, development, immunology, neuroscience, microbiology, physiology and medicine, pharmacology, biochemistry, cell biology, bioinformatics, and systems biology. Submit your research that provides new concepts and new understanding of biological signal transduction for consideration.

Subscribing to *Science Signaling* ensures that you and your lab have the latest cell signaling resources. From basic science to design of therapeutics, from molecules to networks and systems design, read the best source – *Science Signaling*.

Science Signaling



Adopt-a-Painting



Native Vanilla hanging from the Wile Orange in the Seychelles.

Time has taken its toll on the 832 paintings in the Marianne North Gallery, a show of botanical art and landscapes at the Royal Botanic Gardens, Kew, outside London that has been on continuous display since 1882. A restoration project is under way with the help of a £1.87 million grant from the Heritage Lottery Fund, but another £1 million is needed. So the gallery is inviting members of the public to “adopt” a painting for £500, £750, or £1000. So far, 187 of the works have been taken. The collection, including many vanished landscapes, has a unique value as a “testament of what we’ve done to the world,” says Kew conservator Jonathan Farley.

Flood Theory Revised

Was the story of Noah’s Ark inspired by a real event? In 1997, two marine geologists proposed that about 7500 years ago a torrent of water from the Mediterranean swelled the Black Sea, scattering early farmers into Europe and giving rise to the biblical flood myth. But the tide has been turning against the idea (*Science*, 17 August 2007, p. 886). Now a study taking a new approach to the question has concluded that the flood was little more than a trickle.

A team led by Liviu Giosan, a marine geologist at the Woods Hole Oceanographic Institution in Massachusetts, bored a 42-meter core into sediments in the delta of the Danube River in Romania, where it empties into the Black Sea. The delta’s geography has remained stable over the millennia, so the team considers it a better indicator of ancient sea levels than the Black Sea sediments used in earlier analyses. The team members also radiocarbon-dated mollusks from the sediments. In the January issue of *Quaternary Science Reviews*, they report that when rising Mediterranean waters started flowing into it, the Black Sea was at least 50 meters higher than the original estimate—greatly reducing the potential for flooding.

“It’s a fascinating piece of work,” says Chris Turney, a geologist at the University of Exeter in the U.K. Giosan and William Ryan of the

Lamont-Doherty Earth Observatory in Palisades, New York, a co-author of the 1997 study, plan to resolve the debate once and for all by applying state-of-the-art dating techniques to both Danube and Black Sea sediments.

Fishy Four Eyes

For the first time, scientists have discovered a vertebrate that uses mirrors to see.

The brownsnout spookfish, a 10-centimeter denizen of tropical deep-sea waters, has taken an unbeaten path during its eye evolution, researchers report this month in *Current Biology*. To keep watch on things both above and below, the fish has developed eyes with two parts. One captures the dim remnants of sunlight from the surface, using a conventional lens to focus light. The other faces downward, picking up the even dimmer flashes of bioluminescence from both predators and prey, such as small copepods. For this, instead of a lens it uses mirrors—tiny reflective crystals that harness wayward flashes and beam a high-contrast image onto the retina. The mirrors snare more light than the lens, which absorbs some photons as it refracts.

“It’s a neat trick,” says Sönke Johnsen, a visual ecologist at Duke University in Durham, North Carolina.

“Nobody’s ever seen anything like this in vertebrates.” Study author Ronald Douglas, a vision scientist at City University London, agrees: “It seems such a good idea that I’m surprised that other animals haven’t evolved it.”



Spookfish.

CREATURES OF THE NIGHT

Once nearly eradicated, bedbugs are making a rapid comeback in cities in the United States and Europe. The nasty bloodsuckers have been kept in check for decades largely thanks to insecticides called pyrethroids. Now, they’re growing increasingly resistant to the compounds.

To find out why, researchers led by John Clark, a toxicologist at the University of Massachusetts, Amherst, ran genetic comparisons between pyrethroid-resistant and nonresistant bedbugs. In the current issue of the *Journal of Medical Entomology*, Clark’s team reports that the resistant bugs carried two mutations in the gene that encodes the sodium channels in their nerve cells. Pyrethroids force those channels to stay open, paralyzing and killing the bugs. The mutations prevent the insecticides from binding. Scientists have found 26 other related mutations in cockroaches and other resistant insects, Clark says.



“It’s bad news” for pyrethroids, says Coby Schal, an entomologist at North Carolina State University in Raleigh, who thinks sodium-channel resistance is likely to spread rapidly to other bedbug colonies. With few insecticides safe for home use, Schal says, researchers are racing to find new compounds.

Science Careers is the lens that magnifies opportunities.

Visit our
ENHANCED
WEBSITE!



Magnifying your opportunities is our main focus. We're your source for connecting with the industry's top employers. We're the experts and primary tool for accessing the latest and most relevant career information across the globe.

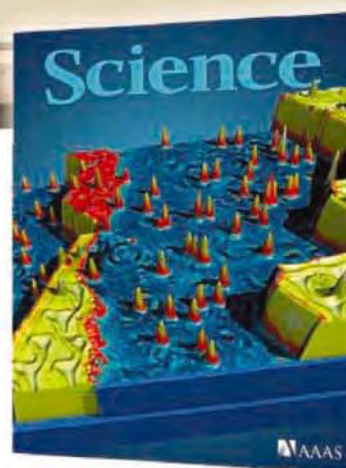
Our newly designed website offers improved features that help you magnify career opportunities and your personal potential. Whether you're seeking a new job, career advancement in your chosen field, or ways to stay current on industry trends, *Science Careers* will broaden your scope for a brighter future.

Improved Website Features:

- » Relevant Job E-mail Alerts
- » Improved Resume Uploading
- » Content Specific Multimedia Section
- » Facebook Profile

Job Search Functionality:

- » Save and Sort Jobs
- » Track Your Activity
- » Search by Geography
- » Enhanced Job Sorting



Your Future Awaits.

Science Careers
From the journal *Science* 

ScienceCareers.org



Three Q's >>

The new president of the French Academy of Sciences, **Jean Salençon**, is an international expert in soil mechanics and earthquake-resistance construction at the École Polytechnique in Palaiseau. Vice president of the academy since 2007, he succeeds biologist Jules Hoffmann.

Q: What are your priorities as president?

The academy has a key role in fostering interest in science, which is declining in France. People don't listen to scientists anymore. The debate about genetically modified organisms, for instance, is often based more on passion than on scientific arguments. Some of the debates you see on TV are amazing.

Q: How do you plan to change that?

We want to help improve science teaching at all levels, and we want to have a clearer presence in the media.

Q: A controversial new law makes universities autonomous. What's your position?

I think it was unavoidable. But now we need better tools to evaluate how universities are doing, and that's where I want the academy to help. The French complain a lot about the "Shanghai ranking" [a global assessment of universities], which only looks at scientific output, not at teaching and professional training. We may not come up with an alternative ranking, but we'll define the criteria that an evaluation should be based on.

DEATHS

WAR ZONE. A 36-year-old anthropologist has become the third social scientist to be killed while working with the U.S. Army's Human Terrain System in Iraq and Afghanistan. Paula Loyd (right) died on 7 January 2009 from burns received in a November 2008 attack in Afghanistan.

Loyd went to Afghanistan in September last year and was embedded with a unit of the 1st Infantry Division. On 5 November, according to news reports, she approached a man carrying a fuel jug in the village of Maiwand in the southern part of the country, where she was conducting interviews. The man ignited the fuel and threw it on Loyd, causing second- and third-degree burns. She was transferred to Brooke Army Medical Center in San Antonio, Texas, where she later died.



This wasn't Loyd's first tour of Afghanistan: She previously worked there for the United Nations Assistance Mission, to improve working arrangements between humanitarian groups and military forces, and for the U.S. Agency for International Development.

Michael Bhatia, a political scientist in the program, was killed by a roadside bomb in Afghanistan in May 2008. About 2 months later, Nicole Suveges, an economist working

for BAE Systems, died when a bomb destroyed a community building in Sadr City, Baghdad.

AWARDS

DECORATED. A Spanish foundation has created \$530,000 prizes to honor the lifetime achievement of researchers in eight major fields of study.

The first winner of the Frontier of Knowledge awards by the Madrid-based BBVA Foundation is Columbia University geochemist Wallace Broecker for his work on the mechanism of abrupt climate change. The 77-year-old Broecker, who has funded the work of other climate scientists with money from previous awards such as the Crafoord Prize, says this latest honor will augment the pot. Given his age and frugal lifestyle, he says, he's unlikely to spend the bounty on himself.

Stay tuned for announcements covering achievements in development, biomedicine, the arts, basic science, information and communication technologies, ecology and conservation biology, and economics, finance, and management.

Charles Dinarello of the University of Colorado School of Medicine in Denver, along with **Tadamitsu Kishimoto** and **Toshio Hirano** of Osaka University in Japan, will share the Royal Swedish Academy of Sciences' \$500,000 Crafoord Prize, being awarded this year in the field of polyarthritis. They are being recognized for exploring the role of signaling proteins known as interleukins in polyarthritis and other autoimmune diseases. The work has led to the development of drugs to treat these conditions.

A Life in Science

INNOVATOR. J. Lamar Worzel enjoyed dropping bombs. In the 1930s, the geophysicist packed explosives into inner tubes, sent them to the floor of the Atlantic Ocean, and deciphered the blasts' reverberations to chart sea-floor sediments. Those findings helped U.S. submarines evade detection during World War II. Among the devices that Worzel and his colleagues invented were deep-sea cameras that discovered marine life in the abyssal ocean. He also figured out how to precisely measure gravity from a rocking ship—to chart Earth's crust—and to drill cores 3.6 kilometers deep. "We never allowed ourselves to think that anything we decided to do was impossible," he wrote in 2001.

In 1949, Worzel cofounded Columbia University's Lamont-Doherty Earth Observatory, where he worked until leaving for the University of Texas, Austin, in 1972. He died of a heart attack on 26 December 2008 at the age of 89. "He was one of the greats in 20th century geophysics," says Robert Froesch, a retired theoretical physicist who studied ocean acoustics at Woods Hole Oceanographic Institution and elsewhere.



Disoriented
pelicans

449

Ebola shows up
in pigs

451

EUROPE

Acquittals in CJD Trial Divide French Scientists

PARIS—Few criminal investigations drag on so long that one of the accused dies, and fewer draw upon the opinions of someone soon to win a Nobel Prize. But a court case here in which both have happened finally reached a verdict last week. Three French judges acquitted six doctors and pharmacists of charges of involuntary homicide and aggravated fraud after a stunningly prolonged investigation centering on the distribution of human growth hormone contaminated with

dren and 18 years after the criminal investigation began. So far, 116 of the youngsters have died from Creutzfeldt-Jakob disease (CJD), a human illness similar to mad cow disease, and three more have recently shown symptoms.

The French scientific community remains split on the case. “No one committed a real fault or negligence,” says one witness, neurologist Yves Agid, who was formerly in charge of monitoring CJD cases in France and is scientific director at the Institute of Brain and Spinal

Cord Disorders here. “At the time, no one could imagine that patients would contract CJD from human growth hormone.”

But virologist Luc Montagnier, also a witness in the trial and a winner of this year’s Nobel Prize in physiology or medicine, says the ruling arouses concern. “I fear we may have not learned any lessons from this case and will face other and bigger public health

scandals in the absence of adequate scientific and medical caution over the effects of new treatments on young people and future generations,” he says.

In 1980, Montagnier recommended a series of precautions to be taken in the gathering and processing of pituitary glands but says he was ignored. He argues that the authorities should have halted the use of cadaver-derived HGH when the first case of CJD was linked to the product in the United States. “This disaster could have been partly avoided,” Montagnier told *Science*. Montagnier adds that he was “surprised and saddened” by the court’s failure to attribute responsibility, and he was also critical of the fact that since the scandal broke, there has been little research into technology that could detect early signs of CJD.

The criminal case dragged on as the number of deaths grew over the years. They added to the prosecution’s case, but each required an investigation, says Jean-François Funcke, one of the victims’ lawyers. The defendants tried to persuade higher courts to throw the case out, the statistics matching infected batches of HGH to the patients were complicated, and charges of corruption involved inquiries abroad, he adds.

The public prosecutor had demanded 4-year suspended sentences for the two main defendants, pediatrician-endocrinologist Jean-Claude Job, who headed the now-defunct association in charge of collecting the hormone-containing pituitary glands from cadavers and who died after the trial ended, and Fernand Dray, who was in charge of purifying the material at the Pasteur Institute. Dray was also accused of corruption over the foreign HGH purchases, but the charges were dropped because the statute of limitations had expired.

The criminal court case had proceeded despite a dismissive 2005 report from the French National Institute for Health and Medical Research that concluded: “It is not reasonable to expect the players involved in the production of growth hormone to have guessed there was a possible risk of CJD from a treatment used since the 1960s” without a single incidence of disease. That report was prepared by an international group including Stanley Prusiner, who won the Nobel Prize for his discovery of prions, and prion expert Paul Brown, formerly of the U.S. National Institute of Neurological Disorders and Stroke in Bethesda, Maryland.

Two years earlier, however, a French civil appeal court had upheld an earlier ruling that the Pasteur Institute was responsible for the 2001 death of 30-year-old Pascale Fachin from CJD contracted from contaminated HGH. The institute was fined €322,000. The criminal court last week did award civil damages to families who hadn’t already accepted a compensation offer from the state. And the public prosecutor said he would appeal the acquittals of Dray, Marc Mollet, former chief of the Central Hospital Pharmacy in Paris, who faced a 2-year suspended sentence, and Elisabeth Mugnier, a pediatrician who faced a 1-year suspended sentence. The appeal hearing should be held in 2010. —BARBARA CASASSUS

Barbara Casassus is a writer in Paris.



Final verdict? Fernand Dray leaves the courtroom after his acquittal, but appeals loom.

deadly prions in the 1980s. The nearly 2-decade-old saga may not be over, however, as prosecutors immediately appealed.

Around the world, human growth hormone (HGH) used to be isolated from the pituitary glands of cadavers before the recombinant product came on the market. And much of the French trial centered on whether the accused used appropriate purification standards, an issue that resulted in several prominent scientists being called to the witness stand. The Pasteur Institute, which was involved in purifying the hormone, had already been fined by a civil court, but whether someone had committed a crime remained an open matter.

The defendants’ 14 January acquittals come more than 25 years after high-risk batches of HGH were administered to 968 French chil-



ECOLOGY

Western U.S. Forests Suffer Death by Degrees

An insidious problem has taken hold in the forests of the American West, quietly thinning their ranks. Mortality rates in seemingly healthy conifer stands have doubled in the past several decades. Often, new trees aren't replacing dying ones, setting the stage for a potentially dramatic change in forest structure, says Phillip J. van Mantgem, a forest ecologist at the U.S. Geological Survey (USGS) in Arcata, California. Warmer temperatures and subsequent water shortfalls are the likely cause of the trees' increased death rate, he and his colleagues report on page 521.

"This is a stunningly important paper," says David Breshears, an ecologist at the University of Arizona, Tucson. For years, he and others have lamented massive diebacks that occur when fungal and insect pests ravage stands of trees. "What's harder to detect," he explains, is any subtle but significant shift in the trees' background death rate. "They have done a very thorough job" of documenting it.

In 2005, mortality rates weren't even on van Mantgem's radar. But while he was evaluating long-term data about forests in California's Sierra Nevada mountains for changes in species composition and other forest characteristics, he noticed an upward trend in tree deaths. At first he thought it was an artifact. Once he and his colleagues became convinced that the trend was real, they looked to see how widespread it might be.

Forest ecologist Nathan Stephenson of USGS in Three Rivers, California, combed the literature and canvassed his colleagues for long-term sites in the western United States where forest experts had tracked mortality and other parameters at regular intervals. They considered only old-growth



Slow demise. A comprehensive study shows that forests are losing trees faster now than they were 40 years ago.

forests, as these well-established communities would be less likely to undergo changes that could confound the analysis. "They were extremely rigorous in site selection," says Nate McDowell, an ecologist at Los Alamos National Laboratory in New Mexico.

All told, they wound up with 76 sites in the Pacific Northwest, California, Idaho, Colorado, and Arizona. They found that in the Pacific Northwest, mortality rates jumped to 1.3% today from 0.3% in the 1970s; in California, that percentage went to 1.7% from 1% in 1983; mortality in the interior forests climbed to 0.6% from 0.2% in roughly the same period. "It's not just one local spot," says van Mantgem. In contrast, they detected no trends in recruitment, the number of seedlings that survive to become mature trees. New growth is often failing to replace dying trees, he notes. Oliver Phillips, a tropical ecologist at the University of Leeds in the United Kingdom, says mortality rates have similarly increased in the tropics, but forest growth rates have increased there, more than compensating for the loss.

At first glance, a shift of a percent or less may seem insignificant. "The change in forests is subtle so far," says Stephenson. But just as a small percent difference in interest rates can compound the cost of a loan, a small difference in mortality rates can have a big effect over time. As the forest thins, ever smaller trees become dominant, affecting the land's carbon storage capacity and ability to support wildlife.

Next, the researchers evaluated the possible causes of the increased mortality rate. No matter how they sliced and analyzed the tree data—by size, type, elevation, and location—they still detected the increase in mortality. Air pollution couldn't be blamed because the increase occurred in pristine as well as polluted areas.

Ultimately, "the finger seems to be pointed to warming," says Breshears. Temperatures in the United States have risen about 0.4°C per decade in the past 40 years. Snowpack of the regions examined diminished over the time period they studied and is melting earlier, effectively lengthening the summer drought. Warmer air also leads to more evaporative loss, exacerbating the effect.

Michael Goulden, an ecosystem ecologist at the University of California, Irvine, thinks the data fall short of pinning the problem on global warming, as regional warming related to natural climatic variation could be to blame. But Julio Betancourt of USGS in Tucson, Arizona, disagrees. "Models suggest that most of this change was due to the buildup of greenhouse gases," he says. Moreover, local Pacific Northwest and Southwest climates tend to fluctuate in opposite directions.

However, Betancourt, who is not a co-author of the paper, stresses that forest researchers need to focus on seedlings, not mortality, in these threatened ecosystems. "If there is an affordable point of intervention, a way to adaptively manage for climate change," he points out, "it may be in how we manage seedlings, not mature forests and adult trees."

—ELIZABETH PENNISI

ScienceInsider

Recovery Plan Unveiled

As *Science* went to press last week, House Democrats proposed an \$825 billion economic stimulus plan that includes spending \$20 billion on a variety of federal research programs. See *ScienceInsider* for ongoing coverage, <http://blogs.sciencemag.org/scienceinsider>



CONSERVATION BIOLOGY

Debate Continues Over Rainforest Fate—With a Climate Twist

WASHINGTON, D.C.—Depending on whom you talk to, the future of tropical rainforest biodiversity is either “truly catastrophic” or not as bad as feared.

The common wisdom tends toward the catastrophic, says tropical ecologist William Laurance of the Smithsonian Tropical Research Institute (STRI), who is based in Brazil. According to some estimates, he notes, tropical forests are vanishing at a rate of 13 million hectares per year. Two prominent conservation biologists have predicted that only 5% to 10% of tropical old-growth forests would survive in 2050, and they gloomily forecast extinctions of up to 75% of the species.

But that view was challenged by two papers published in 2006, both by Joseph Wright of STRI and Helene Muller-Landau of the University of Minnesota, Twin Cities. They argued that a trend toward urbanism would mean fewer people living in forests and thus a slowing rate of deforestation. They predicted that more than a third of tropical forests overall would remain in 2030. Moreover, the regrowth of forests on abandoned farms would provide a refuge for tropical species. So in the end, 16% to 35% of species would be threatened with extinction, they estimated.

The reaction was fierce. Many biologists felt Wright and Muller-Landau's conclusions would undermine attempts to preserve more rainforest. Laurance, who wrote a high-profile rebuttal in *Trends in Ecology and Evolution*, says one scientist commented: “Their argument is just plain dangerous. We should hit them hard—and with one voice.”

As the public faces of the debate, Wright and Laurance decided to host two symposia, one at STRI in Panama last August and another here at the Smithsonian's National Museum of Natural History last week, to evaluate recent evidence on the threat to tropical biodiversity. Their talks, before an audience of 400 at the natural history museum, were illustrated with

good-natured caricatures of each other as pro wrestlers, devils, and angels. The bout isn't over: Still unsettled are key points such as the amount of tropical forest that will remain in 2030, the biodiversity contained in degraded and recovering forests, and the effectiveness of nature reserves. But the speakers were united in their concerns that climate change may pose even greater risks of unprecedented disturbance to biodiversity than they realized 3 years ago.

Speakers presented evidence that gave cause for both hope and concern. On the negative side, Gregory Asner of the Carnegie Institution of Washington's Department of Global Ecology in Stanford, California, noted that small-scale selective logging affects 28%

her research on regrowing Central American forests, which are often planted with coffee under the canopy. In an unpublished study of northeast Costa Rica, her team found that 90% of old-growth tree species were present in secondary forests. “That's a pretty promising picture,” she said. Secondary forests can't substitute for old-growth reserves (the source of seeds, for example), she conceded, but a network of secondary forests could eventually reconstruct a landscape that would work for many species.

That will be important, because the existing reserves are in trouble, said Laurance, who presented preliminary results of a survey of 60 tropical reserves worldwide. After interviewing several experts at each, he found that biodiversity appears to be declining while threats are on the rise. “Far more reserves are getting worse than [are] getting better,” he told the audience. “The overall trend is one of worsening conditions.” Wright says the parks aren't as remote as they used to be, but many

tropical reserves are generally successful.

Wright firmly agrees that the situation for tropical species could deteriorate as the region warms. That's already clear for highland species—some 165 frog species have gone extinct as warmer climates enable a deadly fungus to thrive. Wright noted that a temperature increase will likely be harmful to lowland tropical species as well. He showed a new analysis suggesting that species living near the equator will have to disperse much farther, up to 2000 kilometers or more, to find climates that match



Patchwork. Tropical forests continue to be cut down and converted to agriculture, such as these soybean fields in Mato Grosso state in western Brazil.

of tropical forest worldwide. “The take-home message is that selective logging, compared to other forms, is massive globally,” Asner said. The figures will be reported in a special issue of *Conservation Biology* devoted to the symposium. Although selective logging itself is less destructive than clear-cutting, new roads lead to increased hunting, fires, and other disturbances, Asner noted. On the plus side, however, he reported that 1.7% of forests worldwide have been regrowing since the 1990s, and up to 2.4% in Central America.

These regrowing forests can house a substantial amount of biodiversity (*Science*, 13 June 2008, p. 1436). Robin Chazdon of the University of Connecticut, Storrs, described

what they're used to. Some researchers have noted that species may be able to adapt (*Science*, 10 October 2008, p. 206). But not Nigel Stork of the University of Melbourne in Australia, who said that climate change “will tip the scales toward massive extinctions.”

Whatever the extent of the threat, everyone agreed with Thomas Lovejoy of the Heinz Center here that preserving tropical forest would yield multiple benefits: storing more carbon, rather than releasing it from burning, and maintaining habitat. For that to happen, the wealthy countries will have to pitch in more than they are now, added Wright: “We're asking the poorest countries in the world to solve this biodiversity threat by themselves.”

—ERIK STOKSTAD

CREDIT: PAULO WHITAKER/REUTERS/LANDOV

WILDLIFE BIOLOGY

Confused Pelicans May Have Lingered Too Long Up North

When pelicans start showing up in grocery store parking lots, backyards, and on roadways, something is seriously wrong. The large seabirds normally stay close to the shoreline and keep plenty of distance from humans. But in recent weeks, hundreds of disoriented and emaciated brown pelicans have turned up in strange places along the Pacific coast from the Baja peninsula to Washington state, prompting concern for this once-imperiled bird now on the verge of removal from the endangered species list.

More than 460 sick and dead pelicans were reported between 10 December and 14 January, says Rebecca Dmytryk, a spokesperson for the International Bird Rescue Research Center (IBRRC), a nonprofit organization headquartered in Fairfield, California. Although young pelicans often succumb to harsh weather during their first winter, Dmytryk says many of the affected birds are adults.

Brown pelicans have rebounded since the 1960s and '70s, when exposure to DDT and other environmental toxicants pushed some populations to the brink, says Daniel Anderson, an avian ecologist at the University of California, Davis. Both the federal government and the state of California are considering removing the birds from their respective endangered species lists as early as this spring. So far, the current outbreak doesn't seem dire enough to alter that decision, Anderson says, but federal and state agencies are keeping an eye on it.

One early suspect has been domoic acid, a neurotoxin produced by algae that has caused previous outbreaks of neurological problems in birds and other marine animals. But the symptoms don't entirely fit, says Heather Nevill, a veterinarian working with IBRRC. Domoic acid can cause erratic behavior and disorientation, but it also typically causes seizures and a characteristic head-weaving motion—neither of which has been seen in the recent cases.

The timing would also be unusual, because domoic acid toxicity is usually associated with algal blooms in springtime, says microbial ecologist David Caron of the University of Southern California in Los Angeles. Five of 14 water samples collected by Caron's lab in southern California in early January did test positive for the toxin but at very low concentrations. As *Science* went to press late last week, Caron's lab had tested blood and other samples from 18 afflicted pelicans. Four had detectable levels of domoic acid, but only two had levels comparable to those found previously in pelicans with classic symptoms of domoic acid



Lost? Earlier this month, a disoriented pelican ended up in a parking lot in Culver City, California.

toxicity, he says. These preliminary results suggest to Caron that domoic acid could be a contributing factor to the mysterious outbreak but not the primary cause.

Another leading suspect is a sudden cold snap that caught thousands of pelicans that lingered longer than usual at the northern edge of their range. "Twenty years ago, you couldn't find pelicans north of California in November," says Deborah Jaques, a wildlife biologist with Pacific Eco Logic, a consulting firm in Astoria, Oregon, near the Washington border. But the birds have been creeping northward recently, and a mild fall in 2008 may have

enticed them to stay even longer before migrating south. Jaques says several thousand pelicans lingered near Astoria into mid-December, when the first big winter storm made its belated arrival. "This was unprecedented in terms of the numbers of pelicans that were here, how late they were here, and the severity of the storm," Jaques says.

Pelicans fare poorly in subfreezing weather, in part because their feathers aren't completely water-repellent and they need to dry off on land after diving for fish. Temperatures below freezing would have made it harder for the birds to dry off, increasing their risk of hypothermia. The cold could also explain other symptoms Nevill and colleagues have seen in rescued pelicans: lesions on the feet and splotches of discoloration on the neck pouches that look suspiciously like frostbite. She and others think it's possible that the blast of cold may have weakened the pelicans, perhaps impairing their ability to hunt as they made their way south and perhaps making them more susceptible to domoic acid or other hazards they encountered along the way.

Still, the case is far from closed. Necropsies being carried out by the California Department of Fish and Game and the National Wildlife Health Center in Madison, Wisconsin, should provide valuable clues in the coming weeks. "We're keeping our minds open," Nevill says. "We want to make sure we've covered all the bases." —GREG MILLER

AWARDS

Two Americans Win Japan Prize

This year's Japan Prize goes to two U.S. academics, one a long-time advocate for sustainability and the other a radiologist who pioneered a standard tool for medical imaging.

Dennis Meadows, a professor emeritus at the University of New Hampshire, Durham, fueled the burgeoning environmental movement with a 1972 paper, *The Limits to Growth*, that highlighted the impact of pollution and the depletion of natural resources on the planet. Meadows, 66, has expanded on that work to advocate for a sustainable society.

David Kuhl, 79, a professor at the University of Michigan, Ann Arbor, developed a method in the 1950s to image organs and tissues by injecting radioactive isotopes into the body. It became the foundation for positron emission tomography, which has become a standard tool for evaluating tumors and tissue damage inside the brain.

Each year, the Science and Technology Foundation of Japan chooses two fields. This year's categories were for "contributions toward a sustainable society in harmony with nature" and "technological integration of medical science and engineering."

—YUDHIJIT BHATTACHARJEE



Meadows



Kuhl



Fungal infection. *Septoria* kills tissue on wheat leaves, hindering the plant's growth.

AGRICULTURE

European Pesticide Rules Promote Resistance, Researchers Warn

Despite intense opposition from farmer groups and scientists, the European Parliament voted last week to approve new regulations that could ultimately outlaw up to one-quarter of the pesticides on the European market. The legislation mandates a new licensing strategy inspired by the so-called precautionary principle, which calls for substances to be considered potentially harmful until proven safe for human health and the environment.

Concerned that pesticides would be immediately banned, farmers had warned of devastated crop yields: "EU pesticides ban will 'wipe out' carrot crop," declared one British newspaper. Although not endorsing such dire forecasts, some agricultural scientists opposed the regulations for other reasons: They say that any reduction in available pesticides will accelerate the development of plant pests' and pathogens' resistance to the remaining agents. They also question the scientific grounding of the hazard criterion.

"The portfolio [of pesticides] that we have is already compromised in some cases by resistance," says John Lucas of the U.K. agricultural institute Rothamsted Research in Harpenden, a vocal opponent of the new licensing rules. He and his colleagues fear that pesticide resistance could become as problematic as the multiresistant bacteria strains causing havoc in hospitals.

Over the years, agricultural scientists have fought a cat-and-mouse game with insects and plant pathogens, developing new substances as the pests become more resistant to the older ones. Because novel pesticides can take a decade or more to develop, the scientists are concerned that they won't be able to keep up, as permits for existing ones expire and aren't renewed. Some worry especially

about losing the azoles, a group of compounds used to manage plant diseases, including septoria leaf blotch, caused by the fungus *Mycosphaerella graminicola*. The most important wheat crop disease in northwestern Europe, septoria was originally controlled by several types of fungicides. But since the 1980s, *M. graminicola* has developed widespread resistance to two pesticide classes, leaving the azoles as the last line of defense.

The rules approved by the European Parliament on 13 January were watered down compared with the first proposal, which would have outlawed about 85% of pesticides currently in use, according to an assessment by the U.K. Pesticide Safety Directorate (PSD). The approved regulations could still lead to the ban of 14% to 23% of pesticides, the PSD estimates.

According to the European Parliament, the new legislation will be applied gradually, with "no sudden or large-scale withdrawal of products from the market," and there should "be ample time for farmers to adapt by using alternatives or non-chemical methods, or for the pesticides industry to devise replacements." The rules also include 5-year permit exceptions for substances deemed hazardous but needed to control serious dangers to plant health, including the development of resistance.

The 5-year rule will "give us some breathing space," says Lucas, who is nevertheless skeptical about its implementation. Time for research is also essential for developing an alternative to pesticide usage: disease-resistant crops. James Brown, who researches ways to make wheat varieties both septoria-resistant and high-yielding at the John Innes Centre in Norwich, U.K., says, "This is a gradual

process." He warns that "diseases don't stay the same." For instance, breeding barley that resists ramularia, a disease that emerged in 1998, "will take at least 10 years." In the meantime, he says, "fungicides are necessary to back up varieties' resistance" to disease.

The pesticide regulations' dependence on the precautionary principle riles many. "This hazard-assessment argument is really where the big problem lies," says Lucas. "As scientists, we find it very worrying that things go through that don't really stack up in terms of scientific evidence."

Alan Boobis, who studies toxic mechanisms of drugs and environmental chemicals at Imperial College London, agrees. "I feel that action is being taken on the basis of a policy position that doesn't reflect the state of the science," Boobis says, arguing that pesticides are one of the most thoroughly evaluated types of products on the market.

Last month, Lucas delivered to a member of the European Parliament a petition he and 71 other European scientists signed against the ruling. "We would be the first to say that we are not encouraging a solely chemical approach to the control of disease," notes Lucas. But he wonders if even common toothpaste would be approved if everyday life were governed by the same precautionary principle now applied to pesticides.

Emma Hockridge, a campaigner for the Soil Association, which supports the new rules, says she recognizes that narrowing down pesticide diversity can lead to increased resistance of certain pests. "But this highlights the fact that any agricultural system which is heavily reliant on pesticides for crop management is inherently unsustainable in the long term," says Hockridge, adding that natural management methods promote healthier and more robust crops.

For Mark Whalon, director of the Pesticides Alternatives Laboratory at Michigan State University in East Lansing, the issue has implications beyond European boundaries. In an age of globalization, if unwanted pest resistance arises in Europe, it will likely make its way to the United States, Whalon says. An organic farmer, Whalon understands the calls for a greener and safer environment. But as editor of the Arthropods Resistant to Pesticides Database, he also takes the resistance issue very seriously. He notes that eliminating pesticides primarily based on human health concerns could leave farmers with ones that are more dangerous to the ecosystems around crops. "Just because it is safer for humans doesn't make a pesticide safer for the environment," he warns.

—SARA COELHO

CREDIT: LAETITIA CHARTRAIN/JOHN INNES CENTRE

EMERGING INFECTIOUS DISEASES

Scientists Puzzle Over Ebola-Reston Virus in Pigs

An international team of human- and animal-health experts is in the Philippines this month, studying the first known outbreak of Ebola-Reston virus in pigs. The virus, which is related to the Ebola virus that causes the highly fatal Ebola hemorrhagic fever, had previously been found only in monkeys and a few humans who had been in contact with the sick animals. It has not caused any known incidents of serious illness or death in humans. But experts are concerned “because this is new, because it is unexpected, because the virus is slightly different [from previous isolates], and because it is in pigs,” which live in close proximity to humans, says Julie Hall, an infectious disease expert for the World Health Organization (WHO) and a member of the investigative team.

“The finding is cause for further study but not further alarm,” says Stuart Nichol, a virologist at the U.S. Centers for Disease Control and Prevention in Atlanta. He says ongoing investigations may lead to a better understanding of Ebola viruses.

Ebola viruses belong to the Filoviridae family and come in five strains: Zaïre, Sudan, Côte d’Ivoire, Bundibugyo, and Reston. The Zaïre, Sudan, and Bundibugyo strains have caused outbreaks of Ebola hemorrhagic fever among humans in Africa, killing up to 90% of those infected. Ebola-Reston was first isolated in 1989 from cynomolgus macaques imported from the Philippines for medical research in the United States. Unusual numbers of the monkeys started dying while in a quarantine facility in Reston, Virginia. About 1000 monkeys died or were euthanized. Subsequently, 21 animal handlers at the Philippine exporter and four employees of the quarantine facility were found to have antibodies to the virus, indicating that they had been infected, but just one reported flulike symptoms. Further outbreaks in monkeys in the Philippines were reported in 1992 and 1996.

An increase in pig mortality on several farms in central Luzon, the Philippines’ largest island, in 2007 and 2008 prompted an investigation by Philippine agencies. Last October, international reference laboratories studying samples supplied by the Philippines confirmed that the pigs were infected with a highly virulent strain of porcine reproductive and respiratory syndrome as well as the Ebola-Reston virus. Which virus is responsible for the increased mortality is not yet clear.

The presence of Ebola-Reston virus on pig farms increases the odds of human exposure and infection. Previous human infections occurred in young men, who happened to be employees at both the Philippine exporter and the Reston lab animal supplier, Hall says. “We now have that virus in pigs that live in very close contact not just with



fit, healthy, young men, but with pregnant women, children, and people with underlying medical conditions,” Hall says. Initial laboratory tests on animal handlers and slaughterhouse workers who might have been exposed were negative, the Philippine Department of Health has reported.

At the request of the Philippine govern-

ment, WHO, the United Nations Food and Agriculture Organization, and the Paris-based World Organisation for Animal Health assembled an 18-member team that began its 10-day investigation on 6 January. So far, they have more questions than answers. It is not clear whether the virus alone causes clinical illness in pigs, how easily it spreads among the animals, or how it invaded the separate farms. The implications of the slight genetic differences in this strain are also not known.

Answers to some of these questions should trickle in over the next several weeks. The international agencies and their local counterparts are planning further studies to determine, among other issues, whether the virus is in wider circulation in pigs and what its natural habitat might be. Meanwhile, the government is being cautious, quarantining the affected farms, even though there are no longer signs of illness among their pigs, and suspending all pork exports.

Gary Kobinger, a virologist at Canada’s National Microbiology Laboratory in Winnipeg, says there have long been rumors of unusual die-offs of pigs before Ebola outbreaks among humans in Africa. “The question is: Is it possible that pigs are hosts that amplify and transmit the virus to other animals and humans?” he asks. —DENNIS NORMILE

TEACHING EVOLUTION

Educators Decry New Louisiana Policy

Science teachers in Louisiana have been given permission to use supplementary material in the classroom in a move that many scientists and educators regard as a backdoor attempt to allow creationism and its variants into the classroom.

Last year, as part of a wave of so-called academic freedom bills, Louisiana legislators passed a law covering the teaching of “controversial” scientific theories that include evolution, origins of life, and global warming (*Science*, 20 June 2008, p. 1572). State education officials initially drafted policy language explicitly prohibiting teachers from teaching intelligent design. But that language was dropped before last week’s unanimous vote by the Louisiana State Board of Elementary and Secondary Education, along with a disclaimer saying

that religion should not be taught under the guise of critical thinking.

Supporters, including the Seattle, Washington-based Discovery Institute and the Louisiana Family Forum, say the policy will foster critical thinking in students. But opponents say that more is at stake. “We fully expect to see the Discovery Institute’s book, *Explore Evolution*, popping up in school districts across the state,” says Barbara Forrest, a philosopher at Southeastern Louisiana University in Hammond. Patsy Peebles, a retired science teacher who helped the education department draft the earlier policy language, says there’s no mistaking the meaning of the last-minute change in the board’s policy: “The creationists got what they wanted.”

—YUDHIJIT BHATTACHARJEE

THE TRANSITION

Proposed Regulatory Czar Has Long And Perplexing Track Record

President-elect Barack Obama's choice to manage the regulatory policies of his new Administration has triggered a mixture of consternation and delight among conservatives and liberals. Cass Sunstein, who teaches law at Harvard University and the University of Chicago in Illinois, has written two dozen books and hundreds of articles on topics as diverse as animal rights and cost-benefit analysis. Despite that prodigious scholarly record, there's a surprising lack of consensus about his likely impact on the Office of Information and Regulatory Affairs (OIRA), a White House office that wields broad power over every federal regulatory agency and that sparked controversy under President George W. Bush.

Sunstein has long kept a foot in opposing regulatory camps. He's a contributing editor for the liberal magazine *The American Prospect* and wrote an entire book praising the "second Bill of Rights" proposed by President Franklin D. Roosevelt that would have guaranteed every American a job, a

home, and medical care. Yet Sunstein is also co-chair of the staunchly free-enterprise Center for Regulatory and Market Studies at the American Enterprise Institute in Washington, D.C. And he sounds like his two predecessors at OIRA—John Graham and Susan Dudley (*Science*, 21 March 2003, p. 1836; 18 May 2007, p. 973)—when he criticizes the public's tendency to get worked up over risks that appear, in the cold light of cost-benefit analysis, to be relatively small: abandoned toxic waste dumps, genetically engineered crops, or mad cow disease. "Unjustified fear is one of the most serious problems facing modern societies," he wrote in 2002.

Initial reaction to his pending nomination focused on his likely use of cost-benefit analysis in formulating regulations. An editorial in *The Wall Street Journal* called it "a promising sign," whereas Rena Steinzor, an advocate of tighter regulation who teaches environmental law at the University of Maryland School of Law in Baltimore, sees Sunstein as "a strange, disconcerting choice."



Ruler of the rules. Cass Sunstein has been tabbed to oversee Obama's regulatory policies.

Sunstein's detractors say he sometimes exhibits a naïve trust in scientists' ability to provide precise and objective answers. "Sunstein will take quantitative risk assessments from people who have a clear ax to grind and treat them as gospel," says Thomas McGarity of the University of Texas, Austin, law school. Another critic, David Driesen of the Syracuse University College of Law in New York, says that efforts to regulate arsenic in drinking water demonstrate the shortcomings of ▶

BIOTECHNOLOGY

U.S. Appellate Court Weighs 'Obvious' Patents

These days, any competent graduate student can take a known protein and come up with the nucleotide sequence that encodes it. Does that mean the gene's code is obvious, in a legal sense, and therefore cannot be patented?

A federal court is mulling that question after hearing oral arguments earlier this month in a case, *in re Kubin*, that involves a 2000 patent application that was rejected by the U.S. Patent and Trademark Office (PTO). Academic and industry scientists hope the answer, expected by early spring, is no. A yes answer would make it harder for researchers to patent discoveries, say biotech lawyers, stymieing innovation and investment.

Scientists at Immunex, a Seattle, Washington-based company later acquired by Amgen, sought a patent on a gene that encodes a protein, called NAIL, found on certain white blood cells that protect the body from disease. In 2007, a PTO adjudicating board rejected the application, saying that obtaining the gene required little more

than "routine skill" in biotechnology. Other scientists had previously isolated NAIL, PTO pointed out, and the steps subsequently needed to obtain the genetic sequence were "conventional methods" described in a laboratory manual. The Washington, D.C.-based U.S. Court of Appeals for the Federal Circuit took the case after Amgen appealed.

By law, patents can be granted for discoveries found to be new, useful, and not obvi-



High barrier. Scientists failed to win a patent on a gene encoding a protein found on certain immune system cells.

ous. But a string of recent court decisions have tossed out inventions in various fields after finding them obvious. Law professor Mark Lemley of Stanford University in Palo Alto, California, calls those decisions, which include a 2007 Supreme Court ruling in a case involving brake pedals, a "significant change" in a system that has historically been friendly to biotechnology patenting. After analyzing the questions raised by the three-judge panel at the 8 January hearing, law professor Chris Holman of the University of Missouri, Kansas City, says that the biotech community "might lose on the issue of obviousness."

Holman found special significance in an observation by one judge that the patent office made a "factual finding" that obtaining a gene sequence from a known protein was "routine." "The court tends to defer to the patent office on such findings," he says. Another judge called a 1997 patent in which researchers isolated the NAIL protein on a gel called a Western blot "of some consequence" because the scientists suggested subsequent steps that might yield the gene.

The 2007 Supreme Court case, *KSR v. Teleflex*, made it easier to reject patent

CREDITS (TOP TO BOTTOM): U. CHICAGO NEWS OFFICE; EYE OF SCIENCE/PHOTO RESEARCHERS INC.

cost-benefit analysis. The scientific committees have proposed a range of estimates for the number of people likely to get cancer because of exposure to the chemical. Plug those numbers into a cost-benefit calculation, says Driesen, and “the range turns out to be so large, it’s not useful.”

Some of Sunstein’s colleagues say that his views on risk analysis are more subtle than either critics or supporters give him credit for. “I think both sides will be surprised,” says Richard Revesz, dean of the law school at New York University. The tools of cost-benefit analysis in the past “were captured by antiregulatory academic and interest groups” and misused, says Revesz. He predicts that Sunstein will deploy those same tools in support of novel regulatory initiatives.

All sides expect Sunstein to play a formidable role within the new Administration, not least because he has the ear of the president. Sunstein, who has known Obama for 15 years and advised him during the campaign, recently married Samantha Power, a professor at Harvard’s Kennedy School of Government. Part of the campaign’s inner circle, Power resigned after calling Obama’s then-rival, Senator Hillary Clinton (D-NY), a “monster” but later joined the transition team. —**DAN CHARLES**

Dan Charles is a freelance writer in Washington, D.C.

claims on the grounds that the discovery is obvious. The court ruled that an inventor could not claim a patent after following steps PTO found “obvious to try.” But attorney Hans Sauer of the Biotechnology Industry Organization (BIO) in Washington, D.C., finds the “obvious to try” standard misleading in this case and for gene-hunting in general. Scientists “have a reasonably good chance to get from the blot to the gene,” he says. “But that doesn’t mean the sequence of the gene itself would be obvious to them.”

Having PTO disqualify applications for DNA patents as it did in the Kubin case would “threaten the development of new drugs, diagnostic tests, and other biotechnology-derived products,” BIO argued in its brief. An adverse ruling could put into doubt the validity of tens of thousands of biotech patents, others say. Even so, attorney Kevin Noonan of the popular Patent Docs blog sees a silver lining. He thinks the court might rule favorably on a secondary issue in Kubin that would allow scientists to receive patents after filing slightly less detailed applications that make broader claims, covering more technology.

—**ELI KINTISCH**

PHYSICS

Photon Sieve Lights a Smooth Path To Entangled Quantum Weirdness

Entanglement, a seemingly impossible link between distant particles, is key to physicists’ plans for revolutionary quantum computers and uncrackable quantum communications systems. Creating entangled pairs of light particles, or photons, is a delicate business. Now, physicists from Japan and the United Kingdom have found a way to do it by simply passing ordinary photons through a novel optical filter.

“This is pretty cool,” says Alan Migdall of the National Institute of Standards and Technology in Gaithersburg, Maryland. “I haven’t seen an approach like this before.” Still, he and others say it’s too soon to tell whether the new method, described on page 483, will outshine techniques that generate pairs of photons entangled from “birth.”

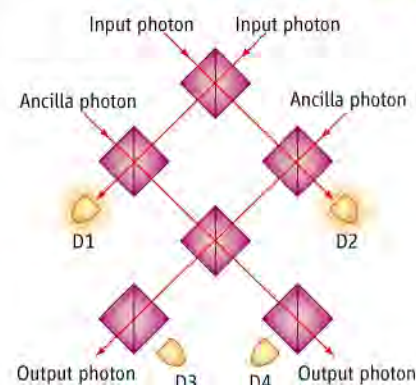
Entanglement connects quantum particles no matter how far apart they are. Imagine two photons speeding away from each other. Each can be polarized horizontally, vertically, or—under the weird laws of quantum mechanics—both horizontally and vertically at the same time. Such a “diagonally” polarized photon can maintain its both-ways state until someone measures its polarization; then it will “collapse” into either the horizontal or vertical state.

Physicists can entangle two diagonally polarized photons so that both must collapse into the same state. So if an experimenter measures one photon and it collapses into horizontal polarization, then the other photon will instantly do the same, no matter the distance. In quantum communications schemes, entangled photons can convey secret messages because an eavesdropper will spoil the entanglement and reveal his or her presence. They might someday ferry information within quantum computers able to tackle problems that stymie conventional machines.

To generate entangled pairs, physicists have relied on “nonlinear” materials that cause photons to multiply or change frequencies. For example, in a technique called parametric down-conversion, a crystal converts one high-frequency photon into two identical lower-frequency photons. In the new approach, by contrast, Shigeki Takeuchi of Hokkaido University in Sapporo, Japan, and colleagues use conventional “linear” optical elements—mirrors and partially reflective “beam splitters”—to make an entanglement filter. The device “acts not just on one photon but on the combination of the polarizations of two photons,” Takeuchi says.

The mazelike filter takes two unentangled, diagonally polarized photons as input. Because each is polarized both horizontally and vertically, the quantum state describing the pair has a part in which both are horizontal, a part in which both are vertical, and parts in which the first is horizontal and the second is vertical and

INPUT STATE: $\uparrow\uparrow + \downarrow\downarrow + \uparrow\downarrow + \downarrow\uparrow$



ENTANGLED STATE: $\uparrow\uparrow + \downarrow\downarrow$



Partially polarizing beam splitter



Single photon detector

Light maze. Two vertically or horizontally polarized photons can bounce through as only detectors 1 and 2 fire. A mixed pair won’t make it through.

vice versa. The filter lets through only the vertical-vertical and horizontal-horizontal parts—the ones involved in entanglement.

As the photons bounce and split their way through the maze, they encounter two additional “ancilla” photons. A phenomenon called quantum interference affects the photons’ tendency to stick together or separate as they pass through the beam splitters. Two of the four photons must trigger certain detectors in the maze to signal that the other two have been entangled, which happens 1/16 of the time.

At the moment, the experiment produces only a few entangled pairs a minute. Nonlinear methods churn out millions per second, notes Paul Kwiat of the University of Illinois, Urbana-Champaign. But with the linear optics, he says, “you can ratchet up” to bigger circuits and more entangled photons much more easily. With improvement, the entanglement filter might light the way toward more ambitious devices.

—**ADRIAN CHO**



Friendship as a Health Factor

In a string of hot articles, two social scientists report that obesity, smoking, and other facets of health “spread” in networks. As the two friends expand their theory, doubters sharpen their questions

BOSTON—On the first snowy day in December, Nicholas Christakis and James Fowler are ensconced in Christakis’s rambling home in Concord, Massachusetts, plotting their next conquest. Christakis, at his desk, is nearly hidden behind two enormous Apple computer screens that beam dizzying network patterns of lines and circles representing community ties. Fowler sits cross-legged and barefoot on the couch, a laptop balanced on his knees. The pair are deep at work on their upcoming book, *Connected: The Surprising Power of Social Networks and How They Shape Our Lives*. On a mock cover taped to the wall, an orange goldfish leaps from one bowl of fish into another. The two men haven’t left the house in 48 hours, and Christakis’s watch stopped some time ago.

Christakis, a social scientist and hospice physician—cheerful, given his line of work—and Fowler, an easygoing political scientist, hatched a plan about 6 years ago to study how social relations influence health. Their initial scheme required a massive number of volunteers and \$25 million. It

didn’t take off, as funders balked at the price tag. But soon after, they stumbled upon something even better that would catapult their careers: a collection of loose-leaf papers locked in a record room in Framingham, Massachusetts, home to patient files of the nearly 15,000 participants in the Framingham Heart Study, begun in 1948.

Christakis, who has joint appointments at Harvard Medical School and in Harvard University’s sociology department, recalls as “delicious” the moment when a woman overseeing data collection for the Framingham study mentioned a critical detail. Christakis was wondering aloud how Framingham had kept its hold on so many people for so long. “‘Well, we have these tracking sheets,’” Christakis recalls her explaining, as she pulled a green sheaf from a cabinet nearby. For each participant, the forms requested home address, family physician—and at the bottom asked, Name a close friend who can find you in case we can’t. Instantly, Christakis saw that a social network spanning 30 years was buried in that chart room. “Exactly the data that we

were planning to spend millions of dollars to collect going forward had already been collected,” says Fowler.

Since then, Christakis and Fowler, from his perch at the University of California, San Diego, have pieced together and computerized the Framingham network, matching it with health over time. In a provocative set of papers, they’ve documented that every facet of health examined so far appears to “spread” from person to person. Obesity spreads. Happiness and unhappiness spread. Smoking



Dynamic duo. Nicholas Christakis (left) and James Fowler are dissecting social networks, gaining fans and foes in the process.

Online sciencemag.org

S Podcast interview
with author
Jennifer Couzin.

habits spread. The work has landed the two everywhere from the front page of *The New York Times* (which wrote that obesity can spread “like a virus”) to the TV news parody *The Colbert Report*. With the fame have come skeptics, who suggest that Christakis and Fowler are drawing conclusions that go beyond their data.

The work has also propelled the field of social networks and health into the spotlight—and, potentially, into medical care, for which findings could be used to modify behaviors that affect health. But the few efforts to apply network insights to patients have been mixed, in part because determining what causes network effects can be enormously difficult, and modifying them is even tougher (see sidebar, p. 456). Even if social interactions influence everything from heart disease to weight to mental health, intervening is far more daunting than proffering up a drug, says sociologist James Moody of Duke University in Durham, North Carolina, who has studied social networks among adolescents: “I can’t write a prescription script for getting new friends.”

Building blocks

Christakis, 46, and Fowler, 8 years younger, came to social networks from different starting points. Christakis, while caring for the elderly in their last months, became fascinated by the widower’s effect, a phenomenon first investigated in 1858 in which one spouse’s death is often closely followed by the other’s. Fowler, completing his dissertation at Harvard on voting patterns, was intrigued by how social interactions influence voter choice. One of Fowler’s advisers introduced the unlikely pair. “It was thrilling to be taken so seriously,” says Fowler now. These days, the two have a video link set up between their homes in Massachusetts and California and chat at all hours of the day and night.

Social networks have been studied for decades, but it’s only recently that researchers have aggressively applied them to health-related questions. Early studies in this field focused on schools: whether, for example, a child in a school filled with smart children is more likely to excel than one in a school of underperformers. “Everyone thinks that, but it’s darn hard to tell” if it’s true, says Ethan Cohen-Cole, an economist at the Federal Reserve Bank of Boston, who studies social networks. Because so many factors feed into school performance, or weight, it’s enormously difficult to separate out the effects of social interactions, says Cohen-Cole.

One tack is to minimize confounding

factors by searching for rare networks that form randomly. An economics professor at Dartmouth College took this approach, reporting in 2001 that freshmen who happened to be assigned roommates who were smarter than they were would perform better academically. Another method is to focus on individuals whose networks are unusually self-contained, such as teenagers, whose entire social scene tends to revolve around their high school.

This was the strategy of the National Longitudinal Study of Adolescent Health, or Add Health. Begun in the 1990s, it surveyed 90,000 U.S. junior high and high schoolers. “We interviewed every kid at every school” and asked each to identify close male and



female friends, says Peter Bearman, a sociologist at Columbia University who helped design Add Health. “You could characterize the social structure of every school” and identify where each student sat—at the center or around the less popular edges.

Add Health, which is still following participants, has yielded hundreds of papers and many interesting observations about sexual health, drug use, isolation, and more. Bearman was struck by one in particular, that girls whose friends were not friends with each other—what he calls an “unbalanced network”—were much more likely to have suicidal thoughts than boys in the same situation. Bearman believes physicians ought to ask adolescents about the shape of their peer

group—but like most people studying networks in academia, he has no idea whether the work has been applied.

“For kids, their band, their friends, their work—it’s all in the same physical space,” says Moody, who also participated in Add Health. “If you try to do this for adults, it’s much more difficult.”

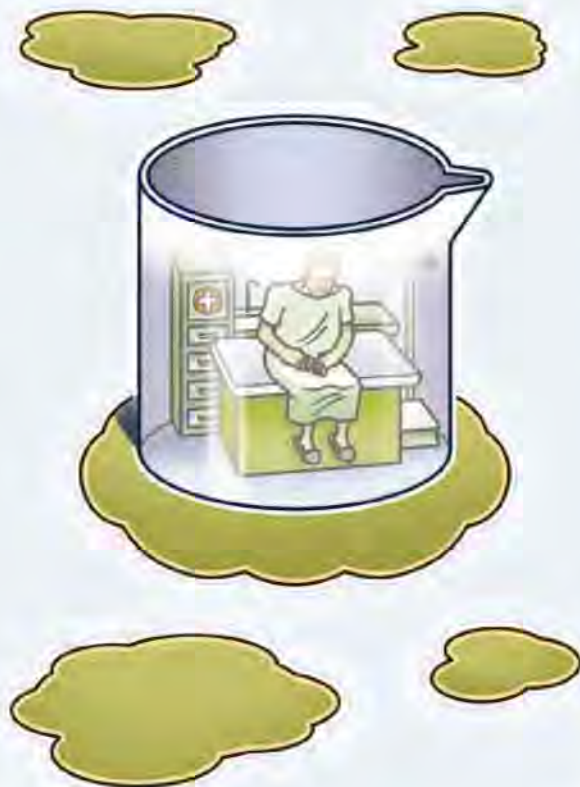
Triumph

Fowler speaks of his joint venture with Christakis in epic terms. “We have an opportunity to peer inside human society,” he says, “the same way Leeuwenhoek peered inside a cell” 3 centuries ago with the earliest microscopes.

That opportunity stems directly from the Framingham network. One great advantage it offered over earlier social networks is that participants were monitored roughly every 3 years for a long period, and Christakis and Fowler could see changes in participants’ weight as the years passed. This could include friends who gained weight at different times, making it easier to link one’s weight gain to the other’s.

Christakis and Fowler chose to focus first on obesity, because weight is an objective measure that was recorded for many years. In the summer of 2007, they described in *The New England Journal of Medicine (NEJM)* their analysis of 12,000 people. About half were offspring of the original 1940s cohort, and the rest were parents and children who also participated in the study (and had named their own friends); the group was followed from 1971 to 2003. Christakis and Fowler found that an individual’s chance of becoming obese increased 57% if someone named as a friend became obese in the same time interval. More surprisingly, the effect surfaced, but to a lesser degree, even when a direct friend wasn’t involved: Obesity in a friend’s friend (or any social contact) boosted the chance of obesity by 20%, and in a friend’s friend’s friend, by 10%. There was no effect beyond three degrees of separation—a pattern that the two have seen in subsequent studies of other health effects. The impact was also weaker among friends of the opposite sex, and there was no effect among neighbors.

The two researchers followed up with a paper the next spring, in May 2008, on smoking. (While obesity increased in the United States during the Framingham years, smoking became less prevalent.) Again writing in *NEJM*, the two showed patterns similar to those for obesity—if a spouse quit smoking,



WITH ISOLATION COMES ILL HEALTH

BOSTON—Epidemiologist Lisa Berkman has been fascinated for years by social isolation, the flip side of social networks. It's a state she and others believe has dire consequences, increasing the risk of certain diseases and earlier death. Attempts to transform this knowledge into action have been discouraging, however: The first ambitious efforts to blunt the harmful effects of solitude have not worked, but Berkman is still seeking ways to mitigate them. She's just beginning a 2-year, \$20 million intervention study funded by the U.S. National Institutes of Health (NIH).

Berkman, of the Harvard School of Public Health located here, says she was drawn to study isolation back

in the 1980s, when she traced social patterns among 7000 people in Alameda County, California. She found that those who scored low on a scale measuring social integration were 2.5 to 3 times more likely to die over the next 7 years than those who scored high. That in itself wasn't a shock, because it's reasonable to assume that isolation is associated with risky behaviors. But Berkman ruled out specific risks, such as drinking alcohol, one by one—and the risk of death stayed high, about 2 to 2.5 times the norm. "What social isolation was doing was making you more susceptible or less resilient to any disease you might get," she says. The work has been replicated in more than a dozen studies around the world.

an individual's chance of quitting increased 67%, and for a friend the figure was 36%. There were subtle distinctions, too. Those with more education were more influenced by others and had a greater influence themselves. The same "spread" pattern held, with friends of friends having an effect. Christakis and Fowler wrote in the *British Medical Journal* in December that happiness and unhappiness disperse in much the same fashion.

They also have papers on alcoholism and depression in the works. Early this year, they expect to publish research on twins from the Add Health study, showing that the structure of one's social network, such as interconnections between friends, is partly inherited.

The research has gotten a remarkable amount of attention. Top medical journals, which don't normally feature social-network research, have published all three of Christakis and Fowler's Framingham papers, in which they describe noninfectious disease with terms such as "person-to-person spread." And the attention has transformed the authors' careers. Christakis and Fowler landed a 5-year, \$11 million grant from the National Institute on Aging in April to study cardiovascular disease, cancer, obesity, violence, and substance use in networks. Their book, slated to appear in early 2010, is expected to be

translated into more than a dozen languages. They've appeared 2 years running in *Time Magazine's* Year in Medicine. Even Fowler's high school in tiny Seminole, Oklahoma, in September inducted him into its hall of fame.

Pushback

Before the first Framingham paper appeared, Christakis's wife warned her husband that he'd be accused of wasting taxpayer money by looking at such a simple, obvious question, because of course friends influence one another. He and Fowler girded themselves for such an attack. Instead, people were incredulous, Christakis says. "We get, 'Outrageous! How can you be claiming obesity spreads?'"

That, say the doubters, is because identifying patterns among friends is not the same as proving that one friend causes another to do something. "They really have not shown adequately" that one person's obesity, or efforts to quit smoking, explain why another person gains weight or quits smoking, says Theodore Iwashyna, a critical-care specialist and social scientist at the University of Michigan, Ann Arbor, and one of Christakis's first graduate students. Iwashyna, who stresses that such challenges are faced in any social-network study, is enthusiastic about the "freaking cool" connections his mentor has demonstrated. But, he asks, what's behind them?

Social scientists point to two other possible explanations for the clustering of friends

with similar characteristics. The first, called "homophily," is the tendency of individuals to associate with people similar to themselves. The second is shared environment. For example, a fast-food restaurant might pop up in a neighborhood, contributing to weight gain among people living nearby. In both cases, one person's weight gain is not the reason for another's.

Christakis and Fowler acknowledge both pitfalls in their writings and emphasize that they've accounted for them. Indeed, says Fowler, "there's not a single argument a critic has made to us that we haven't thought of." Homophily, they have determined, can't explain all the effects because of changes in the Framingham participants that show up over time. For example, two contacts might start off slender; over time, one gains weight, followed by the other. Shared environment has its own limitations. Some clustering, particularly for smoking and obesity, pops up across geographic distances (as when members of the Framingham study moved out of town) but doesn't appear among neighbors on the same block. Furthermore, Christakis and Fowler find that the strength of an effect depends on the strength of a friendship. The weight gain, for example, or boost in happiness, only occurs when one person named another as a friend; the effect did not run in the other direction if that person did not name the other. "It's really subtle," says Christakis. And, Fowler chimes in, "completely ignored by all our critics."

But unlike her social science colleagues Nicholas Christakis of Harvard Medical School and James Fowler of the University of California, San Diego, who beam confidence that social effects are causing changes in health (see main text), Berkman is not certain that a cause-and-effect linkage has been proved, at least where social isolation is concerned. She concedes that isolation may be a result rather than a cause of disease.

Adding to her mixed feelings is that she's had "some really spectacular failures." In 1995, Berkman chaired a nearly \$40 million NIH study designed to bolster social networks to prevent a second heart attack in those who'd had one before. The intervention did improve social support and reduced depression but had no effect on

heart disease. A second network intervention to help stroke victims had equally dismal results. It's a "totally legitimate interpretation" that the studies failed because social isolation doesn't cause cardiovascular disease after all, says Berkman, but that is not what she believes. Her theory is that the "exposure"—isolation—had already done too much harm, so that late intervention accomplished little physiologically. She also says it's difficult to change a social network enough to make a difference.

In the new NIH-funded study, Berkman and others are turning to workplace interventions, focusing on 3000 nursing home employees and information technologists. Half of the 60 sites will implement family-friendly policies and half will not. The idea is to see if giving



Determined. Lisa Berkman aims to blunt the negative health effects of social isolation.

employees more time to spend at home and with friends will bolster their social networks. Berkman acknowledges that the outcome seems obvious—presumably having an amiable boss and a flexible work environment is good for one's health.

But "the truth is we don't know, and the truth is we've been lousy at producing change," Berkman says. "In fact, I'm incredibly wary that we're going to show health effects." Many more scientists believe "that we should be thinking of molecular biology to solve these problems than to think about how work is organized, or how our social world is organized." She and her colleagues will be following workers, their spouses, and their children, examining everything from heart disease and cancer to biomarkers of health such as levels of cholesterol, blood pressure, and C-reactive protein. If changes in the workplace can modify these physiological effects, says Berkman, "that's huge. That's totally huge."

—J.C.

Some of the most vocal detractors of Christakis and Fowler's work are economists who study social networks, in particular Cohen-Cole and his graduate school friend Jason Fletcher, a health economist at Yale University. Working with data from Add Health, the study of teens in high schools around the country, the two tried and failed to replicate the published obesity results. (Two other groups say they have replicated Christakis and Fowler's findings using Add Health, but one noted that evidence for obesity's contagion was "only suggestive at best.") In December, Cohen-Cole and Fletcher published a damning paper in the *British Medical Journal*, applying Christakis and Fowler's methodology to three traits they did not consider transmissible: acne, height, and headaches. Again turning to the Add Health school networks, in which students were surveyed three times over the years, they reported that all three "spread," although in some cases the effects were weak.

Differences with critics run deep. Whereas Cohen-Cole and Fletcher express disbelief that acne or height could appear to spread, Christakis and Fowler think it's quite plausible, especially because Add Health relied on teenagers to report their own health habits. They say that a teen whose friends have acne, for example, may be more aware of his own and more likely to mention it—or the group might share a similar diet that leaves them prone to, or protected from, bad skin. Those with tall friends might be more likely to exaggerate their height. But they also

might be more likely to exercise together, which has been shown to boost height slightly in growing adolescents, says Christakis.

So what traits should not be altered by social networks? Well, says Christakis, eye color and birth order, and anything else that is wholly genetic. Everything else, they agree, is fair game.

Network makeovers

Those wishing to intervene in real-life social networks must first settle on what's behind the health changes documented. "If kids are getting fatter because their friends are getting fatter, what you need to do as a policy-maker is very different than if they're getting fatter because there's a McDonald's nearby," says Cohen-Cole.

Even though there's no unanimity yet, interest in applying network findings is keen. Christakis says that he and Fowler have been contacted by companies interested in smoking cessation, by the White House drug policy office, and by an eating-disorders clinic wondering whether to include girls with varying weights in group therapy sessions in hopes that those who are a bit heavier will help shift the lightest ones to a healthier weight.

But few people have actually tried to modify networks to change health, and those who have have experienced mixed results. Psychologist Rena Wing of Brown University reported that when one spouse participated in a weight-loss program, the other lost nearly 5 pounds, compared with no weight

loss for spouses of nonparticipants. Whether the effects spread beyond one person wasn't examined. Still, such ripple effects, which Fletcher is also studying in smoking cessation, have strong implications. "We know the costs of the pill," he says, "but we're not counting all the benefits."

Physicians are still a long way from adopting any of this work. The implications "are often not translated into messages that resonate with people who are delivering medical care," says Carol Ford, an adolescent medicine physician at the University of North Carolina, Chapel Hill. In efforts to prevent the spread of sexually transmitted diseases, she says, networks can reveal which partners are most important to focus on.

"I do think people in medicine are paying attention," says Duke's Moody, but "it's one thing to show something matters. It's another to show you can do something with it," especially in a world where most doctors spend mere minutes with each patient.

But he and some others see networks adding an entirely new dimension to considerations of health. "For so long, science, medicine, and lots of other fields have succeeded by cutting things into small pieces," he says. "The way science works is isolating smaller and smaller microunits. ... What the network model does is say, that can only take you so far. There's an effect that occurs at the population level," even if capturing it, understanding it, and making use of it still has a long way to go.

—JENNIFER COUZIN



Galloping Glaciers of Greenland Have Reined Themselves In

Things were looking bad around southeast Greenland a few years ago. There, the streams of ice flowing from the great ice sheet into the sea had begun speeding up in the late 1990s. Then, two of the biggest Greenland outlet glaciers really took off, and losses from the ice to the sea eventually doubled. Some climatologists speculated that global warming might have pushed Greenland past a tipping point into a scary new regime of wildly heightened ice loss and an ever-faster rise in sea level.

So much for Greenland ice's Armageddon. "It has come to an end," glaciologist Tavi Murray of Swansea University in the United Kingdom said during a session at the meeting. "There seems to have been a synchronous switch-off" of the speed-up, she said. Nearly everywhere around southeast Greenland, outlet glacier flows have returned to the levels of 2000. An increasingly warmer climate will no doubt eat away at the Greenland ice sheet for centuries, glaciologists say, but no one should be extrapolating the ice's recent wild behavior into the future.

News of a broad slowdown comes from a wide-ranging survey of glacier conditions across southeastern Greenland. Researchers reported in 2007 that two of the area's major outlet glaciers—Helheim and Kangerdlugssuaq—had slowed by the previous summer. But at the meeting, Murray and 10 of her Swansea colleagues reported results from their 2007 and 2008 surveys of the shape and appearance of the 14 largest outlet glaciers of southeast Greenland. When glaciers speed up, they thin, and their lower, leading edge that floats on the sea retreats. So the Swansea researchers flew laser altimeters over the glaciers to estimate

their changing volumes and, indirectly, their changing velocities. They also studied satellite images and aerial photographs in order to track the movements of natural markings on the ice.

Taken together, the data show "there's a pattern of speeding up to maximum velocity and then slowing down since 2005," Murray said. "It's amazing; they sped up and slowed down together. They're not in runaway acceleration. Something happened that has switched off" the acceleration event of 2003 to 2005.

A short-lived speed-up makes sense if something had given the glaciers some sort of jolt at their lower ends, says glaciologist Richard Alley of Pennsylvania State University in State College. Two possibilities for a disturbance are the warmer air over southern Greenland in recent years and warmer coastal seawater. Either could have eaten away, weakened, and begun to break up the floating seaward ends of outlet glaciers, he says. That would have weakened the glacier's grip on its bounding rock and sent a wave of glacier thinning and acceleration inland. But given time, a glacier would regain its footing—like a fighter rolling with a punch—thicken again, and slow down to its original speed, he says.

That's just what glacial modeler Faezeh Nick of Durham University in the United Kingdom and her colleagues found when they modeled the flow of Helheim Glacier, as they report this week in *Nature Geoscience*. In their model, Helheim, and presumably similar outlet glaciers, is extremely sensitive to disturbances at its margin but can adjust rapidly even as the disturbance continues. "Our results imply that the recent rates of

Glacial two-step. Helheim Glacier's flow to the sea sped up in 2005, as evidenced by the 5-kilometer retreat of its leading edge (left panel to middle panel), but by 2006 it had slowed back down.

mass loss in Greenland's outlet glaciers are transient," the group writes, "and should not be extrapolated into the future."

Not that Greenland's ice is safe, says Alley. "If you turn the thermostat too high, it will melt," he notes. And the glaciers of the West Antarctic Ice Sheet (WAIS), some of which have already picked up speed, don't have the shallow rocky underpinnings that allow Greenland's glaciers to regain their equilibrium. "With nothing to hold on to," he says, "we think [WAIS] will run away."

Tang Hints of a Watery Interior for Enceladus

The search for habitable environs off-Earth is all about liquid water, and Saturn's icy moon Enceladus is looking more and more as though it has the precious substance. The latest evidence comes from Saturn's faint E ring, formed from icy particles spewed out of the moon. At the meeting, planetary scientists reported that the ring particles include the chemicals they would see if a salty ocean lurks beneath the moon's surface.

The key to "tasting" the salty ring grains was the Cosmic Dust Analyzer (CDA) on board the Cassini spacecraft orbiting Saturn. Its mass spectrometer identifies the ions created when hypervelocity particles hit the CDA and explode. At the meeting, planetary scientist Frank Postberg of the Max Planck Institute for Nuclear Physics in Heidelberg, Germany—where the CDA was developed and is operated—and seven colleagues reported the clear detection of

sodium in the E ring's ice particles. Six percent of the particles are rich in sodium and contain salts such as sodium chloride and sodium bicarbonate, along with smaller amounts of potassium. Cassini has traced the ice grains to a towering plume rising from Enceladus's south pole.

The CDA results are what would be expected if water from a deep ocean makes it to the surface and blasts from the fissures of the south pole, the group says. The salts—resembling terrestrial sea salt—are just the ones that liquid water would extract from rock thought to lie deep within the moon. In a poster presentation, CDA team members headed by dynamicist Jürgen Schmidt of the University of Potsdam in Germany argued that the Enceladus plumes must blast out tiny water droplets, not just water vapor. Only liquid could carry off the salts, they say.

Taken together, the salty ice grains appear to counter earlier arguments that Enceladus's plumes arise from frozen, not liquid, water. Geophysicist Susan Kieffer of the University of Illinois, Urbana-Champaign, had pointed out that liquid water could not possibly hold as much gas as Cassini has found in the plumes, but gas-trapping water ice called clathrate could. Planetary scientist Andrew Ingersoll of the California Institute of Technology in Pasadena and the Cassini camera team agrees. "She's right," he says, but "it seems to me, Postberg holds the key to having it both ways." The low-sodium particles could have condensed from vapor coming off clathrates, he says, and the high-sodium grains could come from liquid water. Time will tell whether such a compromise will fly.

The Many Dangers of Greenhouse Acid

If global warming has its hungry polar bears, ocean acidification by greenhouse carbon dioxide has its declining coral reefs. But poster children can be misleading. "It is not good to think about coral reefs as epitomizing all issues of acidification," marine biologist Donald Potts of the University of California, Santa Cruz, warned during a session at the meeting. Other speakers showed that marine life is in peril almost across the board.

Geochemist Justin Ries of the University of North Carolina, Chapel Hill, and colleagues reported that most sorts of calcifying organisms—creatures that grow calcium carbonate skeletons or shells—suffered when pH sank much below the 8.2 of surface ocean seawater. They grew 18 species from eight major calcifying groups in the laboratory for 6 months under a range of carbon dioxide concentrations, including levels expected in the next decade, by the end of the century, and beyond.

Although some species actually increased calcification with modest increases in carbon dioxide, most species—including periwinkles, oysters, urchins, and calcareous green algae—eventually formed less calcium carbonate under greater acidification. There were exceptions. One species of mussel showed no ill effects, and surprisingly, the crustaceans—an edible shrimp, an Ameri-

can lobster, and a blue crab—actually grew thicker shells under even the most severe acidification. But looking at the types of carbonate formed, the group found that only a tube-building worm could protect itself by producing a greater proportion of a more acid-resistant carbonate mineral.

For "higher" marine animals such as squids and fishes, the problems center on respiration—and both carbon dioxide and oxygen come into play. Marine geochemists Peter Brewer and Edward Peltzer of the Monterey Bay Aquarium Research Institute in Moss Landing, California, pointed out that the higher the ratio of carbon dioxide to oxygen dissolved in seawater, the harder it is for the animals to gather oxygen. Seawater carbon dioxide is going up with rising atmospheric levels, they noted, and dissolved oxygen is decreasing in deeper waters as the warming of surface waters slows ocean circulation.

To demonstrate why that's a risky combination, Brewer showed a video of a remotely operated vehicle they used to trap a small squid at a depth of 700 meters and immerse it in a higher-carbon dioxide, lower-oxygen brew. The squid dropped motionless to the bottom of the test vessel. "We can expect multiple impacts as we go forward into this strange CO₂ world," Brewer observed. **—RICHARD A. KERR**



Ouch. Extreme carbon dioxide levels led to dissolution (*bottom*) of normal sea urchin spines (*top*). Scale bars = 1 cm.

Snapshots From the Meeting >>

Following martian water. The news from Mars scientists in search of water was mostly upbeat. Radar probing from orbit shows that the Frozen Sea—supposedly dirt-covered ice—"is not ice," but lava, said planetary geophysicist Roger Phillips of

Southwest Research Institute in Boulder, Colorado. That's the bad news. More encouragingly, spectroscopist Bethany Ehlmann of Brown University reported spectroscopic signs that something had long ago altered minerals in and around impact craters. That alteration looks typical of hot groundwater. And Alfred McEwen of the University of Arizona, Tucson,

showed orbital images of what may be the oldest rock now on the surface. Large impacts probably lifted the so-called megabreccia from deep in the crust. It consists of great boulders embedded in a fine matrix containing water-altered minerals. McEwen's bottom line: "These may be the best places in the solar system to study ... clues to the origin(s) of life."

Some thermometer. Paleoceanographers analyze microscopic plankton remains from a few square centimeters of sea floor to gauge past ocean temperature at that one spot. But paleoclimatologist Melissa Headley of Scripps Institution of Oceanography in San Diego, California, and her colleagues wanted to read the average temperature at one geologic moment of the whole ocean—top to bottom globally—so they took a 1-kilogram chunk of old glacial ice and measured its krypton and xenon gas content. Because the total amount of the noble gases in the atmosphere and ocean remains constant over time and their solubility in water depends on temperature, the changing amount down an ice core provides a whole-ocean temperature history. Their record suggests that changes in the far south of the Southern Ocean helped drive greenhouse warming at the end of the last ice age, 18,000 years ago. **—R.A.K.**



Profound. Jumbled, deep-crustal rock exposed by impacts was once wet and possibly habitable.

CREDITS (TOP TO BOTTOM): TOM KLEINDINST; NASA/JPL/UNIVERSITY OF ARIZONA



LETTERS

edited by Jennifer Sills

Bailing Out Creatures Great and Small

WE ARE FACING A CRISIS OF GLOBAL PROPORTIONS, WITH IMPLICATIONS FOR PEOPLE'S livelihoods, well-being, and quality of life. Such circumstances warrant serious and immediate action, and an impressive commitment of, say, \$700 billion (with apologies to the Paulson/U.S. Treasury Plan) does not seem unnecessarily extravagant.

How does one conceptualize as large a number as 700 billion? Let us put it in the context of the species extinction crisis. An estimated 10 million species populate the earth. To ward against extinction, we could equitably award \$70,000 to each and every one of these 10 million species from our \$700 billion cash injection. The intertidal bryozoans of Scotland's West Coast would alone receive more than \$3 million. In Borneo, the 350 or so species of dipterocarp trees could form a union to demand existence rights, using their \$25 million to lobby for viable landscape mosaics in which they could persist alongside competing land uses. Should this not be sufficient, they could team up with their obligately resident invertebrates, ensuring that funds would not be restrictive. The 43 species of ants from E. O. Wilson's single leguminous tree at the Tambopata Reserve in Peru (1) could pool their resources to buy about 150,000 hectares of Amazonian forest (at \$20 per hectare). The 163 species of beetles occurring exclusively in the tree species *Luehea seemannii* (2) could add an additional 570,000 hectares. Even copepods, those diminutive denizens of the deep, would receive just short of \$1 billion, yet their ubiquity

will ensure that they would have little need of such financial security. Consider though, the jellyfish tree *Medusagyné oppositifolia* from the Seychelles. Even \$70,000 should be enough to save its few remaining individuals, which would no doubt appreciate efforts to promote their populations' longevity by investing in simple nursery facilities and a modest propagation and planting program. The endangered Indonesian "Pakis ata" fern



Lygodium circinnatum would benefit greatly from a \$70,000 cash injection toward its conservation through propagation, and \$700,000 would go a long way in securing the future of the 10 endangered British insects recently featured on Royal Mail stamps.

Species that are doing just fine, on the other hand, could bank their share of funds. The roughly 7.5 million species not considered at risk could bank their collective \$525 billion, hedging their bets against some future need. The interest thereby generated could subsidize species with greater financial and conservation needs and, if reinvested, could maintain the capital stock.

Some species will undoubtedly be declared genetically bankrupt and lost forever, but many more will be offered a lifeline to recovery, flooding the global ecological system with confidence. Growth will be restored.

But where would \$700 billion come from? From borrowing, of course. We have been borrowing from Nature's capital for nigh on the last few centuries—is it not time we paid some back?

JABOURY GHAZOU

Institute of Terrestrial Ecosystems, ETH Zurich, Universitätsstrasse 16, Zurich, Switzerland. E-mail: jaboury.ghazoul@env.ethz.ch

References

1. E. O. Wilson, *Biotropica* **19**, 245 (1987).
2. T. L. Erwin, *Coleopter. Bull.* **36**, 74 (1982).

Proposed French Reforms Miss the Mark

BOTH THE EDITORIAL "LONG ROAD TO RE-form in France" by E. Brézin and A. Triller (27 June 2008, p. 1695) and the News of the Week story "Will French science swallow Zerhouni's strong medicine?" by M. Enserink (28 November 2008, p. 1312) convey the message that shortsighted, leftist scientists are fiercely fighting an overdue modernization of our scientific organization. As someone with practical experience in the French system, I find this position strikingly biased.

The coexistence of INSERM, CNRS, and CEA was not a source of major complication for French scientists as long as our governments kept them functional. We could choose to deal with only one of them, and scientists controlled the direction of each institution. Horrific complications began only when, mainly for ideological reasons, the government began withdrawing real money from INSERM, CNRS, and CEA, and instead redistributed it through a bewildering and ever-increasing number of new program-based agencies.

The French system has long been an example of scientific freedom. Instead of capitalizing on that, France has been desperately trying to kill its own system and to emulate the American way of managing scientists. A system based on fierce selection of scientists—at the expense of wasting qualified people—may be acceptable in America, where the reservoir of scientists extends to the rest of the world. However, in France, scien-

CREDIT: JOE SUTLIF



T cell lineage

466



Tracing life's beginnings

471

tists are much too scarce a resource to be cavalierly dismissed. The French government should not implement a management system based on fear and insecurity at a time when young scientists are already deterred by the treatment of scientists and are fleeing scientific careers. Moreover, before declaring that French and American universities have the same mission, we must recognize the profound differences between the two in functions, resources, and organization.

DIDIER JOB

INSERM U836, Institut des Neurosciences, Université Joseph Fourier, Site Santé à La Tronche, 38 042 Grenoble Cedex 9, France. E-mail: didier.job@ujf-grenoble.fr

Ban Impact Factor Manipulation

THE LETTERS "NEUTRALIZING THE IMPACT factor culture" by A. L. Notkins and "Impact factor fever" by P. Cherubini (10 October 2008, p. 191) discussed the negative effect of the impact factor (IF). Although the IF system has serious flaws (1), for the moment there is nothing better to measure quality of scientific output (2). Instead of trying to get rid of the IF, we should try to make the IF a more reliable number and to prevent misuse.

One way that journals can manipulate their impact factors is by increasing journal self-citation (1). For example, a journal can publish summaries of its own previously published articles, along with relevant self-citations. A journal can also publish editorials and readers' comments on its own published articles—again, with citations. In perhaps the

most questionable editorial policy, editors suggest revision of a submitted manuscript's reference list to include specific relevant articles published in the editor's journal (1). Some have advocated removing all journal self-citations from the IF citation count (3). Every journal has the right to increase its impact factor by attracting the best papers. Disingenuously manipulating impact factor, however, should be banned.

CHRISTIAN WALLNER

Department of Anatomy and Embryology, Academic Medical Center, Meibergdreef 15, Amsterdam, 1105 AZ, Netherlands. E-mail: c.wallner@amc.uva.nl

References

1. M. E. Falagas, V. G. Alexiou, *Arch. Immunol. Ther. Exp. (Warsz.)* **56**, 223 (2008).
2. C. Hoeffel, *Allergy* **53**, 1225 (1998).
3. A. Fassoulaki, K. Papilas, A. Paraskeva, K. Patrís, *Acta Anaesthesiol. Scand.* **46**, 902 (2002).

GOP Must Embrace Science Again

SCIENCE HAS DISAPPEARED FROM REPUBLICAN policy and rhetoric over the past 8 years. It is now almost radical for a Republican to fight for an evidence-based policy process that has not been distorted by political considerations. In this election cycle, large groups of scientists backed Barack Obama. An astonishing 76 Nobel Laureates signed a letter endorsing him (1). Meanwhile, it was hard to find representatives from the McCain campaign who would talk about his science policies.

Derisive statements from Republican leaders about experiments involving grizzly bear DNA (2) and fruit fly studies (3) related to medical discoveries have revealed a lack of understanding about what science and engineering mean for our country. Throughout the campaign, it was clear that science was not a high priority.

This has not always been the case. It was widely known that the first President Bush relied heavily on his science adviser, Allan Bromley. As Bromley wrote in the preface to his book *The President's Scientists*, "No President in memory has been more sensitive than he [George Bush] to the importance of science and technology nor more willing to

actively support them as an investment in the national future" (4).

The new Republican stance toward science isn't Republican and doesn't work—not for effective policy nor for winning elections. Republican ideals such as a strong national defense and security at home depend on science. Limited government and fiscal responsibility are possible when we fund programs that are evidence-based. Basic research stimulates the economy and leads to breakthroughs that are brought to market by private companies.

Learning the right lessons from this election will make all the difference two years from now. For the Republican Party to become relevant again, support of science can't be solely a Democratic issue. It is a national one.

ROBERT WHITE

Palo Alto, CA, USA. E-mail: white@ece.cmu.edu

References

1. A copy of the letter can be found at http://sefora.org/wp-content/uploads/2008/10/nobel_letter_v6.pdf.
2. W. Broad, C. Dean, "Rivals' visions differ on unleashing innovation," *New York Times*, 17 October 2008, A1.
3. L. Stein, "Palin takes on fruit flies—and loses," *Scientific American*, 27 October 2008; available at www.sciam.com/blog/60-second-science/post.cfm?id=palin-takes-on-fruit-flies--and-los-2008-10-27.
4. D. A. Bromley, *The President's Scientists: Reminiscences of a White House Science Advisor* (Yale Univ. Press, New Haven, CT, 1994), p. xiv.

A Word of Caution on the Coca-Cola Way

THE NEWS OF THE WEEK STORY "MALARIA drugs, the Coca-Cola way" (M. Enserink, 21 November 2008, p. 1174) highlighted the vital need for malaria drugs to reach the target market at affordable prices in the poorest countries in the world. The proposed solution, likened to Coca-Cola distribution, is to allow local pharmaceutical dealers to buy medicine directly from the manufacturer at a discount; the Global Fund, World Bank, and others would pay the difference.

This strategy comes with a risk: product diversion. When goods are priced considerably more in one market than another, dishonest local traders buy the goods at the local cheap price and quietly ship them, at profit, to a more expensive market. Before plans are completed to spend public and charitable funds on the "Coca-Cola Way," those responsible must take adequate steps to protect the supply chain.

GRAHAM SATCHWELL

Woodlands House, Science Pharma Limited, Palestine, Andover, Hampshire SP11 7EH, UK. E-mail: graham.satchwell@sciencepharma.co.uk

Letters to the Editor

Letters (~300 words) discuss material published in *Science* in the previous 3 months or issues of general interest. They can be submitted through the Web (www.submit2science.org) or by regular mail (1200 New York Ave., NW, Washington, DC 20005, USA). Letters are not acknowledged upon receipt, nor are authors generally consulted before publication. Whether published in full or in part, letters are subject to editing for clarity and space.

WATER RESOURCES

Data Drought, Data Flood

Jared Farmer

Located on either side of the Grand Canyon, Hoover Dam and Glen Canyon Dam can each hold back about two years' flow of the Colorado River. The resulting reservoirs, Lake Mead and Lake Powell, are listed in encyclopedias as the two largest by volume in the United States. Yet both stand half empty today. According to James Lawrence Powell (the executive director of the National Physical Science Consortium), the present is the future. In the coming era of global warming, Lake Powell may never reach "full pool" again.

The root problem, Powell argues in *Dead Pool*, is that water managers in the Southwest have belatedly and incompletely come to grips with two sets of scientific data—one historical and descriptive, the other theoretical and predictive.

The first set concerns the average historic flow of the Colorado. Insufficient data led to bad policy in 1922, when the Senate ratified the Colorado River Compact. By the terms of this interstate agreement, the Upper Basin (Utah, Wyoming, Colorado, and New Mexico) could use up to 7.5 million acre-feet (MAF) of the river per year—averaged over ten years—provided that the Lower Basin (California, Nevada, and Arizona) received the same amount first. On the basis of streamflow measurements, government scientists had calculated that the Colorado carried 18.5 MAF per year on average. By allocating "only" 15 MAF, the Compact seemingly left a comfortable cushion for yet-to-be-determined Mexican water rights, Native American water rights, and the vagaries of climate.

Unfortunately, the data—a 26-year sample from a 5-million-year-old river—came from a wet period. The average flow of the Colorado for the 20th century turned out to be just about 15 MAF. And recent dendrochronological research suggests that the average over the past millennium was lower still. In other words, politicians overallocated the river. For decades, the Lower Basin lived on bor-



Drought-lowered lake. Bathtub rings encircling the waters impounded behind Glen Canyon Dam.

rowed water—and borrowed time—as the Upper Basin did not fully use its share. But since 1999 the combination of persistently dry weather and explosive metropolitan growth has exposed cracks in the system. A mega-drought—the kind of dry spell recorded repeatedly in tree rings—could induce systemic failure. In a belated response to streamflow recalculations, the seven Colorado River states in December 2007 signed a cooperative agreement that allows joint management of Lakes Mead and Powell in times of drought.

According to the author—a scientific gadfly—the new pact is already out of date. Here's where the second data set comes in. Recent climate modeling—some of it published in *Science* (1–3)—predicts that global warming will produce outstandingly large effects on the U.S. Southwest. Increased temperatures will lead to smaller snowpacks in the Rockies, and these will melt sooner and more completely. As a result, snowmelt will rush downstream before the peak-use months, more of it will evaporate from low-elevation reservoirs, and more of it will be absorbed by dried-out soil. Warming will also cause mountain ice to sublimate at a

higher rate. For all of these reasons, less liquid will be available in the lower Colorado for human consumption.

Using simple open-source spreadsheet software that simulates the flow of the Colorado River (4), Powell tries to quantify the probable impact of global warming. His projections are provocative. Contradicting the U.S. Bureau of Reclamation's forecasts, Powell's trend lines point to systemic failure by 2050. The urban Southwest could violently contract, and Phoenix could depopulate in "a *Grapes of Wrath*-like exodus in reverse."

How can policy-makers avert this doomsday scenario? Powell touches on various proposals, starting with cloud seeding, importation of water from the Columbia River, and ocean water desalination. The first, at a scale large enough to solve the problem, is scientific fantasy; and the second seems like economic and political wishfulness. In contrast, desalination holds promise—although cost-effective, carbon-neutral technology remains elusive without nuclear power. Other partial solutions include subterranean water banking, water conservation and recycling, the retirement of irrigated farms, and the swapping of water rights among different political entities in the river basin.

The vulnerability of the Southwest's water regime has an indicator site: Lake Powell behind Glen Canyon Dam. This impoundment took a "quick" 17 years to fill—and that was during a wet period, 1963–1980. In a warmer, drier future, the Bureau of Reclamation could be forced to operate Glen Canyon Dam at "dead pool": minimal storage with no power production and outflow matching inflow. Maintained at its lowest level, Lake Powell might fill with sediment in decades rather than centuries. Environmentalists have long wished to drain "Lake Foul" and restore the legendary beauty of Glen Canyon; their passionate wish might yet be granted if cold-blooded decision-making prevails. The author argues that there will only be enough water for one big reservoir on the Colorado and that Lake Powell should be sacrificed for a maximal Lake Mead, which services Las Vegas directly and holds greater hydroelectric capacity.

Dead Pool won't win awards for original research or splendid writing. It does, however, offer a solid primer on the history of use of Colorado River water and the science of climate change. The legal, political, economic, and social ramifications of Powell's predictions would require a book of their own. But the author's main purpose is science

Dead Pool
Lake Powell, Global
Warming, and the Future
of Water in the West

by James Lawrence
Powell

University of California
Press, Berkeley, 2008.
298 pp. \$27.50, £19.95.
ISBN 9780520254770.

The reviewer is at the Department of History, State University of New York, Stony Brook, NY 11794, USA. E-mail: jared.farmer@stonybrook.edu

advocacy. Powell wants regional policy-makers to respond to the flood of data on global warming. Otherwise, he says, westerners will find themselves in a megadrought of their own making.

References

1. E. R. Cook, C. A. Woodhouse, C. M. Eakin, D. M. Meko, D. W. Stahle, *Science* **306**, 1015–1018 (2004).
2. R. Seager et al., *Science* **316**, 1181–1184 (2007).
3. T. P. Barnett et al., *Science* **319**, 1080–1083 (2008).
4. www.onthecolorado.org/cross.cfm.

10.1126/science.1169644

LINGUISTICS

Pondering Grammar and God

Andreea S. Calude

Contemplate your life as it is now, the things you hold most dear to you, family, and the beliefs and values you have adopted and hold true. What would your life become if you were to lose them all? Who might you be? These are questions that Dan Everett faced in the course of his fieldwork among the Pirahã people of the Amazonian jungle. *Don't Sleep, There Are Snakes* offers Everett's personal account of the language and life of the tribe and, at the same time, a close-up of his life and experiences in making sense of this new world.

As a trained linguist and devoted Christian, Everett (now in the Department of Languages, Literatures, and Cultures at Illinois State University) set out with his wife and three children to bring the word of God to the Pirahãs. Aiming to succeed where other missionaries had failed, he tried to master the famously difficult Pirahã language (for which the tribe is notorious in linguistics circles) and to break their recalcitrant rigidity toward alien faiths. In a twist of fate, Everett lost all: God, wife, and even linguistic ideology. The Pirahãs left him stripped of these but, in return, provided their own take on life. They taught him about the “immedi-

acy of experience”—the principle he locates at the heart of the Pirahã language and culture. According to Everett, living and speaking for the moment allows the tribe's members to enjoy each day as it comes, to avoid stress and the burnouts that result from worrying about the future, and to disregard the regret and guilt of the past.

The book has two parts. The first describes everyday life within the tribe. Although lacking any temporal organization, this narrative talks in an honest and raw voice about birth, death, eating, hunting, rituals, spirits, sex, family and kinship, growing up, and community among the Pirahãs. The people and stories are intertwined with Everett's own life: as a husband fighting to save his wife and daughter from a near-fatal bout of malaria, as a linguist and fieldworker coping with first-language and first-culture biases, as a Christian coming to terms with dissipating faith, and as a foreigner in a community plotting to kill him. Despite a few confusing aspects of the story (such as how the individual Pirahãs mentioned in the book interact with one another), the prose lures the

siderable extent, innate. Like many of the beliefs the author held when he arrived in the Amazon, generative grammar was soon questioned and discarded because it had “little enlightening to say about the Pirahã language.” The “straight head,” as the Pirahãs term their

language, appears to lack terms for color, number, (distant) past events, and quantifiers. Everett goes so far as to claim that the language lacks recursion, the ability to put one phrase or sentence inside another (in a “matrioshka-doll effect,” as eloquently put by Everett). The absence of recursion is extremely difficult to swallow—not just by Chomskyans, but by any linguist. These claims remain

highly controversial and many linguists dismiss them; however, a field often benefits from the reexamination of some of its more cemented assumptions. Nonetheless, although such health checks are good for the field, they are often extremely tough on those who instigate them.

It is not clear for whom the second part of the book was written. The discussions there are too simple and introductory for the practicing linguist and probably too long and clamoring for the lay reader—although Everett offers good explanations of some basic ideas from linguistics (such as the concepts of tones and tonal languages and the distinction between phonemes and allophones). To his merit, however, the author includes several transcripts of conversations with the Pirahãs. His willingness to present these demonstrates his confidence in his interpretations, and the transcripts add credibility to his argument.

The book is fascinating. In part, that is because Everett provides a personal glimpse of a tribal people living in a remote jungle. More important, we see the world of the Pirahãs through the lens of a unique source: someone whose own world is turned upside down and who possesses an inquisitive and adventurous mind that is, at times, very much in conflict with itself. In addition, *Don't Sleep, There Are Snakes* may serve to bring the furor of linguistics and language research to readers who would otherwise never catch sight of it.

10.1126/science.1169622

Don't Sleep, There Are Snakes

Life and Language in the Amazonian Jungle

by Daniel L. Everett

Pantheon, New York, 2008.

304 pp. \$26.95, C\$32.

ISBN 9780375425028.

Profile, London, 2008. £15.

ISBN 9781846680304.



Immersed among the Pirahãs. Everett with Kaaboboá.

reader with vivid and unexpected incidents that leave one pondering when the movie might be coming out.

The second part focuses on the linguistic aspects of Everett's Amazonian experiences (primarily on the Pirahã language and, more generally, on the author's own ideas). The author trained within the generativist school, founded by Noam Chomsky, that has largely dominated the linguistics arena over the past 50 years. Generativists endorse the idea of an innate universal grammar and propose that language acquisition is, at least to some con-

The reviewer is at the School of Biological Sciences, University of Reading, Reading RG6 6BX, UK. E-mail: acalude@gmail.com

GLOBAL BIOLOGICAL RESOURCES

Could Access Requirements Stifle Your Research?

Sikina Jinnah¹ and Stefan Jungcru²

Scientists from developed and developing countries have expressed concerns about overly restrictive government-imposed requirements to gain access to biological resources needed for academic research (1–5). Indian scientists, for example, have been concerned that exceedingly burdensome international access regulations are driving away international collaborators in fields such as taxonomy, where India has enormous biological potential but limited domestic expertise (6). Scientists globally expressed outrage in 2007

While other nongovernmental stakeholders such as indigenous groups and trade associations have been active participants in the ABS discussions, to date, academic scientists have been relatively silent. Participation does not guarantee that new guidelines will reflect all aspects of scientific concern; however, it would be unfortunate if decisions were made in the absence of scientific voices highlighting how future rules will affect the academic research community. With the negotiations on the ABS regime due to conclude in 2010,

the window for scientific input in the process is quickly closing.

The CBD aims not only to conserve biological diversity but also to address sustainable development-related conservation issues. Specifically, the CBD aims to negotiate rules that facilitate foreign access to genetic resources in biodiversity-rich countries and to ensure that local communities and governments that provide access to those resources are protected from commercial exploitation by powerful foreign interests.

Providers of resources would also be fairly compensated under the future regime. These discussions mostly take place in the Ad Hoc Open-Ended Working Group on Access and Benefit-Sharing (ABSOG), which was created in 2000 (see figure). They focus on issues such as the following: (i) how to ensure prior informed consent from knowledge holders or provider countries before accessing genetic resources and associated traditional knowledge; (ii) how to access genetic resources based on mutually agreed terms between the user and provider countries; and (iii) how sharing benefits arising from the use of these resources could take place. In 2004, the CBD mandated its ABSOG to negotiate an international agreement related to ABS (8), and significant progress has been made in the past year, with many of the basic components starting to

As the rules for foreign access to biological resources are being negotiated, academic researchers and organizations should make their opinions known.

come into focus (9). However, there are still areas of controversy and areas where the implications for the research community have not been fully appreciated.

The most pertinent issue for research academics is whether or not the ABS regime will allow exemptions for samples extracted exclusively for noncommercial academic research. Although this issue has been mentioned at various ABSOG meetings, the final decision has not yet been made. The discussion suffers from a lack of understanding about how academics use biological resources and how to differentiate noncommercial and academic research from commercial research and development.

If an exemption for academic research is not included, or conditions for exemption are so strict as to exclude many researchers, three additional issues are of particular importance to the academic research community. First, ABS negotiators are currently divided over whether “derivatives” of biological material should be subject to benefit-sharing rules and, if so, how derivatives should be defined. In other words, must benefits arising from the use of intermediate research products (such as synthetic processes or isolated gene sequences) as opposed to raw materials (such as plant specimens collected directly from the field) be shared? A broad definition of derivatives would subject intermediate research products and possibly final products, such as new biocatalysts, pharmaceutical products, or even consumer goods, such as coffee, to benefit-sharing obligations. Further, under a broad definition, if derivatives of noncommercial research become the basis for future commercial utilization, researchers could be held responsible for downstream benefit-sharing.

Second, ABS negotiators are divided over whether or not biological material accessed before 1992, when the CBD became legally binding on its member governments, should be covered. Its inclusion would likely require burdensome compliance requirements, because, for example, the necessary information to identify original suppliers of biological material may not have been recorded. So far, practical difficulties associated with this issue have not been reflected in the working document that is currently guiding the ABSOG's discussions (10).



Access. Delegates of the African Group and other biodiversity-rich countries seeking common ground on conditions for access to genetic resources during a meeting of the ABSOG in Geneva in January 2008.

when the primatologist, Marc van Roosmalen, was sentenced to almost 16 years in prison in Brazil for possession of monkeys at his rehabilitation center without appropriate permits (7). The Association for Tropical Biology and Conservation circulated a petition on his behalf, signed by over 250 scientists from 31 countries, condemning the sentence and calling van Roosmalen's situation “indicative of government restrictions on scientists.” Whether such problems are ameliorated or exacerbated in the future may depend on results of the Convention on Biological Diversity's (CBD's) ongoing negotiations to develop an international “regime” for access and benefit-sharing (ABS).

¹Watson Institute for International Studies, Brown University, Providence, RI 02912, USA; sikina_jinnah@brown.edu.

²International Institute for Sustainable Development, Winnipeg, R3B 0Y4, Canada; stefan@iisd.org.

Finally, of critical importance to researchers is the question of whether the CBD should develop international ABS standards, or should allow contracts to be negotiated on a case-by-case basis, subject to minimum standards in different sectors. This issue is one where scientists' field experience would be of tremendous value, as it was during the negotiations of the 2002 International Treaty on Plant Genetic Resources for Food and Agriculture (ITPGRFA) (11–15). The research community could provide similar practical guidance as to the benefits and drawbacks of harmonized, case-tailored, or hybrid approaches to negotiating access to biological research materials.

How can academic scientists get involved? The first step is raising awareness within the academic community about how they may be affected by the results of the negotiations. The CBD secretariat posts documents that detail the issues to be discussed before any ABSWG meeting on its Web site (16). During ABSWG meetings, the International Institute for Sustainable Development's *Earth Negotiations Bulletin* provides daily coverage of what is discussed during the meeting, as well as a summary and analysis of the meetings' outcomes (17). Finally, various nongovernmental organizations, such as Botanic Gardens Conservation International, Bioversity International, or the Swiss Academy of Sciences, regularly post informational materials on their Web sites (18–20).

Second, researchers should engage more actively in the negotiation process. Research institutions and international academic organizations can participate as observers in meetings of the ABSWG. The scientific community should develop a harmonized voice on ABS issues by using existing informal networks and professional associations, such as the Association for Tropical Biology and Conservation. These groups can both continue lobbying domestic governments responsible for negotiating the ABS regime and directly participate in the international negotiations. Bodies qualified in the fields of biodiversity conservation or sustainable use can register as observers at most CBD meetings (21). Although observers do not have voting rights, they are encouraged to take the floor at meetings to voice their opinions. More important, these venues provide scientists direct access to their countries' negotiators to discuss their views.

In addition, frequently, CBD member governments request submissions on a specific issue from both member governments and "other stakeholders." Observer organizations can submit documents in these situations, which the CBD secretariat will make available to member governments before an upcoming

meeting. For example, at the most recent CBD Conference of the Parties (COP) in May 2008, member governments requested relevant stakeholders to submit views, proposals, or operational text and supporting rationales on the potential components of the regime (22). Although documents submitted in response to this request are not yet publicly available on the CBD Web site, they might include suggestions for definitions, or practical mechanisms to facilitate access, benefit-sharing, compliance, and capacity building. This is an opportunity for scientific professional organizations, such as the Society for Conservation Biology, to pool member experience and to prepare a paper on, for example, experiences with overly restrictive access requirements, such as those faced by entomologists in India, when a collaborative project to study the insects of the Western Ghats was derailed by the Indian National Biodiversity Authority for biopiracy concerns (23).

This is not to say to that scientists necessarily have a unified voice on this topic. For example, historical collaborative asymmetries between developed- and developing-country scientists with regard to funding priorities, division of labor, and authorship benefits (24) have highlighted some of the legitimate reasons why provider-country scientists may be reluctant to support open access (25). Nevertheless, this debate has been notably absent from the ABSWG's discussions.

Further, CBD member governments also decided to convene three expert meetings to assist in technical aspects of the regime. The first meeting, held in December 2008, was of particular interest to research scientists because noncommercial research, including how such research might be affected by a future ABS regime, was one of the topics for discussion (26). Participating experts for these meetings are typically nominated by member countries. A good way to be considered for participation is by attending international negotiations, meeting with home-country delegates, and expressing interest in participation.

In addition, a workshop on ABS in Non-Commercial Biodiversity Research, organized by the Barcode of Life Initiative and other science organizations, was held in November 2008. Participants from 10 national science agencies and international organizations exchanged views on the issues to be addressed by the expert meetings, such as ways to distinguish commercial and noncommercial research. The views and recommendations of the workshop have been submitted to the CBD expert meetings (27). Such meetings and workshops provide excellent opportunities for scientists to participate more actively in the ABS negotia-

tions. There are also opportunities now for peer review of studies on technical and legal issues that have been commissioned by the CBD.

There are, of course, many other avenues for participation in the international ABS negotiations. We have described here those entry points that have the highest potential for influence given the short time-line for conclusion of the negotiations by 2010. There are three more meetings of the ABSWG scheduled (28) before the regime is signed and sealed. Industry, environmental, and indigenous organizations are certain to continue making their voices heard. Why not academics too?

References and Notes

1. M. D. Madhusudan *et al.*, *Curr. Sci.* **91**, 1015 (2006).
2. K. ten Kate, *Science* **295**, 2371 (2002).
3. K. S. Bawa, *Curr. Sci.* **91**, 1005 (2006).
4. R. Pethiyagoda *et al.*, *Curr. Sci.* **92**, 426 (2007).
5. A. Revkin, *New York Times*, 7 May 2002, p. F1.
6. K. T. Prathapan *et al.*, *Curr. Sci.* **94**, 170 (2008).
7. E. Check, T. Hayden, *Nature* **448**, 634 (2007).
8. The ABSWG deals with ABS requirements for international users, not domestic ABS requirements that would apply to in-country scientists.
9. See *Earth Negotiations Bulletin* reports in vol. 9, no. 398 (2007); no. 416 (2008); and no. 452 (2008), from the International Institute for Sustainable Development, Winnipeg, Canada; available at www.iisd.ca/vol09/.
10. See Annex of CBD COP9 Decision IX/12; www.cbd.int/decisions.
11. C. Fowler, *Science* **297**, 157 (2002).
12. R. Sauvé, J. Watts, *Agric. Syst.* **78**, 307 (2003).
13. S. Jungcurt, *Institutional Interplay in International Environmental Governance: Policy Interdependence and Strategic Interaction in the Regime Complex on Plant Genetic Resources for Food and Agriculture* (Shaker, Aachen, Germany, 2008).
14. H. D. Cooper, *Rev. Eur. Community Int. Environ. Law* **11**, 1 (2002).
15. C. Fowler, *Genet. Resour. Crop Evol.* **51**, 609 (2004).
16. Access and Benefit-Sharing, CBD, www.cbd.int/abs.
17. Available at www.iisd.ca.
18. Botanic Gardens Conservation International, www.bgc.org.
19. Bioversity International, www.bioversityinternational.org.
20. Access and Benefit-Sharing, <http://abs.scnat.ch>.
21. To register, the chief executive or president of an organization must submit an official letter to the CBD executive secretary indicating names, titles, and contact details of proposed attendees.
22. CBD COP9 Decision IX/12, www.cbd.int/decisions.
23. K. S. Jayaraman, *Nature* **452**, 7 (2008).
24. J. Gaillard, *Knowl. Technol. Policy* **7**, 31 (1994).
25. E. Masood, *SciDevNet News*, 15 April 2004; www.scidev.net/en/news/developing-world-slow-to-share-biodiversity-data.html.
26. This Technical Expert Group convened 2 to 5 December 2008 in Windhoek, Namibia. For further information contact secretariat@cbd.int.
27. The workshop was held 16 to 19 November 2008 in Bonn, Germany. Submissions are available at www.cbd.int/.
28. Tentative dates and venues for these meetings are ABS7: 2 to 8 April 2009, Paris, France; ABS8: 9 to 15 November 2009, Kuala Lumpur, Malaysia; and ABS9: 1 to 7 April 2010, Bogotá, Colombia.
29. Supported by NSF, University of California (U.C.) at Berkeley Institute for International Studies, U.C. Institute for Global Conflict and Cooperation, Soroptimist International, German Foundation for Nature Conservation (DBU). We thank our colleagues of the *Earth Negotiations Bulletin* and its donors, as well as ABSWG Cochair T. Hodges, B. Fraleigh, and P. Chasek.

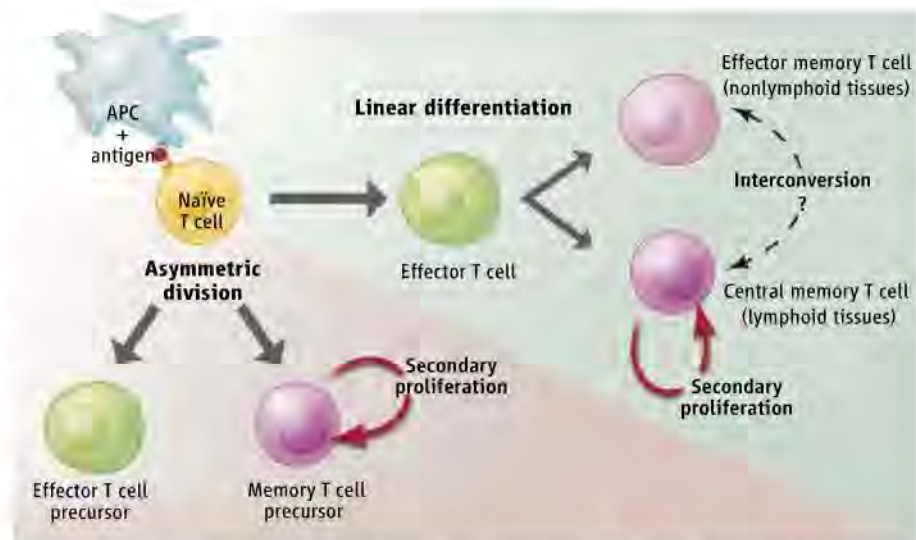
Ex Uno Plura

Sonia Feau and Stephen P. Schoenberger

The response of a specific subset of immune cells (T cells) to infection is characterized by the capacity to become functionally specialized in response to the particular pathogen and, consequently, to shift T cell population dynamics. Two reports in this issue, by Bannard *et al.* on page 505 (1) and Texeiro *et al.* on page 502 (2), shed new light on how the distinct subsets of T cells that mediate acute versus long-term protection to infection can arise from a single precursor.

Our long-term health and survival depend on the ability of a subset of T cells ($CD8^+$) to quickly generate a potent population of effector T cells that can limit an ongoing infection, as well as memory T cells that provide long-term immunity should the same pathogens be reencountered. Accordingly, two main subsets of $CD8^+$ T cells, distinguishable by their location, function, and longevity, are generated in response to vaccination or acute infection. Effector cells are short-lived and numerous, comprising 90 to 95% of $CD8^+$ T cells at peak response, and can deploy a variety of cytokine and cell contact-dependent cytotoxic mechanisms to eradicate infected cells and thereby control acute infection. Memory T cells serve as a long-term “insurance policy” by providing a swift and effective response to reinfection by the same pathogen. There is further heterogeneity within this memory cell population. Cytotoxic effector memory T cells act as sentinels in the blood and peripheral tissues where reinfection is most likely to occur, and central memory T cells in the secondary lymphoid organs undergo a second round of clonal expansion upon reencounter of their inducing antigen (3).

Given the phenotypic and functional heterogeneity among the $CD8^+$ T cell responders, a central goal has been to determine the ontogeny and lineage relationships among their apparently disparate constituent subsets. Of the several models that have been proposed, two posit that the effector and memory T cells measured after infection or immunization descend from either distinct or common precursors. A single naïve $CD8^+$ T cell (mature but not yet stimulated by a foreign antigen) can give rise to each of the effector and memory subsets measurable after acute infection, indi-



From one, many. The development of the distinct types of memory $CD8^+$ T cells from a single clonal precursor might occur according to the asymmetric cell division model, in which a stimulated naïve T cell produces two daughter cells with distinct fates—one giving rise to effector T cells and the other to memory T cells. Only the latter can undergo secondary expansion in response to antigen. In the linear T cell differentiation model, memory T cells that descend from effector T cells retain the capacity for secondary clonal expansion.

cating that naïve cells are pluripotent and that specific fates are determined either coincident with or after the first round of cell division (4). In addition, the first round of $CD8^+$ T cell division is asymmetric with respect to the partitioning of key molecules, producing one daughter cell that serves as a precursor to the effector cell subset whereas the other daughter cell is destined to become the memory cell precursor (5) (see the figure). This model predicts that primary effector T cells are incapable of secondary expansion, a hallmark function of the memory subset. The second model proposes that memory cells arise directly from effector T cells, with their specific subspecialty and location (effector versus central memory T cells) determined by additional events, and perhaps being subject to interconversion (6, 7). Under this model, effector cells would either possess replicative function or differentiate directly into memory cells. A key difference between these models, therefore, lies in whether bona fide effector cells retain the ability to undergo a secondary proliferative response.

Bannard *et al.* approached the question of lineage relationship by devising an elegant experimental system through which $CD8^+$ T cells differentiating into the effector lineage in response to viral infection can be conditionally and irreversibly marked to allow their secondary proliferative response to be measured after

T cells that respond quickly to infection and later to reinfection arise from a single precursor cell type.

rechallenge. This was achieved by creating transgenic mice in which treating the animals with the compound tamoxifen induced the expression of a fluorescent reporter protein, but only in cells that expressed Granzyme B, a cytolytic granule protein that mediates cytotoxicity in $CD8^+$ T cells (8, 9). Thus, Bannard *et al.* could follow the repertoire of endogenous, antigen-specific T cells responding to infection in an animal and avoid the artifacts in clonal expansion and differentiation that can occur in approaches that use the adoptive transfer of transgenic T cells (10–12). By administering tamoxifen at various times after viral infection, Bannard *et al.* found that $CD8^+$ T cells that have differentiated into the effector lineage can nonetheless display a secondary replicative potential upon rechallenge that is comparable with that of all virus-specific $CD8^+$ T cells. This finding would not have been predicted by the asymmetric division model, and shows that cells that have acquired effector cell function during primary infection can indeed display the secondary replicative capacity of memory cells, a result that is consistent with a linear differentiation model.

The ability of memory $CD8^+$ T cells to mount a secondary proliferative response appears to be “programmed” by inductive signals transmitted to clonal precursors during their initial priming and executed by their

Laboratory of Cellular Immunology, La Jolla Institute for Allergy and Immunology, La Jolla, CA 92037, USA. E-mail: sps@liai.org

clonal progeny upon restimulation by the same antigen. These include signals provided by a subset of helper T cells ($CD4^+$) and the cytokine interleukin-2 (13–17). Teixeira *et al.* show that the T cell receptor, a heterodimeric protein that serves as the antigen-specific sensor for T cells, also helps to generate the intracellular signals necessary for a primed T cell to differentiate into a memory cell. The authors found that antigen-specific $CD8^+$ T cells expressing a T cell receptor bearing a single point mutation in the transmembrane domain portion of the β chain undergo a primary response to antigen that is indistinguishable from that of cells bearing a wild-type version of the same receptor. Despite this normal primary response, the cells with the mutated T cell receptor are nonetheless unable to mount a secondary proliferative response to antigenic rechallenge, thus failing a key test of the ability to function as memory cells. This finding supports the idea that secondary clonal expansion is a discrete functional capacity that is conferred, among other signals, by T cell receptor

stimuli that are qualitatively distinct from those that lead to differentiation into an effector cell. Given that the relevant signals were received by the clonal precursors for both effector and memory cells, this “action at a distance” suggests that unique signaling events within a clonal precursor cell are integrated into a distinct program of gene expression that regulates the fate of its daughter cells. Consistent with this idea, Teixeira *et al.* found that cells expressing the T cell receptor with the mutation displayed differences in recruiting an intracellular signaling protein (protein kinase C- θ) to the “immune synapse” formed between a T cell and an antigen-presenting cell (APC) and in translocation of the transcription factor nuclear factor κ B to the nucleus. Though it is unknown how the pattern of gene expression in $CD8^+$ T cells expressing the mutated T cell receptor might differ from that of their wild-type counterparts after primary and secondary stimulation with antigen, this information should add to the list of molecules expressed in $CD8^+$ T cells that help establish and maintain the mem-

ory state. In this way the operationally defined state of immune memory can be put on a more rigorous and defined molecular foundation that will facilitate the next generation of experimental studies.

References

1. O. Bannard, M. Kraman, D. T. Fearon, *Science* **323**, 505 (2009).
2. E. Teixeira *et al.*, *Science* **323**, 502 (2009).
3. F. Sallusto, J. Geginat, A. Lanzavecchia, *Annu. Rev. Immunol.* **22**, 745 (2004).
4. C. Stemberger *et al.*, *Immunity* **27**, 985 (2007).
5. J. T. Chang *et al.*, *Science* **315**, 1687 (2007).
6. J. T. Opferman, B. T. Ober, P. G. Ashton-Rickardt, *Science* **283**, 1745 (1999).
7. E. J. Wherry *et al.*, *Nat. Immunol.* **4**, 225 (2003).
8. R. Feil, J. Wagner, D. Metzger, P. Chambon, *Biochem. Biophys. Res. Commun.* **237**, 752 (1997).
9. S. Srinivas *et al.*, *BMC Dev. Biol.* **1**, 4 (2001).
10. V. P. Badovinac, J. S. Haring, J. T. Harty, *Immunity* **26**, 827 (2007).
11. J. Jacob, D. Baltimore, *Nature* **399**, 593 (1999).
12. A. L. Marzo *et al.*, *Nat. Immunol.* **6**, 793 (2005).
13. E. M. Janssen *et al.*, *Nature* **434**, 88 (2005).
14. E. M. Janssen *et al.*, *Nature* **421**, 852 (2003).
15. D. J. Shedlock, H. Shen, *Science* **300**, 337 (2003).
16. J. C. Sun, M. J. Bevan, *Science* **300**, 339 (2003).
17. M. A. Williams, A. J. Tyznik, M. J. Bevan, *Nature* **441**, 890 (2006).

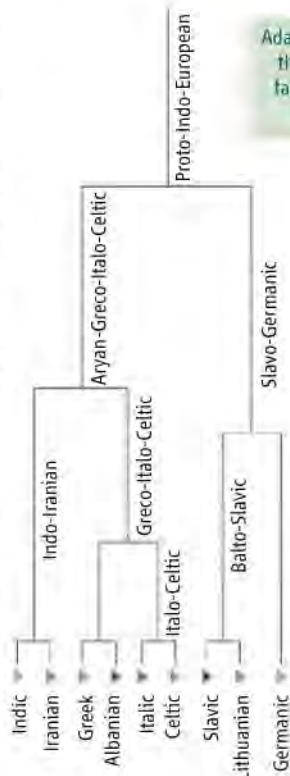
10.1126/science.1169409

ANTHROPOLOGY

Where Bacteria and Languages Concur

Colin Renfrew

Two articles in this issue mark a substantial advance in our understanding of human population history in the Pacific area. On page 479, Gray *et al.* (1) report a computational linguistic analysis that offers a detailed and precise scenario for the dispersal and development of the Austronesian languages, and by implication of human populations among the Pacific islands. The authors come down decisively in favor of one of the two major models for the peopling of the Pacific. On page 527, Moodley *et al.* (2) come to the same conclusion as Gray *et al.* about the source and trajectory of spread of the human populations in question, based on results from a seemingly unrelated field: the archaeo-



Adaptation of the family tree for the Indo-European language family, produced by Augustus Schleicher in 1863 (10)

genetics of human gastric bacterial parasites. In the rapidly developing field of computational historical linguistics (3), this impressive reassessment of the Pacific languages and its corroboration from a very different source are likely to have an impact in linguistic studies far beyond the Pacific area.

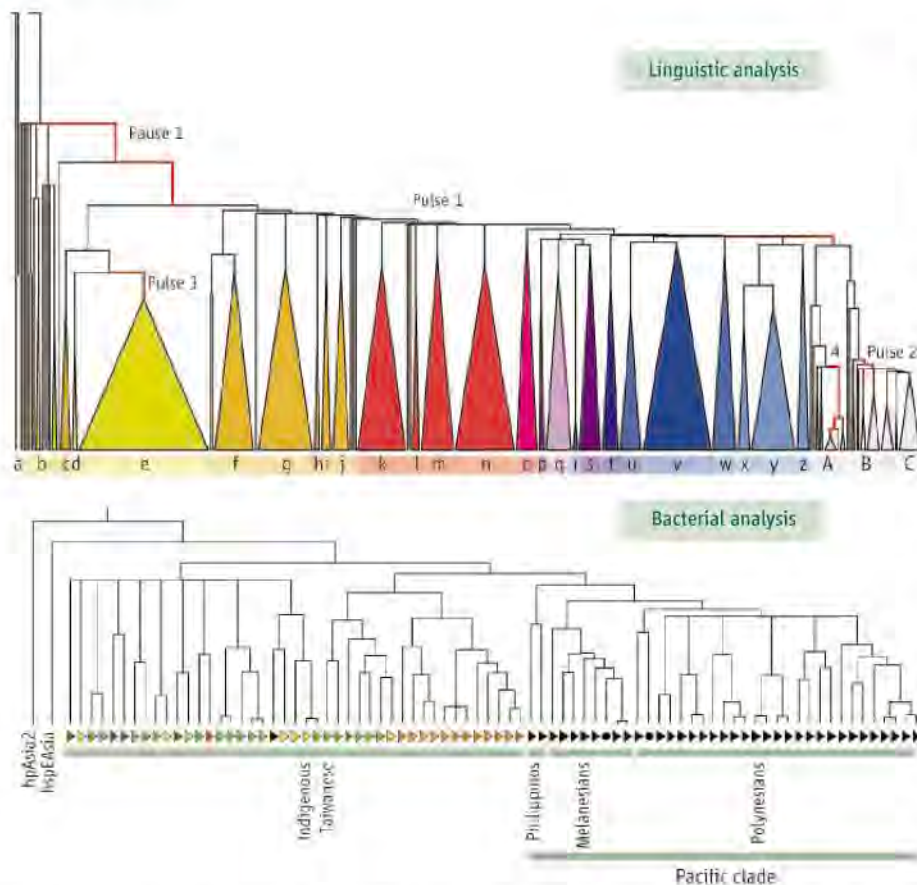
The reconstruction of Pacific population history, especially in Polynesia, has been a focus of archaeological interest for many years. The recognition of a characteristically decorated pottery

Genetic data from human gastric bacteria provide independent support for a linguistic analysis of Pacific population dispersals.

style as a marker left by the first human inhabitants of western Polynesia is one of the contributions made by prehistoric archaeology (4). Because this pottery is associated with the first crop cultivators in the area, agricultural dispersal is often seen as a vehicle for language dispersal.

The languages of Polynesia are part of the widely distributed Austronesian language family, one of the largest language families in the world (5). Its more than 1000 constituent languages include the Micronesian and Polynesian subfamilies as well as the languages of Malaya, much of Indonesia, the Philippines, Taiwan, and Madagascar. The origin of this family has been disputed. One theory, favored by many linguists, places the homeland of the Austronesian languages in Taiwan (6), where languages of several Austronesian subfamilies are located and where farming communities existed as early as 5000 years ago. This theory envisages a farming-language dispersal from Taiwan to the Philippines and then to West Polynesia, starting around 5000 years ago. The alternate, gradualist model sees the process starting very much earlier in island Southeast

The McDonald Institute for Archaeological Research, University of Cambridge, Cambridge CB2 3ER, UK. E-mail: renfrew@mcdonald.cam.ac.uk



Phylogenetic trees for Pacific human populations. (Top) Tree derived from linguistic data by Gray *et al.* (Bottom) Tree based on DNA analysis of the bacterium *H. pylori* by Moodley *et al.*

Asia (7). Genetic studies have given conflicting results, and human mitochondrial DNA data do not seem to point to a Taiwanese origin for the populations that now speak Austronesian languages (8). The archaeogenetic evidence is, however, not easy to interpret, and there may have been substantial gene flow in recent colonial times (9).

Gray *et al.* now apply computer-based phylogenetic methods to this problem. Language trees have been a tool in historical linguistics since the 19th century (see the first figure) (10), but the computational analysis enables a more systematic investigation, which also offers a chronology for the various stages. Gray and Atkinson previously used the same method to study the Indo-European language family (11), but that analysis has not yet found favor with most historical linguists. The present analysis of the Pacific languages is, however, based on a very much larger database of more than 400 languages [compared with 87 languages in (11)]. Moreover, it relies for its lexical data on the work of Blust (12) and other linguists generally regarded as the leading authorities on the Austronesian languages.

A remarkably clear scenario emerges (see the second figure, top panel). The dating rests

on 10 externally dated calibration points, of which the more ancient are based on the archaeological data for the Austronesian entry into the Philippines, Micronesia, and Eastern Polynesia (13). The overall scenario, however, derives from the topology of the tree, which does not depend on the archaeology. In the scenario, an Austronesian origin in Taiwan ~5200 years ago was followed by a first pause, and then a major pulse or migration dispersal reaching across the Pacific as far as Micronesia ~3000 years ago. A second pause occurred after the settlement of Western Polynesia around 2800 years ago. A second migration after 1500 years ago led to the peopling of Central and Eastern Polynesia. The level of detail offered by the analysis is impressive, and because the method relies on archaeologically or historically established calibration points, the nodes in the tree—that is, the splitting points resulting from human dispersals—can be dated to within a few centuries.

Support for this picture comes from Moodley *et al.*'s genetic analysis of samples for the bacterial parasite *Helicobacter pylori*, taken from the genetic tracts of Pacific human populations. The data also strongly favor a Taiwanese origin, producing a tree (see the sec-

ond figure, bottom panel) that is similar in many ways to the linguistic tree of Gray *et al.* The analysis relies on the observation that, although most human populations share a gastric flora of *H. pylori*, at a molecular genetic level these bacteria differ from continent to continent. These differences are likely to be the product of genetic drift following the splitting and separation of populations. These processes enable reconstruction of a phylogenetic tree similar to that derived from human mitochondrial or Y-chromosome DNA (14). The dates in the bacterial analysis have large error margins and are again derived from archaeologically dependent calibration points. So the fact that both papers date the dispersal from Taiwan to ~5000 years ago is not so much a corroboration but a result of using the same archaeological data. But the topology and detail of the two trees are genuinely independent.

It will be interesting to see how well the topologies of the two trees correlate at a more detailed level, as clearly they do in general structure. The use of modern genetic data to reconstruct phylogenetic trees shows that the past is still “within us” (15) today. Our past is within us in a different sense when the vocabularies of specific modern languages are the basis for historical analysis. And the past is within us in a very literal way when the early history of humankind is reconstructed based on the bacterial flora in our guts. The convergence between the approaches suggests that a synthesis between linguistic and genetic interpretations of human history may soon be possible on a worldwide basis.

References

1. R. D. Gray, A. J. Drummond, S. J. Greenhill, *Science* **323**, 479 (2009).
2. Y. Moodley *et al.*, *Science* **323**, 527 (2009).
3. C. Renfrew, P. Forster, Eds., *Phylogenetic Methods in the Prehistory of Languages* (McDonald Institute for Archaeological Research, Cambridge, UK, 2006).
4. P. V. Kirch, *The Lapita Peoples* (Blackwell, Cambridge, MA, 1997).
5. M. Ruhlén, in *A Guide to the World's Languages* (Stanford Univ. Press, Stanford, CA, 1991), pp. 160–172.
6. P. Bellwood, in *First Farmers, The Origins of Agricultural Societies* (Blackwell, Malden, MA, 2005), pp. 128–145.
7. J. Allen, *Pac. Prehist.* **19**, 186 (1984).
8. S. Oppenheimer, M. Richards, *Sci. Prog.* **84**, 157 (2001).
9. M. E. Hurles *et al.*, *Am. J. Hum. Genet.* **72**, 1282 (2003).
10. A. Schleicher, *Die Darwinische Theorie und die Sprachwissenschaft* (H. Boehlau, Weimar, 1863).
11. R. D. Gray, Q. D. Atkinson, *Nature* **426**, 435 (2003).
12. R. Blust, *The Austronesian Languages* (Pacific Linguistics, Canberra, in press).
13. A. Pawley, in *Examining the Farming/Language Dispersal Hypothesis*, P. Bellwood, C. Renfrew, Eds. (McDonald Institute for Archaeological Research, Cambridge, UK, 2002), pp. 251–274.
14. D. Falush *et al.*, *Science* **299**, 1582 (2003).
15. C. Renfrew, P. Forster, M. E. Hurles, *Nat. Genet.* **26**, 253 (2000).

PHYSICS

Teleporting a Quantum State to Distant Matter

M. S. Kim and Jaeyoon Cho

One of the many paradoxes introduced by quantum mechanics is entanglement. When two or more objects are entangled, knowing the quantum states of individual objects separately does not enable us to know the whole system because of their strong correlation. Quantum information processing exploits these entangled states in applications such as computation and cryptography, and one of its most useful tools is teleportation (1), which transfers a quantum state between two systems in separate locations. On page 486 of this issue, Olmschenk *et al.* report the teleportation of a quantum state between two ytterbium ions (Yb^+) that are separated by a distance of 1 m (2). Although photon states have been teleported over much longer distances (3, 4), the teleportation of quantum states of stationary particles with mass over macroscopic distances has important practical implications such as the simultaneous transfer and storage of a quantum state at a fixed remote place.

Quantum teleportation requires two communication channels, one for classical information and the other for entangled quantum states, set up between the sender ("Alice") and the receiver ("Bob"). Alice performs a joint measurement between her particle of their entangled pair and a particle prepared in a quantum bit or qubit—which, like a classical bit, has values of 0 and 1 but can also be in a superposition of two quantum states—which she wants to send to Bob. Upon Alice's measurement, Bob's particle is left in a quantum state that can be recovered with simple transformations as Alice's qubit; Alice sends the results of her measurement (1) to Bob along the classical channel, then he knows if he has the correct qubit that Alice teleported, or must recover it with what is called a unitary transformation.

In 1997, Bouwmeester *et al.* reported the first experimental realization of quantum teleportation for photon states (3). A pair of photons, which are entangled in their polarization states, was generated from a higher-energy photon through parametric down-conversion, and by the joint measurement of one of the pair and the original photon, the other photon

comes to embody the quantum state of the original photon (or can be converted to it via a unitary transformation). However, the quantum teleportation of states between two matter systems at macroscopic distances was not to be realized for another 10 years.

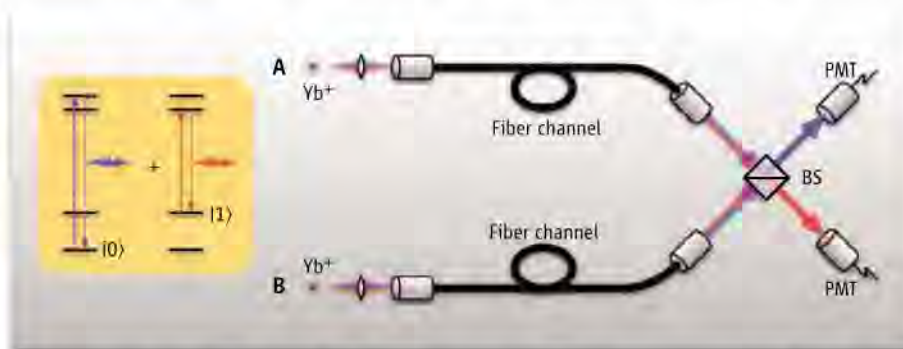
Quantum teleportation of electronic-level quantum states was initially performed between pairs of ions trapped in a harmonic potential a few micrometers in size (5, 6). This physical system may be useful for quantum gate operations between nonadjacent qubits, but the experimental principle could not be extended to long-distance teleportation because of the molecular dimensions of a harmonic potential within which entanglement generation and joint measurement can be performed.

Spins, atoms, and ions are well suited for logical gate operations and storage, whereas photons are advantageous for long-distance communication. Thus, the development of

A quantum state is teleported between two atoms that are 1 meter apart through their entanglement with photons.

ter, they interfered and exited together in one of the two output ports. However, when the two photons were distinguishable, they did not interfere. Beugnon *et al.* earlier reported a similar result, but the atoms were separated by only 6 μm (9). This so-called Hong-Ou-Mandel interferometer (10) works because of the quantum nature of single photons and is frequently used to prove the indistinguishability of two single photons. Experiments (7) and (8) are important building blocks for Olmschenk *et al.*'s teleportation (2).

Matsukevich and Kuzmich noted that atom-photon coupling becomes stronger by increasing the number of atoms in a trap, and showed quantum state transfer between photons and atomic clouds (11). Earlier, a pair of nonclassically corrected photons was generated by an atomic cloud (12, 13). Quantum teleportation between photons, with the atomic cloud used as a memory, was successfully performed (14). This achievement was



Entanglement swaps with atoms. (Left) A laser pulse excites the electronic energy state (from the lower S levels to the upper P levels). A subsequently emitted photon in either blue or red is entangled with the atom. **(Right)** The two emitted photons are mixed on a beam splitter (BS). Teleportation is successful if a different-color photon is detected in each of the photomultiplier tubes (PMT).

atom-photon entanglement has been an important prerequisite to the transmission of quantum states over long distances between atoms by photonic qubit states. For example, Blinov *et al.* (7) connected the two polarization states of a photon with the two possible states of an atom after it emitted a photon. The same group later showed quantum interference of two single photons emitted from two Yb^+ ions in their respective traps, which are a distance of 1 m apart (8). When two indistinguishable photons were sent into two input ports of a beam split-

ter, they followed by the experimental proof of entangling two atomic clouds with photons as a mediator (15).

Olmschenk *et al.* do not follow the standard teleportation protocol because of the difficulty in establishing an entangled channel. They use entanglement swapping instead, which makes the scheme versatile and efficient as it allows expansion into a series of quantum teleportation.

In their experiment, two Yb^+ ions are stored in independent traps that are separated by 1 m.

School of Mathematics and Physics, Queen's University Belfast, BT7 1NN, UK. E-mail: m.s.kim@qub.ac.uk (M.S.K.); chooor@gmail.com (J.C.)

The quantum state $\alpha|0\rangle + \beta|1\rangle$, composed of electronic energy levels, to be teleported is written onto atom A with a microwave pulse. Another microwave pulse prepares atom B in a definite superposition state $|0\rangle + |1\rangle$. Next, an ultrafast laser pulse puts each atom into an excited state (see the figure, left panel). The excited atoms then emit a photon and return back to their initial states (either $|0\rangle$ or $|1\rangle$); the emitted photon's energy depends on the electronic state in which the atom initially resided. The energy of the emitted photon becomes entangled with the atomic state.

The two photons from the two atoms are jointly measured with a beam splitter, which mixes the two input photons (see the figure, right panel), and the atom-photon entanglement is transferred to interatom entanglement, which is the entanglement swap. Next, atom A is measured to yield 0 or 1, and the measurement outcome is sent to atom B. This final mea-

surement causes atom B to embody the initial quantum state $\alpha|0\rangle + \beta|1\rangle$ of atom A (again, via a unitary transformation). The authors confirmed the success of the quantum teleportation through full tomography of the atomic state.

There are several advantages to Olmschenk *et al.*'s experimental approach. Single atoms in free space are used in both ends of the teleportation, so the state preparation and measurement are easy. The single atoms also ensure the emission of single photons. The use of photons for a quantum channel opens the possibility for teleportation to reach long distances. This experiment is an important step toward the realization of quantum repeaters with built-in memory (16), which is a key component in long-distance quantum communication. With the recent experimental advances, the theoretically presumed quantum paradoxes are slowly revolutionizing information technology.

References and Notes

1. C. H. Bennett *et al.*, *Phys. Rev. Lett.* **70**, 1895 (1993).
2. S. Olmschenk, *et al.*, *Science* **323**, 486 (2009).
3. D. Bouwmeester *et al.*, *Nature* **390**, 575 (1997).
4. H. de Riedmatten *et al.*, *Phys. Rev. Lett.* **92**, 047904 (2004).
5. M. Riebe *et al.*, *Nature* **429**, 734 (2004).
6. M. D. Barrett *et al.*, *Nature* **429**, 737 (2004).
7. B. B. Blinov, D. L. Moehring, L.-M. Duan, C. Monroe, *Nature* **428**, 153 (2004).
8. P. Maunz *et al.*, *Nat. Phys.* **3**, 538 (2007).
9. J. Beugnon *et al.*, *Nature* **440**, 779 (2006).
10. C. K. Hong, Z. Y. Ou, L. Mandel, *Phys. Rev. Lett.* **59**, 2044 (1987).
11. D. N. Matsukevich, A. Kuzmich, *Science* **306**, 663 (2004).
12. A. Kuzmich *et al.*, *Nature* **423**, 731 (2003).
13. C. H. van der Wal *et al.*, *Science* **301**, 196 (2003).
14. Y.-A. Chen *et al.*, *Nat. Phys.* **4**, 103 (2008).
15. Z.-S. Yuan *et al.*, *Nature* **454**, 1098 (2008).
16. L.-M. Duan, M. D. Lukin, J. I. Cirac, P. Zoller, *Nature* **414**, 413 (2001).
17. We acknowledge the UK Engineering and Physical Sciences Research Council and the UK Quantum Information Processing Interdisciplinary Research Centre at Oxford for financial support.

10.1126/science.1169279

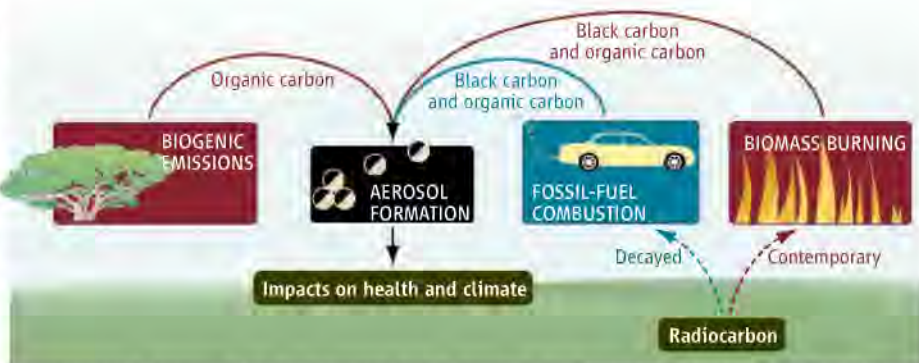
ATMOSPHERE

Sources of Asian Haze

Sönke Szidat

Carbonaceous aerosols—that is, the carbon-containing aerosol fraction, such as soot—can affect both climate and human health, especially in regions where the atmosphere contains high levels of such particles. Yet, knowledge of the sources of the aerosols is limited. On page 495 of this issue, Gustafsson *et al.* (1) use radiocarbon (^{14}C) analysis as an atmospheric tracer to quantify biomass and fossil-fuel contributions to the atmospheric “brown clouds” (2) over South Asia, a persistent and large-scale pollution layer of haze. The results resolve a discrepancy between measurements of other atmospheric tracers and calculations of emission-based inventories for carbonaceous aerosols.

Typically, urban particulate matter comprises ~40% carbonaceous aerosol (total carbon) (3), which is traditionally divided into black carbon and organic carbon. Black carbon is optically absorptive and chemically little reactive. It is emitted during oxygen-deficient combustion of biomass and fossil fuels (see the figure) (4, 5). Biomass burning is dominated on a global scale by fires due to slash-and-burn land clearance, waste burning in agriculture and forestry, and residential wood combustion for heating and cooking. As for fossil-fuel



Source apportionment. Radiocarbon analysis allows fossil and nonfossil sources of black carbon and organic carbon to be identified. [Adapted from (12)]

burning, submicrometer soot particles (consisting mostly of black carbon) are mainly produced in diesel engines and during heating with hard and brown coal. Organic carbon contains lighter, nonabsorptive organic compounds, which are directly emitted or formed by atmospheric oxidation of precursor gases (5, 6); both anthropogenic and biogenic sources are known.

The consequences of high carbonaceous-aerosol concentrations are especially severe in the case of the tropical atmospheric brown clouds (2). First, pollution from particulate matter is responsible for cardiovascular and respiratory diseases, inducing acute symptoms, chronic diseases, or even mortality (7, 8); this is intensified in South Asia due to

high concentrations of black carbon, which is carcinogenic in addition to the other health effects (7). Second, the haze layer causes cooling and takes up air moisture persistently so that rain events become rarer during the dry season, but are intensified when they occur (2).

Efforts to reduce the extent of atmospheric brown clouds require knowledge of their sources. Several approaches have been used to apportion sources and quantify emissions, but all have drawbacks (5, 6, 9). Emission-based inventories evaluate all potential emission processes of an atmospheric species on a local scale and extrapolate them to a larger scale (4). This estimation is reasonably accurate and precise for species with few different emission

Department of Chemistry and Biochemistry, University of Berne, Freiestrasse 3, 3012 Berne, Switzerland. E-mail: szidat@iac.unibe.ch

processes, but not satisfactory for complex source patterns. Receptor-based techniques aim to reconstruct emissions by measuring ambient concentrations of source-specific tracers such as the inorganic composition, organic marker compounds (10), or black carbon/total carbon ratios (11) and comparing these with known source profiles. However, the aerosol may be altered chemically during atmospheric transport from the source sites to the receptor site, such that the source profiles lose validity with distance from the origin.

In contrast to these techniques, analysis of the long-lived radioactive isotope ^{14}C unambiguously separates fossil from nonfossil sources, because ^{14}C has completely decayed in fossil fuels, whereas modern materials have the contemporary radiocarbon level (1, 12–14). It is thus a unique source apportionment tool (9, 10). The carbon isotopic composition of the carbonaceous aerosol is practically stable during transport from the source

sites to the receptor site, allowing receptor-based identification of sources even if they are remote from the emissions and have undergone chemical transformations.

Gustafsson *et al.* use ^{14}C to distinguish fossil-fuel and biomass-burning contributions to the total carbonaceous aerosol and to black carbon for pollution events in South Asia. They find a much larger contribution of biomass combustion to black carbon emissions (46 and 68% for two different black carbon fractions) than do other tracer techniques [for example, 10 to 40% from black carbon/total carbon ratios (11)]. The study shows that the importance of biomass burning for local and global black carbon budgets has been underestimated. This was previously pointed out for urban, rural, and remote areas in Europe (12–14), but never were the consequences as severe as for the Asian haze.

There is an urgent need for further studies of this kind. Only the application of diverse state-of-

the-art techniques will allow the complex source mixture of carbonaceous aerosols to be disentangled. Here, radiocarbon analysis of the fossil and nonfossil sources will be a powerful tool.

References

1. Ö. Gustafsson *et al.*, *Science* **323**, 495 (2009).
2. V. Ramanathan, P. J. Crutzen, *Atmos. Environ.* **37**, 4033 (2003).
3. U. Pöschl, *Angew. Chem. Int. Ed.* **44**, 7520 (2005).
4. T. C. Bond *et al.*, *J. Geophys. Res.* **109**, D14203 (2004).
5. M. Kanakidou *et al.*, *Atmos. Chem. Phys.* **5**, 1053 (2005).
6. S. Fuzzi *et al.*, *Atmos. Chem. Phys.* **6**, 2017 (2006).
7. A. M. Knaapen, P. J. A. Borm, C. Albrecht, R. P. F. Schins, *Int. J. Cancer* **109**, 799 (2004).
8. C. A. Pope III, D. W. Dockery, *J. Air Waste Manage. Assoc.* **56**, 709 (2006).
9. M. O. Andreae, A. Gelencsér, *Atmos. Chem. Phys.* **6**, 3131 (2006).
10. M. Viana *et al.*, *J. Aerosol Sci.* **39**, 827 (2008).
11. O. I. Mayol-Bracero *et al.*, *J. Geophys. Res.* **107**, 8030 (2002).
12. S. Zidat *et al.*, *J. Geophys. Res.* **111**, D07206 (2006).
13. S. Zidat *et al.*, *Geophys. Res. Lett.* **34**, L05820 (2007).
14. A. Gelencsér *et al.*, *J. Geophys. Res.* **112**, D23504 (2007).

10.1126/science.1169407

GEOCHEMISTRY

Life on an Anaerobic Planet

Frances Westall

Living organisms on the anaerobic planet that was Earth three and a half billion years ago were small, and the signatures that they left behind in rocks are subtle. These signatures—including the remains of cells, cell colonies, and microbial mats; the degraded remnants of organic molecules that once formed the microorganisms; and characteristic isotopic fractionations of carbon and sulfur—are very similar to those produced by modern prokaryotic cells (1). However, because of their great age, the signatures are the subject of heated debate. Were they really made by microorganisms, or are they merely the result of abiogenic precipitations on a prebiotic Earth?

These questions are not trivial. Recent experiments have shown that some morphologies formed by microorganisms in nature can be imitated in laboratory conditions by abiogenic mineral and/or organic polymers (2, 3), although it is unclear whether such structures could have been produced on a prebiotic Earth. On the other hand, natural processes in hydrothermal environments can produce abiogenic carbon with isotopic signatures similar to those produced by microbial fractionation (4).

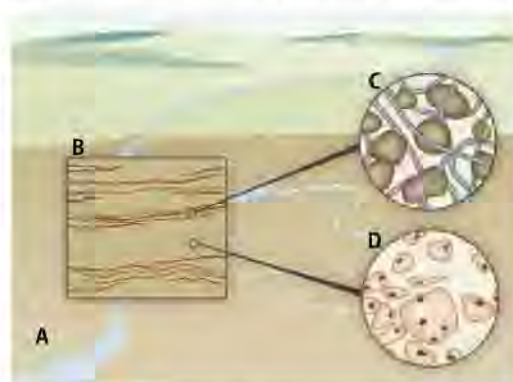
Carbonaceous molecules carried in hydrothermal fluids may also be precipitated as structures resembling the fossilized remains of microorganisms (5).

Of the oldest signatures of life, stromatolites are among the most readily recognizable. Representing the calcified remains of photosynthetic microbial mats (6), stromatolites are typically vertical, three-dimensional constructions that reach macroscopic proportions. Their shape and structure may change as a result of subtle environmental changes, as documented in 3.4-billion-year-old sediments in the Pilbara in northwestern Australia (7). Some authors

It remains highly challenging to unambiguously identify signatures of small anaerobic life forms on the early Earth.

have argued for abiological origins of these stromatolites (2, 8), but it is unlikely that non-living constructions would produce such environmentally controlled responses (7).

Stromatolites are rare in the ancient rock record, but there are other signatures of such mats. Modern microbial mats are dominated by oxygen-producing photosynthesizers, such as cyanobacteria. Putative fossilized remains of such organisms were discovered in the Pilbara sediments (9), implying existence of oxygen-producing microorganisms by this time, but they were recently reinterpreted as probable hydrothermal precipitations (5). The interpreta-



A window into the past. (A) A tidal channel meanders across exposed mud during low-tide conditions. This environment would have been common 3.4 to 3.2 billion years ago, just as it is today. (B) A vertical section cut into the mud reveals multiple, finely laminated strata characterized by microbial mat-dominated and sediment-dominated layers. (C) The filamentous microbial mats trap and bind detrital particles, thus stabilizing the sediment surfaces and forming an integral part of the sediments. The interactions of the filaments with the sedimentary environment lead to structural features that can be preserved in the rock record, dating back to the oldest well-preserved sedi-

ment. (D) In the waterlogged sediment layers between the microbial mats, chemolithotrophic microorganisms (black spots) colonize the surfaces of volcanic grains. They were probably the most common microorganisms on the early anaerobic Earth, but their signatures are extremely subtle and challenging to reveal.

Centre de Biophysique Moléculaire, CNRS et Université d'Orléans, Rue Charles Sadron, 45071 Orléans cedex 2, France. E-mail: Frances.Westall@cnrs-orleans.fr

tion of the carbon isotope ratios in 3.8- to 3.3-billion-year-old sediments from Greenland, South Africa, and Australia as signs of photosynthetic microorganisms (10–15) has also been called into question (4).

Organic carbon molecules produced by microorganisms leave typical degradation products in rocks, and it was on the basis of such molecules that the oldest molecular evidence for oxygenic photosynthesis was identified in 2.7-billion-year-old oil-rich rocks in the Pilbara (16), now reidentified as recent contamination (17). In rocks almost a billion years older, the molecules are even more degraded, and there is little to distinguish them from the prebiotic organic molecules found in meteorites. Nevertheless, measurements on 3.5-million-year-old samples from the Pilbara have shown that small-scale structural details of the conformation of certain organic molecules (such as a predominance of odd over even carbon numbers in spectra produced by pyrolysis gas chromatograph-mass spectrometry of the remnant carbon) can be traced back to living organisms (18). However, these measurements were performed on a bulk rock sample, and there is no context information about the environment of formation of the rocks or the kinds of life forms they could contain.

In contrast to the macroscopically identifiable stromatolites, other microbial signatures are far more subtle and hence more challenging to identify in the rock record, although they are more common. Biolaminated sediments, for instance, are formed by the rhythmic alternation of sticky photosynthetic microbial mats, formed on the surfaces of inter- to supratidal sediments, and intervening layers of sediment (19, 20) (see the figure). The resulting textural signatures include laminations caused by the stabilization of sediment surfaces, rippled and ripped-up mats produced by wave action, or even desiccation cracks in exposed mats. Compositionally, the layers may have higher carbon contents. These structural, textural, and compositional signatures of the nonstromatolite-forming microbial mats can be preserved in the rock record.

Silicified biolaminated sediments have been identified in 3.5- to 2.9-billion-year-old rocks in South Africa and Australia (11, 12, 15, 20, 21). From 3.4-billion-year-old sediments in the Barberton greenstone belt in South Africa, Tice and Lowe (12) recorded portions of microbial mats, formed in shallow littoral waters, that have been broken up by physical stress and redeposited in deeper water environments as rolled-up fragments (11). In the same area, we have documented overturning and mechanical shearing of a 3.3-billion-year-old filamentous microbial mat under flowing

water (15). Filaments in the latter mat had average diameters of 0.25 μm , with lengths reaching several tens of micrometers. Portions of resedimented mats from the Pilbara contained similar-sized filaments in 3.4-billion-year-old intertidal sediments (14). Such filaments, and other microorganisms (14), may be characteristic of life at that period: that is, anaerobic and small in size.

Searching for signatures of life in the oldest well-preserved sediments is difficult because of degradation of the materials and the pitfalls represented by confusing abiogenic biosignature mimics. And because life was small and anaerobic, its signatures are subtle and more challenging to identify unambiguously. However, the past half decade has seen a breakthrough in the methods used to identify biosignatures, opening the way for a future that will reveal the profusion of life on an anaerobic planet.

References

1. F. Westall, G. Southam, *AGU Geophys. Monogr.* **164**, 283 (2006).
2. N. McLoughlin *et al.*, *Geobiology* **6**, 95 (2008).
3. J. M. Garcia-Ruiz *et al.*, *Science* **302**, 1194 (2003).

4. M. van Zuilen, A. Lepland, G. Arrhenius, *Nature* **418**, 627 (2002).
5. M. D. Brasier *et al.*, *Nature* **416**, 76 (2002).
6. P. T. Visscher, J. Stolz, *Paleogeog. Paleoclimatol. Paleocol.* **119**, 87 (2005).
7. A. C. Allwood *et al.*, *Nature* **441**, 714 (2006).
8. D. R. Lowe, *Geology* **22**, 287 (1994).
9. J. W. Schopf, *Science* **260**, 640 (1993).
10. M. Schidlowski, *Precambrian Res.* **106**, 117 (2001).
11. M. M. Walsh, D. R. Lowe, in *Geologic Evolution of the Barberton Greenstone Belt, South Africa*, D. R. Lowe, G. R. Byerly, Eds., *Geol. Soc. Am. Spec. Paper* 329 (Geol. Soc. America, Boulder, CO, 1999), pp. 115–132.
12. M. Tice, D. R. Lowe, *Nature* **431**, 549 (2004).
13. Y. Ueno, H. Yoshioka, S. Maruyama, Y. Isozaki, *Geochim. Cosmochim. Acta* **68**, 573 (2004).
14. F. Westall *et al.*, in *Processes on the Early Earth*, W. U. Reimold, R. Gibson, Eds., *Geol. Soc. Am. Spec. Paper* 405 (GSA, Boulder, CO, 2006), pp. 105–131.
15. F. Westall *et al.*, *Phil. Trans. R. Soc. B* **361**, 1857 (2006).
16. J. J. Brocks, G. A. Logan, R. Buick, R. E. Summons, *Science* **285**, 1033 (1999).
17. B. Rasmussen, I. R. Fletcher, J. Brocks, M. R. Kilburn, *Nature* **455**, 1101 (2008).
18. S. Derenne *et al.*, *Earth Planet. Sci. Lett.* **272**, 476 (2008).
19. G. Gerdes, W. E. Krumbein, in *Biolaminated Deposits*, S. Bhattacharya *et al.*, Eds. (Springer, Berlin, 1987), vol. 9, pp. 1–180.
20. N. Noffke, *Earth Sci. Rev.*, published online 10 September 2008; 10.1016/j.earscirev.2008.08.002.
21. N. Noffke *et al.*, *Geology* **34**, 253 (2006).

10.1126/science.1167220

CELL BIOLOGY

Protein Filaments Caught in the Act

Grant J. Jensen

Advances in electron microscopy have allowed bacterial DNA-segregating protein filaments to be visualized.

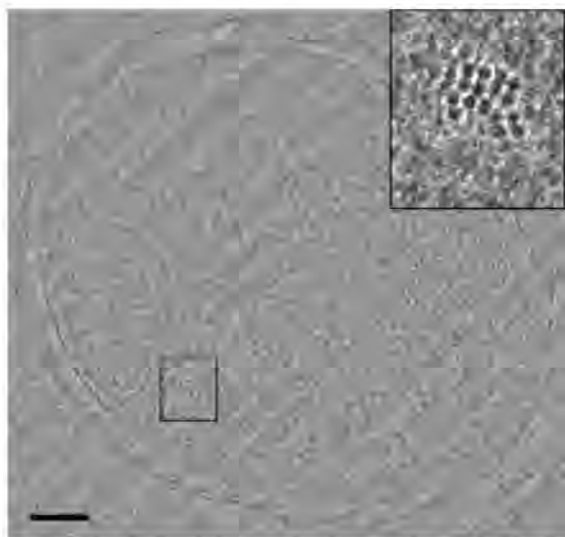
Cells can be thought of as little chemical processing plants, but they also accomplish some marvelous physical and mechanical tasks such as shaping themselves into characteristic forms, moving toward nutrients, organizing their complex interiors, replicating and then segregating their DNA, and dividing (1). It has long been understood how in eukaryotes most of this work is done by cytoskeletal filaments—long protein polymers that are used like cables, tracks, and beams in the machinery of the cell. But until about a decade ago, it was a mystery as to how bacterial cells did the same tasks. None of the existing technologies, including “traditional” electron microscopy methods, had convincingly revealed analogous cytoskeletal filaments in bacteria. As a result, the lack of a cytoskeleton became widely regarded as a distinguishing characteristic of

prokaryotic cells. Now, on page 509 of this issue (2), Salje *et al.* show direct images of an important bacterial cytoskeletal filament responsible for DNA segregation.

The findings of Salje *et al.* add to a series of discoveries that have firmly debunked the idea that prokaryotes lack a cytoskeleton (3). First, improvements in light and immunoelectron microscopy led to the identification of several bacterial proteins whose elongated localization patterns suggested that they were polymerizing into filaments (4). Next, a series of stunning crystal structures showed that many of these proteins had the same structures as known eukaryotic cytoskeletal proteins (5). In vitro biochemistry then demonstrated how some of these proteins did in fact form dynamic filaments with all the properties required to perform cytoskeletal functions (6). But seeing is believing, and the development of cryoelectron microscopy (cryo-EM) methods has in just the past few years allowed a number of bacterial cytoskeletal filaments to be imaged directly, inside cells, doing their jobs.

Division of Biology 114-96 and Howard Hughes Medical Institute, California Institute of Technology, Pasadena, CA 91125, USA. E-mail: jensen@caltech.edu

The key was that the development of cryo-EM methods allowed samples to be imaged frozen in a near-native, lifelike state, thus bypassing the harsh preparative procedures of chemical fixation, dehydration, plastic embedment, and staining required by traditional electron microscopy. Because cytoskeletal filaments have now been seen frequently within bacteria through cryo-EM techniques, it appears that the harsher “traditional” techniques simply failed to preserve such fine structures. As a second major recent advance, electron tomographic methods have been developed that allow entire small cells, not just sections of cells, to be imaged in three dimensions (7). This allows filaments that



Freeze frame. Cryo-EM projection image of a vitreous section of an *E. coli* cell containing a high-copy plasmid with the ParMRC segregation system. A single bundle of ~16 ParM cytoskeletal filaments is seen at the lower left (and inset), cut in cross section and projected down the filaments' long axis so they appear as small dots. Scale bar, 100 nm. [Reproduced from (2)]

bend and curve, and therefore might be missed in a single planar section, to be recognized and followed.

Unfortunately, although these advances have opened a completely new window into the ultrastructure of several bacterial species (8), they were not immediately applicable to the bacterium *Escherichia coli* because the high-energy electrons typically used in cryo-EM can only penetrate about 0.5 μm of biological material before being inelastically scattered (and thus lost to the image). *E. coli* cells are, unfortunately, just larger than this, and are therefore problematically thick. This is a major disappointment, because *E. coli* is by far the most studied bacterium (and possibly the most studied cell of any type), and images of its putative cytoskeleton are in high demand, as so much is already known about

its complex cell biology. To overcome this challenge, Salje *et al.* first cryosectioned frozen *E. coli* cells and then imaged the frozen sections. This resulted in the first direct in vivo images of an *E. coli* cytoskeletal filament, the plasmid-segregating protein ParM.

ParM is part of the simplest cellular DNA (plasmid) segregation system discovered to date, involving only two proteins: ParM, which self-assembles into a dynamic filament, and ParR, an adaptor protein that anchors the tips of ParM filaments to plasmids at a special short DNA sequence called *parC*. ParM filaments segregate plasmids by binding through ParR to two identical copies of the plasmid (one at each end of the filament), growing until they extend across the cell from one pole to the other, and then releasing the plasmids near the poles. This greatly improves the chances that when the cell then divides at its mid-plane, each daughter cell will receive its own copy of the plasmid (9). Although these points had all been established previously, ParM filament bundles had never actually been seen directly inside cells. Salje *et al.* froze cells at high pressure (which prevents formation of large ice crystals that would have distorted the cellular ultrastructure), cryosectioned them to produce slabs thin enough for cryo-EM, and then recorded either projection images or full tomograms of the frozen sections—a strategy that has been named CEMOVIS (“cryo-EM of vitreous sections”) (10). Filament bundles were unambiguously recognized in the images.

Although cryo-EM methods do allow cellular structures to be imaged in a native state, there are as yet no effective labels that can be used to identify molecules of interest. Previous studies had identified specific protein filaments by varying the expression level of a candidate protein (i.e., from absent to highly overexpressed) or the stability of the filament it formed, and then observing which filaments in the cell exhibited corresponding changes in their number or length (11, 12). Salje *et al.* did the same, imaging cells overexpressing ParM protein alone, cells harboring high-copy-number and then low-copy-number plasmids bearing the ParMRC machinery, and finally control cells lacking ParM entirely. In a technological first, however, Salje *et al.* further strengthened their case by showing that the putative ParM fila-

ments they saw had the same characteristic spacings between filaments, and between monomers along a single filament, as did ParM filaments assembled in vitro from purified ParM protein. In the cells harboring the low-copy-number plasmid, they occasionally saw small bundles of just three to five filaments near the edge of the nucleoid (the nucleus-like region in the cytoplasm of a prokaryotic cell where DNA localizes). Biologically, these images strongly support the model that there is one filament for each plasmid pair (13), and further reveal that the filaments and plasmids are somehow bundled together at the edge of the nucleoid (see the figure).

These findings point the way toward new questions and opportunities. It is unclear, for instance, how the filaments are bundled together, or why the ParM filaments were consistently seen within the periphery of the nucleoid. Similar cryosectioning approaches may allow images of the proteins FtsZ, MreB, MinCDE, and other putative cytoskeletal machinery in *E. coli* to be obtained (although each will present its own special challenges because of their different abundances, positions, curvature, and sizes). Analyses of the characteristic spacings (structural “signatures”) of other filaments may help identify them, just as it did ParM. Finally, as one of a burst of pioneering applications of CEMOVIS, the study of Salje *et al.* further justifies hopes that we will one day be able to produce three-dimensional maps of even large (eukaryotic) cells to this same degree of “molecular resolution” through tomography of serial vitreous sections.

References

1. D. M. Morris, G. J. Jensen, *Annu. Rev. Biochem.* **77**, 583 (2008).
2. J. Salje, B. Zuber, J. Lowe, *Science* **323**, 509 (2009); published online 18 December 2008 (10.1126/science.1164346).
3. K. A. Michie, J. Löwe, *Annu. Rev. Biochem.* **75**, 467 (2006).
4. W. Margolin, *Trends Microbiol.* **6**, 233 (1998).
5. L. A. Amos, F. van den Ent, J. Lowe, *Curr. Opin. Cell Biol.* **16**, 24 (2004).
6. E. C. Garner, C. S. Campbell, D. B. Weibel, R. D. Mullins, *Science* **315**, 1270 (2007).
7. V. Lucic, F. Forster, W. Baumeister, *Annu. Rev. Biochem.* **74**, 833 (2005).
8. G. J. Jensen, A. Briegel, *Curr. Opin. Struct. Biol.* **17**, 260 (2007).
9. C. S. Campbell, R. D. Mullins, *J. Cell Biol.* **179**, 1059 (2007).
10. A. Al-Amoudi *et al.*, *EMBO J.* **23**, 3583 (2004).
11. Z. Li, M. J. Trimble, Y. V. Brun, G. J. Jensen, *EMBO J.* **26**, 4694 (2007).
12. A. Kornelli, Z. Li, D. K. Newman, G. J. Jensen, *Science* **311**, 242 (2006); published online 22 December 2005 (10.1126/science.1123231).
13. J. Salje, J. Lowe, *EMBO J.* **27**, 2230 (2008).

10.1126/science.1169829

Membrane Fusion: Grappling with SNARE and SM Proteins

Thomas C. Südhof¹ and James E. Rothman²

The two universally required components of the intracellular membrane fusion machinery, SNARE and SM (Sec1/Munc18-like) proteins, play complementary roles in fusion. Vesicular and target membrane-localized SNARE proteins zipper up into an α -helical bundle that pulls the two membranes tightly together to exert the force required for fusion. SM proteins, shaped like clasps, bind to trans-SNARE complexes to direct their fusogenic action. Individual fusion reactions are executed by distinct combinations of SNARE and SM proteins to ensure specificity, and are controlled by regulators that embed the SM-SNARE fusion machinery into a physiological context. This regulation is spectacularly apparent in the exquisite speed and precision of synaptic exocytosis, where synaptotagmin (the calcium-ion sensor for fusion) cooperates with complexin (the clamp activator) to control the precisely timed release of neurotransmitters that initiates synaptic transmission and underlies brain function.

Life in eukaryotes depends on the fusion of membranous organelles. Every vital process relies on the orderly execution of membrane fusion, from the exquisite compartmental organization of all cells to the precise timing of synaptic transmission in the brain. SNARE and SM proteins have long been known to be required for fusion, but precisely how they cooperate has been unclear until very recently. Moreover, because this universal fusion machinery is constitutively “on,” the necessity for control of fusion—as needed for all of biology, from cell division and migration to hormone signaling and synaptic transmission—requires a superimposed dynamic control mechanism that grapples with the SNARE and SM proteins, clamps them down when not needed, and activates them when they are.

Here, we review recent advances and suggest a simple and unified view of the mechanisms by which SNARE and SM proteins function together as the universal fusion machinery, responsible for all intracellular membrane fusion except that involving mitochondria. We present a simple and coherent picture of how membrane fusion is executed and controlled, providing a foundation for understanding physiology and its chronic imbalances that contribute to diseases as diverse as diabetes, immune deficiency, and Parkinson's disease.

SNARE Proteins: The Force Generators

NSF (*N*-ethylmaleimide-sensitive factor) and SNAP (soluble NSF attachment protein; note that this protein is not related to the “SNAP”-type SNARE proteins described below) were purified on the basis of their requirement for transport

vesicle fusion in a cell-free system (1–3). SNARE proteins were identified to be receptors for SNAP and NSF (hence the name SNARE, derived from SNAP receptor) as a complex of three membrane proteins proposed to bridge the exocytic vesicle to the plasma membrane (4). These proteins—syntaxin-1 and SNAP-25, emanating from the presynaptic plasma membrane, and vesicle-associated membrane protein (VAMP; also called synaptobrevin), located in the synaptic vesicle—had previously been individually sequenced and localized (5–9). They were also

recognized, along with many synaptic vesicle proteins and yeast secretion genes, as members of conserved gene families directly or indirectly implicated in vesicle transport (10–15). Consistent with their proposed central importance in fusion (4), the synaptic SNARE proteins were additionally identified as targets for botulinum and tetanus toxins, exquisitely specific proteases that block synaptic vesicle fusion (16–18).

Finding the membrane-bridging SNARE complex at the synapse focused attention on these three proteins (and their homologs in other organelles and tissues) as being at the heart of membrane fusion and suggested that synaptic SNARE proteins and their ubiquitously expressed homologs are universal fusion proteins—a concept broadly referred to as the SNARE hypothesis (4). The SNARE hypothesis also postulated that SNAREs fall into two broad categories, v-SNAREs in transport vesicles and t-SNAREs in target membranes, that pair specifically to add compartmental specificity to membrane fusion. A comprehensive test of hundreds of combinations of SNAREs derived from the yeast genome indicated that the compartmental specificity of the yeast cell correlates in almost every case with the physical chemistry of isolated SNAREs. Only a dozen or so SNARE combinations are fusogenic, corresponding to the known transport processes in the cell (19–21); hence, SNAREs can impart considerable specificity to membrane fusion.

The structure of SNARE proteins and the architecture of SNARE complexes illustrate their

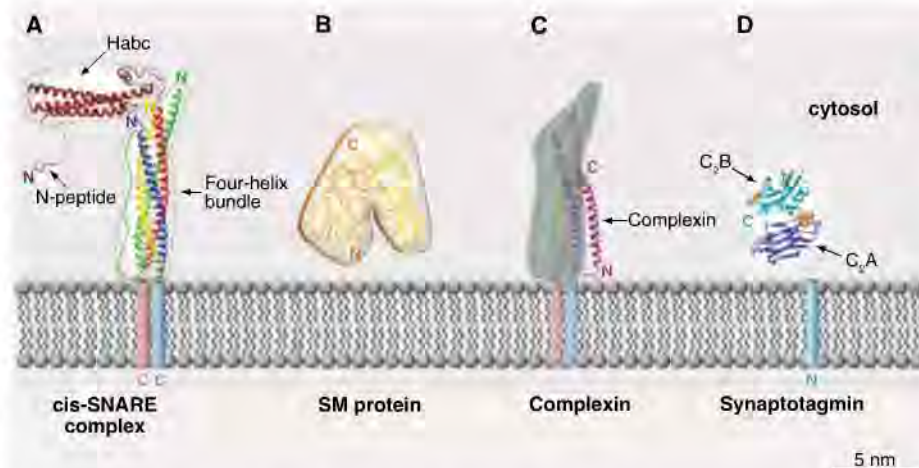


Fig. 1. Structure of SNARE and SM proteins and some proteins that grapple with them. (A) SNARE complex (also called cis-SNARE complex) of VAMP/synaptobrevin (blue helix), syntaxin (red helix), and SNAP-25 [green and yellow helices for the N- and C-terminal domains, respectively; adapted from (23)]. The Habc domain of syntaxin-1A [brown helices, adapted from (69)] is positioned arbitrarily. (B) An SM protein, highlighting its arch-like structure [Munc18-1, adapted from (38)]. (C) Complexin, bound to the SNARE complex [complexin-1, shown in magenta, adapted from (67)], has a helical region that binds at the interface of the v- and t-SNAREs in an antiparallel orientation. (D) Synaptotagmin, the calcium sensor for synchronous synaptic transmission [synaptotagmin-1, adapted from (70, 71)], with its membrane-proximal (C₂A) and membrane-distal (C₂B) C₂ domains labeled and the position of critical bound calcium ions (orange) shown. All proteins are at the same scale, and the bilayer thickness is approximately on the same scale.

¹Department of Cellular and Molecular Physiology, Stanford University, Palo Alto, CA 94304, USA. E-mail: tcs1@stanford.edu

²Department of Cell Biology, Yale University School of Medicine, 333 Cedar Street, New Haven, CT 06520, USA. E-mail: james.rothman@yale.edu

mechanism (Fig. 1). Individual SNARE proteins are unfolded, but they spontaneously assemble into a remarkably stable (22) four-helix bundle (23) that forms between membranes as a “trans-SNARE complex” (also known as a “SNAREpin”) that catalyzes fusion by forcing membranes closely together as it zippers up, exerting force against any attempted separation of its helices from each other (Fig. 2A) (24, 25). Each SNAREpin releases about $35 k_B T$ of energy (equivalent to about 20 kcal/mol) as it zippers up (26). The activation energy for lipid bilayer fusion is in the range of 50 to 100 $k_B T$ (27), and so three or more individual SNAREpins suitably arranged will provide enough energy to drive fusion, in line with current estimates (28). In the postfusion state (Fig. 2B), the fully zippered SNARE complex (emanating from the fused membrane) is termed the “cis-SNARE complex.”

Current evidence suggests that SNARE complex formation promotes membrane fusion by simple mechanical force, because their normally polypeptide membrane anchors can be replaced by passive lipid structures that span both leaflets (29). Moreover, the linker region between the SNARE motif and the transmembrane region is critical (30, 31) as a force transducer that translates the energy released upon trans-SNARE complex zippering into a catalytic force that fuses the apposing bilayers.

Overall, fusion is driven by an adenosine triphosphate (ATP)-dependent cycle of SNARE association and dissociation. In this cycle, the bilayer merger is thermodynamically coupled to exergonic folding of SNARE proteins, followed by their endergonic unfolding by a specialized adenosine triphosphatase (ATPase), NSF, that returns them to their initial state for another round. This simple thermodynamic mechanism has been demonstrated in the spontaneous fusion of artificial lipid vesicles containing purified v- and t-SNARE proteins (25). Once assembled, SNARE complexes are recycled by the ATPase NSF and its adaptor protein, SNAP, the latter binding directly to the SNARE complex (32, 33). NSF is a hexamer that presumably uses three to six ATPs with each catalytic cycle (totaling about 20 to 40 kcal/mol) to disrupt the SNARE complex.

SNARE proteins are diverse (typically 20 to 30% protein sequence identity as a superfamily), but each contains a characteristic ~70-residue “SNARE motif” with heptad repeats (34). It is this motif that forms the four-helix bundle. Most but not all SNARE proteins are membrane-anchored (at their C-terminal ends) and contain a single SNARE motif, except for SNAP-class SNAREs, which contain two motifs and are specialized for exocytosis. Within the four-helix bundle, four classes of SNARE motifs are structurally distinguished [referred to as R-, Qa-, Qb, and Qc-SNARE motifs (34)]. All SNARE complexes contain one member of each class: The R-SNARE usually corresponds to the v-SNARE, and the Q-SNAREs usually correspond to the

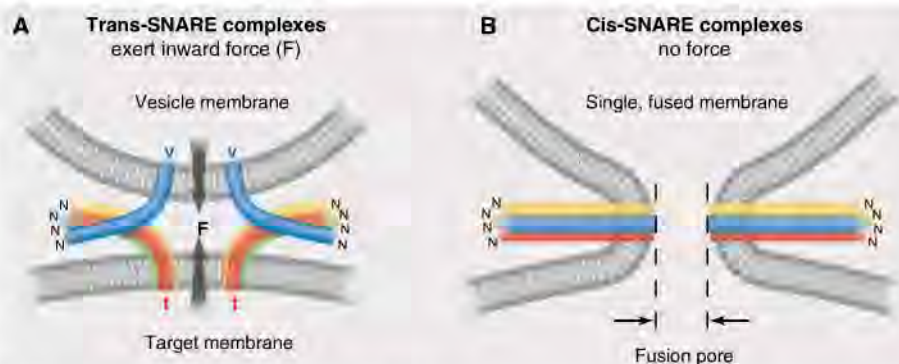


Fig. 2. (A) The zippering model for SNARE-catalyzed membrane fusion. Three helices anchored in one membrane (the t-SNARE) assemble with the fourth helix anchored in the other membrane (v-SNARE) to form trans-SNARE complexes, or SNAREpins. Assembly proceeds progressively from the membrane-distal N termini toward the membrane-proximal C termini of the SNAREs. This generates an inward force vector (F) that pulls the bilayers together, forcing them to fuse. Complete zippering is sterically prevented until fusion occurs, so that fusion and the completion of zippering are thermodynamically coupled. **(B)** Therefore, when fusion has occurred, the force vanishes and the SNAREs are in the low-energy cis-SNARE complex.

t-SNAREs. Physiologically, fusion is mediated by SNARE complexes containing one of each of the SNARE classes [this is referred to as the R/Q rule (23, 34)]. Frequently, the v-SNARE is uniquely positioned in a separate membrane from the three t-SNAREs in order for fusion to occur (19). This topological restriction reveals distinct but not well-understood roles for the v- and t-SNARE components in the force-generating mechanism.

Although it is clear that SNAREs drive fusion thermodynamically, estimates of catalytic potency vary widely among the kinds of defined systems where isolated SNARE kinetics can be studied. Fusion kinetics range from tens of milliseconds for single events (35, 36) to tens of minutes for populations in the earliest studies (25) and depend strongly on SNARE concentration and local membrane architecture, indicating that one or more additional proteins may be needed under physiological conditions. In fact, whereas SM proteins can be dispensed with *in vitro* at high SNARE concentrations (see below), the system *in vivo* universally requires an SM protein as a subunit of the t-SNARE complex to clasp the assembling SNARE complexes.

SM Proteins: Clasping SNAREpins

SM proteins have been linked to membrane fusion since the synaptic SM protein (Munc18-1) was isolated bound to the synaptic t-SNARE syntaxin-1 (37), but only recently has a clear view emerged of how SM proteins work in fusion. SM proteins associate with SNARE proteins in multiple ways, including as clasps binding both the v-SNARE and t-SNARE components of zippering SNARE complexes. It now seems likely that SM proteins organize trans-SNARE complexes (i.e., SNAREpins) spatially and temporally.

SM proteins (Fig. 1B) are composed of a conserved ~600-amino acid sequence that folds into an arch-shaped “clasp” structure (38). SM proteins interact with SNAREs in different ways.

First, they bind to the individual synaptic t-SNARE subunit syntaxin-1, forming a complex that includes part of the SNARE motif, thus disabling the formation of SNARE complexes (Fig. 3A). Here, the SM protein embraces a four-helix bundle formed exclusively within the syntaxin. In addition to its SNARE motif, syntaxin-1 also contains a three-helix bundle that comprises its globular, N-terminal “Habc” domain that folds back and binds the helical SNARE motif to form the “closed” syntaxin conformation (38, 39). In this arrangement, the SM protein clasps these four helices—the three from the Habc domain and the fourth from the SNARE motif. Only syntaxins among the SNARE superfamily assume such a stable intramolecular closed conformation, yet this structure reveals a general feature of SM proteins: They are fundamentally designed to clasp a four-helix bundle. As discussed below, this can also be the four-helix bundle of a zippering SNAREpin.

The early discovery of this mode of binding to the closed conformation of syntaxin-1 led to the suggestion that SM proteins act as negative regulators. However, an SM protein is positively required in all fusion reactions, and all genetic screens involving fusion reactions identified, among other genes, those encoding SM proteins [e.g., see (10, 40)]. As well, reverse genetic deletion of the major synaptic SM protein (Munc18-1) blocks exocytosis without altering synapse formation (41) even more completely than the strong effect of deleting VAMP/synaptobrevin (42). Thus, SM proteins could not only be negative regulators.

Recently this mechanistic gap was resolved when a second, distinct mechanism of interaction between SM and SNARE proteins was found (Fig. 3B), explaining how SM proteins could promote fusion (43, 44). Here, the SM protein is anchored by its N-terminal lobe to a specific N-terminal peptide sequence of the syntaxin (43, 44). This

binding leaves the arch-shaped body of the SM protein free to fold back on the SNAREpin and clasp across the zippering four-helix bundle near the membrane (Fig. 3C).

Of course, this can only happen when the v-SNARE (one helix) combines with the t-SNARE (three helices) to comprise four helices, potentially enabling SM proteins to cooperate in trans-SNARE complex assembly and organization, spatially and temporally, thereby stimulating SNARE-mediated fusion upon tethering to syntaxin's N terminus (45, 46). Targeted mutagenesis and biophysical studies indicate that the SM protein contacts residues on the surface of both the v- and t-SNARE in the SNARE complex (45, 46), as expected from clasping (Fig. 3C).

Thus, SM proteins are—together with SNARE proteins—the universal components of the fusion machinery, equally essential for membrane fusion in the cell and capable of promoting compartmental specificity. Yet this clear-cut *in vivo* requirement for SM proteins was not evident in defined fusion assays, which in retrospect had used higher than physiological concentrations of SNAREs. By maximizing fusion by SNAREs in the absence of SM proteins, defined systems indeed established the inherent thermodynamic sufficiency of SNARE proteins for fusion, but at the same time somehow bypassed the vital requirement for SM proteins in the complexity of a cellular environment. We ascribe this difference to the relatively low SNARE concentrations in cells, presumably kept low to allow effective regulation of their activity (47).

Exactly how SM proteins cooperate with SNARE complexes for fusion is not yet known. We suggest a kinetic role in which SM proteins cooperate with SNAREs by helping them assemble into productive topological arrangements at the interface of two membranes (such as ring-like arrangements that could facilitate the opening of fusion pores), possibly by restricting the diffusion of SNAREs into the space between fusing membranes (48). Thus, SM proteins likely act as catalysts for SNAREs, which in turn are catalysts for membrane fusion. The HOPS complex containing the SM protein Vps33 appears to act in this manner (49). Additionally, SM proteins might contribute to a SNARE-dependent organization of lipid microdomains in fusing membranes. We also note that binding of SM protein to SNARE proteins likely performs additional functions in fusion that seamlessly merge with their universal roles in fusion—for example, in vesicle tethering and in regulating the speed of fusion (50).

In sum, the universal fusion machinery (Fig. 3C) consists of a v-SNARE protein and a t-SNARE complex, the latter comprising a syntaxin “heavy

chain” with one or two associated nonsyntaxin SNARE “light chains,” and a cognate SM protein bound to the N terminus of the syntaxin. The t-SNARE complex engages the cognate v-SNARE in the opposing membrane, and as these two SNAREs zipper up toward the membrane, the SM protein cooperates in fusion, at least in part, by circumferentially clasping the assembling trans-SNARE complex.

Complexins: Grappling with SNAREs for Synaptic Transmission

Different intracellular fusion reactions are subject to distinct regulatory processes that adapt the universal fusion machinery to organismal physiology. These regulators prevent rampant fusion events that would otherwise occur, because membrane fusion is driven by a thermodynamically

the pancreas and neurotransmitter release at the synapse, the latter underlying all information processing in the brain. Synaptic and other exocytic SNAREs are first activated and then clamped by complexin (52–54) and are finally triggered by Ca^{2+} binding to synaptotagmin, which reverses the action of complexin and allows fusion to be completed (55, 56).

At the synapse, at any one time, there are only a handful of synaptic vesicles docked at the presynaptic plasma membrane, and these are the most advanced in the fusion process—referred to as being “primed for fusion” or “readily releasable.” When Ca^{2+} enters the nerve terminal as the result of an arriving action potential, this ion selectively triggers fusion of these few vesicles, often in less than a millisecond, faster than any other membrane fusion event (57). The primed

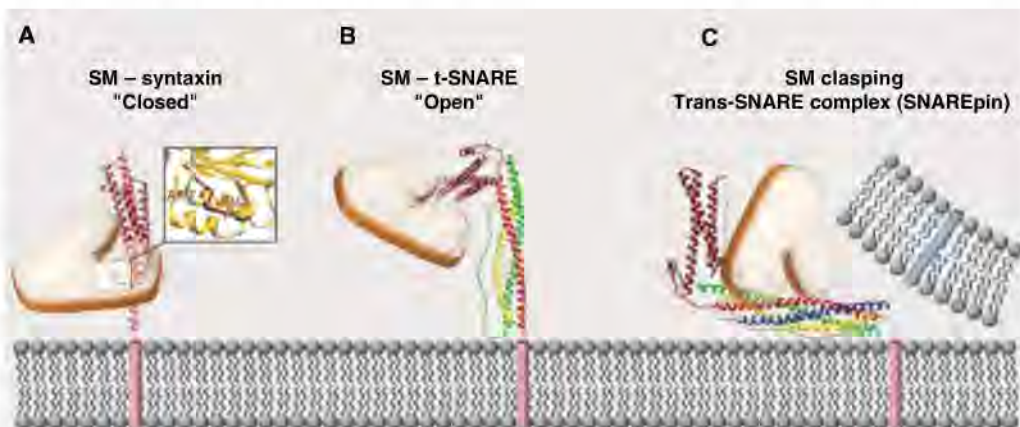


Fig. 3. SM proteins are designed to bind four-helix bundles. (A) The “closed” conformation of syntaxin-1, in which the SM protein Munc18-1 binds the four-helix bundle composed of syntaxin’s own Habc domain (three helices, in brown) and its own SNARE motif helix [fourth helix, in red; adapted from (38)]. This closed state has so far only been found with syntaxins involved in exocytosis. Inset: SM proteins are universally attached to Habc domains by a specialized sequence at the N terminus of Habc [adapted from (38, 43, 44)]. (B) The “open” conformation of a t-SNARE complex, consisting of a t-SNARE and its cognate SM protein bound to the N-peptide of its syntaxin’s Habc domain. This is believed to be the universal state in which t-SNAREs are open (i.e., reactive) with cognate v-SNAREs to form trans-SNARE complexes (C), resulting in fusion. Positions of the protein domains in (B) and (C) are arbitrary; (C) illustrates SNAREs and SM proteins, the universal fusion machinery.

spontaneous process of protein folding. Equally importantly, these regulators poise the fusion machinery in an active state to allow rapid and synchronous fusion in response to a trigger. By grappling (i.e., “seizing at close quarters”) the SNAREs, regulatory proteins can accomplish orderly clamping and activation, holding the machinery in a “cocked” state that only needs a small triggering stimulus to burst forward. A grapple can be used either to prevent or induce an action; by their nature, grapples are capable of inhibiting a process, activating a process, or both under differing conditions.

Complexin and synaptotagmin are probably the best understood grappling proteins in membrane fusion (51). Together, these two proteins account for the precise timing and regulation of the secretion of hormones such as insulin from

vesicles are distinguished from the rest—and are kinetically the most advanced—because their v-SNAREs have already formed partially zippered trans-SNARE complexes with the plasma membrane t-SNAREs, as evidenced by the fact that complexin acts upstream of Ca^{2+} -triggered fusion, but nonetheless requires SNARE complex binding for function (52, 58). Complexin acts as the quintessential grappling protein that elevates zippered SNARE complexes into this activated but frozen state, and releases them when Ca^{2+} enters and binds to synaptotagmin.

Synaptotagmin (Fig. 1D) is a synaptic (or secretory) vesicle protein containing two protein kinase C-like C_2 domains, leading to the suggestion that it acts as the Ca^{2+} sensor for exocytosis (59). The fact that synaptotagmin binds Ca^{2+} (60) and SNARE proteins (5, 61, 62), and

that its C₂ domains function as autonomous Ca²⁺-binding domains [indeed, they were the first C₂ domains for which this was revealed (63)], gave credence to this hypothesis. Synaptotagmin is required in mice for the tightly regulated, synchronous (i.e., rapid and coordinated) synaptic exocytosis characteristic of neurotransmission, but not for synaptic vesicle fusion per se (64). Reducing the Ca²⁺-binding affinity of synaptotagmin in mice caused a correspondingly reduced Ca²⁺ sensitivity of fusion, which is thus determined by Ca²⁺ binding to synaptotagmin (55, 56), formally proving that synaptotagmin is the calcium sensor for fusion. In triggering synaptic fusion, synaptotagmin binds to both phospholipids and SNARE complexes in a Ca²⁺-regulated manner (56).

Strikingly, deletion of complexin causes a precise phenocopy of the synaptotagmin deletion—a loss of Ca²⁺-triggered synchronous release but not of fusion, because asynchronous release is unimpaired (52)—which suggests that complexin somehow functions to activate SNARE complexes for subsequent synaptotagmin action. In addition, complexin clamps fusion, as evidenced both by inhibition of SNARE-mediated fusion in vitro (54, 65) and by increased spontaneous synaptic fusion in complexin-deficient synapses (58, 66). Then, Ca²⁺ binding to synaptotagmin releases the complexin clamp and triggers fusion by binding to SNARE complexes and phospholipids.

Very recent work has revealed how precisely complexin might control fusion in cooperation with synaptotagmin. Complexin contains a central α helix that binds at the interface of the v- and t-SNARE adjacent to the membrane (Fig. 1C) (67). It also contains an accessory helix and an unstructured N-terminal sequence that are located proximal to the membrane, where the final stages of zippering take place. Elsewhere in this issue (58) it is reported that SNARE binding by the central helix of complexin and its accessory helix are required for activation and clamping of fusion, whereas the N-terminal unstructured sequence is required for activation but not clamping. The accessory helix may clamp fusion by forming an alternate four-helix bundle with the membrane-proximal portion of the t-SNARE, thereby preventing the v-SNARE from completing its zippering and triggering fusion (68). This creates a “toggle switch” that can reversibly clamp fusion at a late stage. The N-terminal complexin sequence, in turn, may independently interact with the trans-SNARE complex where it inserts into the fusing membranes, because a point mutation in synaptobrevin at the membrane prevents activation by complexin (58).

How might complexin and synaptotagmin interface with each other during Ca²⁺-triggered fusion to control this toggle switch? Synaptotagmin competes with complexin for binding to assembled SNARE complexes, releasing complexin in a Ca²⁺-dependent manner (54), the

simplest possible molecular mechanism for Ca²⁺ coupling. Thus, complexin and synaptotagmin act on SNARE complexes in a pas de deux that is choreographed by Ca²⁺ and enables the supreme speed and precision of synaptic transmission, although many details—for example, the nature of other Ca²⁺ sensors for fusion—remain to be discovered.

Perspective

Intracellular membrane fusion in eukaryotes is executed by a conserved and universal fusion machinery composed of SNARE and SM proteins. Fusion results from the thermodynamic coupling of protein folding (assembly of v-SNAREs with t-SNAREs, spatially and temporally organized by SM proteins) to bilayer perturbation. Energy made available from folding is productively channeled into the bilayer so that, on balance, fusion is the favored, spontaneous reaction. Nonetheless, fusion is tightly regulated in a spatial and temporal manner, most strikingly at the synapse, where the regulation of fusion enables information processing by the brain. We are just beginning to understand how this regulation works, but in the case of the synapse we have learned some of the molecular details through the recent elucidation of the interplay among complexin, SNAREs, and synaptotagmin. There are a plethora of proteins and compounds that fragmentary evidence suggests may regulate synaptic and other fusion processes—including the large families of Rab GTPases, tethering proteins, and phosphoinositides—but the underlying principles are likely the same, driven by the simple mechanism we have described.

References and Notes

- D. O. Clary, I. C. Griff, J. E. Rothman, *Cell* **61**, 709 (1990).
- V. Malhotra, L. Orci, B. S. Glick, M. R. Block, J. E. Rothman, *Cell* **54**, 221 (1988).
- D. W. Wilson et al., *Nature* **339**, 355 (1989).
- T. Sollner et al., *Nature* **362**, 318 (1993).
- M. K. Bennett, N. Calakos, R. H. Scheller, *Science* **257**, 255 (1992).
- A. Inoue, K. Obata, K. Akagawa, *J. Biol. Chem.* **267**, 10613 (1992).
- G. A. Oyler et al., *J. Cell Biol.* **109**, 3039 (1989).
- W. S. Trimble, D. M. Cowan, R. H. Scheller, *Proc. Natl. Acad. Sci. U.S.A.* **85**, 4538 (1988).
- T. C. Südhof, M. Baumert, M. S. Perin, R. Jahn, *Neuron* **2**, 1475 (1989).
- P. Novick, C. Field, R. Schekman, *Cell* **21**, 205 (1980).
- C. Dascher, R. Ossig, D. Gallwitz, H. D. Schmitt, *Mol. Cell. Biol.* **11**, 872 (1991).
- J. Shim, A. P. Newman, S. Ferro-Novick, *J. Cell Biol.* **113**, 55 (1991).
- K. G. Hardwick, H. R. Pelham, *J. Cell Biol.* **119**, 513 (1992).
- G. Schiavo et al., *Nature* **359**, 832 (1992).
- E. Link et al., *Biochem. Biophys. Res. Commun.* **189**, 1017 (1992).
- J. Blasi et al., *Nature* **365**, 160 (1993).
- J. Blasi et al., *EMBO J.* **12**, 4821 (1993).
- G. Schiavo et al., *J. Biol. Chem.* **268**, 23784 (1993).
- F. Parlati et al., *Nature* **407**, 194 (2000).
- R. Fukuda et al., *Nature* **407**, 198 (2000).
- J. A. McNew et al., *Nature* **407**, 153 (2000).
- T. Hayashi et al., *EMBO J.* **13**, 5051 (1994).
- R. B. Sutton, D. Fasshauer, R. Jahn, A. T. Brünger, *Nature* **395**, 347 (1998).

- P. I. Hanson, R. Roth, H. Morisaki, R. Jahn, J. E. Heuser, *Cell* **90**, 523 (1997).
- T. Weber et al., *Cell* **92**, 759 (1998).
- F. Li et al., *Nat. Struct. Mol. Biol.* **14**, 890 (2007).
- F. S. Cohen, G. B. Melikyan, *J. Membr. Biol.* **199**, 1 (2004).
- Y. Hua, R. H. Scheller, *Proc. Natl. Acad. Sci. U.S.A.* **98**, 8065 (2001).
- J. A. McNew et al., *J. Cell Biol.* **150**, 105 (2000).
- F. Deak, O. H. Shin, E. T. Kavalali, T. C. Südhof, *J. Neurosci.* **26**, 6668 (2006).
- J. A. McNew, T. Weber, D. M. Engelman, T. H. Sollner, J. E. Rothman, *Mol. Cell* **4**, 415 (1999).
- A. Mayer, W. Wickner, A. Haas, *Cell* **85**, 83 (1996).
- T. Sollner, M. K. Bennett, S. W. Whiteheart, R. H. Scheller, J. E. Rothman, *Cell* **75**, 409 (1993).
- T. H. Kloepper, C. N. Kienle, D. Fasshauer, *Mol. Biol. Cell* **18**, 3463 (2007).
- M. E. Bowen, K. Weninger, A. T. Brunger, S. Chu, *Biophys. J.* **87**, 3569 (2004).
- T. Y. Yoon, B. Okumus, F. Zhang, Y. K. Shin, T. Ha, *Proc. Natl. Acad. Sci. U.S.A.* **103**, 19731 (2006).
- Y. Hata, C. A. Slaughter, T. C. Südhof, *Nature* **366**, 347 (1993).
- K. M. S. Misura, R. H. Scheller, W. I. Weis, *Nature* **404**, 355 (2000).
- I. Dulubova et al., *EMBO J.* **18**, 4372 (1999).
- S. Brenner, *Genetics* **77**, 71 (1974).
- M. Verhage et al., *Science* **287**, 864 (2000).
- S. Schoch et al., *Science* **294**, 1117 (2001).
- T. Yamaguchi et al., *Dev. Cell* **2**, 295 (2002).
- I. Dulubova et al., *EMBO J.* **21**, 3620 (2002).
- J. S. Shen, D. C. Tareste, F. Paumet, J. E. Rothman, T. J. Melia, *Cell* **128**, 183 (2007).
- I. Dulubova et al., *Proc. Natl. Acad. Sci. U.S.A.* **104**, 2697 (2007).
- D. Tareste, J. Shen, T. J. Melia, J. E. Rothman, *Proc. Natl. Acad. Sci. U.S.A.* **105**, 2380 (2008).
- J. Rizo, X. Chen, D. Arac, *Trends Cell Biol.* **16**, 339 (2006).
- C. Stroupe, K. M. Collins, R. A. Fratti, W. Wickner, *EMBO J.* **25**, 1579 (2006).
- S. H. Gerber et al., *Science* **321**, 1507 (2008); published online 14 August 2008 (10.1126/science.1163174).
- J. Rizo, C. Rosenmund, *Nat. Struct. Mol. Biol.* **15**, 665 (2008).
- K. Reim et al., *Cell* **104**, 71 (2001).
- C. G. Giraudo, W. S. Eng, T. J. Melia, J. E. Rothman, *Science* **313**, 676 (2006); published online 22 June 2006 (10.1126/science.1129450).
- J. Tang et al., *Cell* **126**, 1175 (2006).
- R. Fernandez-Chacon et al., *Nature* **410**, 41 (2001).
- Z. P. Pang, O. H. Shin, A. C. Meyer, C. Rosenmund, T. C. Südhof, *J. Neurosci.* **26**, 12556 (2006).
- B. L. Sabatini, W. G. Regehr, *Nature* **384**, 170 (1996).
- A. Maximov, J. Tang, X. Yang, Z. P. Pang, T. C. Südhof, *Science* **323**, 516 (2009).
- M. S. Perin, V. A. Fried, G. A. Mignery, R. Jahn, T. C. Südhof, *Nature* **345**, 260 (1990).
- N. Brose, A. G. Petrenko, T. C. Südhof, R. Jahn, *Science* **256**, 1021 (1992).
- C. Li et al., *Nature* **375**, 594 (1995).
- E. R. Chapman, P. I. Hanson, S. An, R. Jahn, *J. Biol. Chem.* **270**, 23667 (1995).
- B. A. Davletov, T. C. Südhof, *J. Biol. Chem.* **268**, 26386 (1993).
- M. Geppert et al., *Cell* **79**, 717 (1994).
- J. R. Schaub, X. Lu, B. Doneske, Y. K. Shin, J. A. McNew, *Nat. Struct. Mol. Biol.* **13**, 748 (2006).
- S. Huntwork, J. T. Littleton, *Nat. Neurosci.* **10**, 1235 (2007).
- X. Chen et al., *Neuron* **33**, 397 (2002).
- C. G. Giraudo et al., *Science* **323**, 512 (2009).
- I. Fernandez et al., *Cell* **94**, 841 (1998).
- R. B. Sutton, B. A. Davletov, A. M. Berghuis, T. C. Südhof, S. R. Sprang, *Cell* **80**, 929 (1995).
- I. Fernandez et al., *Neuron* **32**, 1057 (2001).
- Supported by NIH grants to T.C.S. and J.E.R. T.C.S. is an HHMI investigator.

10.1126/science.1161748

Earth's Degassing: A Missing Ethane and Propane Source

Giuseppe Etiope^{1*} and Paolo Ciccio²

Ethane (C_2H_6) and propane (C_3H_8) are gaseous hydrocarbons that contribute to photochemical pollution and ozone production in the atmosphere. Global annual emissions are estimated at 9.57 Tg and 9.61 Tg, respectively (1, 2), and include biogenic and anthropogenic sources (plants, oceans, fossil fuel, agricultural waste, and biomass burning). Yet, emission rates needed to explain present atmospheric amounts of ethane are estimated at ~ 15 Tg year⁻¹ (3), which is about ~ 5 Tg year⁻¹ higher than rates in the current inventories. Isotope measurements combined with modeling confirm that inventories are underestimated and show that global predictions better approach tropospheric amounts of ethane if at least 1 Tg year⁻¹ is added from sources located in the Northern Hemisphere (2). Here, we provide evidence that a substantial part of the missing ethane source can be attributed to Earth's natural degassing.

Recent research suggests that geologic sources of methane (CH_4), including gas manifestations and microseepage from petroliferous (sedimentary) and geothermal areas, represent the second most important natural emission of this gas to the troposphere, after wetlands (4–6). Thermogenic (organic), or subordinatedly microbial, methane dominates natural gas seepage in sedimentary basins, whereas geothermal and volcanic emissions are dominated by CO_2 (or H_2O). However, the released gas always contains small amounts of light alkanes, mainly ethane and propane, which are present at hundreds or thousands of parts per million by volume (ppmv) in petroleum gas (sometimes exceeding 1% in thermogenic gas and oil seeps) and at parts per billion by volume (ppbv) in geothermal and volcanic manifestations. More than 10,000 petroleum seeps occur in more than 80 countries, and most of them release thermogenic gas (5, 7). We analyzed a robust data set consisting of methane, ethane, and propane concentrations in surface gas manifestations from 238 sites throughout the world, including nine mean values representing nine different petroleum basins, based on more than 4000 soil-gas samples (7). Emission

rates of ethane and propane were estimated from median ethane/methane and propane/methane ratios calculated for each of the six source cate-

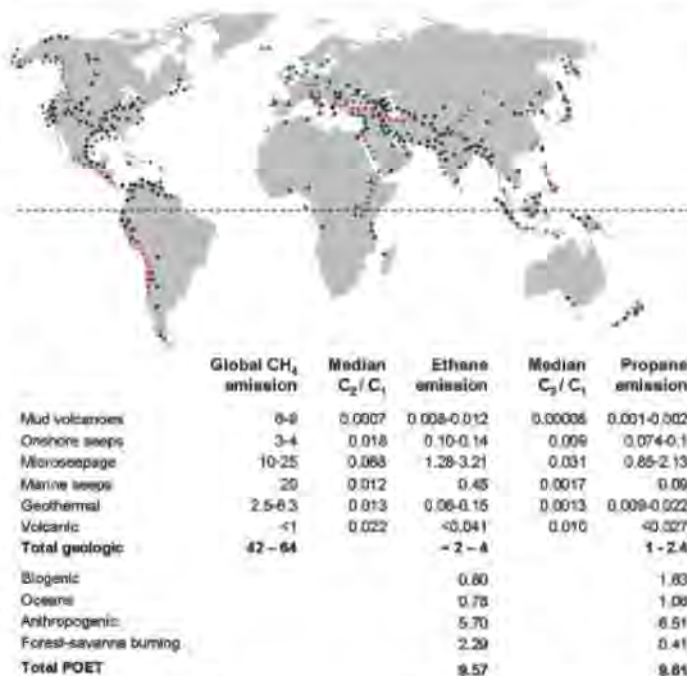


Fig. 1. Global distribution of geologic sources of gaseous hydrocarbons (black dots indicate main petroleum seepage areas; red, main geothermal and volcanic areas; and blue, submarine seepage on continental shelves) and estimates of ethane and propane emissions (Tg year⁻¹) compared with other natural and manmade sources. Geosources distribution is derived from published maps and literature (7). Figure does not include diffuse microseepage of gas from soil, potentially occurring in all sedimentary basins with hydrocarbon production (8). Global CH_4 emissions are from (5). See (7) and references therein for more explanations and uncertainties. Median ethane/methane (C_2/C_1) and propane/methane (C_3/C_1) ratios are derived from published concentration data (more than 230 gas manifestations and more than 4000 soil-gas samples) as described in (7). Biogenic, ocean, anthropogenic, and biomass-burning emissions are from POET inventory, base year 2000 (2), whose large uncertainties are discussed by (9).

gories for which global methane emission was previously estimated (5) (namely, mud volcanoes, gas seeps, microseepage, marine seepage, geothermal manifestations, and volcanoes). The output of ethane and propane from these sources was obtained by scaling to methane emissions. In Fig. 1, results are summarized and compared with other known sources. Our estimates suggest a global geologic source of ethane in the range of 2 to 4 Tg year⁻¹, with propane in the range of 1 to 2.4 Tg year⁻¹, indicating that geologic seepage can be higher than other natural sources (even considering the lowest estimates). Microseepage appears

to be the major geosource, which, in its upper estimate, would affect strongly the total emission. Such a source will need more thorough investigation in the future. Considering microseepage's lower estimate only, geoethane emission would account for about 17% of the total global source. Total ethane emission is projected beyond 11.57 Tg year⁻¹, approaching model prediction (2, 3). Geologic source accounts for at least 10% of total propane emission.

As indicated in Fig. 1, geologic emissions are mainly distributed throughout the Northern Hemisphere, where the surface of the continents and shallow seas with tectonically active (i.e., seepage prone) petroleum-bearing sedimentary and geothermal basins is larger. They could therefore represent those additional ethane sources required by models (2).

Although 3 to 6 Tg year⁻¹ of ethane plus propane have a limited impact in tropospheric ozone production, their discovery fills a gap in trace gas budgets and increases the relative importance of natural emissions. Our results challenge conventional views that consider geologic emissions as negligible hydrocarbon sources for the atmosphere.

References and Notes

1. C. Granier *et al.*, GEIA-ACCENT database (2005), available at www.geiacenter.org.
2. O. Stein, J. Rudolph, *J. Geophys. Res.* **112**, 10.1029/2006JD008062 (2007).
3. J. Rudolph, *J. Geophys. Res.* **100**, 11369 (1995).
4. G. Etiope, *Atmos. Environ.* **38**, 3099 (2004).
5. G. Etiope, K. R. Lassey, R. W. Klusman, E. Boschi, *Geophys. Res. Lett.* **35**, 10.1029/2008GL033623 (2008).
6. K. L. Denman *et al.*, in *Climate Change 2007: Fourth Annual Report of the Intergovernmental Panel on Climate Change*, S. Solomon *et al.*, Eds. (Cambridge Univ. Press, Cambridge, 2007), chapt. 7, pp. 449–587.
7. Materials and methods are available as supporting material on Science Online.
8. G. Etiope, R. W. Klusman, *Chemosphere* **49**, 777 (2002).
9. J. J. Olivier *et al.*, POET report no. 2 (2003), available at www.geiacenter.org.

Supporting Online Material

www.sciencemag.org/cgi/content/full/323/5913/478/DC1
Materials and Methods
Table S1
References

15 September 2008; accepted 20 November 2008
10.1126/science.1165904

¹Istituto Nazionale di Geofisica e Vulcanologia, Sezione Roma 2, via V. Murata 605, 00143 Rome, Italy. ²Istituto di Metodologie Chimiche, CNR, 00016 Monterotondo Scalo, Italy.

*To whom correspondence should be addressed. E-mail: Etiope@ingv.it

Language Phylogenies Reveal Expansion Pulses and Pauses in Pacific Settlement

R. D. Gray,¹ A. J. Drummond,² S. J. Greenhill¹

Debates about human prehistory often center on the role that population expansions play in shaping biological and cultural diversity. Hypotheses on the origin of the Austronesian settlers of the Pacific are divided between a recent “pulse-pause” expansion from Taiwan and an older “slow-boat” diffusion from Wallacea. We used lexical data and Bayesian phylogenetic methods to construct a phylogeny of 400 languages. In agreement with the pulse-pause scenario, the language trees place the Austronesian origin in Taiwan approximately 5230 years ago and reveal a series of settlement pauses and expansion pulses linked to technological and social innovations. These results are robust to assumptions about the rooting and calibration of the trees and demonstrate the combined power of linguistic scholarship, database technologies, and computational phylogenetic methods for resolving questions about human prehistory.

A fundamental goal of the human sciences is to understand the major factors that have shaped the diversity of our species. At one extreme, innovationist models argue that advances in technology and social organization have driven population expansions and shaped the patterns of cultural and biological diversity (1, 2). At the other extreme, diffusionist/wave models (3) argue that innovations and population expansions are not critically linked, and new technologies diffuse between societies. The settlement of the Pacific ocean by Austronesian speakers (hereafter we will use the term “Austronesian” to refer to these people) is one of the most remarkable prehistoric human expansions. The innovationist “pulse-pause” scenario posits that the Austronesians originated in Taiwan around 5500 years ago and spread through the Pacific in a sequence of expansion pulses and settlement pauses (2, 4–6). According to this scenario, the first pause occurred after the settlement of Taiwan and was followed by a rapid expansion pulse as the Austronesians spread over 7000 km from the Philippines to Polynesia in less than 1200 years. As the Austronesians spread through these regions, they integrated with existing populations and innovated new technologies, including the Lapita cultural complex (5). The archaeological evidence suggests the Austronesians reached the previously uninhabited islands of the Reefs/Santa Cruz around 3000 to 3200 years before the present (B.P.) (7), New Caledonia, and Vanuatu around 3000 years B.P., and Tonga, Samoa and Fiji in Western Polynesia in the period between 2900 to 3200 years B.P. (8, 9). This initial rapid pulse was followed by a second pause in Western

Polynesia coinciding with the development of pre-Polynesian society (6, 10), before a second expansion phase into Eastern Polynesia between 1200 and 1800 years B.P., settling Tahiti, the Cook Islands, Tuamotu, Marquesas, Hawaii, Rapanui, and New Zealand.

In contrast, proponents of the slow-boat scenario argue that the Austronesians emerged from an extensive sociocultural network of maritime exchange in Wallacea (in the region of modern day Sulawesi and the Moluccas) around 13,000 to 17,000 years B.P. based on the dating of mitochondrial lineages (11, 12). This Wallacean slow-boat scenario differs from an alternate slow-boat model that, in agreement with the pulse-pause scenario, postulates an East Asian/Taiwanese origin (13, 14). According to the Wallacean slow-boat scenario, the spread of the Austronesians was driven by the submerging of the Sunda shelf at the end of the last ice age (15). These floods triggered population expansions from the Austronesian homeland in Wallacea in a two-pronged expansion. One of these prongs moved north through the Philippines and into Taiwan. The second expansion prong spread east along the New Guinea coast and into Oceania and Polynesia (following the same route described for the pulse-pause scenario). The pulse-pause and slow-boat scenarios differ substantially in where they locate the Austronesian homeland, in the expansion sequence they postulate, and in the age and timing of this expansion. Genetic studies of Pacific settlement (13, 16–18) have been hampered by problems in separating ancient from recent admixture (19) and difficulties in precisely dating the mitochondrial and Y chromosome haplogroups found in the Pacific (20, 21).

We used phylogenetic analyses of languages to trace the history of human populations because language is linked to other cultural traits (22), contains large amounts of information (23), and

evolves at a rapid rate (24). Gray and Jordan’s (25) previous parsimony analysis of Austronesian lexical data found support for the expansion sequence predicted by the pulse-pause scenario but limitations of the data and methods used meant that the predictions about the timing of Pacific settlement could not be tested.

Lexical data. The Austronesian language family is the one of the largest in the world, with around 1200 languages spread from Taiwan to New Zealand and Madagascar to Easter Island. We have constructed a large database of Austronesian basic vocabulary (23, 26), which stores 210 items of basic vocabulary from each language, including words for animals, kinship terms, simple verbs, colors, and numbers. Basic vocabulary is both relatively stable over time and generally less likely to be borrowed between languages (27). From this database, a team of linguists identified the sets of homologous words (“cognates”) following the linguistic comparative method (28). We extracted the cognate sets for 400 well-attested languages for analysis. These languages comprise a third of the entire family and include a representative sample of each recognized Austronesian subgroup. We included two non-Austronesian languages as outgroups to “root” the trees: an archaic variant of the Sino-Tibetan language Chinese that was spoken between 2300 and 2900 years B.P. and the Tai-Kadai language Buyang (28). These languages are not traditionally part of the Austronesian family, but a number of cognates have been identified (29). The cognate sets for all 210 meanings across these 400 languages were encoded into a binary matrix. Identified “borrowings” between languages were removed from further analyses. Simulation studies have shown that the amount of undetected borrowing needs to be very substantial (>20%) to substantially bias either the tree topology or the date estimates (30). The resulting matrix contained a total of 34,440 characters (twice the length of whole mitochondrial genomes), and 6436 of these characters were parsimony informative.

Language tree topology. To test the predictions about the origin, sequence, and timing of the Austronesian expansion, we constructed trees using Bayesian phylogenetic methods under a number of models of cognate evolution (28). The best-performing model had a single parameter for cognate gains and losses and modeled character-specific rate variation using a covarion approach where characters could switch between fast and slow rates at different branches on the tree (31).

Early attempts to estimate Austronesian language relationships using lexicostatistical methods (32) produced trees that were dramatically different from those obtained by linguists using the comparative method (33). In contrast, the Bayesian phylogenetic trees (Fig. 1 and fig. S5) we obtained from our basic vocabulary data were congruent with the traditional subgroups identified by phonological and morphological evidence, such as the loss of the Proto-Oceanic uvular trill *R

¹Department of Psychology, University of Auckland, Private Bag 92019, Auckland 1142, New Zealand. ²Department of Computer Science, University of Auckland, Private Bag 92019, Auckland 1142, New Zealand.

in the Central Pacific subgroup (34) or the lowering of high vowels in morphemes identifying Central-Eastern Malayo-Polynesian (35). The trees support 26 of the 34 putative Austronesian language subgroups and linkages discussed in (28). Of the remaining seven unsupported groups, two are linkages that lack exclusively shared innovations (Central and Western Malayo-Polynesian), and one is only supported by a single sound

change (East Formosan). The remaining five (Western Oceanic, Malayo-Chamic, Greater Central Philippines, Greater Barito, and Barrier Islands/North Sumatra) may be obscured in our analyses because of conflicting signals caused by undetected borrowing between neighboring languages. Our results place the Formosan languages of Taiwan at the base of the trees immediately after the outgroups (Fig. 1). Fol-

lowing these are the languages of the Philippines, Borneo/Sulawesi, Central Malayo-Polynesia, South Halmahera/West New Guinea, and the Oceanic languages. This chained topology is precisely the structure predicted by the pulse-pause scenario.

One potential problem with this analysis is that Old Chinese may be too distantly related to Austronesian to reliably root the tree, whereas

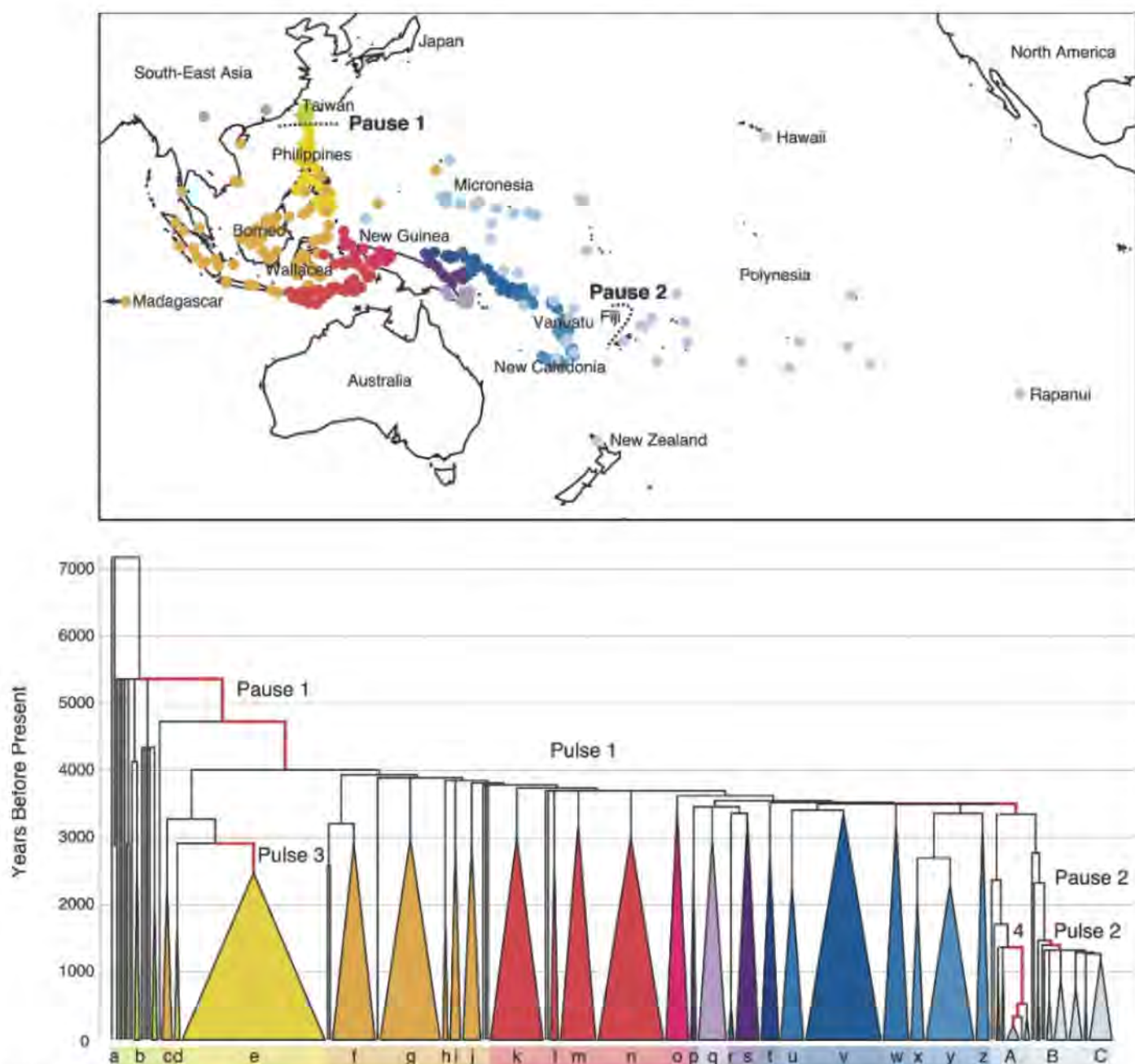


Fig. 1. Map and maximum clade credibility tree of 400 Austronesian languages. The tree shows four major expansion pulses and two pauses in Pacific settlement. Branches colored red are those identified as having significant increases in language diversification rates. Major language subgroups are color-coded and labeled as follows: a, Outgroups (Buyang, Old Chinese); b, Formosan; c, Sama-Bajaw; d, Gorontalo-Mongondowic; e, Philippine; f, Barito; g, Malayo-Sumbawan; h, Greater South Sulawesi; i,

Sangiric; j, Celebic; k, Bima-Sumba; l, Yamdena-North Bomberai; m, Central Maluku; n, Timor; o, South Halmahera-West New Guinea; p, Schouten (North New Guinea); q, Papuan Tip; r, Willaumez (Meso-Melanesian); s, North New Guinea; t, Admiralties; u, South-East Solomonian; v, Meso-Melanesian; w, Temotu; x, South Vanuatu; y, North Vanuatu; z, Loyalties/New Caledonia; A, Micronesian; B, Polynesian; and C, Eastern Polynesian.

Buyang and the other Tai-Kadai languages may be a sister group to Malayo-Polynesian (29). To investigate the reliability of the Taiwanese rooting, we conducted a separate analysis using a

stochastic-Dollo model of cognate evolution (28), which can estimate where the root should be without specifying outgroups (36). This additional analysis placed Old Chinese and Buyang at

the base of the tree, followed by the Formosan languages with 100% posterior probability.

Age of Austronesian. The second key difference between the settlement scenarios is the age of the Austronesian language family. The pulse-pause scenario predicts an origin of Austronesian between 5000 to 6000 years B.P., whereas the Wallacean slow boat scenario predicts an older age of between 13,000 to 17,000 years B.P. To test between these predictions, we estimated the age of Proto-Austronesian by using a penalized likelihood rate-smoothing approach (37). Rather than assuming constant rates of lexical replacement, this method uses calibrations to smooth the observed rates of character change across the trees. We calibrated 10 nodes on the trees with archaeological date estimates and known settlement times (28). The languages Old Chinese and Old Javanese were calibrated to the ages when they were spoken, and Favorlang and Siraya were calibrated to their data collection times. All other languages were treated as contemporaneous.

The divergence time estimates for the age of the Austronesian language family support the pulse-pause scenario (Fig. 2). The estimated root age of Austronesian across all the post-burn-in trees has a mean of 5230 years [95% highest posterior density (HPD) interval, 4750 to 5800 years B.P.]. The divergence time estimates were robust across a range of calibrations and different models (28). In particular, estimating the root age of Austronesian without the Proto-Malayo-Polynesian constraint had a trivial effect on the estimated age (mean, 5230 years; 95% HPD, 4730 to 5790 years B.P.). To thoroughly assess the impact of different calibrations, we estimated the age of Proto-Austronesian on the Maximum Clade Credibility tree for all possible calibration combinations. The resulting distribution of the age of Proto-Austronesian had a median of 5110 years (28).

Our estimates for the age of the Austronesian expansion are considerably younger than the deep age estimates of the slow-boat scenario (11, 12, 15). One possibility is that these deep estimates are artifacts due to problems with accurately dating genetic change. There is increasing evidence that rates of genetic change estimated over thousands of years are substantially higher than the long-term substitution rate (21). This violation of the molecular clock leads to the systematic overestimation of recent divergence times. The difficulties of obtaining accurate molecular dates are probably compounded by the use of the error-prone *rho* dating method (20), especially when it is applied to sequences of high-rate heterogeneity such as hypervariable region 1 (HVR-1).

Another possibility is that the genes and languages have quite different histories. However, both Austronesian expansion scenarios envisage a coupling between genetic and linguistic histories. In the pulse-pause scenario, the considerable diversity of Formosan languages reflects the Taiwanese origin of Austronesian. In contrast, the Wallacean slow-boat scenario argues that Taiwan

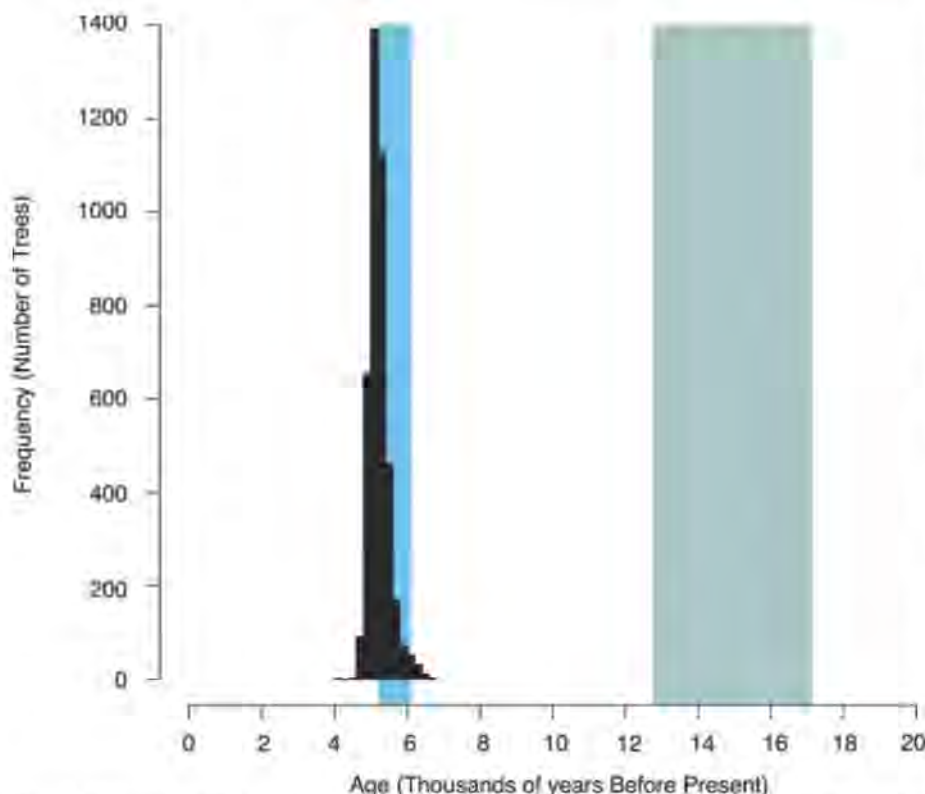


Fig. 2. Histogram of the estimated age of the Austronesian language family. The light blue bar shows the age range predicted by the pulse-pause scenario (5000 to 6000 years B.P.), and the gray bar shows that predicted by the slow-boat scenario (13,000 to 17,000 years B.P.).

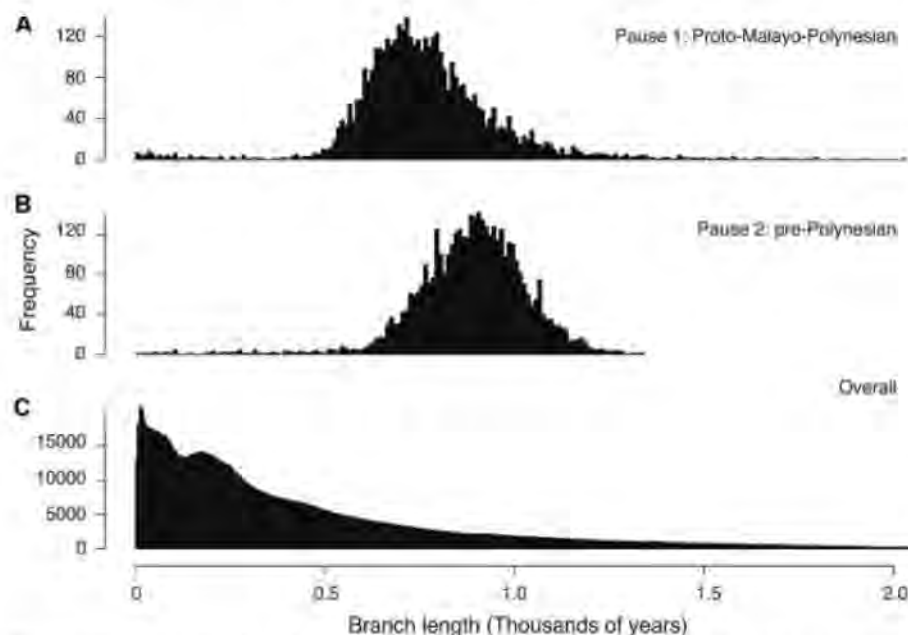


Fig. 3. Histograms of the branch length distributions. (A) The distribution of the Proto-Malayo-Polynesian pause, (B) the distribution of the pre-Polynesian pause, and (C) the overall branch-length distribution.

is an “Austronesian backwater” (12) and that the initial diversity of Malayo-Polynesian languages has been obscured by language-leveling as a result of extensive socioeconomic networks (11). Recent genetic studies of complete mitochondrial sequences (18) and genome-wide autosomal markers (14, 16) also show that, despite considerable admixture in Near Oceania (38), there is a clear signature linking Austronesian speakers from Taiwan to Polynesia. Even at a fine geographic scale on the east Indonesian island of Sumba, there are strong correlations between languages, genes, and geography (39). The Austronesian expansion has therefore produced a close initial coupling between genes and languages that has subsequently broken down in some regions such as Near Oceania (38).

Pulses and pauses. If language diversification (cladogenesis) is linked to population expansions, then expansion pulses should leave a series of short branches in the phylogenies because there will be little time for linguistic changes to accumulate before speech communities fragment. In contrast, when the geographic spread of cultures is constrained by physical or social boundaries, the rate of linguistic diversification should decrease leading to longer branches (anagenesis). The pulse-pause scenario predicts the existence of two settlement pauses: the first occurring before the settlement of the Philippines and corresponding with the development of the Proto-Malayo-Polynesian language around 3800 to 4500 years B.P. (4, 6), and the second occurring after the settlement of Western Polynesia by 2800 years B.P., before the expansion into Central and Marginal Eastern Polynesia (4, 6, 10). This Western Polynesian settlement coincides with the development of the temporally brief Proto-Central Pacific dialect network in Fiji, Tonga, and Samoa (10), with the Polynesian languages emerging from the eastern part of this dialect network sometime later. This second pause is therefore harder to place cleanly on a tree, but should correlate with the development of a pre-Polynesian stage.

To test for the predicted signature of settlement pauses, we extracted all the internal branch lengths from the posterior distribution of the dated trees. We compared the branches corresponding to the Proto-Malayo-Polynesian and pre-Polynesian stages with all other internal branches in the trees (Fig. 3). This is a conservative test because the pauses may be spread across a number of branches (Fig. 1). The Proto-Malayo-Polynesian and pre-Polynesian branches were longer than 81 and 85%, respectively, of a random sample of branches from the overall branch-length distribution (28). A rank-sum test suggests a low probability ($P = 0.057$) of obtaining these ranks or higher by chance.

If these settlement pauses were followed by expansion pulses, then the trees should also show increases in language diversification rates after the pauses. To test this possibility, we modeled diversification rates as a change-point process down the estimated language phylogeny. At each

branch in the tree, we used an indicator variable to model whether the rate of language diversification changed below the branch and a relative rate variable to specify the new rate of diversification relative to the rate on the parent branch. If no change is indicated on a given branch, the diversification rate of the parent language is inherited. We employed a full language-diversification model in which the number, phylogenetic location, and magnitude of the changes in diversification rate were all estimated directly from the data by using Bayesian stochastic variable selection within a Markov chain Monte Carlo method (28).

The posterior estimate of the number of changes in diversification was 4.3 (95% credible set: 1 to 7) with a total of 10 branches showing strong evidence of changes [Bayes Factor (BF) > 20] in diversification rates (Fig. 2 and fig. S4). The pulse with the highest posterior probability occurred in three of the branches leading to Proto-Malayo-Polynesian (BF = 397, 79, and 33, respectively). The second identified pulse occurred in two of the branches after the pre-Polynesian stage (BF = 29 and 36). The location of these two pulses is in agreement with those predicted by the pulse-pause scenario. Changes in diversification rate were also evident in three other locations. The third pulse was found in the branch leading to the Philippines languages (BF = 38) after another lengthy pause. Our results place the age of this pulse around 2500 years B.P. This is consistent with arguments that the Greater Central Philippines subgroup expanded at the expense of other lineages between 2000 and 2500 years B.P., reducing linguistic diversity in the region (40). A fourth pulse was evident in three of the branches leading to the Micronesian languages (BF = 66, 29, and 23). Within this Micronesian group the Trukic languages contain the fastest (single-population) rates in the entire family. The final branch to show a significant increase in diversification rates is that leading to both the Micronesian and Polynesian subgroups and suggests that there might be a common underlying factor between the subsequent pulses into Polynesia and Micronesia (Fig. 1 and fig. S4).

Discussion. Our results show that the diversification of Austronesian languages was closely coupled with geographic expansions. The availability of appropriate social and technological resources probably determined the timing of the expansion pulses and settlement pauses. The first pause between the settlement of Taiwan and the Philippines may have been due to the difficulties in crossing the 350-km Bashi channel between Taiwan and the Philippines (4, 6). The invention of the outrigger canoe and its sail may have enabled the Austronesians to move across this channel before spreading rapidly over the 7000 km from the Philippines to Polynesia (4). This is supported by linguistic reconstructions showing that the terminology associated with the outrigger canoe complex can only be traced back to Proto-Malayo-Polynesian and not Proto-Austronesian (41). One possible reason for the second long

pause in Western Polynesia is that the final pulse into the far-flung islands of Eastern Polynesia required further technological advances. These might have included the ability to estimate latitude from the stars, the ability to sail across the prevailing easterly tradewinds, and the use of double-hulled canoes with greater stability and carrying capacity (4, 42). Alternatively, the vast distances between these islands might have required the development of new social strategies for dealing with the greater isolation found in Eastern Polynesia (42). These technological and social advances in Eastern Polynesia may also underlie the fourth pulse into Micronesia.

The language phylogenies reveal the rapidity of major cultural development in the Pacific. As the Austronesians spread along New Guinea and into the Solomons, they developed the Lapita cultural complex through interaction with the existing populations in Near Oceania (5, 10). This complex includes distinctive and often elaborately decorated pottery, adzes/axes, shell ornaments, tattooing, and bark-cloth (10). The phylogenies show that there was only a very small time-window for this complex to develop. Based on the age of the Eastern Malayo-Polynesian clade the Austronesians entered the South Halmahera/West New Guinea region at around 3680 years B.P. (95% HPD, 3640 to 3,710 years B.P.), and had reached Remote Oceania by 3575 years B.P. (95% HPD, 3560 to 3590 years B.P.). The high levels of male-biased admixture detected in Polynesian genetic studies (13, 14) must either have occurred over this very short time span (approximately four generations), with Melanesian males actively incorporated into the Austronesian expansion, or there was extended post-settlement contact between Near Oceania and Polynesia. The results presented here show the combined power of Bayesian phylogenetic methods and large lexical databases to resolve questions about human prehistory. Just as molecular phylogenies provide the fundamental framework for studies of biological evolution, language phylogenies open up the exciting possibility of a Darwinian approach to cultural evolution based on rigorous phylogenetic methods (43).

References and Notes

1. J. Diamond, *Guns, Germs, and Steel* (Norton, New York, 1997).
2. J. Diamond, P. Bellwood, *Science* **300**, 597 (2003).
3. R. L. Welsch, J. Terrell, J. A. Nadolski, *Am. Anthropol.* **94**, 568 (1992).
4. R. Blust, in *Selected Papers from the Eighth International Conference on Austronesian Linguistics*, E. Zeitoun, P. J. K. Li, Eds. (Symposium Series of the Institute of Linguistics, Academia Sinica, Taipei, Taiwan, 1999), vol. 1, pp. 31–94.
5. R. C. Green, in *Pacific Archaeology: Assessments and Prospects. Proceedings of the International Conference for the 50th Anniversary of the First Lapita Excavation, Kone-Noumea 2002*, C. Sand, Ed. (Département Archéologie, Service des Musées et du Patrimoine., Noumea, Nouvelle-Calédonie, 2003), pp. 95–120.
6. A. Pawley, in *Examining the Farming/Language Dispersal Hypothesis*, P. Bellwood, C. Renfrew, Eds. (McDonald Institute for Archaeological Research, Cambridge, 2002), pp. 251–274.

7. R. C. Green, M. Jones, P. Sheppard, *Archaeol. Ocean.* **43**, 49 (2008).
8. D. V. Burley, W. R. Dickinson, *Proc. Natl. Acad. Sci. U.S.A.* **98**, 11829 (2001).
9. P. D. Nunn *et al.*, *Archaeol. Ocean.* **39**, 139 (2004).
10. P. Kirch, R. Green, *Hawaiki, Ancestral Polynesia: An Essay in Historical Anthropology* (Cambridge Univ. Press, Cambridge, UK, 2001).
11. C. Hill *et al.*, *Am. J. Hum. Genet.* **80**, 29 (2007).
12. S. Oppenheimer, M. Richards, *Sci. Prog.* **84**, 157 (2001).
13. M. Kayser *et al.*, *Mol. Biol. Evol.* **23**, 2234 (2006).
14. M. Kayser *et al.*, *Am. J. Hum. Genet.* **82**, 194 (2008).
15. P. Soares *et al.*, *Mol. Biol. Evol.* **25**, 1209 (2008).
16. J. S. Friedlaender *et al.*, *PLoS Genet.* **4**, e19 (2008).
17. T. Melton *et al.*, *Am. J. Hum. Genet.* **57**, 403 (1995).
18. J. A. Trejaut *et al.*, *PLoS Biol.* **3**, e247 (2005).
19. M. E. Hurler *et al.*, *Am. J. Hum. Genet.* **72**, 1282 (2003).
20. M. P. Cox, *Hum. Biol.* **80**, 335 (2008).
21. S. Y. Ho, B. Shapiro, M. J. Phillips, A. Cooper, A. J. Drummond, *Syst. Biol.* **56**, 515 (2007).
22. R. Mace, M. Pagel, *Curr. Anthropol.* **35**, 549 (1994).
23. S. J. Greenhill, R. Blust, R. D. Gray, *Evol. Bioinform.* **4**, 271 (2008).
24. M. Pagel, Q. D. Atkinson, A. Meade, *Nature* **449**, 717 (2007).
25. R. D. Gray, F. M. Jordan, *Nature* **405**, 1052 (2000).
26. Available at <http://language.psy.auckland.ac.nz/austronesian>.
27. S. M. Embleton, *Statistics in Historical Linguistics* (Studienverlag Brockmeyer, Bochum, 1986).
28. Materials and methods are available as supporting material on Science Online.
29. L. Sagart, in *The Peopling of East Asia: Putting Together Archaeology, Linguistics and Genetics*, L. Sagart, R. Blench, A. Sanchez-Mazas, Eds. (Routledge-Curzon, London, 2005), pp. 161–176.
30. Q. Atkinson, G. Nicholls, D. Welch, R. D. Gray, *Trans. Philol. Soc.* **103**, 193 (2005).
31. D. Penny, B. J. McComish, M. A. Charleston, M. D. Hendy, *J. Mol. Evol.* **53**, 711 (2001).
32. I. Dyen, in *Indiana University Publications in Anthropology and Linguistics: Memoir 19 of the International Journal of American Linguistics* (Indiana University, Bloomington, IN, 1965).
33. G. W. Grace, *Ocean. Linguist.* **5**, 361 (1964).
34. J. Lynch, M. Ross, T. Crowley, *The Oceanic Languages* (Curzon, Richmond, UK, 2002).
35. R. Blust, *Ocean. Linguist.* **32**, 241 (1993).
36. G. K. Nicholls, R. D. Gray, *J. Roy. Stat. Soc. B Met.* **70**, 545 (2008).
37. M. J. Sanderson, *Mol. Biol. Evol.* **14**, 1218 (1997).
38. K. Hunley *et al.*, *PLoS Genet.* **4**, e1000239 (2008).
39. S. J. Lansing *et al.*, *Proc. Natl. Acad. Sci. U.S.A.* **104**, 16022 (2007).
40. R. Blust, in *Current Issues in Philippine Linguistics and Anthropology: Parangal kay Lawrence A. Reid*, H. Liao, C. R. Galvez Rubino, Eds. (The Linguistic Society of the Philippines and Summer Institute of Linguistics, Manila, 2005), pp. 31–68.
41. A. Pawley, M. Pawley, in *Austronesian Terminologies: Continuity and Change*, A. Pawley, M. Ross, Eds. (Australian National University, Canberra, 1994), pp. 329–361.
42. G. Irwin, *J. Polyn. Soc.* **107**, 111 (1998).
43. R. D. Gray, S. J. Greenhill, R. M. Ross, *Biol. Theory* **2**, 360 (2007).
44. We thank R. Blust, J. Lynch, J. Marck, C. Nickelsen, M. Ross, L. Sagart, and all contributors to the Austronesian Basic Vocabulary Database for their assistance with lexical data and cognate judgments. We gratefully acknowledge BeSTGRID (www.bestgrid.org) for Web hosting and A. Meade, M. Pagel, and the Centre for Advanced Computing and Emerging Technologies at the University of Reading for computational support. R. Blust, M. Corballis, R. Green, F. Jordan, M. Pagel, R. Ross, and M. Suchard commented on the manuscript. Funding was provided by the Royal Society of New Zealand Marsden Fund and a Bright Futures doctoral scholarship to S.G.

Supporting Online Material

www.sciencemag.org/cgi/content/full/323/5913/479/DC1
Materials and Methods
SOM Text
Figs. S1 to S5
Tables S1 to S3
References

6 October 2008; accepted 10 December 2008
10.1126/science.1166858

REPORTS

An Entanglement Filter

Ryo Okamoto,^{1,2*} Jeremy L. O'Brien,^{3*} Holger F. Hofmann,⁴ Tomohisa Nagata,^{1,2} Keiji Sasaki,¹ Shigeki Takeuchi^{1,2†}

The ability to filter quantum states is a key capability in quantum information science and technology, in which one-qubit filters, or polarizers, have found wide application. Filtering on the basis of entanglement requires extension to multi-qubit filters with qubit-qubit interactions. We demonstrated an optical entanglement filter that passes a pair of photons if they have the desired correlations of their polarization. Such devices have many important applications to quantum technologies.

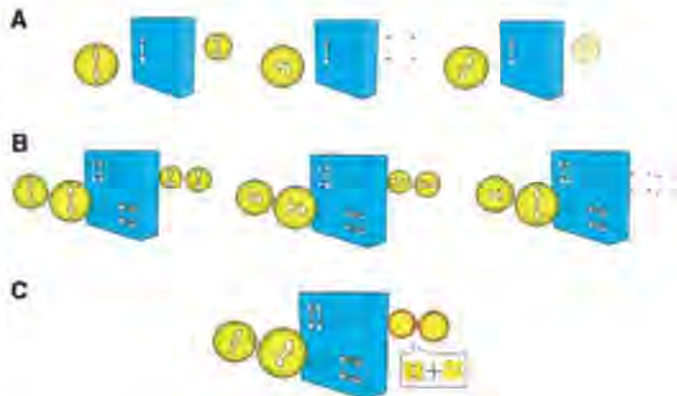
Filters, which pass the desired and reject the unwanted (material, signal, frequency, or polarization, for example), are one of the most important scientific and technological tools available to us. Quantum information science and technology is concerned with harnessing quantum mechanical effects to gain exponential improvement of and new functionality for particular tasks in communication (1), computation (2), measurement (3), and lithography (4). Perhaps the most distinctive of these quantum mechanical features is entanglement. Filters that act on the

quantum correlations associated with entanglement must operate nonlocally on multiple quantum systems, typically two-level qubits. Such a device has been proposed for photonic qubits (5); however, the technical requirements to build such a device, an optical circuit with two ancillary

photons and multiple quantum gates, requiring both quantum interference and classical interference in several nested interferometers, have been lacking.

We demonstrate an entanglement filter made by combining two key recent technological approaches: a displaced-Sagnac architecture (6) and partially polarizing beam splitters (PPBSs) (7–9). The entangling capability of the filter was verified, distinguishing it from classical ones. Because our entanglement filter acts on photonic qubits, it is promising for quantum technologies; photons are the logical choice for communication (1, 10), metrology (6, 11), and lithography (12) and are a leading approach to information processing (13). The filter can be used for the creation as well as the purification of entanglement (14, 15), which will be important in realizing quan-

Fig. 1. The function of a polarization filter and an entanglement filter. (A) Polarization filters pass only the certain polarization component of single photons. (B) Entanglement filters pass a pair of photons only if they share the same horizontal or vertical polarization. (C) Because the quantum coherence between these two possibilities is preserved during the process, the output state is entangled when two diagonally polarized photons are input.



¹Research Institute for Electronic Science, Hokkaido University, Sapporo 060-0812, Japan. ²The Institute of Scientific and Industrial Research, Osaka University, Mihogaoka 8-1, Ibaraki, Osaka 567-0047, Japan. ³Centre for Quantum Photonics, H. H. Wills Physics Laboratory and Department of Electrical and Electronic Engineering, University of Bristol, Merchant Venturers Building, Woodland Road, Bristol BS8 1UB, UK. ⁴Graduate School of Advanced Sciences of Matter, Hiroshima University, Hiroshima 739-8530, Japan.

*These authors contributed equally to this work.

†To whom correspondence should be addressed. E-mail: takeuchi@es.hokudai.ac.jp

tum relays and repeaters for long-distance quantum communication.

The most common examples of a filter for photonic qubits is a polarizer that transmits only the horizontal component of the incident photons (Fig. 1A). Polarization filters are crucial for the initialization and readout of photonic qubits as well as for the measurement-related effects, such as the quantum Zeno effect (16, 17). More sophisticated photonic filters that transmit only single-photon states while rejecting higher-photon-number states have also been realized by using ancillary photons and photon detection to induce the required optical nonlinearity (18–20). The concept of a polarization filter can be extended to a higher dimensional Hilbert space of multi-qubits, and one may anticipate that the necessary qubit-qubit interactions will also require the use of ancillary photons.

The two-photon polarization filter proposed in (5) is a device that transmits photon pairs only if they share the same horizontal or vertical polarization without decreasing the quantum coherence between these two possibilities (Fig. 1B). Because this filter is not sensitive to the individual polarization of the photons, it can preserve and even create entanglement between the photons passed through it (Fig. 1C). The filter achieves this two-qubit filtering effect by using two ancilla photons as probes that detect whether or not the two input photons are in the desired states. Detection of the ancilla photons indicates a successful filter operation, requiring no post-selection in the output. This is a substantial difference between this filter and the function realized by output postselection on a polarizing beam splitter (14, 21), in which it is necessary to eliminate the cases in which both photons exit on the same side. Because our filter should reliably produce the correct two-photon output in separate ports of the device, it can be integrated into larger quantum information networks, just like a one-qubit polarization filter. It is therefore possible to apply it to a wide range of problems, such as encoding quantum information in multiple

qubits and entanglement purification from mixed entangled states.

The operation of this filter can be summarized by a single operator \hat{S} describing the effect on an arbitrary two photon input state (5):

$$\hat{S} = \frac{1}{4}(|HH\rangle\langle HH| - |VV\rangle\langle VV|) \quad (1)$$

where $|HH\rangle$ and $|VV\rangle$ denotes the state in which both incident photons are horizontally (H) and vertically (V) polarized, respectively. This operator filters out the $|HV\rangle$ and $|VH\rangle$ components of the two-photon state without reducing the coherence between the remaining $|HH\rangle$ and $|VV\rangle$ components. The negative sign between the terms is a consequence of the phase difference between two-photon reflection and two-photon transmission at the beam splitters. The factor of $1/4$ is an expression of the transmission probability of $1/16$ for $|HH\rangle$ and $|VV\rangle$. However, the detection of the ancilla photons indicates a successful transmission of the two input photons, so that it is not necessary to detect the output photons in order to know that they were successfully transmitted.

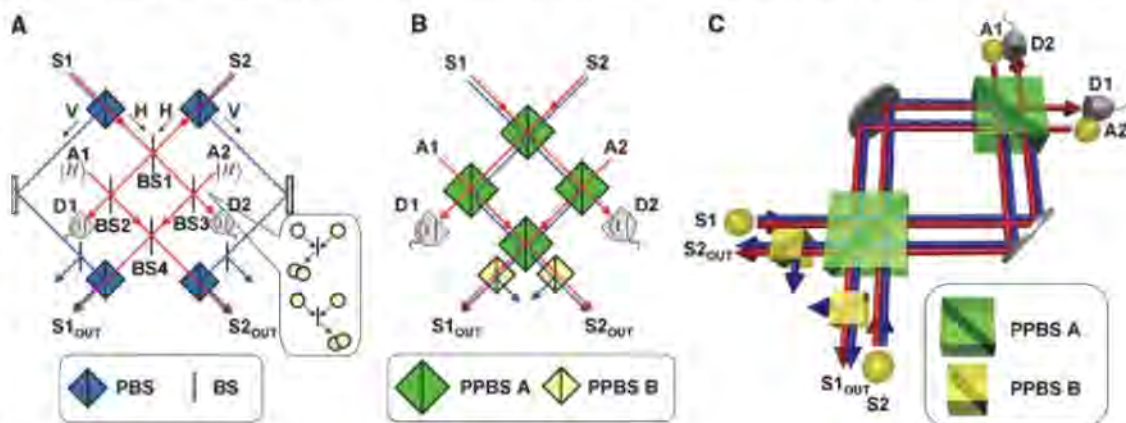
To understand the unique quantum properties of this filter, it is useful to consider the effects of its filtering process on two diagonally polarized photons. Because diagonal polarizations are coherent superpositions of horizontal and vertical polarizations ($|P\rangle \equiv \frac{1}{\sqrt{2}}(|H\rangle + |V\rangle)$; $|M\rangle \equiv \frac{1}{\sqrt{2}}(|H\rangle - |V\rangle)$), two diagonally polarized photons have a well-defined coherence between their $|HH\rangle$ and $|VV\rangle$ components that determines whether their diagonal polarizations are parallel (+) [that is, $|PP\rangle/|MM\rangle = 1/2(|HH\rangle + |VV\rangle \pm \dots)$] or orthogonal (−) [that is, $|PM\rangle/|MP\rangle = 1/2(|HH\rangle - |VV\rangle \pm \dots)$]. The operator \hat{S} preserves the magnitude of this coherence but flips the sign (Eq. 1). Therefore, the correlation between the diagonal polarizations is inverted; parallel inputs result in the superpositions of the orthogonal outputs and vice versa. Moreover, the coherence between $|HH\rangle$

and $|VV\rangle$ indicates a correlation between the circular polarizations—opposite directions (+) or the same direction (−). Thus, filtering out the $|HV\rangle$ and $|VH\rangle$ components of two diagonally polarized input photons also generates correlations between the circular polarizations of the photons, indicating the generation of entanglement.

A schematic of the optical quantum circuit for the entanglement filter (Fig. 2A) shows that multiphoton interferences occur at each of the four beam splitters, BS1 to BS4. The crucial ones are BS2 and BS3. The working principle of the quantum circuit is as follows: Whenever one of the ancilla photons meets a single-input photon at BS2 or BS3, two-photon quantum interference between the reflection of both photons and the exchange of ancilla and input photons reduces the probability of finding a single photon at D1 or D2 to zero (Fig. 2A, inset) (22). Thus, a single horizontally polarized photon cannot pass the circuit, resulting in the elimination of the $|HV\rangle$ and $|VH\rangle$ components. However, the $|HH\rangle$ component can pass because the two input photons will both arrive at BS2 or BS3 together (the two H photons undergo quantum interference at BS1). In that case, the negative probability amplitude corresponding to the exchange of the ancilla photon and one of the input photons is higher than the positive probability amplitude for three-photon reflection, and the $|HH\rangle$ component is transmitted with a flipped phase.

To realize the quantum optical circuit of Fig. 2A, we have combined two recent technological approaches in order to simplify and stabilize quantum optical circuits: the displaced-Sagnac architecture (6) and PPBSs (7–9). In this case, the PPBSs reflect vertically polarized photons perfectly while transmitting/reflecting horizontally polarized photons with 50% probability. By replacing all the beam splitters (BS1 to BS4) with such PPBSs, we can remove the four polarizing beam splitters that were used to separate the two polarizations (Fig. 2B). The remaining optical path interferometer is realized as a displaced Sagnac interferometer (Fig. 2C).

Fig. 2. Optical quantum circuit for the nondestructive entanglement filter. (A) The original circuit includes concatenated path-interferometers together with four quantum interferences. PBS, polarizing beam splitter, which reflects vertical polarization component and transmits horizontal polarization; BS, beam splitter, whose reflectance/transmittance is 1/2 for horizontal/vertical polarization component. (Inset) Two-photon interference at BS2 and BS3. The blue line indicates optical paths for vertically polarized components, and the red line indicates optical paths for horizontally polarized components. (B) A semisimplified circuit made by using PPBSs. The reflectance of PPBS A for horizontally and vertically polarized photons is 1/2 and 1, respectively. The



transmittance of PPBS B for horizontally and vertically polarized photons is 1/2 and 1, respectively. (C) The final simplified system used in our experiment. Now the system includes one super-stable optical path-interferometer realized by using displaced Sagnac architecture.

transmittance of PPBS B for horizontally and vertically polarized photons is 1/2 and 1, respectively. (C) The final simplified system used in our experiment. Now the system includes one super-stable optical path-interferometer realized by using displaced Sagnac architecture.

In this setup, all the four polarization modes of two-input photons pass through all the optical components inside the interferometer so that the path differences between those four polarization modes are robust against drifts or vibrations of optical components.

We used photons generated via type-I spontaneous parametric down-conversion (23). The pump laser pulses (82 MHz at 390 nm) pass through a beta-barium borate crystal twice to generate two pairs of photons. Two photons in one of the pairs are used as the signal photons, and the two photons in the other pair are used as the ancillary photons. The visibility of the Hong-Ou-Mandel dip (22) was $96 \pm 1\%$ for two photons in the same pair and $85 \pm 5\%$ for photons from different pairs. To test the performance of our quantum filter circuit, we used coincidence measurements between the four threshold detectors at D1, D2, and the two outputs rather than using photon number-discriminating detectors (24–27) for D1 and D2 because we needed to analyze the polarization state of the output to confirm correct operation. We performed this polarization analysis using pairs of half-wave plates and quarter-wave plates together with polarizing beam splitters.

First, we checked the essential operation of the filter circuit. We prepared input-signal photons in the four combinations of H and V polarizations (which we call the Z-basis states) and observed how those input states are filtered by the circuit (Fig. 3). It is clear from the experimental data that the photon pairs are transmitted through the filter when the two input photons share the same polarization (HH or VV), and most of the pairs are filtered out when the two input photons have different polarizations (HV or VH). The fidelity of this process can be defined as the ratio of correctly transmitted photon pairs to the total number of transmitted photon pairs. For the filter's operation on horizontal and vertical polarizations, the fidelity is $F_{Z \rightarrow Z} = 0.80$.

Next, it was necessary to test the preservation of quantum coherence between the $|HH\rangle$ and the $|VV\rangle$ components transmitted by the filter. As explained above, this can be done by using diagonally polarized photons in the input. We prepared pairs of photons in all combinations of diagonal linear polarizations $|P\rangle$ and $|M\rangle$ (the X-basis states) as signal inputs. The input photons are then in an equal superposition of the four different horizontal/vertical polarization states $|HH\rangle$, $|HV\rangle$, $|VH\rangle$, and $|VV\rangle$ (with different signs of the coherences for each of the four different inputs). The filter should transmit only the HH and the VV components while preserving the quantum coherence between them. As a result, the ideal output states are entangled states with maximal correlations in both the circular and the diagonal polarizations. To test this entanglement generation, we first detected the output photons in the right-circular $|R\rangle \equiv (|H\rangle + i|V\rangle)/\sqrt{2}$ and left-circular $|L\rangle \equiv (|H\rangle - i|V\rangle)/\sqrt{2}$ polarizations (Y basis). The predicted correlations between the circular polarizations of the output were observed with a fidelity of $F_{X \rightarrow Y} = 0.68$. To complete the test of entanglement generation, we also detected the diagonal polarizations of the output to test whether the polarization correlation was correctly flipped by the filter. The fidelity of this filter operation was $F_{X \rightarrow X} = 0.60$. Taken together, the three experimental tests are sufficient for the evaluation of the quantum filter operation. Because almost all the errors conserve horizontal/vertical polarization [supporting online material (SOM) text], the probability of the correct operation \hat{S} is given by the process fidelity

$$F_p = (F_{Z \rightarrow Z} + F_{X \rightarrow Y} + F_{X \rightarrow X} - 1)/2 = 0.54 \quad (2)$$

The entanglement capability of the filter can be evaluated as $C = 2F_p - 1 = 0.08$, and so our experimental results provide clear evidence of the entangling capability of the quantum filter operation.

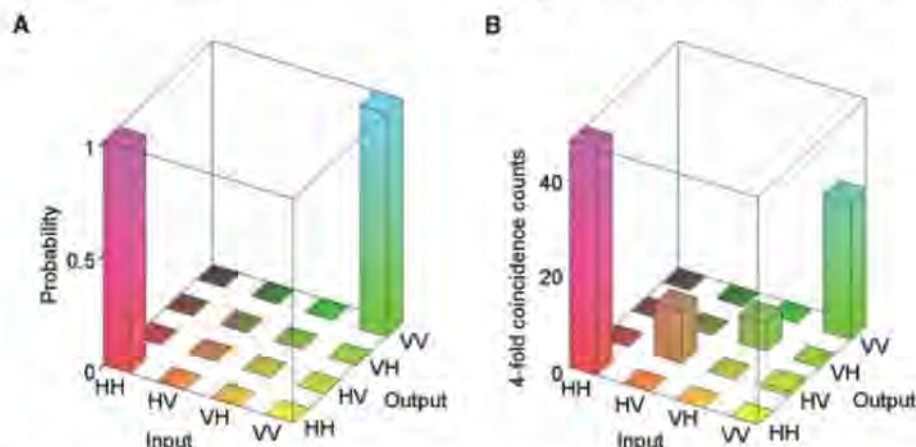


Fig. 3. Experimental results. Input-signal photons are prepared in H or V polarization and are measured on an H/V basis. (A) Theoretically predicted probabilities and (B) fourfold coincidence count rates [counts per 800 s] of the four detectors D1 to D4 are shown. The events in which two pairs of photons are simultaneously incident to the ancillary inputs and no photons are incident to the signal inputs are subtracted, as confirmed by a reference experiment without input photons (6 coincidence counts per 800 s for each of four cases with HH outputs).

The entanglement filter will be a key element in the control of multiphoton quantum states, with a wide range of applications in entanglement-based quantum communication and quantum information processing. For the present tests of the performance of the quantum filter circuit, we used threshold detectors to monitor the output state. For applications in which the output state cannot be monitored, high-efficiency number-resolving photon detectors (24–27) could be used at D1 and D2 to generate the heralding signals. Such a circuit could be used for on-demand generation of entangled photons or non-destructive entanglement purification and could be implemented using an integrated waveguide architecture (28).

References and Notes

1. N. Gisin, G. Ribordy, W. Tittel, H. Zbinden, *Rev. Mod. Phys.* **74**, 145 (2002).
2. M. A. Nielsen, I. L. Chuang, *Quantum Computation and Quantum Information* (Cambridge Univ. Press, Cambridge, UK, 2000).
3. V. Giovannetti, S. Lloyd, L. Maccone, *Science* **306**, 1330 (2004).
4. A. N. Boto et al., *Phys. Rev. Lett.* **85**, 2733 (2000).
5. H. F. Hofmann, S. Takeuchi, *Phys. Rev. Lett.* **88**, 147901 (2002).
6. T. Nagata, R. Okamoto, J. L. O'Brien, K. Sasaki, S. Takeuchi, *Science* **316**, 726 (2007).
7. N. K. Langford et al., *Phys. Rev. Lett.* **95**, 210504 (2005).
8. N. Kiesel, C. Schmid, U. Weber, R. Ursin, H. Weinfurter, *Phys. Rev. Lett.* **95**, 210505 (2005).
9. R. Okamoto, H. F. Hofmann, S. Takeuchi, K. Sasaki, *Phys. Rev. Lett.* **95**, 210506 (2005).
10. N. Gisin, R. Thew, *Nature Photonics* **1**, 165 (2007).
11. B. L. Higgins, D. W. Berry, S. D. Bartlett, H. M. Wiseman, G. J. Pryde, *Nature* **450**, 393 (2007).
12. M. D'Angelo, M. V. Chekhova, Y. Shih, *Phys. Rev. Lett.* **87**, 013602 (2001).
13. J. L. O'Brien, *Science* **318**, 1567 (2007).
14. J.-W. Pan, C. Simon, C. Brukner, A. Zeilinger, *Nature* **410**, 1067 (2001).
15. T. Yamamoto, M. Koashi, S. K. Özdemir, N. Imoto, *Nature* **421**, 343 (2003).
16. B. Misra, E. C. G. Sudarshan, *J. Math. Phys.* **18**, 756 (1977).
17. P. G. Kwiat et al., *Phys. Rev. Lett.* **83**, 4725 (1999).
18. K. Sanaka, *Phys. Rev. A* **71**, 021801 (2005).
19. K. Sanaka, K. J. Resch, A. Zeilinger, *Phys. Rev. Lett.* **96**, 083601 (2006).
20. K. J. Resch et al., *Phys. Rev. Lett.* **98**, 203602 (2007).
21. T. B. Pittman, B. C. Jacobs, J. D. Franson, *Phys. Rev. A* **64**, 062311 (2001).
22. C. K. Hong, Z. Y. Ou, L. Mandel, *Phys. Rev. Lett.* **59**, 2044 (1987).
23. D. C. Burnham, D. L. Weinberg, *Phys. Rev. Lett.* **25**, 84 (1970).
24. S. Takeuchi, J. Kim, Y. Yamamoto, H. H. Hogue, *Appl. Phys. Lett.* **74**, 1063 (1999).
25. J. Kim, S. Takeuchi, Y. Yamamoto, H. H. Hogue, *Appl. Phys. Lett.* **74**, 902 (1999).
26. E. J. Gansen et al., *Nature Photonics* **1**, 585 (2007).
27. B. E. Kardynal, Z. L. Yuan, A. J. Shields, *Nature Photonics* **2**, 425 (2008).
28. A. Politi, M. J. Cryan, J. G. Rarity, S. Yu, J. L. O'Brien, *Science* **320**, 646 (2008).
29. This work was supported by the Japan Science and Technology Agency, Ministry of Internal Affairs and Communication, Japan Society for the Promotion of Science, 21st Century Center of Excellence Program, Special Coordination Funds for Promoting Science and Technology, Japan, and Engineering and Physical Sciences Research Council, UK.

Supporting Online Material

www.sciencemag.org/cgi/content/full/323/5913/483/DC1
SOM Text

14 October 2008; accepted 16 December 2008
10.1126/science.1167182

Quantum Teleportation Between Distant Matter Qubits

S. Olmschenk,^{1*} D. N. Matsukevich,¹ P. Maunz,¹ D. Hayes,¹ L.-M. Duan,² C. Monroe¹

Quantum teleportation is the faithful transfer of quantum states between systems, relying on the prior establishment of entanglement and using only classical communication during the transmission. We report teleportation of quantum information between atomic quantum memories separated by about 1 meter. A quantum bit stored in a single trapped ytterbium ion (Yb^+) is teleported to a second Yb^+ atom with an average fidelity of 90% over a complete set of states. The teleportation protocol is based on the heralded entanglement of the atoms through interference and detection of photons emitted from each atom and guided through optical fibers. This scheme may be used for scalable quantum computation and quantum communication.

A defining feature of quantum physics is the inherent uncertainty of physical properties, despite the fact that we observe only definite states after a measurement. The conventional interpretation is that the measurement process itself can irreversibly influence the quantum system under study. The field of quantum information science makes use of this notion and frames quantum mechanics in terms of the storage, processing, and communication of information. In particular, the back-action of measurement underlies the quantum “no cloning” theorem, which states that it is impossible to generate identical copies of an unknown quantum state (1). Nevertheless, a quantum state can still be transferred from one system to another by the process of quantum teleportation (2). A quantum state initially stored in system A can be teleported to system B by using the resource of quantum entanglement or the quantum correlation between systems that do not have well-defined individual properties. Relaying the result of a destructive measurement of system A allows the original quantum state to be recovered at system B without ever having traversed the space between the systems. The ability to teleport quantum information is an essential ingredient for the long-distance quantum communication afforded by quantum repeaters (3) and may be a vital component to achieve the exponential processing speed-up promised by quantum computation (4).

The experimental implementation of teleportation has been accomplished in optical systems by using down-converted photons (5, 6) and squeezed light with continuous variable entanglement (7). Teleportation has also been accomplished between photons and a single atomic ensemble (8, 9). Because photons are able to carry quantum information and establish entanglement over long distances, these experiments demonstrated the nonlocal behavior of tele-

portation. However, a quantum memory is required at both transmitting and receiving sites in order to scale this protocol to quantum networks and propagate quantum information over multiple nodes (10). Deterministic teleportation between quantum memories has been demonstrated with trapped atomic ions in close proximity to one another, relying on the mutual Coulomb interaction (11–13). In contrast to the optical systems, these implementations feature long-lived coherences stored in good quantum memories but lack the ability to easily transmit quantum information over long distances.

We present the implementation of a heralded teleportation protocol where the advantages from both optical systems and quantum memories are combined to teleport quantum states between two trapped ytterbium ion (Yb^+) quantum bits (qubits) over a distance of about 1 m. We fully characterized the system by performing tomography on the teleported states, enabling complete

process tomography of the teleportation protocol. The measured average teleportation fidelity of $90\% \pm 2\%$ [$90(2)\%$] over a set of mutually unbiased basis states, which is well above the $2/3$ fidelity threshold that could be achieved classically, unequivocally demonstrates the quantum nature of the process (14, 15). Our teleportation protocol represents the implementation of a probabilistic measurement-based gate that could be used to generate entangled states for scalable quantum computation (16, 17).

A schematic of the experimental setup (Fig. 1) shows a single Yb^+ atom confined and Doppler laser-cooled in each of two nearly identical radio-frequency (rf) Paul traps, located in independent vacuum chambers (18–21). An ion will typically remain in the trap for several weeks. The qubit states in each atom are chosen to be the first-order magnetic field-insensitive hyperfine “clock” states of the $^2S_{1/2}$ level, $|F=0, m_F=0\rangle$ and $|F=1, m_F=0\rangle$, which are separated by 12.6 GHz and defined to be $|0\rangle$ and $|1\rangle$, respectively. In this notation, F is the total angular momentum of the atom, and m_F is its projection along a quantization axis defined by an external magnetic field B . The qubit exhibits coherence times observed to be greater than 2.5 s and thus serves as an excellent quantum memory (20).

For the teleportation protocol (Fig. 2A), the states of the atomic qubits are initialized with a 1- μs pulse of 369.5-nm light resonant with the $^2S_{1/2} |F=1\rangle \leftrightarrow ^2P_{1/2} |F=1\rangle$ transition that optically pumps the ions to $|0\rangle$ with probability greater than 99% (20). We can then prepare any superposition of $|0\rangle$ and $|1\rangle$ by applying a resonant microwave pulse with controlled phase and duration (0 to 16 μs) directly to one of the trap electrodes. The quantum state to be tele-

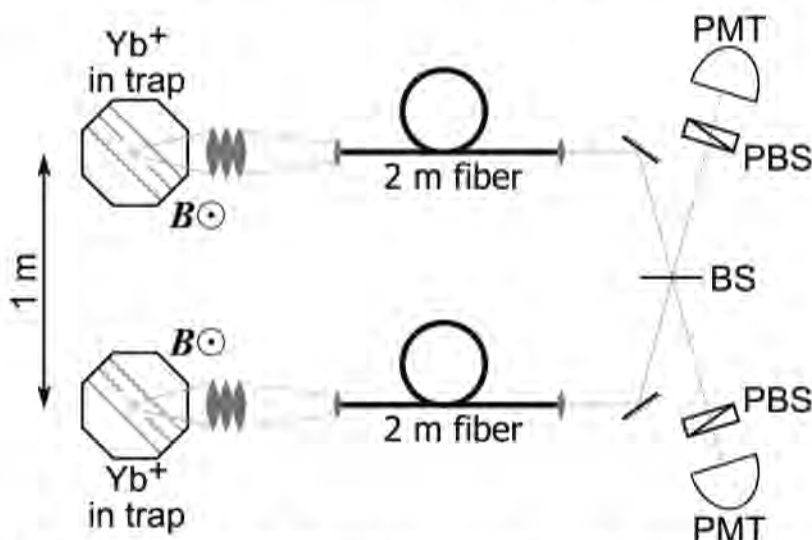


Fig. 1. The experimental setup. Two Yb^+ ions are trapped in independent vacuum chambers. An externally applied magnetic field B determines a quantization axis for defining the polarization of photons emitted by each atom. Spontaneously emitted photons are collected with an objective lens, coupled into a single-mode fiber, and directed to interfere on a beamsplitter (BS). Polarizing beamsplitters (PBSs) filter out photons resulting from σ decays in the atoms. The remaining π -polarized photons are detected by single-photon counting PMTs.

¹Joint Quantum Institute (JQI) and Department of Physics, University of Maryland, College Park, MD 20742, USA. ²FOCUS Center and Department of Physics, University of Michigan, Ann Arbor, MI 48109, USA.

*To whom correspondence should be addressed. E-mail: smolms@umd.edu

ported is written to ion *A* by using this microwave pulse, which prepares ion *A* in the state $|\Psi(t_1)\rangle_A = \alpha|0\rangle_A + \beta|1\rangle_A$. A separate microwave pulse prepares ion *B* in the definite state $|\Psi(t_1)\rangle_B = |0\rangle_B + |1\rangle_B$, where for simplicity we neglect normalization factors and assume ideal state evolution throughout our discussion. After this state preparation, each ion is excited to the $^2P_{1/2}$ level with near-unit probability by an ultrafast laser pulse (≈ 1 ps) having a linear polarization aligned parallel to the quantization axis (π -polarized) and a central wavelength of 369.5 nm. Due to the polarization of the pulse and atomic selection rules, the broadband pulse coherently transfers $|0\rangle$ to $^2P_{1/2}[F=1, m_F=0]$ and $|1\rangle$ to $^2P_{1/2}[F=0, m_F=0]$ (Fig. 2B) (22). Because the duration of this pulse is much shorter than the $\tau \approx 8$ ns natural lifetime of the $^2P_{1/2}$ level, each ion spontaneously emits a single photon while returning to the $^2S_{1/2}$ ground state (18). The emitted photons at 369.5 nm can each be collected along a direction perpendicular to the quantization axis by objective lenses of numerical aperture $NA = 0.23$ and coupled into single-mode fibers. Observation along this direction allows for polarization filtering of the emitted photons because those produced by π and σ transitions appear as orthogonally polarized (23). Considering only π decays results in each ion being entangled with the frequency of its emitted photon such that

$$\begin{aligned} |\Psi(t_2)\rangle_A &= \alpha|0\rangle_A|v_{\text{blue}}\rangle_A + \beta|1\rangle_A|v_{\text{red}}\rangle_A \\ |\Psi(t_2)\rangle_B &= |0\rangle_B|v_{\text{blue}}\rangle_B + |1\rangle_B|v_{\text{red}}\rangle_B \end{aligned} \quad (1)$$

where $|v_{\text{blue}}\rangle$ and $|v_{\text{red}}\rangle$ are single photon states having well-resolved frequencies ν_{blue} and ν_{red} , each with a bandwidth of $1/(2\pi\tau) \approx 20$ MHz and frequency difference $\nu_{\text{blue}} - \nu_{\text{red}} = 14.7$ GHz. The outputs of the fibers are directed to interfere at a 50:50 nonpolarizing beamsplitter, with

a measured mode overlap greater than 98%. Because of the quantum interference of the two photons, a simultaneous detection at both output ports of the beamsplitter occurs only if the photons are in the state $|\Psi^-\rangle_{\text{photons}} = |v_{\text{blue}}\rangle_A|v_{\text{red}}\rangle_B - |v_{\text{red}}\rangle_A|v_{\text{blue}}\rangle_B$ (24–26), which projects the ions into the entangled state (27):

$$\begin{aligned} \langle\Psi^-(t_3)|_{\text{photons}}(|\Psi(t_3)\rangle_A \otimes |\Psi(t_3)\rangle_B) &= \\ |\Psi(t_3)\rangle_{\text{ions}} &= \alpha|0\rangle_A|1\rangle_B - \beta|1\rangle_A|0\rangle_B \end{aligned} \quad (2)$$

A coincident detection of two photons is therefore the heralding event that announces the success of the ion-ion entangling gate operation $\frac{1}{2}\hat{\sigma}_3^A(\hat{\sigma}_0^B\hat{\sigma}_0^B - \hat{\sigma}_3^B\hat{\sigma}_3^B)$, where $\hat{\sigma}_0^i$ is the identity and $\hat{\sigma}_3^i$ the z -Pauli operator acting on the i th qubit (16). In the current setup, this entangling gate only succeeds with probability $P_{\text{gate}} \approx 2.2 \times 10^{-8}$, limited by the efficiency of collecting and detecting both spontaneously emitted photons. Therefore, the previous steps (state preparation and pulsed excitation) are repeated at a rate of 40 to 75 kHz, including intermittent cooling, until the gate operation is successful (every 12 min, on average). Because each attempt is independent of all others, this protocol allows for a sequence of unknown and unrelated input states. After the entanglement has been confirmed by the heralding event, another pulse of microwaves transforms the state of ion *A* through the rotation operator $R_y(\pi/2)$, altering the state of the ions given in Eq. 2 to

$$\begin{aligned} |\Psi(t_4)\rangle_{\text{ions}} &= \alpha(|0\rangle_A + |1\rangle_A)|1\rangle_B - \\ &\quad \beta(-|0\rangle_A + |1\rangle_A)|0\rangle_B \end{aligned} \quad (3)$$

We then measure the state of ion *A* with standard fluorescence techniques, by illuminating the ion with laser light at 369.5 nm, resonant with the $^2S_{1/2}[F=1] \leftrightarrow ^2P_{1/2}[F=0]$ transition. If the ion is in the state $|1\rangle$, it scatters many photons, whereas if the ion is in the state $|0\rangle$ the

light is off-resonance and almost no photons are scattered. By detecting the fluorescence of the atom with a single-photon counting photomultiplier tube (PMT), we discriminate between $|0\rangle$ and $|1\rangle$ with an error of about 2% (20).

Measuring ion *A* projects ion *B* into one of the two states:

$$\begin{aligned} |\Psi(t_5)\rangle_B &= \alpha|1\rangle_B + \beta|0\rangle_B \text{ (if measured } |0\rangle_A) \\ |\Psi(t_5)\rangle_B &= \alpha|1\rangle_B - \beta|0\rangle_B \text{ (if measured } |1\rangle_A) \end{aligned} \quad (4)$$

The result of the measurement on ion *A* is relayed through a classical communication channel and used to determine the necessary phase of a conditional microwave π pulse applied to ion *B* to recover the state initially written to ion *A*; measuring $|0\rangle_A$ requires the rotation $R_y(\pi)$, whereas $|1\rangle_A$ demands $R_y(\pi)$. Afterward, the state of ion *B* is ideally $|\Psi(t_6)\rangle_B = \alpha|0\rangle_B + \beta|1\rangle_B$, which completes the teleportation of the quantum state between the two distant matter qubits.

The teleportation protocol we present differs from the original proposal (2) in that we use four qubits (two atoms and two photons) rather than three, and our implementation is intrinsically probabilistic because the two-photon Bell states are not all deterministically distinguishable (5, 26, 27). Nevertheless, the heralding event of the two-photon coincident detection still allows our teleportation protocol to succeed without postselection (15). In addition, establishing the quantum channel between the (atomic) quantum memories with photons and entanglement swapping allows the atoms to be separated by a large distance from the outset.

A successful implementation of this teleportation protocol requires the transmission of two classical bits of information: one to announce

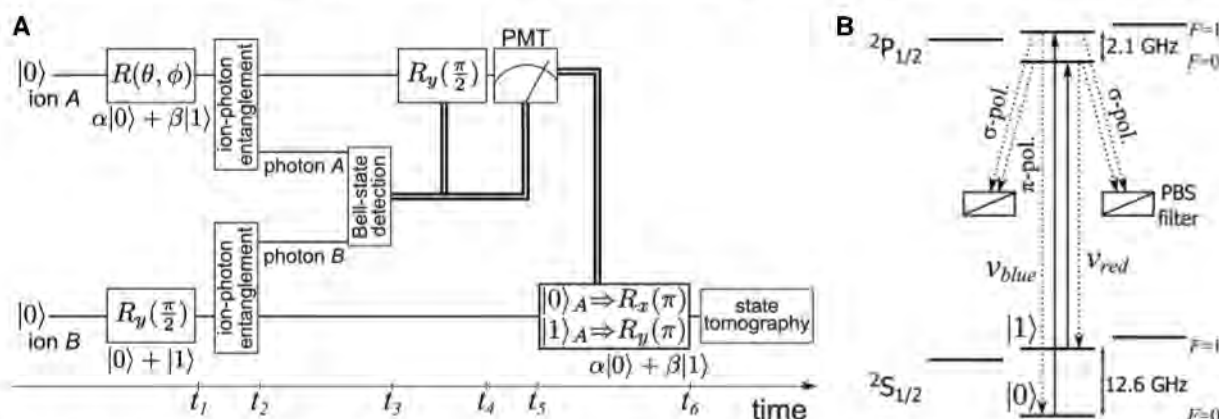


Fig. 2. (A) Schematic of the teleportation protocol. Each ion is first initialized to $|0\rangle$ by optical pumping. The state to be teleported is written to ion *A* by a microwave pulse, whereas a separate microwave pulse prepares ion *B* in a known superposition (t_1). A laser pulse excites each atom, as shown in (B). The frequency of an emitted π -polarized photon (selected by polarization filtering) is then entangled with the hyperfine levels of the atom (t_2). These two photons interfere at a BS, as illustrated in Fig. 1, resulting in a coincident detection only if the photons are in the $|\Psi^-\rangle_{\text{photons}}$ state, which heralds the success of the ion-

ion entangling gate (t_3). If the gate is successful, ion *A* is rotated by $\pi/2$ (t_4) and measured (t_5). A microwave pulse with phase conditioned on the outcome of the measurement on ion *A* is then applied to ion *B* to complete the teleportation of the quantum state (t_6). **(B)** Ion-photon entanglement process. A broadband picosecond pulse with a central wavelength at 369.5 nm is used to coherently excite $|0\rangle$ and $|1\rangle$ to the $^2P_{1/2}$ level. Because of the atomic selection rules and polarization filtering with PBSs to only observe photons from a π decay, the coherence of the atomic states is retained.

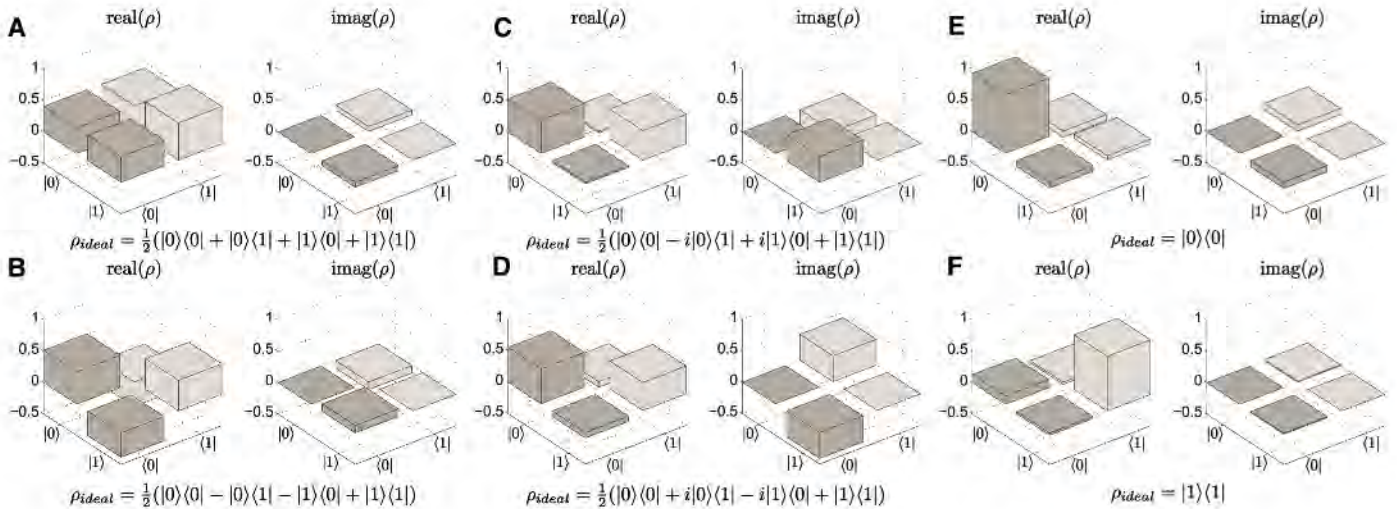


Fig. 3. Tomography of the teleported quantum states. The reconstructed density matrices, ρ , for the six unbiased basis states teleported from ion A to ion B: (A) $|\Psi_{\text{ideal}}\rangle = |0\rangle + |1\rangle$ teleported with fidelity $f = 0.91(3)$, (B) $|\Psi_{\text{ideal}}\rangle = |0\rangle - |1\rangle$ teleported with fidelity $f = 0.88(4)$, (C) $|\Psi_{\text{ideal}}\rangle = |0\rangle + i|1\rangle$ teleported with fidelity $f = 0.92(4)$, (D) $|\Psi_{\text{ideal}}\rangle = |0\rangle - i|1\rangle$ teleported with fidelity $f = 0.91(4)$, (E)

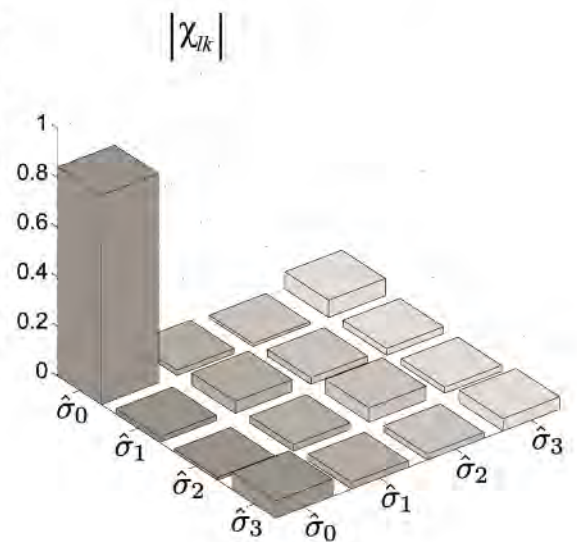
$|\Psi_{\text{ideal}}\rangle = |0\rangle$ teleported with fidelity $f = 0.93(4)$, and (F) $|\Psi_{\text{ideal}}\rangle = |1\rangle$ teleported with fidelity $f = 0.88(4)$. These measurements yield an average teleportation fidelity $f = 0.90(2)$, where we have defined the fidelity as the overlap of the ideal teleported state with the measured density matrix, $f = \langle \Psi_{\text{ideal}} | \rho | \Psi_{\text{ideal}} \rangle$. The data shown comprise a total of 1285 events in 253 hours.

the success of the entangling gate and another to determine the proper final rotation to recover the teleported state at ion B. Although these classical bits do not contain any information about α or β , in the absence of this classical information ion B is left in a mixed state (Eq. 4), and the protocol fails. The required classical communication assures that no information is transferred superluminally (2).

We evaluate the teleportation protocol by performing state tomography on each teleported state. The tomographic reconstruction of the single-qubit density matrix can be completed by measuring the state in three mutually unbiased measurement bases. Because measurement of the ion occurs via the aforementioned state fluorescence technique, measurement in the remaining two bases requires an additional microwave pulse before detection; we define the rotation $\{R_y(\pi/2), R_x(\pi/2), R(0)\}$ before detection to correspond to measurement in the basis $\{x, y, z\}$. The single-qubit density matrix is then reconstructed from these measurements with use of a simple analytical expression (28).

We teleport and perform tomography on the set of six mutually unbiased basis states $|\Psi_{\text{ideal}}\rangle \in \{|0\rangle + |1\rangle, |0\rangle - |1\rangle, |0\rangle + i|1\rangle, |0\rangle - i|1\rangle, |0\rangle, |1\rangle\}$. The reconstructed density matrix, ρ , for each of these teleported states is shown in Fig. 3. The fidelity of the teleportation, defined as the overlap of the ideal teleported state and the measured density matrix $f = \langle \Psi_{\text{ideal}} | \rho | \Psi_{\text{ideal}} \rangle$, for this set of states is measured to be $f = \{0.91(3), 0.88(4), 0.92(4), 0.91(4), 0.93(4), 0.88(4)\}$, yielding an average teleportation fidelity $\bar{f} = 0.90(2)$. The experimental teleportation fidelities surpass the maximum value of $2/3$ that is achievable by classical means, explicitly demonstrating the quantum nature of the process (14, 15).

Fig. 4. Absolute value of the components of the reconstructed process matrix, $|\chi_{lk}|$, with $l, k = 0, 1, 2$, and 3 . The state tomography of the six mutually unbiased basis states teleported between the two ions, displayed in Fig. 3, enables process tomography of the teleportation protocol by a maximum likelihood method. The operators $\hat{\sigma}_i$ are the identity ($i = 0$) and the x -, y -, and z -Pauli matrices ($i = 1, 2$, and 3). As intended, the dominant component of χ is the contribution of the identity operation, yielding an overall process fidelity $f_{\text{process}} = \text{tr}(\chi_{\text{ideal}} \chi) = 0.84(2)$, consistent with the average fidelity cited above.



The reconstructed density matrices also facilitate full characterization of the teleportation protocol by quantum process tomography. We can completely describe the effect of the teleportation protocol on an input state ρ_{in} by determining the process matrix χ , defined by $\rho = \sum_{l,k=0}^3 \chi_{lk} \hat{\sigma}_l \rho_{\text{in}} \hat{\sigma}_k$, where to evaluate our process we take $\rho_{\text{in}} = |\Psi_{\text{ideal}}\rangle\langle \Psi_{\text{ideal}}|$. The ideal process matrix, χ_{ideal} , has only one nonzero component, $(\chi_{\text{ideal}})_{(0)} = 1$, meaning the input state is faithfully teleported. We experimentally determine the process matrix χ (Fig. 4) by using a maximum likelihood method (29) and calculate the process fidelity to be $f_{\text{process}} = \text{tr}(\chi_{\text{ideal}} \chi) = 0.84(2)$. Given that the relation between the average fidelity and process fidelity is $f_{\text{process}} = (3\bar{f} - 1)/2$,

this is consistent with the average fidelity found above (30).

The deviation from unit average fidelity is consistent with known experimental errors. The primary sources that reduce the average fidelity are imperfect state detection (3.5%), photon mode mismatch at the 50:50 beamsplitter (4%), and polarization mixing resulting from the nonzero numerical aperture of the objective lens and from misalignment with respect to the magnetic field (2%). Other sources, including incomplete state preparation, pulsed excitation to the wrong atomic state, dark counts of the PMT leading to false coincidence events, photon polarization rotation while traversing the optical fiber, and multiple excitation resulting from pulsed laser light leakage, are each expected to contribute to the error by much less than 1%. Residual micromotion at the rf-drive frequency of

the ion trap, which alters the spectrum of the emitted photons and degrades the quantum interference, reduces the average fidelity by less than 1%.

The entangling gate central to this teleportation protocol is a heralded, probabilistic process. The net probability for coincident detection of two emitted photons is given by $P_{\text{gate}} = (p_{\text{Bell}})(p_{\pi}\eta T_{\text{fiber}} T_{\text{optics}} \xi (\Delta\Omega/4\pi))^2 \approx 2.2 \times 10^{-8}$, where $p_{\text{Bell}} = 0.25$ accounts for the detection of only one out of the four possible Bell states; $p_{\pi} = 0.5$ is the fraction of photons with the correct polarization (half are filtered out as being produced by σ decays); $\eta = 0.15$ is the quantum efficiency of each PMT; $T_{\text{fiber}} = 0.2$ is the coupling and transmission of each photon through the single-mode optical fiber; $T_{\text{optics}} = 0.95$ is the transmission of each photon through the other optical components; $\xi = 1 - 0.005 = 0.995$, where 0.005 is the branching ratio into the $^2D_{3/2}$ level; and $\Delta\Omega/4\pi = 0.02$ is the solid angle of light collection. The attempt rate of 75 kHz is currently limited by the time of the state preparation microwave pulse, resulting in about one successful teleportation event every 12 min. However, the expression for P_{gate} reveals multiple ways to substantially increase the success rate. The most dramatic increase would be achieved by increasing the effective solid angle of collection, which, for instance, could be accomplished by surround-

ing each ion with an optical cavity. Although improvements that increase the success probability of the gate operation can enhance scalability, even with a low success probability this gate can still be scaled to more complex systems (16).

The fidelity obtained in the current experiment is evidence of the excellent coherence properties of the photonic frequency qubit and the "clock" state atomic qubit. Together, these complementary qubits provide a robust system for applications in quantum information. The teleportation scheme demonstrated here could be used as the elementary constituent of a quantum repeater. Moreover, the entangling gate implemented in this protocol may be used for scalable measurement-based quantum computation.

References and Notes

- W. K. Wootters, W. H. Zurek, *Nature* **299**, 802 (1982).
- C. H. Bennett et al., *Phys. Rev. Lett.* **70**, 1895 (1993).
- H.-J. Briegel, W. Dür, J. I. Cirac, P. Zoller, *Phys. Rev. Lett.* **81**, 5932 (1998).
- D. Gottesman, I. L. Chuang, *Nature* **402**, 390 (1999).
- D. Bouwmeester et al., *Nature* **390**, 575 (1997).
- D. Boschi, S. Branca, F. De Martini, L. Hardy, S. Popescu, *Phys. Rev. Lett.* **80**, 1121 (1998).
- A. Furusawa et al., *Science* **282**, 706 (1998).
- J. F. Sherson et al., *Nature* **443**, 557 (2006).
- Y.-A. Chen et al., *Nat. Phys.* **4**, 103 (2008).
- L.-M. Duan, M. D. Lukin, J. I. Cirac, P. Zoller, *Nature* **414**, 413 (2001).

- M. Riebe et al., *Nature* **429**, 734 (2004).
- M. D. Barrett et al., *Nature* **429**, 737 (2004).
- M. Riebe et al., *N. J. Phys.* **9**, 211 (2007).
- S. Massar, S. Popescu, *Phys. Rev. Lett.* **74**, 1259 (1995).
- S. J. van Enk, N. Lütkenhaus, H. J. Kimble, *Phys. Rev. A* **75**, 052318 (2007).
- L.-M. Duan et al., *Phys. Rev. A* **73**, 062324 (2006).
- R. Van Meter, K. M. Itoh, T. D. Ladd, <http://arxiv.org/abs/quant-ph/0507023>.
- P. Maunz et al., *Nat. Phys.* **3**, 538 (2007).
- D. L. Moehring et al., *Nature* **449**, 68 (2007).
- S. Olmschenk et al., *Phys. Rev. A* **76**, 052314 (2007).
- D. N. Matsukevich, P. Maunz, D. L. Moehring, S. Olmschenk, C. Monroe, *Phys. Rev. Lett.* **100**, 150404 (2008).
- M. J. Madsen et al., *Phys. Rev. Lett.* **97**, 040505 (2006).
- B. B. Blinov, D. L. Moehring, L.-M. Duan, C. Monroe, *Nature* **428**, 153 (2004).
- C. K. Hong, Z. Y. Ou, L. Mandel, *Phys. Rev. Lett.* **59**, 2044 (1987).
- Y. H. Shih, C. O. Alley, *Phys. Rev. Lett.* **61**, 2921 (1988).
- S. L. Braunstein, A. Mann, *Phys. Rev. A* **51**, R1727 (1995).
- C. Simon, W. T. M. Irvine, *Phys. Rev. Lett.* **91**, 110405 (2003).
- J. B. Altepeter, E. R. Jeffrey, P. G. Kwiat, in *Advances in Atomic, Molecular, and Optical Physics*, P. Berman, C. Lin, Eds. (Elsevier, San Diego, CA, 2006), vol. 52, pp. 105–159.
- J. L. O'Brien et al., *Phys. Rev. Lett.* **93**, 080502 (2004).
- M. Horodecki, P. Horodecki, R. Horodecki, *Phys. Rev. A* **60**, 1888 (1999).
- This work is supported by the Intelligence Advanced Research Projects Activity (IARPA) under Army Research Office contract, the NSF Physics at the Information Frontier program, and the NSF Physics Frontier Center at JQI.

14 October 2008; accepted 19 December 2008
10.1126/science.1167209

Femtosecond XANES Study of the Light-Induced Spin Crossover Dynamics in an Iron(II) Complex

Ch. Bressler,¹ C. Milne,¹ V.-T. Pham,¹ A. ElNahhas,¹ R. M. van der Veen,^{1,2} W. Gawelda,^{1,2*} S. Johnson,² P. Beaud,² D. Grolimund,² M. Kaiser,^{1,2} C. N. Borca,² G. Ingold,² R. Abela,² M. Chergui^{1†}

X-ray absorption spectroscopy is a powerful probe of molecular structure, but it has previously been too slow to track the earliest dynamics after photoexcitation. We investigated the ultrafast formation of the lowest quintet state of aqueous iron(II) tris(bipyridine) upon excitation of the singlet metal-to-ligand-charge-transfer (¹MLCT) state by femtosecond optical pump/x-ray probe techniques based on x-ray absorption near-edge structure (XANES). By recording the intensity of a characteristic XANES feature as a function of laser pump/x-ray probe time delay, we find that the quintet state is populated in about 150 femtoseconds. The quintet state is further evidenced by its full XANES spectrum recorded at a 300-femtosecond time delay. These results resolve a long-standing issue about the population mechanism of quintet states in iron(II)-based complexes, which we identify as a simple ¹MLCT→³MLCT→⁵T cascade from the initially excited state. The time scale of the ³MLCT→⁵T relaxation corresponds to the period of the iron-nitrogen stretch vibration.

There is a large class of iron(II)-based molecular complexes that exhibit two electronic states closely spaced in energy: a low-spin (LS) singlet and a high-spin (HS) quintet state. They therefore manifest spin crossover (SCO) behavior, wherein conversion from a LS ground state to a HS excited state (or the reverse) can be induced by small temperature or pressure changes or by light absorption (1, 2).

The SCO phenomenon has been much studied using steady-state (2) and ultrafast (3–6) optical spectroscopies, with the goal of identifying the elementary steps leading to formation of the HS state. A representative energy level diagram of all Fe(II)-based complexes is shown in Fig. 1 (7). The main difference between them concerns the absolute energies of states, not their energetic ordering (2). All crystallographic studies point to an

Fe-N bond elongation by ~0.2 Å in the HS compared to the LS state (1, 2). Theoretical studies show that the Fe-N bond length of the singlet and triplet metal-centered (MC) ^{1,3}T states lies halfway between those of the LS and HS states (7). Obviously, accessing the HS excited state by absorption of light from the LS ground state is forbidden by the spin selection rules. Therefore, the doorway to the HS state is ideally via the singlet metal-to-ligand-charge-transfer (¹MLCT) that exhibits strong absorption bands in the visible spectrum, or via the weakly absorbing and lower-lying ^{1,3}T states (1, 2). The time scale and the route going from the initially excited ¹MLCT state to the lowest-lying quintet state are still the subject of debate. Steady-state spectroscopic studies at cryogenic temperatures showed that excitation into the MC ^{1,3}T states leads to population of the ⁵T₂ state with a quantum efficiency of ~80% (2). Researchers therefore concluded that the relaxation cascade from the ¹MLCT state to the HS ⁵T₂ state proceeds via the intermediate ^{1,3}T states. However, for excitation of the ¹MLCT state, the relaxation process was reported to occur with 100% efficiency at both 10 K (2) and at room

¹Ecole Polytechnique Fédérale de Lausanne, Laboratoire de Spectroscopie Ultrarapide, ISIC, FSB-BSP, CH-1015 Lausanne, Switzerland. ²Swiss Light Source, Paul-Scherrer Institut, CH-5232 Villigen PSI, Switzerland.

*Present address: Laser Processing Group, Instituto de Optica, Consejo Superior de Investigaciones Científicas, Serrano 121, E-28006 Madrid, Spain.

†To whom correspondence should be addressed. E-mail: Majed.chergui@epfl.ch

temperatures (8, 9), thus questioning the involvement of the intermediate ^1T states. Ultrafast laser studies established that the relaxation cascade from the initially excited $^1\text{MLCT}$ state to the lowest excited quintet state $^5\text{T}_2$ is complete in <1 ps (3–5), but this result was indirectly inferred, as neither the intermediate MC states nor the final $^5\text{T}_2$ state have spectroscopic transitions in the region of the probe (>350 nm). McCusker and co-workers (6) proposed that the $^1\text{MLCT}$ state relaxes to a manifold of strongly mixed singlet and triplet MC states down to the quintet state, the latter being considered to be the only one clearly defined by its spin quantum number S . However, the steady-state spectroscopic studies of Hauser and co-workers (2) point to a clear classification of all MC states according to their spin character, thus excluding strong state mixings.

Iron(II)-tris(bipyridine) ($[\text{Fe}^{\text{II}}(\text{bpy})_3]^{2+}$), which is the molecule studied here, serves as a model system for the family of Fe(II)-based SCO complexes. Early events of the relaxation cascade in aqueous $[\text{Fe}^{\text{II}}(\text{bpy})_3]^{2+}$ were recently investigated using femtosecond resolved fluorescence and transient absorption by Gawelda *et al.* (5) upon 400-nm excitation of the $^1\text{MLCT}$ state. They observed a prompt (~ 30 fs) intersystem crossing (ISC) to the $^3\text{MLCT}$ state, followed by a departure from this state within ~ 120 fs (Fig. 1B). The subsequent steps and the arrival into the HS state were not observed directly, and the final step of the photocycle, the radiationless HS \rightarrow LS transition, was identified via the recovery of the ground-state electron bleach with its 665-ps lifetime. For 400-nm excitation, the relaxation cascade from the initially excited $^1\text{MLCT}$ state to the HS state implies dissipation of 2.6 eV of energy in <1 ps and, were it to proceed via the intermediate MC states, it would entail a back electron transfer, followed by at least three ISC events, as well as an Fe–N bond elongation by 0.2 Å. This elongation was recently measured by x-ray absorption spectroscopy (XAS) studies with 50- to 100-ps resolution on $[\text{Fe}^{\text{II}}(\text{tren}(\text{py})_3)]^{2+}$ (10) and $[\text{Fe}^{\text{II}}(\text{bpy})_3]^{2+}$ (11, 12) in solution. The structural change manifests itself through substantial modifications of the x-ray absorption near-edge structure (XANES) at the Fe K-edge, which we exploit in the present study of the ultrafast light-induced SCO of aqueous $[\text{Fe}^{\text{II}}(\text{bpy})_3]^{2+}$.

So far, most x-ray studies with subpicosecond time resolution have used diffraction to investigate strain, coherent phonon dynamics, or melting phenomena in solid materials (13–15). Scattering does not require wavelength tunability, and sources of (monochromatic) femtosecond x-ray pulses (obtained by plasma emission from metal targets struck by intense ultrashort laser pulses) have readily been available for some time now. Diffraction is also a collective phenomenon in crystals, delivering rather strong signals. For chemical and biological systems that may be disordered and diluted in solution, x-ray absorption spectroscopy is a more suitable probe (12, 16, 17). However, it requires rather stable sources of tunable ultrashort x-rays. Subpicosecond x-ray plasma

sources have been implemented for time-resolved XAS studies on the few picoseconds (18) to tens of picoseconds time scale, but their use is challenging because of their poor shot-to-shot stability and low fluxes (19, 20). Synchrotron sources (12, 17) deliver very stable radiation with reasonable fluxes, although the pulse durations lie in the 50- to 150-ps range. The recently developed slicing scheme (21) has allowed the extraction of tunable femtosecond x-ray pulses from a synchrotron and was first implemented for soft x-ray absorption studies of the electronic changes resulting from the photo-induced ultrafast insulator-metal phase transition in VO_2 bulk crystals (22) and the ultrafast demagnetization dynamics in solid nickel (23). For structural determination, hard x-rays (>2 keV) are better suited, and the recent implementation of the slicing scheme for 5 to 20 keV radiation at the Swiss Light Source (SLS, PSI-Villigen) (24) opens the possibility of carry-

ing out ultrafast XANES studies on dilute molecular systems in liquids. By applying this technique, we have succeeded in following the structural changes in real time upon visible light excitation of aqueous $[\text{Fe}^{\text{II}}(\text{bpy})_3]^{2+}$, and moreover we have unraveled the mechanism of the ultrafast spin crossover in this class of molecules.

Briefly (25), a 100- μm -thick free-flowing liquid jet of an aqueous solution of 50 mM $[\text{Fe}^{\text{II}}(\text{bpy})_3]^{2+}$ was excited by an intense 400-nm laser pulse (115-fs pulse width, repetition rate 1 kHz), and a tunable femtosecond hard x-ray pulse from the slicing source was used to probe the system in transmission mode at 2 kHz. The flux of the femtosecond x-ray source was about 10 photons per pulse at 7 keV. We recorded the transient difference absorption spectra by alternating detection of signals from the laser-excited and the unexcited sample, thus achieving a precise intrinsic energy calibration that compensates for

Fig. 1. (A) Representative potential energy curves of Fe(II)-based SCO complexes as a function of the Fe–N bond distance (7). The manifold of MLCT states is shown as a shaded area. $[\text{Fe}^{\text{II}}(\text{bpy})_3]^{2+}$ has predominantly O_h symmetry with a trigonal (D_3) distortion. The MC states are represented by their symmetry character (A, T, and E) in the D_3 group: the LS 1A_1 ground state has a completely filled $e_g^4 a_{1g}^2$ configuration (deriving from the t_{2g}^6 subshell in O_h symmetry), whereas the antibonding e_g (e_g in O_h symmetry) orbital is empty. Per electron that is promoted from the t_{2g} subshell to the e_g subshell (for easier reading we will use the O_h nomenclature hereafter), the metal-ligand bond length increases by as much as 0.1 Å (1, 7). For the series of $^1,^3T(t_{2g}^5 e_g^1)$ states, the Fe–N bond length is expected to lie between the values observed for the ground and the high-spin $^5T_2(t_{2g}^4 e_g^2)$ states. **(B)** Relaxation cascade as determined by ultrafast laser spectroscopy upon excitation of aqueous $[\text{Fe}(\text{bpy})_3]^{2+}$ at 400 nm (5). The intermediate MC states are not shown because they are optically silent in the region >350 nm and were therefore not observed in (5). **(C)** For the $[\text{Fe}(\text{bpy})_3]^{2+}$ complex, the Fe–N bond length is 1.97 Å in the low-spin $^1A_1(t_{2g}^6)$ ground state (32) but increases by 0.2 Å in the high-spin $^5T_2(t_{2g}^4 e_g^2)$ state, as determined by picosecond XAS experiments (11).

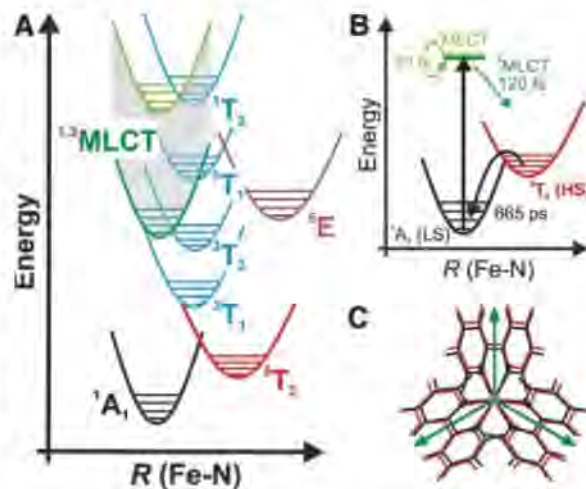
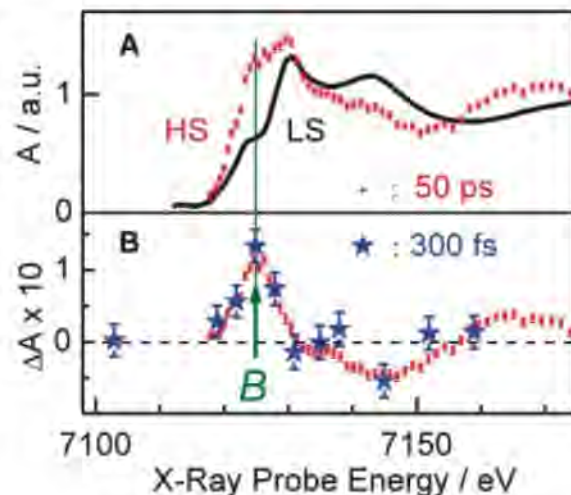


Fig. 2. (A) Fe K-edge XANES spectrum of the LS state of aqueous $[\text{Fe}^{\text{II}}(\text{bpy})_3]^{2+}$ (black trace) and of the HS quintet state (red dots). The latter is determined from the LS spectrum and the transient spectrum (B) measured at a time delay of 50 ps after laser excitation at 400 nm (11). **(B)** Transient XANES spectrum (difference in x-ray absorption between the laser-excited sample and the unexcited sample) recorded 50 ps after laser excitation at 400 nm (red dots) (11). Note the increase in absorption at the so-called B-feature. The blue stars represent the transient spectrum recorded at a time delay of 300 fs in the present work. Error bars, ± 1 SD (25).



drifts of the laser or synchrotron energies and fluxes. The time resolution was <250 fs (25).

Figure 2A shows the Fe K-edge XANES spectra of aqueous $[\text{Fe}^{\text{II}}(\text{bpy})_3]^{2+}$ in its ground (LS) and excited (HS) state. The spectrum of the latter was retrieved from the LS spectrum and the difference spectrum recorded 50 ps after laser excitation (red dots in Fig. 2B) (11). The strongest increase in absorption upon LS to HS conversion occurs at the so-called B-feature (arrow in Fig. 2), which was previously identified as a structure-sensitive above-ionization multiple-scattering resonance (26). The increase in intensity of the B-feature is concomitant with the increase in Fe-N bond distance upon LS to HS conversion, reflecting a well-established correlation between edge absorption intensity and bond distance [see, e.g., (27)]. For the present system, this correlation was confirmed (fig. S1) by a simulation of the XANES spectrum using the Minuit XANES (MXAN) code (11, 28), which additionally shows a nearly linear relationship between the Fe-N bond elongation and the intensity of the B-feature. The B-feature intensity is therefore a signature of the Fe-N bond elongation, and it allows us to distinguish the various states that can be grouped by their similar Fe-N bond distances: (i) the LS ground and the $^1\text{MLCT}$ states; (ii) the $^1\text{MLCT}$ states, which exhibit an elongation of 0.1 Å relative to the ground state (7); and (iii) the ^5T state, which exhibits a 0.2 Å elongation (11). Based on this correlation, we analyze the observed light-induced changes at the B-feature as a function of the time delay between the optical pump pulse and the x-ray probe pulse in the femtosecond to picosecond time domain.

Figure 3 shows the transient signal at the B-feature as a function of time delay (the inset shows an expanded region out to 10 ps). It is characterized by a steep rise followed by a plateau beyond 250 to 300 fs, which suggests that the system has reached the HS state within this time frame. This suggestion is confirmed by the energy scan recorded at a time delay of 300 fs (blue stars in Fig. 2B), which agrees with the transient absorption spectrum recorded at 50-ps time delay. Considering a simple four-level kinetic model $^1\text{A}_1 \rightarrow ^1\text{MLCT} \rightarrow ^3\text{MLCT} \rightarrow ^5\text{T}$, we simulated the signal with no adjustable parameters, assuming (i) an optical/x-ray cross-correlation of 250 fs; (ii) the $^1\text{MLCT}$ and $^3\text{MLCT}$ decay times measured in (5) (Fig. 1B); (iii) the cross sections at the B-feature for the LS and HS states (Fig. 2A), as well as for the intermediate $^1\text{MLCT}$ states, derived from the relationship between the Fe-N bond elongation and the B-feature intensity (25); and (iv) the absorption cross section of the $^3\text{MLCT}$ state(s). For the latter, based on our previous study of the analogous $[\text{Ru}^{\text{II}}(\text{bpy})_3]^{2+}$ molecule (29), the $^1\text{MLCT}$ and LS XANES are expected to be similar, except for a shift to higher energies of the $^1\text{MLCT}$ XANES spectrum, due to the oxidation of the central metal atom (over the time the system remains in the $^1\text{MLCT}$ manifold). At the Fe K-edge, this oxidation state shift amounts to at most +2 eV based on a study of Fe(II)- and Fe(III)-hexacyanide (30).

Figure 3B shows the simulated time evolution of the signal due to the various states, including (solid curves) and excluding (dashed curves) the $^1\text{MLCT}$ states, as well as the resulting total signal (red traces). The blue shift of the $^1\text{MLCT}$ spectrum

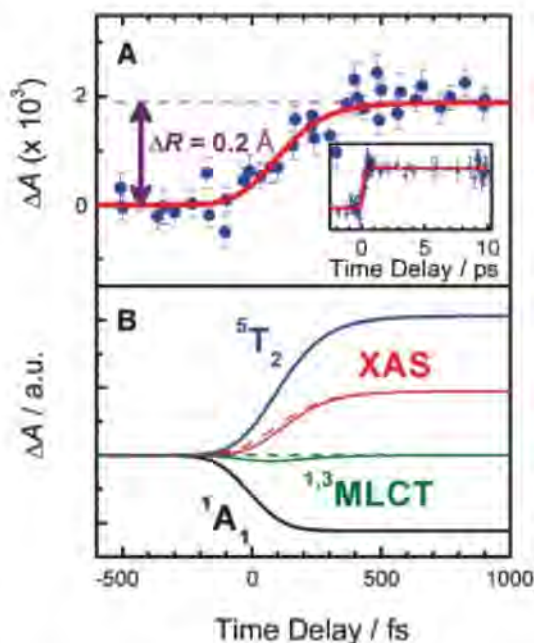
should lead to an initial decrease in absorption of the signal, which we do not observe. The simulations (green trace in Fig. 3B) confirm that our pump-probe correlation time brings this initial signal decrease below our experimental sensitivity, thus accounting for its absence in the data. Also, we note that time zero is hardly affected by inclusion of the signal due to the $^1\text{MLCT}$ state, and its value changes by at most 40 fs when comparing the simulations with and without the (temporary) oxidation shift. Finally, introducing the $^1\text{MLCT}$ state(s) can reproduce the data only for a fitted relaxation time of <60 fs (25). Such a short lifetime, however, is unrealistic because it corresponds to the period of high frequency modes of the system, which in addition would need to be shared among the $^1\text{MLCT}$ states that all have potential curves with identical equilibrium distances and curvatures along the Fe-N coordinate (Fig. 1A). Consequently, the agreement between the experimental and the simulated time trace (Fig. 3A) implies that the rise time (~150 fs) of the x-ray absorption of the HS state corresponds to the decay of the $^3\text{MLCT}$ state (5). Thus, the population of the $^3\text{MLCT}$ state proceeds to the quintet state directly and bypasses the intermediate $^1\text{MLCT}$ states. Furthermore, the derived relaxation time scale corresponds to the period of the Fe-N stretch mode, which lies in the 130- to 160-fs range for all Fe(II)-based complexes, according to Raman studies (31). Therefore, here the observation of the structural dynamics allows us to unambiguously unravel the population relaxation pathway.

Because the $^3\text{MLCT}$ state lies about 1.5 eV above the quintet state (Fig. 1), the latter is populated in high vibrational levels. However, we do not observe vibrational cooling in the quintet state, because XANES spectroscopy is in general not very sensitive to Debye-Waller factors, which reflect the uncertainty in atomic coordinates due to thermal motion.

The general picture of the light-induced SCO process that emerges from this study becomes very simple and is summarized in Fig. 1B. The full cascade reduces a two-step ISC process, $^1\text{MLCT} \rightarrow ^3\text{MLCT} \rightarrow ^5\text{T}$. The bypassing of the intermediate $^1\text{MLCT}$ states resolves the issue of multiple ultrafast ISC steps among states that are quasiparallel with respect to the Fe-N coordinate (Fig. 1A). Dissipation of the energy difference in the ultrafast cascade is accounted for by storage of vibrational energy in the quintet state. Finally, the unit quantum efficiency of the SCO process from the $^1\text{MLCT}$ state into the quintet state makes sense in the context of excluding any leakage back to the ground state (9) through the bypassing of the $^1\text{MLCT}$ states.

Considering that $[\text{Fe}^{\text{II}}(\text{bpy})_3]^{2+}$ is a model system for all Fe(II)-based SCO complexes, we believe that our results are of general validity to this family. These results also underscore the power of ultrafast x-ray absorption spectroscopy for the study of molecular structural dynamics of dilute systems. In the present case, resolving the structural dynamics unravels the pathways of spin and electronic relaxation.

Fig. 3. (A) Time scan of the signal (blue points) at the B-feature (at 712.6 eV) (Fig. 2B) as a function of laser pump/x-ray probe time delay after excitation of aqueous $[\text{Fe}^{\text{II}}(\text{bpy})_3]^{2+}$ at 400 nm. The inset shows a long time scan up to a 10-ps time delay. The red trace is the simulated signal assuming a simple four-step kinetic model $^1\text{A}_1 \rightarrow ^1\text{MLCT} \rightarrow ^3\text{MLCT} \rightarrow ^5\text{T}$ to describe the spin conversion process [see (B)]. The vertical arrow displays the expected effect of the elongation of 0.2 Å for the Fe-N bond elongation ΔR between the LS and HS states. Error bars, ± 1 SD (25). (B) Simulated transient absorption traces of the individual states (black, green, and blue) and total (red) trace based on a four-step kinetic model $^1\text{A}_1 \rightarrow ^1\text{MLCT} \rightarrow ^3\text{MLCT} \rightarrow ^5\text{T}$, with the $^3\text{MLCT} \rightarrow ^5\text{T}$ intersystem crossing taking place in 20 to 30 fs and the depopulation of the $^3\text{MLCT}$ state taking place in 120 fs, as determined by ultrafast fluorescence and transient absorption studies (5). Neglect of the absorption decrease due to the $^1\text{MLCT}$ states (dashed traces) does not affect the final simulated signal. The kinetics were convoluted with a cross-correlation of 250 fs between laser and x-ray pulse.



References and Notes

- P. Gutlich, H. A. Goodwin, *Top. Curr. Chem.* **233**, 1 (2004).
- A. Hauser, *Top. Curr. Chem.* **234**, 155 (2004).
- J. K. McCusker *et al.*, *J. Am. Chem. Soc.* **115**, 298 (1993).
- J. E. Monat, J. K. McCusker, *J. Am. Chem. Soc.* **122**, 4092 (2000).
- W. Gawelda *et al.*, *J. Am. Chem. Soc.* **129**, 8199 (2007).
- C. Brady, J. J. McGarvey, J. K. McCusker, H. Toftlund, D. N. Hendrickson, *Top. Curr. Chem.* **235**, 1 (2004).
- B. Ordejon, C. de Graaf, C. Sousa, *J. Am. Chem. Soc.* **130**, 13961 (2008).
- C. Creutz, M. Chou, T. L. Netzel, M. Okumura, N. Sutin, *J. Am. Chem. Soc.* **102**, 1309 (1980).
- M. A. Bergkamp, C. K. Chang, T. L. Netzel, *J. Phys. Chem.* **87**, 4441 (1983).
- M. Khalil *et al.*, *J. Phys. Chem. A* **110**, 38 (2006).
- W. Gawelda *et al.*, *Phys. Rev. Lett.* **98**, 057401 (2007).
- C. Bressler, R. Abela, M. Chergui, *Z. Kristallogr.* **223**, 307 (2008).
- A. Cavalleri, R. W. Schoenlein, *Top. Appl. Phys.* **92**, 309 (2004).
- M. Bargheer, N. Zhavoronkov, M. Woerner, T. Elsaesser, *Chem. Phys. Chem.* **7**, 783 (2006).
- K. J. Gaffney, H. N. Chapman, *Science* **316**, 1444 (2007).
- L. X. Chen, *Angew. Chem. Int. Ed.* **43**, 2886 (2004).
- C. Bressler, M. Chergui, *Chem. Rev.* **104**, 1781 (2004).
- F. Raksi *et al.*, *J. Chem. Phys.* **104**, 6066 (1996).
- I. V. Tomov, J. Chen, X. Ding, P. M. Rentzepis, *Chem. Phys. Lett.* **389**, 363 (2004).
- T. Lee, Y. Jiang, C. G. Rose-Petruck, F. Benesch, *J. Chem. Phys.* **122**, 084506 (2005).
- R. W. Schoenlein *et al.*, *Science* **287**, 2237 (2000).
- A. Cavalleri *et al.*, *Phys. Rev. Lett.* **95**, 067405 (2005).
- C. Stamm *et al.*, *Nat. Mater.* **6**, 740 (2007).
- P. Beaud *et al.*, *Phys. Rev. Lett.* **99**, 174801 (2007).
- Materials and methods are available as supporting material on Science Online.
- V. Briois, P. Saintcavit, G. J. Long, F. Grandjean, *Inorg. Chem.* **40**, 912 (2001).
- H. Dau, P. Liebisch, M. Haumann, *Anal. Bioanal. Chem.* **376**, 562 (2003).
- M. Benfatto, A. Congiu-Castellano, A. Daniele, S. D. Longa, *J. Synchrotron Radiat.* **8**, 267 (2001).
- W. Gawelda *et al.*, *J. Am. Chem. Soc.* **128**, 5001 (2006).
- A. Bianconi, in *X-ray Absorption Principles, Applications, Techniques of EXAFS, SEXAFS and XANES*, D. C. P. Koningsberger, R. Prins, Eds. (Wiley, New York, 1988), pp. 573–662.
- J. P. Tchuagues, A. Bousseksou, G. Molnar, J. J. McGarvey, F. Varret, *Top. Curr. Chem.* **235**, 85 (2004).
- S. Dick, *Z. Kristallogr., New Cryst. Struct.* **213**, 356 (1998).
- This work was funded by the Swiss National Science Foundation (FNRS), 110464, 107956, 620-066145, and 105239, and by Staatssekretariat für Bildung und Forschung contract COST D35 C06.0016. We are very grateful to A. Hauser (Geneva) for providing us with the samples, as well as for many useful discussions. We also thank M. Benfatto (Rome) for providing us with the MXAN code and for useful discussions.

Supporting Online Material

www.sciencemag.org/cgi/content/full/1165733/DC1

Materials and Methods

Fig. S1

References

25 June 2008; accepted 1 December 2008

Published online 11 December 2008;

10.1126/science.1165733

Include this information when citing this paper.

Complementary Active Sites Cause Size-Selective Reactivity of Aluminum Cluster Anions with Water

Patrick J. Roach,¹ W. Hunter Woodward,¹ A. W. Castleman Jr.,^{1*} Arthur C. Reber,² Shiv N. Khanna²

The reactions of metal clusters with small molecules often depend on cluster size. The selectivity of oxygen reactions with aluminum cluster anions can be well described within an electronic shell model; however, not all reactions are subject to the same fundamental constraints. We observed the size selectivity of aluminum cluster anion reactions with water, which can be attributed to the dissociative chemisorption of water at specific surface sites. The reactivity depends on geometric rather than electronic shell structure. Identical arrangements of multiple active sites in Al_{16}^- , Al_{17}^- , and Al_{18}^- result in the production of H_2 from water.

Metal clusters possess electronic shells that result from quantum confinement of the nearly free valence electrons (1–3). Because the shell structures of clusters and atoms are similar, shell-filling concepts from traditional valence bond theory can be applied to the description of clusters (4, 5). The result of a chemical interaction may then be explained through the energy minimization that results when a cluster closes an incomplete electronic shell (closed shell $n = 2, 8, 18, 20, 34, 40, \dots$), either by direct ionization or through the formation of a covalent or ionic bond (3–11). A cluster can therefore be assigned as a superatom analog of a specific group of the periodic table on the basis of the difference between its valence electron count and the number of electrons required to fill the nearest superatomic shell (8–11).

The previously reported size-selective reactions of Al clusters with O_2 (4, 6–11) result from the superatomic electronic structure. However, the observed selective reactivity of Al cluster anions with water is inconsistent with the closing of superatom shells. For example, Al_{23}^- and Al_{37}^- are both considered by the superatom model to have rare gas-like closed electronic shells (4) yet adsorb water molecules, whereas Al_{14}^- and Al_{46}^- have open electronic shells but do not adsorb water molecules (fig. S1) (12). We investigated what combination of geometric and electronic features could account for this observed reactivity. We found that pure Al cluster anions of certain sizes harbor distinct active sites in which a pair of adjacent Al atoms is responsible for the dissociative chemisorption of water. The complementary active site consists of one Al atom that acts as a Lewis acid and a second Al atom that acts as a Lewis base. The ability of an adjacent pair of different elements to promote similar chemical activity is known in metal oxides (13) and at the interface of dissimilar metals (14) because of the different electron affinity of each element. In the current case, however, we show

that the conditions required for reactivity are met in certain clusters that consist of only a single element. Understanding how a specific shape or size will affect the affinity of a metal cluster toward a specific reagent may facilitate future efforts to design either stable or reactive materials for specific technological applications (15–18).

Reactions between water (12) and anionic Al clusters comprising 7 to 60 atoms (Fig. 1) were observed under multicollosional conditions in a fast-flow reactor (fig. S2) (12). When water was introduced into the fast-flow reactor, products were observed that we have assigned as adducts of Al anion clusters with water. Most clusters adsorbed one or more water molecules with varying intensity, whereas no adducts were observed for other species (fig. S1) (12). The distinct differences in the reactivity of similarly sized clusters suggests that small differences in electronic and geometric structure play an important role in determining the reactivity of aluminum nanostructures with water.

Al_{12}^- is the smallest cluster that reacts to form a product of observable intensity (Fig. 2A); thus, we analyzed this species by a first-principles approach within a gradient-corrected density functional formalism (12). The initial interaction we considered between a water molecule and an Al cluster anion was the nucleophilic attack of water on the Al surface. This reaction requires the donation of lone-pair electrons from water to the lowest unoccupied molecular orbital (LUMO) of the cluster (or LUMO+1 in odd-electron species, as the lone pair interacts most strongly with levels where both spin states are unoccupied) where the probability density of the vacant orbital protrudes out from the cluster structure into vacuum (19–22). Previous rules proposed by Chrétien *et al.* (23) suggest that the susceptibility of a specific species to a nucleophilic reactant is increased as the relative energy of a cluster's LUMO decreases, as compared to other species (fig. S3A) (12). Although the observation of a strong $Al_{12}H_2O^-$ product peak (the LUMO energy of Al_{12}^- is a

¹Departments of Chemistry and Physics, Pennsylvania State University, University Park, PA 16802, USA. ²Department of Physics, Virginia Commonwealth University, Richmond, VA 23284, USA.

*To whom correspondence should be addressed. E-mail: awc@psu.edu

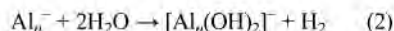
local minimum) is consistent with these rules, similar coincidences are not globally observed. We believe that this inconsistency is not a result of any deficiency in the rules, but rather suggests that the initial charge donation process consistent with nucleophilic bonding is not rate-limiting.

We next considered a reaction coordinate that is initiated by the chemisorption of a water molecule and subsequently undergoes a rate-limited step that results in dissociative chemisorption. The lone-pair electrons from oxygen nucleophilically attack the cluster at a well-defined site where the LUMO+1 protrudes into vacuum. The highest occupied molecular orbital (HOMO) of the chemisorbed intermediate of $\text{Al}_{12}\text{H}_2\text{O}^-$ (Fig. 3B) has an appreciable charge density at an Al site that is adjacent to the location of the initial nucleophilic attack. Charge density can stabilize a nascent Al-H bond (24), which suggests that the water fragments to form a surface-bound OH and H. The proposed rate-limiting transition state (Fig. 3C) is 0.32 eV above the energy of the chemisorbed intermediate (Fig. 3B). Because the system gains 0.52 eV in the initial adsorption of water, this barrier may be overcome to form a dissociatively chemisorbed species that is exothermic by 1.47 eV. To further examine these considerations, we calculated the transition state energy ΔE_T , defined as

$$\Delta E_T = E_B - E_A \quad (1)$$

where E_B is the energy barrier for breaking the OH bond starting from the adsorbed state, and E_A is the initial gain in energy in absorbing the water molecule. Positive values of ΔE_T result from barriers higher than the initial gain in energy and show that the reaction is energetically unfavorable. The progression and variation of ΔE_T as a function of size (fig. S3B) (12) corresponds to the experimentally observed propensity for adduct formation (fig. S1) (12). Thus, the observed selective reactivity trends of Al_n^- ($n = 7$ to 18) with water can be accounted for by this quantity. Further, this analysis suggests that the products observed in the mass spectrum are dissociatively chemisorbed. Consideration of the above reaction coordinate (Fig. 3) shows that the energy of the rate-limiting transition state is controlled by the relative Lewis acidity and Lewis basicity of the adjacent surface sites where the OH and H may bind.

Although most of the observed adducts were consistent with the adsorption of complete H_2O molecules, Al_{16}^- , Al_{17}^- , and Al_{18}^- formed adducts that were distinctly different, being deficient by two or four hydrogen atoms from the stoichiometry of water (Fig. 2). On the basis of this observation, we conclude that molecular hydrogen is being formed on the surface of selected aluminum clusters and released:



Al_{17}^- has a structure that can be described as two sets of adjunct Al atom dimers located on

opposing vertices of a 13-atom icosahedral core (Fig. 4A). Appreciable HOMO density is located on the adjunct dimer, and the LUMO protrudes into vacuum at an adjacent surface site (Fig. 4A and fig. S5). The coincidence of adjacent LUMO and HOMO probability density results in an energetically accessible transition state for

cleaving the water, as discussed above in the case of Al_{12}^- (Fig. 4C). The adsorption of additional water molecules is favored at the site of abundant LUMO density, which is adjacent to the adjunct pair of atoms and opposite from the first dissociatively chemisorbed water (Fig. 4, D and E). The resulting transition state (Fig. 4F) for

Fig. 1. Distribution of Al_n^- ($n = 7$ to 73) clusters reacting with D_2O . Nonpure aluminum clusters are shown in red; m/z , mass/charge ratio.

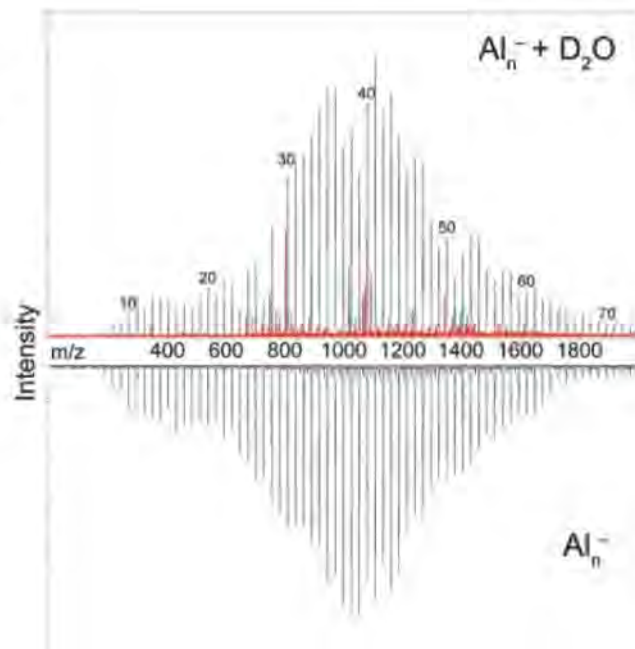
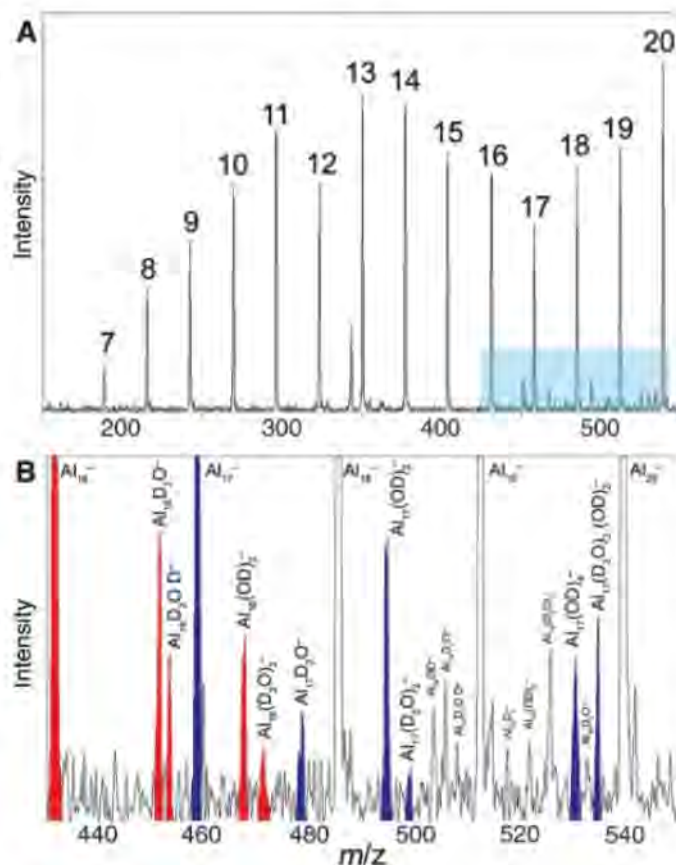


Fig. 2. (A) Reaction of low-mass Al_n^- clusters ($n = 7$ to 20) with D_2O . (B) Expansion of shaded area in (A). Red peaks are Al_{16} species; blue peaks are Al_{17} species.



water splitting at this site is 0.20 eV lower than for the other two possible active sites located at either end of the other adjunct pair.

We propose that the intermediate species (Fig. 4G) contains a sufficient amount of thermal energy from the dissociative chemisorption to allow the recombination of the individual surface-bound hydrogen atoms and the release of H_2 , resulting in the experimental detection of the hydrogen-deficient species. The energy barrier required to remove an H_2 molecule from the activated intermediate (Fig. 4H) is 0.84 eV, whereas the system may contain up to 2.55 eV

of thermal energy from previous reactions. The calculated bond energy of a free H_2 molecule is 4.54 eV. H_2 release is facilitated by a rearrangement of the icosahedral core (Fig. 4G) to a 14-atom core (Fig. 4H), which reduces the transition state by 0.24 eV.

The proposed mechanism (Fig. 4, E to J) resembles Langmuir-Hinshelwood processes that are observed on extended surfaces (25). Alternatives to the proposed mechanism include the interaction of an incoming water molecule with the first dissociatively adsorbed water, similar to an Eley-Rideal mechanism (26, 27). The transition

state for splitting water in an Eley-Rideal-type mechanism requires the previously dissociated H atom to act as the Lewis acid, rather than an Al atom, resulting in a barrier that is 0.23 eV higher than the proposed Langmuir-Hinshelwood-like process. Furthermore, the size selectivity of H_2 liberation is explained by a Langmuir-Hinshelwood mechanism; the Eley-Rideal mechanism requires a free H atom on the cluster surface with a neighboring Lewis acid site, which is likely to be present in many clusters after reacting with a single water molecule, yet only those with paired active sites result in the inferred release of H_2 .

Al_{16}^- and Al_{18}^- react to form adducts that are deficient by two H atoms through the same mechanism as Al_{17}^- . These three clusters have an icosahedral core with two-atom adjuncts atop one vertex possessing similarly comparable locations of high LUMO and HOMO probability density, and one-, two-, or three-atom adjuncts on the opposite vertex (Fig. 4, A, K, and L). The presence of the complementary active sites (highlighted in purple) on the species that are experimentally observed to generate H_2 suggests that all three clusters react in the same way. Comparison of the transition states in Al_{16}^- shows that a mechanism identical to that proposed for Al_{17}^- is energetically feasible. Additionally, a second adjunct dimer exists on Al_{17}^- opposite the first, which may also react and produce $[Al_{17}(OH)_4]^-$, an observation consistent with experiment.

The reactivity of Al anion clusters with water demonstrates the remarkable variance in reactivity seen at the nanoscale. Not only does the reactivity of the clusters vary sharply with size, but certain sizes including Al_{16}^- , Al_{17}^- , and Al_{18}^- (Fig. 2) preferentially produce H_2 with the addition of multiple waters, whereas others only bind water. The adsorption of water onto gas-phase aluminum anion clusters at thermal energies requires the cleavage of an OH bond, which is facilitated by two specific surface sites that act appropriately as a Lewis acid and a Lewis base to accept the fragments. The presence of an active site is a result of irregular charge distribution on the cluster surface, which is most prominent in clusters with geometries that are akin to defects on the cluster surface. It remains to be explored how other reactions are promoted through the production of active pairs and how nanostructures can be designed with a preponderance of such sites.

References and Notes

- W. Knight et al., *Phys. Rev. Lett.* **53**, 510 (1984).
- W. A. de Heer, *Rev. Mod. Phys.* **65**, 611 (1993).
- A. W. Castleman Jr., S. N. Khanna, in *The Chemical Physics of Solid Surfaces: Atomic Clusters*, D. P. Woodruff, Ed. (Elsevier, Oxford, 2007), pp. 409–425.
- R. E. Leuchtner, A. C. Harms, A. W. Castleman Jr., *J. Chem. Phys.* **91**, 2753 (1989).
- S. N. Khanna, P. Jena, *Phys. Rev. B* **51**, 13705 (1995).
- P. J. Roach, A. C. Reber, W. H. Woodward, S. N. Khanna, A. W. Castleman Jr., *Proc. Natl. Acad. Sci. U.S.A.* **104**, 14565 (2007).
- A. C. Reber, S. N. Khanna, P. J. Roach, W. H. Woodward, A. W. Castleman Jr., *J. Am. Chem. Soc.* **129**, 16098 (2007).

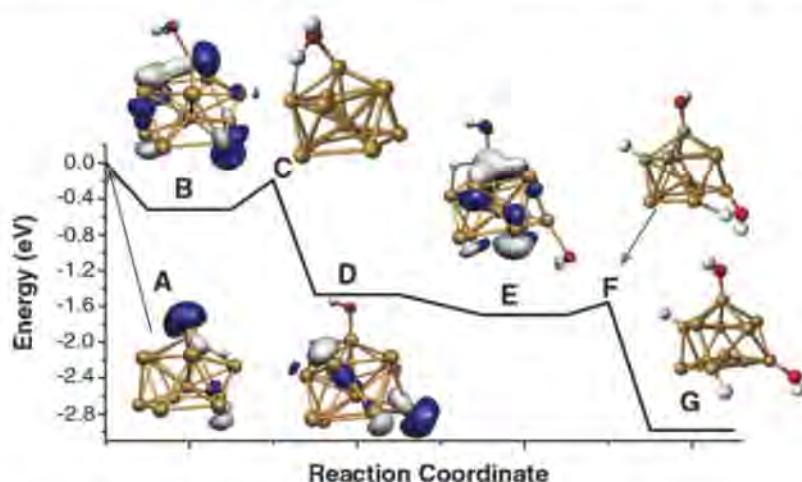
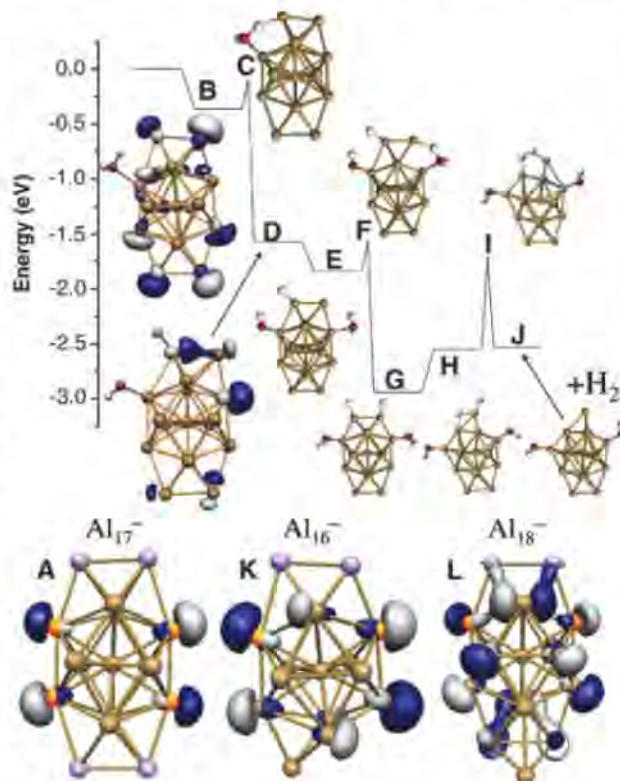


Fig. 3. Reaction coordinates for $Al_{12}^- + 2H_2O$. (A) The calculated LUMO+1 for Al_{12}^- . (B) The HOMO for the chemisorbed $[Al_{12}(H_2O)]^-$ complex. (C) A proposed transition state. (D) The dissociatively chemisorbed product and LUMO+1. (E) The HOMO after a second water is bound to the active site. (F) The transition state for the second water. (G) The final product. Al atoms, yellow-brown; O atoms, red; H atoms, white.

Fig. 4. Reaction coordinate for the formation of H_2 from Al_{17}^- and two H_2O molecules. Colors of atoms are as in Fig. 3; Al atoms representing complementary active sites are shown with the Lewis acid site in orange and the Lewis base site in purple. (A, K, and L) Al_{17}^- , Al_{16}^- , and Al_{18}^- , respectively; the LUMO charge density is plotted for (A) and LUMO+1 is plotted for (K) and (L). (B) One water chemisorbed to the cluster with HOMO charge density. (C) The transition state to dissociative chemisorption. (D) The resulting complex with LUMO+2 charge density. (E) The second water chemisorbed to the adjacent Lewis acid–Lewis base pair. (F) The transition state. (G) A complex with two dissociative chemisorbed waters. (H) The complex rearranged to more efficiently release H_2 . (I) The transition state for H_2 release. (J) The cluster after H_2 is released.



8. D. E. Bergeron, A. W. Castleman Jr., T. Morisato, S. N. Khanna, *Science* **304**, 84 (2004).
9. D. E. Bergeron, P. J. Roach, A. W. Castleman Jr., N. O. Jones, S. N. Khanna, *Science* **307**, 231 (2005).
10. N. O. Jones et al., *J. Chem. Phys.* **124**, 154311 (2006).
11. J. U. Reveles, S. N. Khanna, P. J. Roach, A. W. Castleman Jr., *Proc. Natl. Acad. Sci. U.S.A.* **103**, 18405 (2006).
12. See supporting material on Science Online.
13. A. Guevara-García, A. Martínez, J. V. Ortiz, *J. Chem. Phys.* **122**, 214309 (2005).
14. V. Bonačić-Koutecký et al., *J. Chem. Phys.* **117**, 3120 (2002).
15. J. M. Woodall, J. Ziebarth, C. R. Allen, in *Proceedings of the 2nd Energy Nanotechnology International Conference* (ASME, New York, 2007), ENIC2007-45014.
16. A. Sanchez et al., *J. Phys. Chem. A* **103**, 9573 (1999).
17. H. Hakkinen, W. Abbet, U. Heiz, U. Landman, *Angew. Chem. Int. Ed.* **42**, 1297 (2003).
18. M. Valden, X. Lai, D. W. Goodman, *Science* **281**, 1647 (1998).
19. A. Michaelides, V. A. Ranea, P. L. de Andres, D. A. King, *Phys. Rev. B* **69**, 075409 (2004).
20. D. M. Cox, D. J. Trevor, R. L. Whetten, A. Kaldor, *J. Phys. Chem.* **92**, 421 (1988).
21. T. P. Lippa, S. A. Lyapustina, S.-J. Xu, O. C. Thomas, K. H. Bowen, *Chem. Phys. Lett.* **305**, 75 (1999).
22. Q. Sun, Q. Wang, J. Z. Yu, T. M. Briere, Y. Kawazoe, *Phys. Rev. A* **64**, 053203 (2001).
23. S. Chrétien, M. S. Gordon, H. Metiu, *J. Chem. Phys.* **121**, 3756 (2004).
24. U. Das, K. Raghavachari, *J. Chem. Phys.* **124**, 021101 (2006).
25. P. W. Atkins, *Physical Chemistry* (Oxford Univ. Press, Oxford, 1990).
26. D. D. Eley, E. K. Rideal, *Nature* **146**, 401 (1940).
27. C. Bürgel et al., *J. Am. Chem. Soc.* **130**, 1694 (2008).
28. Supported by Air Force Office of Scientific Research grants FA9550-04-1-0066 and FA9550-05-1-0186.

Supporting Online Material

www.sciencemag.org/cgi/content/full/323/5913/492/DC1
Materials and Methods
Figs. S1 to S5
References

15 September 2008; accepted 10 December 2008
10.1126/science.1165884

Brown Clouds over South Asia: Biomass or Fossil Fuel Combustion?

Örjan Gustafsson,^{1*} Martin Kruså,¹ Zdenek Zencak,¹ Rebecca J. Sheesley,¹ Lennart Granat,² Erik Engström,² P. S. Praveen,³ P. S. P. Rao,⁴ Caroline Leck,² Henning Rodhe²

Carbonaceous aerosols cause strong atmospheric heating and large surface cooling that is as important to South Asian climate forcing as greenhouse gases, yet the aerosol sources are poorly understood. Emission inventory models suggest that biofuel burning accounts for 50 to 90% of emissions, whereas the elemental composition of ambient aerosols points to fossil fuel combustion. We used radiocarbon measurements of winter monsoon aerosols from western India and the Indian Ocean to determine that biomass combustion produced two-thirds of the bulk carbonaceous aerosols, as well as one-half and two-thirds of two black carbon subfractions, respectively. These constraints show that both biomass combustion (such as residential cooking and agricultural burning) and fossil fuel combustion should be targeted to mitigate climate effects and improve air quality.

The radiative effects of carbonaceous aerosols constitute one of the largest uncertainties in climate modeling (1–6). Combustion-derived carbonaceous aerosols have traditionally been associated with pollution in urban areas, but research over the past decade has revealed that the haze they cause may envelop entire subcontinents and ocean basins (3, 7–9). The extensive atmospheric brown cloud (ABC) over South Asia and the Indian Ocean persists during the winter season, and its cooling effect may regionally balance and even surpass the warming effect of greenhouse gases (GHGs) (3, 4, 8), with predicted effects including changed circulation and monsoon patterns with amplified droughts and floods (10, 11), as well as increased melting of Himalayan glaciers (4). A conspicuous feature of the Asian ABC is its unusually high content of airborne black carbon (BC) particles (4, 7, 12, 13). This highly condensed carbonaceous residue of incomplete combustion is the “dark horse” in the current climate debate as sub-

stantial uncertainties exist about its atmospheric longevity (1), aerosol mixing state (14), measurement (15–18), and sources (12, 19–25). Because it is becoming clear that BC represents a continuum of light absorbing carbon (LAC) forms (16–18), exploiting differences in BC analytical techniques may improve the characterization of atmospheric BC. The primary motivation for the ABC BC Radiocarbon (¹⁴C) Campaign (ABC-BC14), the results of which are reported here, was the observational determination of the relative contribution of contemporary biomass versus fossil fuel combustion to both the total carbonaceous aerosols and to two different atmospheric BC isolates.

Though it is now established that there is an unusually high mass fraction of BC in the Asian ABC (4, 7, 12, 13, 23–25), there is a notable discrepancy in source apportionment of this BC between top-down studies relying on measured ratios of BC to total carbon or other aerosol components (12, 24, 25) as compared with bottom-up emission inventories based on fuel consumption and laboratory-derived emission factors (19–23) (Table 1). Several top-down studies conclude that 50 to 90% of the South Asian BC originates from fossil fuel combustion (12, 24, 25). However, employed end-member ratios were from other regions and may not be representative of South Asian combustion processes (21, 23). Further, the BC:organic carbon

(OC) ratio is nonconservative if there is substantial formation of secondary organic aerosols (13, 26). In contrast, bottom-up approaches suggest that only 10 to 30% of the BC loadings originate from fossil fuel combustion (19–23) while recognizing that emission factors (particularly those for biomass combustion) are difficult to constrain because of strong dependency on fuel type and efficiency of combustion (22, 23). This current dichotomy is addressed in the ABC-BC14 Campaign by using radiocarbon abundance (half life $\tau_{1/2} = 5730$ years) as a tool to distinguish between fossil (radiocarbon “dead”) and contemporary biomass (radiocarbon “alive”) combustion sources of the Asian ABC.

The ABC-BC14 Campaign was conducted with identical sampling at two sites (Fig. 1) of the international ABC-Asia project. Aerosol samples for microscale ¹⁴C measurements were collected at the Maldives Climate Observatory at Hanimaadhoo island (MCOH) (6.78°N, 73.18°E) from 31 January to 16 March 2006 and at the mountain top site of the Indian Institute of Tropical Meteorology located at Sinhgad, West India (SIN) (18.35°N, 73.75°E, 1400 meters above sea level) from 27 March to 18 April 2006 (27). The ABC-BC14 Campaign thus overlapped with the previously reported Maldives Autonomous Unmanned Aerial Vehicle Campaign (4) that reported on the vertically resolved aerosol solar heating, and the meteorological context is detailed therein.

Back-trajectory analyses illustrate the typical winter monsoon circulation, with most of the first half of the MCOH samples (31 January to 18 February 2006) reflecting a predominant low-level air mass transport during the preceding 10 days from central India (including the Gangetic Plain) flowing southward along the western Bay of Bengal 2 to 5 days before arrival (fig. S1A). During subsequent collections (19 February to 16 March 2006), most 10-day trajectories originated from the northern Arabian Sea and adjacent land areas in northwest India and Pakistan with transport along the Indian west coast margin (fig. S1B). Most of the surface air masses sampled at SIN were arriving from a sector west and north, originating from Arabian Sea, Arabic peninsula, Pakistan, and northwest India (fig. S1C). Satellite-retrieved optical signals suggest that study locations were

¹Department of Applied Environmental Science, Stockholm University, 10691 Stockholm, Sweden. ²Department of Meteorology, Stockholm University, 10691 Stockholm, Sweden. ³Maldives Climate Observatory at Hanimaadhoo (MCOH), Republic of the Maldives. ⁴Indian Institute of Tropical Meteorology, Dr. Homi Bhabha Road, Pashan, Pune 411 008, India.

*To whom correspondence should be addressed. E-mail: orjan.gustafsson@itm.su.se

influenced by aerosols, presumably brown clouds (Fig. 1).

Ground-based particle soot absorption photometer (PSAP) (550 nm) measurements confirm high abundances of LAC at MCOH and SIN (Fig. 2A). Absorption coefficients of $1 \cdot 10^{-5} \text{ m}^{-1}$ at the onset of the MCOH Campaign increased to a maximum above $3 \cdot 10^{-5} \text{ m}^{-1}$ toward the end of the Gangetic Plain influenced period, followed by a consistent decrease to $5 \cdot 10^{-6} \text{ m}^{-1}$ as trajectories shifted toward the western side of India. The lower-temporal-resolution PSAP data for the SIN campaign varied from 0.3 to $3 \cdot 10^{-5} \text{ m}^{-1}$.

The temporal evolutions of the mass-based carbonaceous aerosol concentrations were broadly consistent with the PSAP data (Fig. 2B). The highest MCOH total organic carbon (TOC) values were associated with air from northern India (4 to $5 \mu\text{g}\cdot\text{m}^{-3}$) decreasing to $1.4 \mu\text{g}\cdot\text{m}^{-3}$ with Arabian Sea origin. Similarly, the elemental carbon (EC), measured using a thermo-optical technique (17, 18, 27, 28), varied from 1.2 to $0.2 \mu\text{g}\cdot\text{m}^{-3}$ (Fig. 2B) for MCOH. The soot carbon (SC) fraction, measured by chemothermal-oxidation (18, 27–29) and representing a more recalcitrant portion of the BC spectrum (15, 16, 18), was lower but followed a similar temporal trend (table S1). The TOC, EC, and SC were all closely coupled ($r^2 = 0.84$ for EC versus SC) (fig. S2), indicating a strong contribution of combustion processes to the total carbonaceous aerosols.

Each of the three carbon isolates exhibited a marked temporal uniformity in radiocarbon signal and hence between the contributions from fossil and contemporary biomass sources. The measured $\Delta^{14}\text{C}$ content of TOC ranged from -239 ± 3 to -145 ± 2 per mil (‰) in MCOH samples and from -235 ± 2 to -187 ± 2 ‰ in SIN samples (Fig. 2C and table S1). This consistency attests to the ability of the series of week-long samples to capture the broader-scale source contributions. Because the optical techniques used to quantify LAC-BC do not physically isolate a carbon mass fraction, a prerequisite for ^{14}C measurement, two techniques commonly used to quantify the combustion-derived carbon mass were employed to isolate carbon (27).

The EC isolate was more fossil-rich than the TOC and ranged from -379 ± 4 to -319 ± 3 ‰ in India and from -595 ± 12 to -430 ± 5 ‰ over the Indian Ocean (Fig. 2C). The more recalcitrant SC fraction had more modern $\Delta^{14}\text{C}$ values, indistinguishable between Indian and Maldivian sites, with averages of -227 ± 37 versus -167 ± 70 ‰, respectively. Hence, there is a component included in the EC isolate but excluded from SC—that is, less recalcitrant but more ^{14}C depleted. We hypothesize that this is fossil “brown carbon” (17) from either domestic coal combustion or fine coal dust released from pulverization of coal for the many coal-fired power plants in India (21, 22). Coal has been one key replacement of wood as domestic fuel (22), and it is conceivable that the BC produced by such small-scale and inefficient coal burning

is escaping detection as SC (16, 18) but is included in EC (24). Further, uncombusted fine coal dust yields larger false positives for EC than SC (18), consistent with differences in $\Delta^{14}\text{C}$ dur-

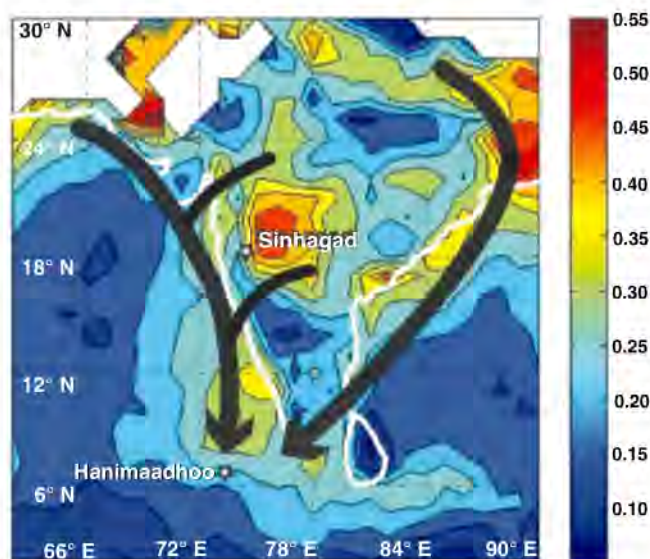
ing the ABC-BC14 study. Sensitivity model calculations explored inclusion of up to 30% of the instrument-inherent pyrolyzed OC in the isolated EC and found that the potential effect

Table 1. Apportionment of Indian carbonaceous aerosols between fossil fuel and biomass combustion. The characteristics of different carbonaceous particle fractions (TOC, BC, EC, SC) are discussed in the text and SOM.

Study	BC from fossil fuel combustion	BC from biomass combustion	Methods/comments
<i>Emission inventories</i>			
India inventory (19, 20)	29%	71%	0.1 Tg/year fossil fuel and 0.25 Tg/year biomass
South Asia inventory (21)	12–45%	55–88%	0.059–0.37 Tg/year fossil fuel and 0.45 Tg/year biomass for India
Global inventory (22)	~30%	~70%	0.18 Tg/year fossil fuel, 0.33 Tg/year biofuel, 0.087 Tg/year open burning for India
South Asia biofuel study (23)	25%	75%	India-specific emission factors and fuel usage
<i>Ambient measurements</i>			
INDOEX* flights over the tropical Indian Ocean (24)	80%	20%	EC:TC ratio for three flights
INDOEX flights over the tropical Indian Ocean (12)	60–90%	10–40%	EC:TC ratio for 13 flights
ABC monitoring in the Maldives (25)	40–50%	30–40%	Positive matrix factorization with EC and multiple elements
Maldives + India (this study)	$32 \pm 5\% \dagger$	$68 \pm 6\%$	Radiocarbon analysis of ambient filter-based SC, range of 66–76% for biomass
Maldives + India (this study)	$54 \pm 8\%$	$46 \pm 8\%$	Radiocarbon analysis of ambient filter-based EC, range of 45–52% for biomass

*INDOEX is the Indian Ocean Experiment. †Standard deviation of 9 samples. ‡Ranges calculated from sensitivity analysis detailed in the SOM text.

Fig. 1. Regional distribution of aerosol optical depth at 550 nm derived from a moderate resolution imaging spectroradiometer (MODIS) instrument aboard the Terra satellite (average for March 2006). The black arrows denote dominant air mass transport patterns in the region during the winter monsoon. The two aerosol sampling sites are shown.



would be within the uncertainty of the reported isotope values [table S2 and supporting online material (SOM) text].

To afford a detailed comparison with earlier bottom-up and top-down source apportionment estimates of carbonaceous aerosols, a simple isotopic mass balance equation (28, 30), based on the $\Delta^{14}\text{C}$ data, was applied to apportion between the fractional contributions of biomass (f_{biomass}) and fossil fuel ($f_{\text{fossil}} = 1 - f_{\text{biomass}}$)

combustion sources to the carbonaceous aerosol components in the investigated samples, as illustrated for EC

$$\Delta^{14}\text{C}_{\text{EC}} = \Delta^{14}\text{C}_{\text{biomass}} \cdot f_{\text{biomass}} + \Delta^{14}\text{C}_{\text{fossil}} \cdot (1 - f_{\text{biomass}}) \quad (1)$$

where $\Delta^{14}\text{C}_{\text{EC}}$ is the measured radiocarbon content of the EC component and $\Delta^{14}\text{C}_{\text{fossil}}$ is

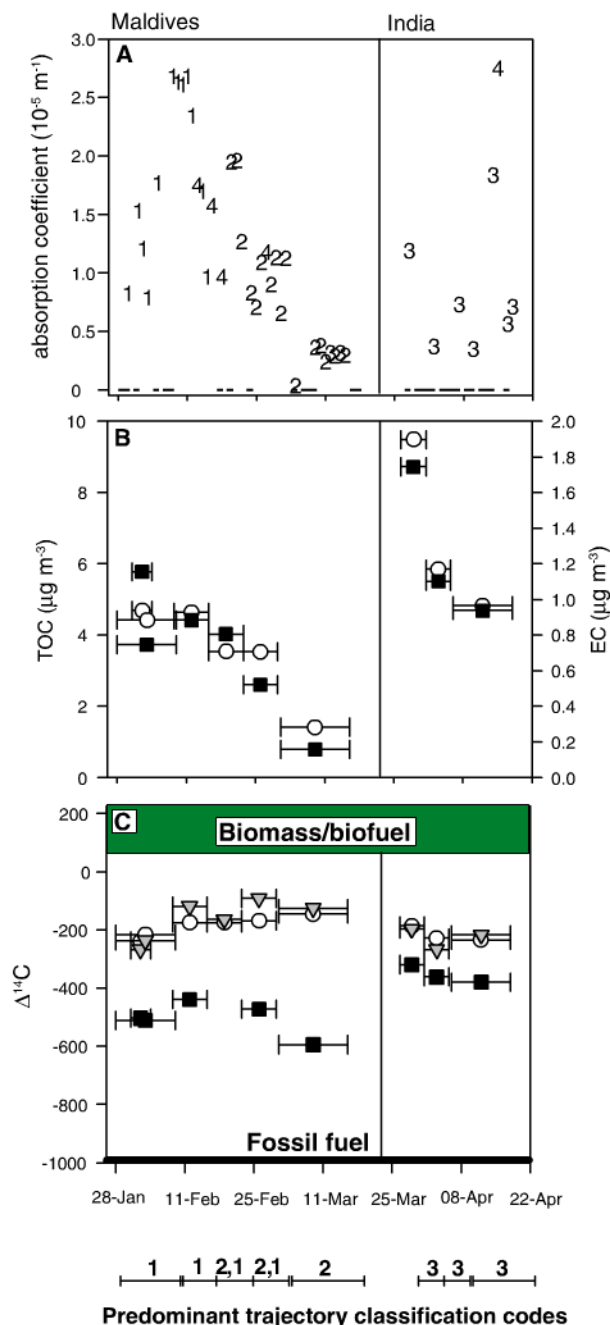
-1000 ‰. The $\Delta^{14}\text{C}_{\text{biomass}}$ end member is between $+70$ and $+225$ ‰. The first $\Delta^{14}\text{C}$ value corresponds to contemporary CO_2 (31), and thus freshly produced biomass, whereas the second $\Delta^{14}\text{C}$ end member is for combustion particles emanating from the combustion of wood (28, 32, 33). The latter $\Delta^{14}\text{C}$ value is higher because it is reflecting the $\Delta^{14}\text{C}$ of biomass that has accumulated over the decades-to-century-long life span of trees, which includes the period after the atmospheric nuclear bomb testing that nearly doubled the $\Delta^{14}\text{C}$ value of CO_2 by the early 1960s. For India, there are several important contemporary biofuel types, including wood fuel and cow dung; additionally, crop residue burning is believed to be an important source of atmospheric BC. To regionally parameterize the contemporary $\Delta^{14}\text{C}_{\text{biomass}}$ end member, the relative contributions of fuel wood (83%) and dung + crop waste (17%) provided by C. Venkataraman *et al.* were employed (23). Hence, an India-tailored $\Delta^{14}\text{C}_{\text{biomass}}$ end member of $+199$ ‰ was used in the model calculations. The sensitivity of the source apportionment results toward this end-member selection is low (Table 1, table S3, and SOM text).

Application of this isotopic mass balance model to these Asian aerosol $\Delta^{14}\text{C}$ values revealed that bulk carbonaceous aerosols (TOC) were $67 \pm 3\%$ (1 SD) of contemporary origin. The EC and SC isolates of the BC continuum were 46 ± 8 and $68 \pm 6\%$ from biomass combustion (Table 1). Although there are not yet any other reports of $\Delta^{14}\text{C}$ for EC isolates, the biomass combustion fraction of SC was 63% for northwest African dust intercepted in the northeast Atlantic Ocean (34), 70 to 88% in wintertime Scandinavia (28), and an averaged 35% in a Swiss alpine valley in the winter (33).

Our ^{14}C -based constraint thus indicates a much larger role for biomass and biofuel burning, compared with earlier top-down studies, while attenuating the biofuel influence relative to bottom-up suggestions. In contrast to the two earlier approaches, the ABC-BC14 results also provide a much tighter source constraint. Dual isotopic probing, combining $\Delta^{14}\text{C}$ with $\delta^{13}\text{C}$ (fig. S3), further underscores biomass combustion. The $\delta^{13}\text{C}$ suggests that wood fuel and other C3 plants are complemented by C4 sources (such as from agricultural slash-and-burn practices) as substantial contributors.

This work demonstrates that both fossil and biomass combustion processes can be blamed for the extensive ABC over South Asia. Improved constraint on the sources is the first step toward enacting effective abatement strategies. The much shorter atmospheric longevity for BC aerosols (approximately days to weeks) compared with GHGs raises the hope of a rapid response of the climate system. However, a consequence of thus decreasing the ABC “global dimmer” would also be to remove its counterbalancing effect on anthropogenic GHGs (1).

Fig. 2. Concentration and radiocarbon-based source apportionment of carbonaceous aerosols over the Maldives and western India. The ABC-BC14 Campaign is divided into two periods with sampling at Hanimaadhoo (Maldives) 31 January to 16 March 2006 and at Sinhagad (India) 27 March to 18 April 2006. (A) Optical measurement (PSAP) of LAC. The data symbols are numbered 1 to 4, which corresponds to the four different source trajectory classes listed below the figure. The dashed symbols at the bottom of the panel represent days with no data. (B) Carbon-mass based concentrations of total organic carbonaceous aerosols (TOC) (open circles) and EC (black squares). (C) Radiocarbon content of TOC, EC, and SC (gray inverted triangles). The radiocarbon end-member ranges are shown for both contemporary biomass/biofuel (upper green field) and for fossil fuel (lower black line) and are further detailed in the text. The predominant air mass source regions over the past 10 days are summarized at the bottom. Horizontal range bars in (B) and (C) represent the collection and integration period for each sample.



Case 1: N. India, eastern Indian margin, S. India
Case 2: Northern Arabian Sea, NW India, Pakistan, western Indian margin
Case 3: Northern Arabian Sea, NW India, Pakistan, Arabian Peninsula
Case 4: Other patterns

References and Notes

- M. O. Andreae, C. D. Jones, P. M. Cox, *Nature* **435**, 1187 (2005).
- P. Forster et al., in *Climate Change 2007: The Physical Science Basis. Contribution of Working Group I to the Fourth Assessment Report of the Intergovernmental Panel on Climate Change*, S. Solomon et al., Eds. (Cambridge Univ. Press, Cambridge, 2007).
- V. Ramanathan, G. Carmichael, *Nat. Geosci.* **1**, 221 (2008).
- V. Ramanathan et al., *Nature* **448**, 575 (2007).
- J. Seinfeld, *Nat. Geosci.* **1**, 15 (2008).
- S. E. Schwartz, R. J. Charlson, H. Rodhe, *Nat. Reports Clim. Change* **2**, 23 (2007).
- J. Lelieveld et al., *Science* **291**, 1031 (2001).
- V. Ramanathan, P. J. Crutzen, J. T. Kiehl, D. Rosenfeld, *Science* **294**, 2119 (2001).
- C. E. Chung, V. Ramanathan, D. Kim, I. A. Podgorny, *J. Geophys. Res. Atmos.* **110**, D24207 (2005).
- S. Menon, J. Hansen, L. Nazarenko, Y. Luo, *Science* **297**, 2250 (2002).
- V. Ramanathan et al., *Proc. Natl. Acad. Sci. U.S.A.* **102**, 5326 (2005).
- O. L. Mayol-Bracero et al., *J. Geophys. Res. Atmos.* **107**, 8030 (2002).
- R. Rengarajan, M. M. Sarin, A. K. Sudheer, *J. Geophys. Res. Atmos.* **112**, D21307 (2007).
- M. Z. Jacobson, *Nature* **409**, 695 (2001).
- L. A. Currie et al., *J. Res. Natl. Inst. Stand. Technol.* **107**, 279 (2002).
- M. Elmquist, G. Cornelissen, Z. Kukulska, Ö. Gustafsson, *Global Biogeochem. Cycles* **20**, GB2009 (2006).
- M. O. Andreae, A. Gelencser, *Atmos. Chem. Phys.* **6**, 3131 (2006).
- K. Hammes et al., *Global Biogeochem. Cycles* **21**, GB3016 (2007).
- M. S. Reddy, C. Venkataraman, *Atmos. Environ.* **36**, 677 (2002).
- M. S. Reddy, C. Venkataraman, *Atmos. Environ.* **36**, 699 (2002).
- R. R. Dickerson et al., *J. Geophys. Res. Atmos.* **107**, 8017 (2002).
- T. C. Bond et al., *J. Geophys. Res. Atmos.* **109**, D14203 (2004).
- C. Venkataraman, G. Habib, A. Eiguren-Fernandez, A. H. Miguel, S. K. Friedlander, *Science* **307**, 1454 (2005).
- T. Novakov et al., *Geophys. Res. Lett.* **27**, 4061 (2000).
- E. A. Stone et al., *J. Geophys. Res. Atmos.* **112**, D22523 (2007).
- C. Neusüß, T. Gnauk, A. Plewka, H. Herrmann, P. K. Quinn, *J. Geophys. Res. Atmos.* **107**, 8031 (2002).
- Aerosols were collected on pre-combusted microquartz filters using high-volume samplers. Mass concentrations of the total organic carbonaceous aerosol (TOC) and the thermo-optical transmission National Institute of Occupational Safety and Health (NIOSH) 5040 protocol EC and chemothermal-oxidation at 375°C SC subfractions of BC were quantified and isolated for offline carbon isotope analysis. Materials and methods details are available as supporting material on Science Online.
- Z. Zencak, M. Elmquist, Ö. Gustafsson, *Atmos. Environ.* **41**, 7895 (2007).
- Ö. Gustafsson et al., *Global Biogeochem. Cycles* **15**, 881 (2001).
- M. Mandalakis et al., *Environ. Sci. Technol.* **39**, 2976 (2005).
- I. Levin, B. Kromer, M. Schmidt, H. Sartorius, *Geophys. Res. Lett.* **30**, 2194 (2003).
- D. B. Klindinst, L. A. Currie, *Environ. Sci. Technol.* **33**, 4146 (1999).
- S. Szidat et al., *Geophys. Res. Lett.* **34**, L05820 (2007).
- T. I. Eglinton et al., *Geochem. Geophys. Geosyst.* **3**, 1050 (2002).
- This is a contribution of the Stockholm University Bert Bolin Centre for Climate Research. We gratefully acknowledge access to and support of the MCOH field site by the Maldives Meteorological Office and H. Nguyen of the international ABC program. We appreciate access to the thermo-optical analyzer at the Department of Applied Environmental Science, Stockholm University. We thank V. Ramanathan (University of California, San Diego, USA) and M. M. Sarin (Physical Research Laboratory, India) for useful discussions. This study was financed by the Swedish Strategic Environmental Research Foundation; the Swedish Research Council; the Swedish Research Council for Environment, Agricultural Sciences, and Spatial Planning; and the Swedish International Development Agency, Department for Research Co-Operation. Ö.G. also acknowledges support as an Academy Researcher from the Swedish Royal Academy of Science.

Supporting Online Material

www.sciencemag.org/cgi/content/full/323/5913/495/DC1

Materials and Methods

SOM Text

Figs. S1 to S3

Tables S1 to S3

References

19 August 2008; accepted 12 December 2008

10.1126/science.1164857

Genetic Interactions Between Transcription Factors Cause Natural Variation in Yeast

Justin Gerke, Kim Lorenz, Barak Cohen*

Our understanding of the genetic basis of phenotypic diversity is limited by the paucity of examples in which multiple, interacting loci have been identified. We show that natural variation in the efficiency of sporulation, the program in yeast that initiates the sexual phase of the life cycle, between oak tree and vineyard strains is due to allelic variation between four nucleotide changes in three transcription factors: *IME1*, *RME1*, and *RSF1*. Furthermore, we identified that selection has shaped quantitative variation in yeast sporulation between strains. These results illustrate how genetic interactions between transcription factors are a major source of phenotypic diversity within species.

Understanding the molecular basis of natural phenotypic diversity is a major challenge in modern genetics (1–6). Knowing how individual genetic polymorphisms combine to produce phenotypic change could strengthen evolutionary theory and advance applications such as personalized medicine (7, 8). Many loci that contribute to variation have been identified across taxa, but only a small fraction has been resolved to the nucleotide level (9, 10). Examples of complex traits in which causative

polymorphisms have been identified at multiple contributing loci are even rarer (11). As a result, the interactions between nucleotide changes in nature, and thus the genetic mechanisms of phenotypic change, are largely unknown.

Crosses of laboratory strains of the yeast *Saccharomyces cerevisiae* have identified genes and polymorphisms governing complex traits (12–21). However, these lines harbor laboratory-engineered gene deletions and deleterious mutations that are pleiotropic for multiple traits, which may obscure the natural genetic architecture. The natural diversity of this species, which includes isolates from clinical, vineyard, and oak tree environments, remains largely untapped (22–24).

Sporulation efficiency is a highly heritable complex trait that varies among natural populations of *S. cerevisiae* (25). Sporulation is a core developmental program that initiates the sexual phase of the yeast life cycle and promotes long-term survival during desiccation or starvation (26). Sporulation is triggered as a response to environmental change (27) and is hypothesized to be under different selective pressures in different habitats (28). Accordingly, wild isolates from North American oak trees and associated soil samples sporulate with efficiencies approaching 100%, but strains isolated from naturally occurring vineyard fermentations sporulate at lower

Table 1. Significant QTL for sporulation efficiency.

Chromosome	Nearest marker	lod score	Variance explained (%)	Additive effect (%)
7	L7.9	86.42	41	20
7	L7.17	4.7	2	4
10	L10.14	68.2	29	16
11	L11.2	3.9	1	–3
13	L13.6	28.7	10	10

Department of Genetics, Washington University School of Medicine, St. Louis, MO 63108, USA.

*To whom correspondence should be addressed. E-mail: cohen@genetics.wustl.edu

rates (25). Genetic dissection of the underlying natural variation in sporulation efficiency provides an opportunity to uncover the nucleotide changes that govern ecologically driven variation.

To identify quantitative trait loci (QTL) governing natural variation in sporulation, we crossed YPS606, a strain isolated from the bark of an oak tree in Pennsylvania that sporulates at 99% efficiency, and BC187, a strain originating from a California wine barrel that sporulates at only 3.5% (25). We developed genetic markers by

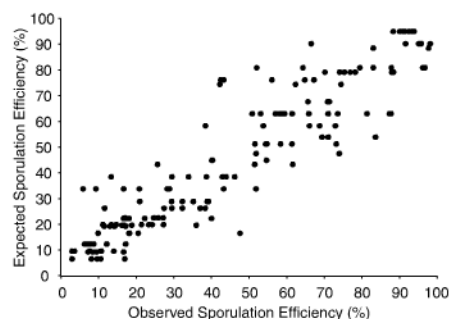


Fig. 1. A linear model of the effects of five QTL on sporulation efficiency. Expected values of sporulation efficiency plotted as a function of observed values for 155 segregants. Expected values are derived from a linear model based on 200 independent segregants (table S2).

shotgun sequencing these parent strains and produced a genetic linkage map of 225 loci typed in 374 recombinant segregants. This map covers the yeast genome at an average of 11 centimorgan intervals (table S1). Composite interval mapping (29) was used to identify five QTL on four chromosomes (fig. S1 and Table 1) that significantly cosegregated with variation in sporulation efficiency with an experiment-wide error rate of $P = 0.05$ [logarithm of the odds ratio for linkage (lod) score > 3.1 , which is significant by permutation analysis]. Alleles from the oak parent at four of the QTL were linked to an increase in sporulation efficiency (markers L7.9, L7.17, L10.14, and L13.6). At the locus on chromosome 11 (marker L11.2), an allele from the poorly sporulating vineyard parent promotes more efficient sporulation in segregating progeny. The presence of a vineyard allele promoting higher sporulation was expected on the basis of previously observed transgressive segregants that sporulate more efficiently than the oak parent (25).

We quantified the total amount of variation explained by these five QTL using a linear model trained on 200 segregants (table S2) (29). In an independent test set of 155 segregants, the model explains 88% of the phenotypic variation [squared correlation coefficient (R^2) = 0.88], with an average prediction error of $\pm 8\%$ (Fig. 1). This indicates that the five QTL explain most of the variation in spor-

ulation efficiency in this cross. To obtain the best fit, the model must incorporate two- and three-way interactions between loci (F-test, $P < 0.001$) (29), indicating that the genetic architecture of sporulation efficiency is nonadditive and complex. Although incorporating the effects of all five loci produces the best-fit model (F-test, $P < 0.001$), only three of the loci have large effects. When the minor QTL (markers L7.17 and L11.2) are ignored, the results are virtually identical ($R^2 = 0.87$, prediction error $\pm 8\%$).

One major QTL (marker L7.9) covers a 100-kb confidence interval on chromosome 7. *RME1*, a transcription factor that suppresses sporulation in specific cell types (30), resides in this peak (fig. S1A). To test whether allelic variation in *RME1* produces variation in sporulation efficiency, we deleted each parental allele of *RME1* in a hybrid background [through reciprocal hemizygosity analysis (18)]. This showed that the allelic contributions of *RME1* from each parent were different, confirming that variation in *RME1* affects sporulation efficiency (Fig. 2A). The coding region of *RME1* contains no amino acid substitutions between the oak and vineyard parents, which suggests that the allelic difference is regulatory. By replacement (29), we confirmed that a single nucleotide insertion/deletion 308 base pairs (bp) upstream of the initiation codon (fig. S2A) accounts for the effect of the *RME1* locus on spor-

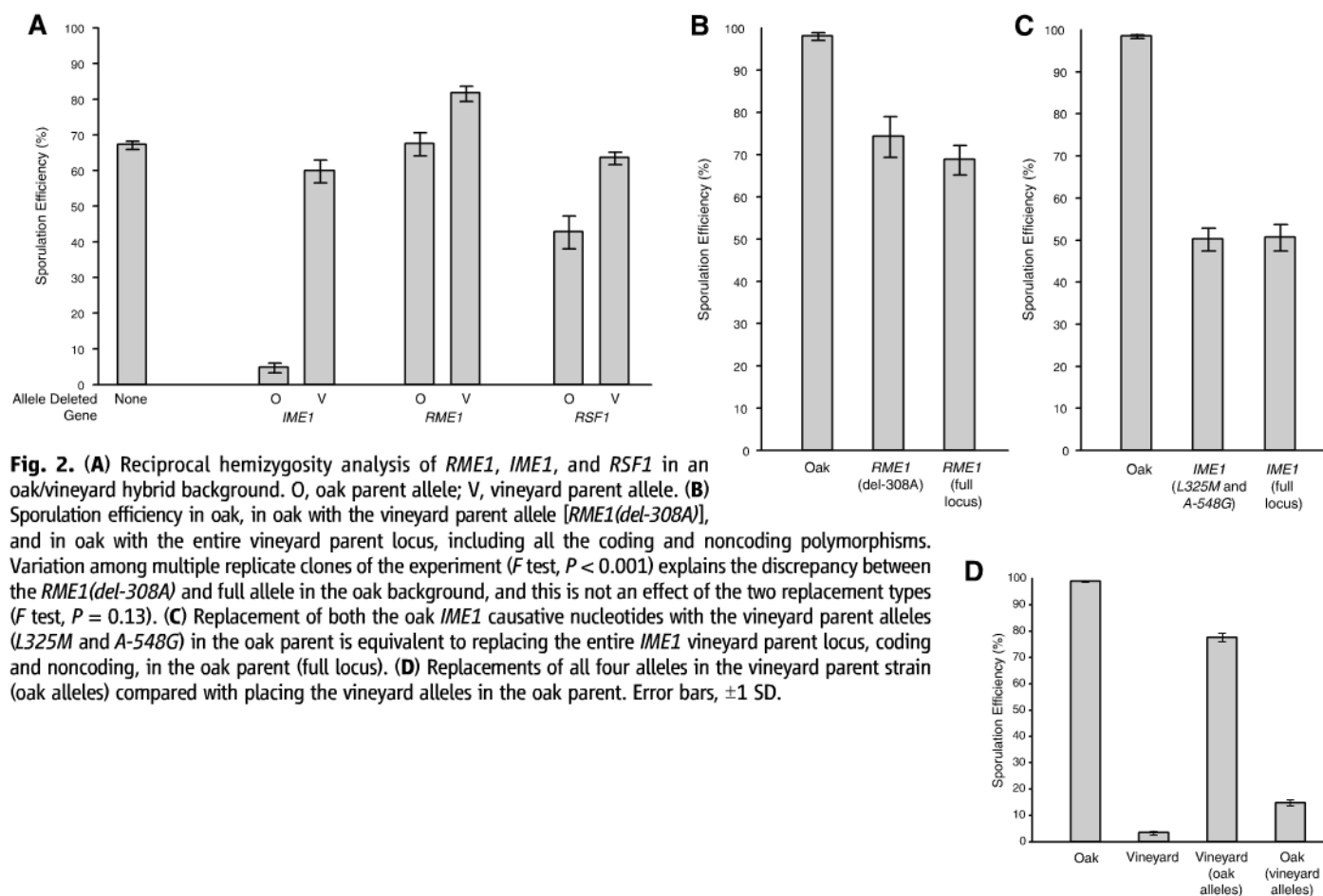


Fig. 2. (A) Reciprocal hemizygosity analysis of *RME1*, *IME1*, and *RSF1* in an oak/vineyard hybrid background. O, oak parent allele; V, vineyard parent allele. (B) Sporulation efficiency in oak, in oak with the vineyard parent allele [*RME1*(*del-308A*)], and in oak with the entire vineyard parent locus, including all the coding and noncoding polymorphisms. Variation among multiple replicate clones of the experiment (F test, $P < 0.001$) explains the discrepancy between the *RME1*(*del-308A*) and full allele in the oak background, and this is not an effect of the two replacement types (F test, $P = 0.13$). (C) Replacement of both the oak *IME1* causative nucleotides with the vineyard parent alleles (L325M and A-548G) in the oak parent is equivalent to replacing the entire *IME1* vineyard parent locus, coding and noncoding, in the oak parent (full locus). (D) Replacements of all four alleles in the vineyard parent strain (oak alleles) compared with placing the vineyard alleles in the oak parent. Error bars, ± 1 SD.

ulation efficiency (Fig. 2B). The vineyard strain allele [*RME1*(*del-308A*)], which has a deletion of a single adenine relative to the oak strain, also reduces sporulation efficiency in laboratory strains (21). This nucleotide change presumably increases the expression of *RME1*, which represses sporulation, as the *RME1*(*del-308A*) allele is expressed at higher levels than the oak allele (25, 31).

A second major QTL (L10.14) located in a 50-kb confidence interval on chromosome 10 also contained a strong candidate gene, *IME1* (fig. S1B). *IME1* is a transcriptional activator and master regulator that initiates yeast sporulation (32). Reciprocal hemizygosity analysis confirmed that *IME1* quantitatively controls sporulation efficiency (Fig. 2A). We identified 8 polymorphisms in the coding region, both synonymous and nonsynonymous, and 39 polymorphisms in the noncoding regions of *IME1* between the oak and vineyard strain. Allele replacements demonstrated that two of these polymorphisms account for the full effect of the *IME1* locus on sporulation efficiency (Fig. 2C). Although other polymorphisms in this region may affect sporulation efficiency, they must be

redundant with the two causative alleles that we identified. We identified a causative nonsynonymous substitution in the vineyard strain, *IME1* (L325M) (fig. S2B), which resides in an Ime1 domain essential for protein-protein interactions with Rim11 and Ume6, which also regulate the initiation of sporulation (33). Mutation of this leucine reduces the ability of Ime1 to activate transcription (34). We also identified a noncoding *IME1*(A-548G) polymorphism in an 11-bp sequence that is conserved among three yeast species closely related to *S. cerevisiae* (fig. S2C).

The third major QTL affecting sporulation occurs in a 100-kb region of chromosome 13 (L13.6, fig. S1D). Reciprocal hemizygosity analysis of genes in this region identified *RSF1* as a candidate gene affecting sporulation efficiency (Fig. 2A). Allele replacements (fig. S3) confirmed that a single derived polymorphism in the vineyard strain—coding for a substitution of a conserved glutamic acid with a glycine *RSF1*(D181G)—is responsible for the allelic effect of *RSF1* (fig. S2D). *RSF1* encodes a transcriptional activator of mitochondrial genes critical for cellular respiration (35). Because a respiratory signal promotes *IME1* expression and sporulation

(36), the vineyard allele likely reduces the function of Rsf1.

In total, we identified four nucleotide changes causing variation in sporulation efficiency by directly affecting three transcription factors governing pathways that regulate the initiation of sporulation. Our QTL model (table S2) includes, however, potentially undiscovered linked alleles that could account for some of the variation. Therefore, we engineered yeast strains isogenic to each parent but carrying the causative alleles from the opposite parent (Fig. 2D) (29). The vineyard parental strain, which sporulates at $3.5 \pm 0.1\%$, increases to $78 \pm 2\%$ when carrying all four oak alleles. In the oak parent, the replacement of these four nucleotides reduced sporulation efficiency from $99 \pm 0.2\%$ to $14.9 \pm 1\%$ and places the phenotype of the oak strain background within the range normally seen only among vineyard strains (Fig. 3).

Our QTL model also predicts that the four causative nucleotides will interact. We therefore compared the phenotypes of strains isogenic to the oak background carrying all possible permutations of the four oak and vineyard alleles. We chose the oak strain background for this experiment because isolates of other species of yeast sporulate efficiently, supporting the idea that the oak strain resembles the ancestral state of sporulation efficiency from which we hypothesize the vineyard parent alleles arose. This is further supported by the fact that three of the four vineyard alleles reducing sporulation [*IME1*(L325M), *IME1*(A-548G), and *RSF1*(D181G)] are derived (fig. S2).

Analysis of the allele replacement strains revealed extensive interactions among the four nucleotides as all possible two-, three-, and four-way interactions are statistically significant in an analysis of variance (table S3). The interactions indicate that the vineyard alleles work synergistically to reduce sporulation efficiency. For example, the *IME1* coding and noncoding polymorphisms interact and double the sum of their individual effects (Fig. 4A). The strongest interactions observed occurred between *RME1*(*del-308A*) and the two polymorphisms at *IME1* (Fig. 4B). The

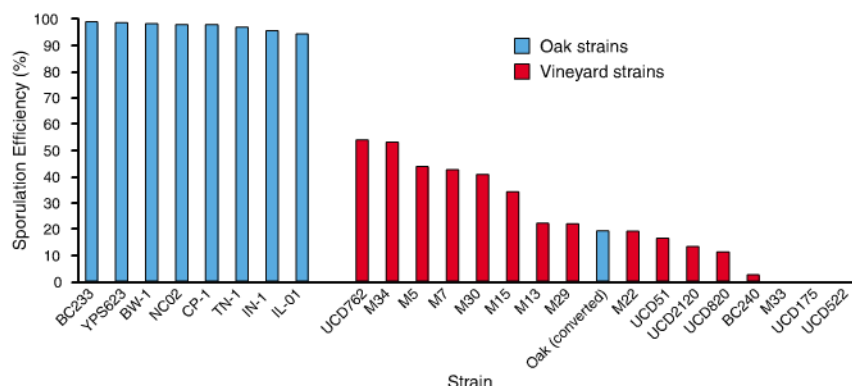


Fig. 3. Variation among oak strains relative to the oak parental strain (BC233) and vineyard strains relative to the vineyard parental strain (BC240) show fixed and variable sporulation efficiencies, respectively. Oak (converted) is the parental oak strain transformed with the four causative nucleotides from the vineyard strain.

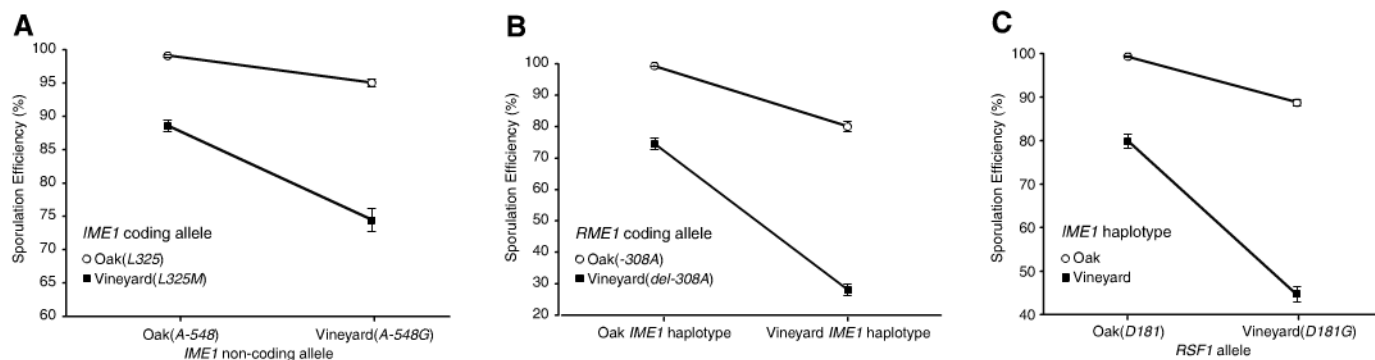


Fig. 4. Single-nucleotide interactions governing sporulation efficiency, as shown by replacing single nucleotides in the oak parent with vineyard parent alleles. (A) The effect of placing the vineyard allele *IME1*(A-548G) in the oak background is greater when the vineyard coding allele *IME1*(L325M) is also present. (B) The effect

of the two causative nucleotides in *IME1* (*IME1* haplotype) is greater when the vineyard *RME1*(*del-308A*) allele is also present. (C) The effect of the *RSF1*(D181G) allele is greater when the vineyard alleles occur at *IME1* (*IME1* haplotype). A full list of interactions is available in table S3. Error bars, ± 1 SD.

RSF1 vineyard allele, which causes less than a 3% change on its own, also was found to interact synergistically with the other vineyard alleles (Fig. 4C) and was responsible for 11%, 13%, and 16% drops in sporulation efficiency through its two-way interactions (table S3). These results illustrate mechanisms by which combinations of alleles can produce a phenotypic change larger than expected from individual effects.

Genetic interactions (epistasis) are often seen between genomic regions affecting quantitative traits (37), and this study demonstrates how a small number of nucleotides can create complex, quantitative variation in phenotype highlighting the importance of single nucleotides on epistasis. This emphasizes the need to incorporate genetic interactions into models that seek to accurately predict phenotype from genotype. If prevalent, genetic interactions between nucleotides will be a major hurdle in the endeavor to connect genetic and phenotypic variation in humans (38). Our identification of epistasis between *RME1* and *IME1* supports the idea that a search for epistasis should incorporate previous knowledge of functional relationships between genes and proteins (39).

We found that alleles reducing sporulation efficiency were at varying frequencies in additional vineyard strains (table S4). The *RME1* polymorphism was found to be ubiquitous, whereas the *IME1* polymorphisms were the rarest. More than half of the vineyard strains harbor at least two of the alleles reducing sporulation, which suggests that the two-way interactions we identified may be producing phenotypic change in nature. However, the four nucleotides we identified are not sufficient to predict all of the differences in sporulation efficiency among vineyard strains. For example, strain UCD51 sporulates less efficiently than M34 and M15 (Fig. 3), despite carrying fewer of the alleles reducing sporulation that we identified (table S4). This suggests that additional alleles reducing sporulation efficiency remain to be identified in the vineyard population.

All four sporulation-reducing alleles were absent from all oak isolates, consistent with the possibility that selection for high sporulation efficiency occurs in woodland environments. This hypothesis was supported by the spectrum of polymorphism in *IME1*, a positive regulator of sporulation (table S5). In oak strains, we observed a lower rate of nonsynonymous substitution relative to synonymous substitutions—which is consistent with purifying selection (Z test, $P < 0.01$) (29). In vineyard strains, the rate of nonsynonymous substitution was not lower than the rate of synonymous substitution, which suggests relaxed selection in vineyard strains (Z test, $P = 0.99$).

Variation at *RSF1* is consistent with selection reducing sporulation efficiency in the vineyard strains. A McDonald-Kreitman test (40) reveals an excess of nonsynonymous polymorphisms in the *S. cerevisiae RSF1* gene relative to its ortholog in *Saccharomyces paradoxus* (Fisher's exact test, $P < 0.001$). These substitutions occurred almost

entirely in the vineyard strains, as eight of nine oak isolates sequenced show no polymorphism at this locus (table S6). This result alone is consistent with relaxed selection on sporulation efficiency, but relaxed selection should still result in a rate of nonsynonymous substitutions lower or equal to the synonymous rate. Instead, the rate of nonsynonymous substitution at *RSF1* in the vineyard strains is significantly greater than the synonymous rate (Z test, $P < 0.02$) (29). This result cannot be explained by relaxed selection and instead suggests selective pressure favoring derived alleles of *RSF1* in vineyard strains.

Selection is hypothesized to favor genetic changes with limited pleiotropy (8). Deletion of *RSF1* causes a severe growth defect when yeast are raised on glycerol (35), and some vineyard strains harbor frame-shifts and premature termination codons in *RSF1* that likely affect both sporulation efficiency and growth rate on glycerol (table S6). We tested whether the *D181G* polymorphism affected growth rate in glycerol and found no effect in the oak parent (t test, $P = 0.99$, $N = 3$) or the vineyard parent (t test, $P = 0.60$, $N = 3$). This suggests that the *D181G* allele is not a complete loss-of-function allele and may alter only a subset of *RSF1* functions.

A major challenge in studying phenotypic change is to find predictable patterns among the genetic differences that create diversity. In this particular case, the causative polymorphisms included both rare and common alleles and occur in both coding and noncoding sequences. One commonality underlying these effects, however, is that all of the changes occur in transcription factors and thus exert their effects through the differential expression of downstream-regulated genes. We argue that change in these transcription factor genes was predictable. *IME1* and *RME1* regulate a battery of functionally related genes whose expression is specific to a single cell type: sporulating cells (41, 42). Therefore, the roles of *IME1* and *RME1* are analogous to those of transcription factors controlling “differentiation gene batteries” that drive terminal cell differentiation in animal development (43). Because these transcription factors coordinately regulate the expression of functionally related genes, changes in their function have the potential for large phenotypic effects (“coordinated pleiotropy”) (2). Furthermore, evolution is hypothesized to favor changes in this type of transcription factor, because their role in a specific cell type limits the potential for deleterious consequences (8, 43, 44). Our results point to transcription factor polymorphism as a major source of natural phenotypic diversity within species.

References and Notes

- G. P. Wagner, V. J. Lynch, *Trends Ecol. Evol.* **23**, 377 (2008).
- G. A. Wray et al., *Mol. Biol. Evol.* **20**, 1377 (2003).
- D. L. Stern, *Evolution* **54**, 1079 (2000).
- H. E. Hoekstra, J. A. Coyne, *Evolution* **61**, 995 (2007).
- S. B. Carroll, *PLoS Biol.* **3**, e245 (2005).
- T. F. Mackay, *Annu. Rev. Genet.* **35**, 303 (2001).

- L. Kruglyak, *Nat. Rev. Genet.* **9**, 314 (2008).
- D. L. Stern, V. Orgogozo, *Evolution* **62**, 2155 (2008).
- J. Flint, R. Mott, *Nat. Rev. Genet.* **2**, 437 (2001).
- A. M. Glazier, J. H. Nadeau, T. J. Aitman, *Science* **298**, 2345 (2002).
- C. C. Steiner, J. N. Weber, H. E. Hoekstra, *PLoS Biol.* **5**, e219 (2007).
- A. Demogines, E. Smith, L. Kruglyak, E. Alani, *PLoS Genet.* **4**, e1000123 (2008).
- A. Demogines, A. Wong, C. Aquadro, E. Alani, *PLoS Genet.* **4**, e1000103 (2008).
- J. A. Heck et al., *Proc. Natl. Acad. Sci. U.S.A.* **103**, 3256 (2006).
- H. Sinha, B. P. Nicholson, L. M. Steinmetz, J. H. McCusker, *PLoS Genet.* **2**, e13 (2006).
- G. Yvert et al., *Nat. Genet.* **35**, 57 (2003).
- R. B. Brem, J. D. Storey, J. Whittle, L. Kruglyak, *Nature* **436**, 701 (2005).
- L. M. Steinmetz et al., *Nature* **416**, 326 (2002).
- G. Ben-Ari et al., *PLoS Genet.* **2**, e195 (2006).
- H. S. Kim, J. C. Fay, *Proc. Natl. Acad. Sci. U.S.A.* **104**, 19387 (2007).
- A. M. Deutschbauer, R. W. Davis, *Nat. Genet.* **37**, 1333 (2005).
- G. I. Naumov, E. S. Naumova, P. D. Sniegowski, *Can. J. Microbiol.* **44**, 1045 (1998).
- P. Marullo et al., *FEMS Yeast Res.* **7**, 941 (2007).
- M. J. McCullough, K. V. Clemons, C. Farina, J. H. McCusker, D. A. Stevens, *J. Clin. Microbiol.* **36**, 557 (1998).
- J. P. Gerke, C. T. Chen, B. A. Cohen, *Genetics* **174**, 985 (2006).
- M. Kupiec, B. Byers, R. E. Esposito, A. P. Mitchell, in *The Molecular and Cellular Biology of the Yeast Saccharomyces: Cell Cycle and Cell Biology*, J. R. Pringle, J. R. Broach, E. W. Jones, Eds. (Cold Spring Harbor Laboratory Press, Cold Spring Harbor, NY, 1997), vol. 3, pp. 889–1036.
- S. M. Honigberg, K. Purnapatre, *J. Cell Sci.* **116**, 2137 (2003).
- I. Nachman, A. Regev, S. Ramanathan, *Cell* **131**, 544 (2007).
- Materials and methods are available as supporting material on Science Online.
- A. P. Mitchell, I. Herskowitz, *Nature* **319**, 738 (1986).
- S. W. Doniger et al., *PLoS Genet.* **4**, e1000183 (2008).
- Y. Kassir, D. Granot, G. Simchen, *Cell* **52**, 853 (1988).
- I. Rubin-Bejerano, S. Mandel, K. Robzyk, Y. Kassir, *Mol. Cell. Biol.* **16**, 2518 (1996).
- H. E. Smith, S. E. Driscoll, R. A. Sia, H. E. Yuan, A. P. Mitchell, *Genetics* **133**, 775 (1993).
- L. Lu, G. Roberts, K. Simon, J. Yu, A. P. Hudson, *Curr. Genet.* **43**, 263 (2003).
- A. Jambhekar, A. Amon, *Curr. Biol.* **18**, 969 (2008).
- O. Carlborg, C. S. Haley, *Nat. Rev. Genet.* **5**, 618 (2004).
- J. H. Moore, *Hum. Hered.* **56**, 73 (2003).
- K. A. Pattin, J. H. Moore, *Hum. Genet.* **124**, 19 (2008).
- J. H. McDonald, M. Kreitman, *Nature* **351**, 652 (1991).
- S. Chu et al., *Science* **282**, 699 (1998).
- M. Primig et al., *Nat. Genet.* **26**, 415 (2000).
- E. H. Davidson, D. H. Erwin, *Science* **311**, 796 (2006).
- V. J. Lynch, G. P. Wagner, *Evolution* **62**, 2131 (2008).
- We thank L. Kyro for technical assistance and J. Fay, B. Engle, H.-S. Kim, and M. Johnston for sharing reagents. We also thank J. Fay, S. Doniger, C. Hittinger, and members of the Cohen laboratory for helpful advice and discussions. Funded by NSF-MCB-0543156. J.P.G. has received support from NHGRI-T32HG000045. Sequences were deposited in GenBank accessions FJ446649 to FJ446698.

Supporting Online Material

www.sciencemag.org/cgi/content/full/323/5913/498/DC1
Materials and Methods

SOM Text

Figs. S1 to S3

Tables S1 to S10

References

25 September 2008; accepted 19 November 2008
10.1126/science.1166426

Different T Cell Receptor Signals Determine CD8⁺ Memory Versus Effector Development

Emma Teixeira,^{1,2†} Mark A. Daniels,^{1,2*} Sara E. Hamilton,^{3*} Adam G. Schrum,^{1,5} Rafael Bragado,⁴ Stephen C. Jameson,³ Ed Palmer^{1†}

Following infection, naïve CD8⁺ T cells bearing pathogen-specific T cell receptors (TCRs) differentiate into a mixed population of short-lived effector and long-lived memory T cells to mediate an adaptive immune response. How the TCR regulates memory T cell development has remained elusive. Using a mutant TCR transgenic model, we found that point mutations in the TCR β transmembrane domain (β TMD) impair the development and function of CD8⁺ memory T cells without affecting primary effector T cell responses. Mutant T cells are deficient in polarizing the TCR and in organizing the nuclear factor κ B signal at the immunological synapse. Thus, effector and memory states of CD8⁺ T cells are separable fates, determined by differential TCR signaling.

It is unclear what determines whether a primed T cell will differentiate into an effector cell and die or will survive and become a long-lived memory cell. Several studies support a linear differentiation model, where memory T cells are descendents of effector cells that differentiate into a memory lineage after antigen has been cleared (1, 2). However, memory T cells have been shown to arise directly from naïve cells, bypassing the effector stage (3–5). This second group of studies suggests that signaling differences may determine the fate of naïve T cells upon infection.

Proinflammatory cytokine signals can favor the generation of effectors versus the development of memory T cells after infection (6, 7). It has also been suggested that cumulative TCR stimulation is required for the generation of memory (8). Other studies have shown that a short period of TCR stimulation is sufficient for programming CD8⁺ T cells to differentiate into memory cells (9, 10). Differentiation and longevity of memory CD4⁺ T cells are dependent on high functional avidities to complete the memory program (11). Several studies have considered the importance of the T cell–APC (antigen-presenting cell) interface in determining the fate of naïve T cells (5, 12). However, much less is known about how and which TCR signals contribute to T cell memory development.

The TCR β -chain transmembrane domain (β TMD) contains a conserved antigen receptor transmembrane (CART) motif (13). The CART motifs in membrane immunoglobulin and in the TCR β chain are involved in the segregation of B cell and CD4⁺ T cell functions (13–15). We

generated OT-1 TCR transgenic mice expressing a point mutation in the β TMD, where the most carboxy-terminal tyrosine residue of the CART motif was replaced by a leucine (CART15 Y→L) (16, 17). TCR expression on mutant T cells was slightly decreased, but the mutant TCR-CD3 complex composition was unaltered (fig. S1). T cell maturation and homeostasis in β TMD mutant mice (β TMDmut) were normal (fig. S1). The OT-1 and β TMDmut OT-1 TCRs recognize the ovalbumin peptide 257 to 264 (OVA_p) bound to H-2K^b (18). No differences were found when wild-type (WT) and mutant T cells were compared for OVA tetramer (OVA_{tet}) binding and OVA_p responsiveness (fig. S1). Thus, the point mutation in β TMD did not affect the ability of the TCR to recognize and respond to ligand.

Next, we studied the capacity of mutant T cells to respond to antigen in vitro. WT and mutant T cells were similar for expression of CD25, CD69, and Fas. However, mutant cells were defective in Fas ligand (FasL) expression (Fig. 1A), similar to Jurkat and murine CD4⁺ T cells, which was linked to impaired nuclear factor- κ B (NF- κ B) signaling (14, 15). We tested β TMDmut T cells for defects in the activation of

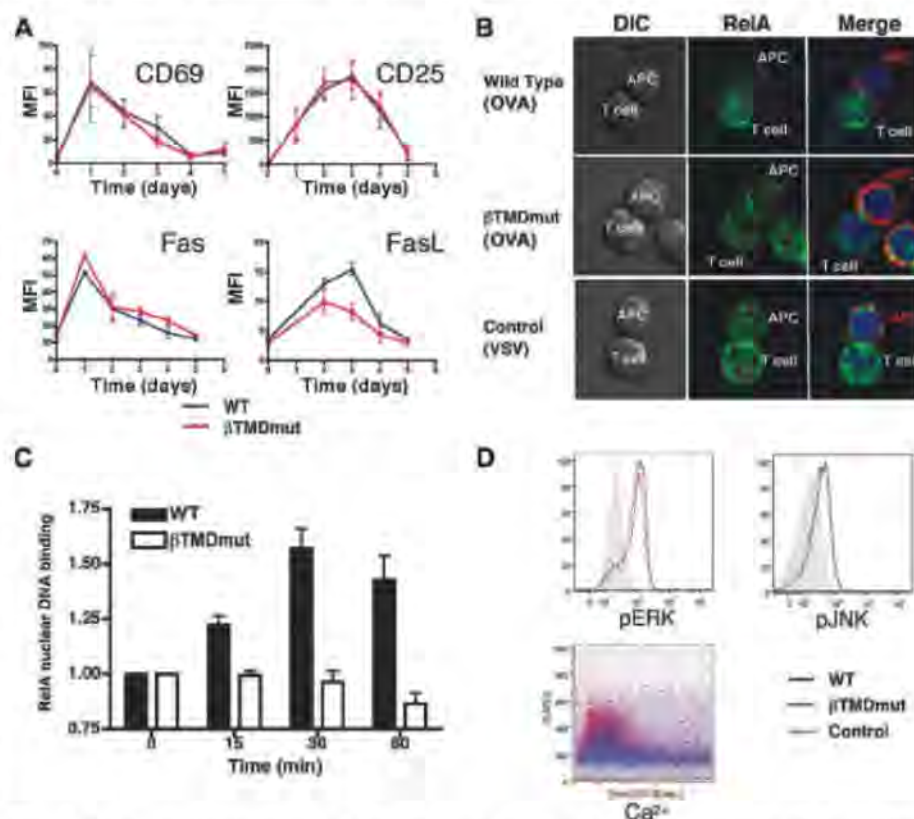


Fig. 1. β TMDmut naïve T cells are defective in NF- κ B signaling. (A) T cells stimulated with 2 μ M OVA_p-pulsed APCs in vitro, showing CD69, CD25, Fas, and FasL ($P = 0.0024$) expression shown as mean fluorescence intensity (MFI). Data represent the means \pm SD of three independent experiments. (B) T cells stimulated as in (A) for 30 min. Vesicular stomatitis virus peptide (VSVp) was a negative control. NF- κ B nuclear translocation determined by confocal microscopy. RelA (green), DRAQ-5 nuclear dye (blue), and CD45.1 (red). Images are representative of $n > 50$ conjugates from three independent experiments. (C) Nuclear extracts from T cells stimulated with OVA_p were tested by enzyme-linked immunosorbent assay (ELISA) for RelA-specific binding to NF- κ B consensus sequence; $P = 0.0003$. (D) T cells stimulated with OVA_p or VSVp (control). ERK and JNK phosphorylation and Ca²⁺ flux were determined by flow cytometry.

¹Experimental Transplantation Immunology, Department of Biomedicine, University Hospital-Basel, Hebelstrasse 20, 4031-Basel, Switzerland. ²Department of Molecular Microbiology and Immunology, University of Missouri, School of Medicine, Center for Cellular and Molecular Immunology, Columbia, MO 65212, USA. ³Center for Immunology and Department of Laboratory Medicine and Pathology, University of Minnesota Medical School, Minneapolis, MN 55454, USA. ⁴Department of Immunology, Fundación Jiménez Díaz, Avenida Reyes Católicos 2, 28040-Madrid, Spain. ⁵Department of Immunology, Mayo Clinic College of Medicine, Rochester, MN 55905, USA.

*These authors have contributed equally to this work. [†]To whom correspondence should be addressed. E-mail: ed.palmer@unibas.ch (E.P.); teixeiropernase@missouri.edu (E.T.)

this or other TCR signaling pathways. Nuclear translocation and DNA binding of NF- κ B were greatly diminished in mutant T cells (Fig. 1, B and C, and fig. S2). However, neither extracellular signal-regulated kinase (ERK), nor c-Jun N-terminal kinase (JNK) phosphorylation, nor Ca^{2+} mobilization was impaired (Fig. 1D).

To study effector development of β TMDmut T cells, low numbers (50 to 500) of CD45.2^+ WT or mutant naïve T cells were transferred into congenic CD45.1^+ recipient mice, followed by infection with recombinant *Listeria monocytogenes*-expressing OVA (LM-OVA). WT and β TMDmut transgenic T cells responded equivalently to LM-OVA, in terms of phenotype, kinetics, and function; this response was also similar to that of the endogenous OVA-responding CD8^+ T cell population (Fig. 2A). At the peak of the primary response, WT and mutant T cells exhibited

identical effector phenotypes (CD62^{low} , interleukin receptor $\text{IL-7R}^{\text{low}}$, $\text{CD43}^{\text{high}}$, CD27^{int} , granzymeB^{high}, IL-2^{low}) (Fig. 2B). On restimulation, interferon- γ (IFN- γ) and tumor necrosis factor- α (TNF- α) expression were similar for both, which indicated that β TMDmut T cells were normal in their effector functions (Fig. 2C). Analogous results were obtained when higher numbers of WT or mutant naïve T cells were used and after OVAp-LPS (lipopolysaccharide) immunization. Mutant and WT T cells were equally efficient at killing in vivo (fig. S3). In addition, there were no differences in CD45.1^+ endogenous responders, WT, or mutant numbers at the peak of the primary immune response in LM-OVA-infected mice (Fig. 2D).

To study the expansion, contraction, and memory phases of the CD8^+ T cell response, we examined lymphocytes from mice that received low

numbers of WT or mutant naïve cells and then were infected with LM-OVA (Fig. 3A). β TMDmut T cells expanded and contracted with kinetics resembling those of WT cells. However, by day 13 to 14, mutant T cells numbers were severely reduced, whereas WT cell numbers contracted more slowly (Fig. 3A). Stable numbers of WT memory T cells were detected by day 46. In contrast, mutant memory cell numbers were at the limit of detection, although similar numbers of endogenous OVA-specific memory CD8^+ T cells were generated (Fig. 3B). Clonal competition can affect differentiation and survival of T cells (19). To check this possibility, we gave mice higher numbers (10^5 to 10^6) of mutant naïve cells and primed them with LM-OVA or OVAp-LPS. Neither condition induced efficient generation of mutant memory T cells (fig. S3). Thus, although mutant T cells differentiated into effectors normally, their memory development was defective. Interleukin receptors IL-15R and IL-7R , important for the survival of CD8^+ memory (20), were equally expressed on both cell types (fig. S3), which indicated that the defect in generating memory T cells was not based solely on competition for survival signals. Thus, the induction of a distinct set of TCR signals, absent in the mutant T cells, is likely required for memory generation.

To compare the functional properties of WT and β TMDmut memory T cells, we tested their ability to mount recall responses. Mice into which low numbers of WT or mutant naïve T cells were previously transferred were reinfected 46 to 50 days post LM-OVA infection. Compared with WT, β TMDmut memory T cells responded poorly to secondary challenge (Fig. 3C). In experiments performed with higher numbers of transferred T cells, mutant memory T cells were deficient in CD25 , leukocyte function-associated antigen-1 (LFA-1), granzyme B, and FasL expression; in CD62L down-regulation; and in IFN- γ and TNF- α expression and secretion (Fig. 3D and fig. S4). β TMDmut memory T cells were also impaired in their cytotoxicity, and they failed to generate a secondary memory pool (fig. S4). Therefore, mutant memory T cells were severely compromised, not only in their numbers but also in their ability to mount secondary responses.

The programming of memory T cell differentiation was tested during the final stages of the primary response. In experiments with LM-OVA, mutant T cells were almost undetectable from day 10 to day 13 after primary immunization (Fig. 3A). However, when we used higher precursor frequencies and immunization with OVAp-LPS, the development of mutant memory T cells could be followed throughout the contraction phase (days 11 and 20). At the peak of the response, WT and mutant cells responded similarly upon antigenic rechallenge. However, by day 11 and day 20, rechallenged mutant T cells were impaired in their expression of several activation, cytolytic, and antiapoptotic proteins (fig. S3). This, together with the fact that mutant cell numbers did not stabilize at the end of the contraction phase (Fig.

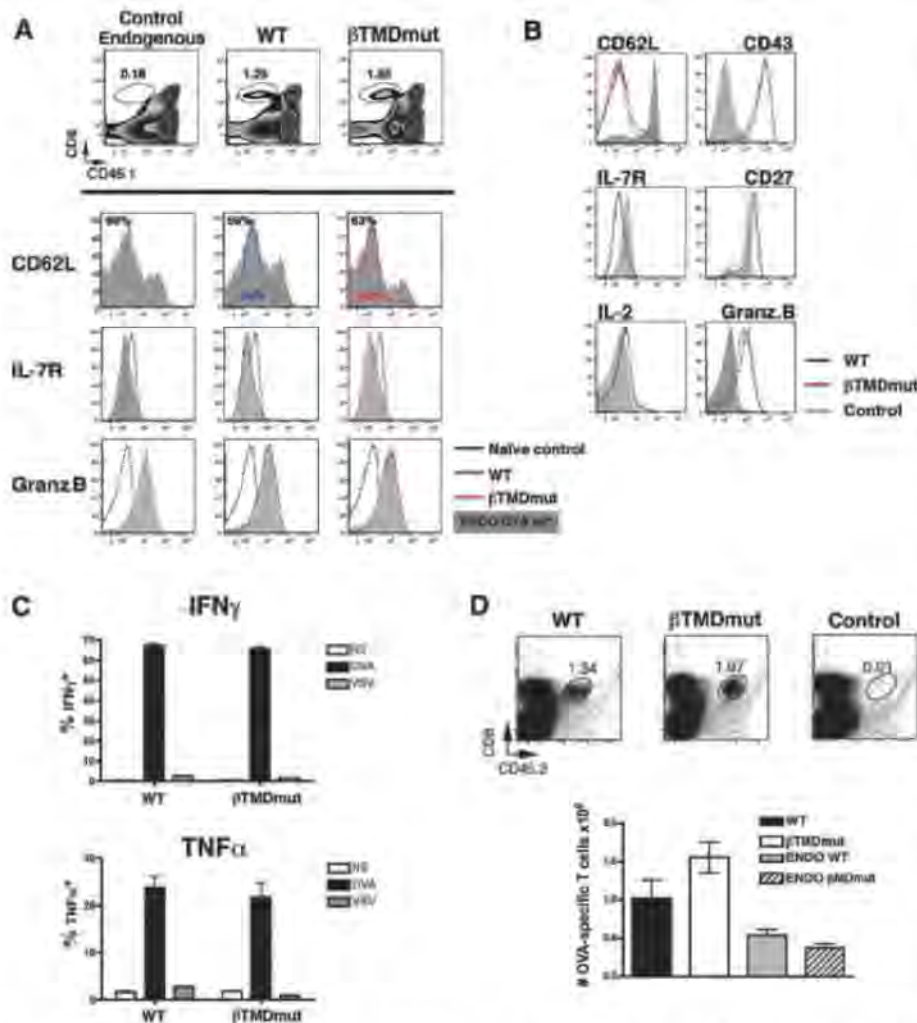


Fig. 2. Normal effector differentiation in β TMDmut T cells. (A) CD45.2^+ naïve T cells were transferred into B6CD45.1^+ mice and immunized with 2×10^4 colony-forming units (CFU) LM-OVA 1 day later. Frequencies and IL-7R, CD62L, and granzymeB expression measured at the peak of the response, day 7. (B) Comparison for expression of markers indicated at day 7 p.i. T cells were restimulated, and IFN- γ or TNF- α expression was measured. (NS, nonstimulated.) Graphs show the percentage (means \pm SD) of WT or mutant cells; $P < 0.004$. (D) CD45.2^+ naïve T cells treated as in (A). Representative plots show frequencies at day 7 p.i. Graph shows number of OVA-specific T cells (means \pm SD). (A to D) Data are representative of more than three independent experiments; $n =$ three mice per group.

3A), strongly indicates that naïve mutant T cells were defective in memory differentiation. Furthermore, considering that mutant cells behaved normally during the primary response, these data suggest that the TCR signals required for generating effector and memory T cells are distinct.

We tested another mutation within the CART motif of the β TMD domain by generating OT-1 TCR transgenic mice with a β TMD mutation in which Ala¹⁶ was replaced by Asn (CART16A→N). β TMD(A→N) T cells were also selectively impaired in memory development, confirming the β TMD (Y→L) phenotype (fig. S5).

To better understand the TCR signals required for memory development, we analyzed some of the biochemical properties of the mutant TCR in memory T cells. Tetramer-binding assays showed that TCRs expressed on WT and mutant memory T cells have similar ligand affinities (Fig. 4A). When stimulated with OVA₃₂₃₋₃₃₉-pulsed APCs, both memory cell types were equally able to mobilize calcium (Fig. 4B). Consequently, the mutant TCR was not blunted in recognizing antigen or in delivering some of the early signals in the context of a memory T cell.

T cells interacting with APCs form conjugates and concentrate signaling molecules at the immunological synapse (IS), which dictates the fate of a naïve T cell (5, 12). It is noteworthy that WT and mutant T cells were similar in maintaining stable interactions with OVA₃₂₃₋₃₃₉-pulsed APCs (figs. S7 to S11). Additionally, proteins important for conjugate formation like LFA-1 and Scribble were polarized to the IS (fig. S7). However, the enrichment of the mutant TCR in the IS (Fig. 4C) and the percentage of mutant T cells polarizing their TCR (fig. S6) were greatly reduced. Because mutant naïve T cells were impaired in NF- κ B induction (Fig. 1C) and the β TMD mutant TCR

was unable to properly polarize to the IS (Fig. 4C), we hypothesized that assembly of NF- κ B signal at the synapse may be affected. As protein kinase C, isoform θ (PKC- θ), is required for NF- κ B activity and colocalizes with the TCR in the IS, we studied the recruitment of PKC- θ to the IS. PKC- θ enrichment within the IS was evident by 15 min in WT cells. However, PKC- θ was not

efficiently recruited to the IS until 60 min of stimulation in mutant cells (Fig. 4C). Nevertheless, this did not rescue the induction of NF- κ B (Fig. 1C). β TMD(A→N) mutant T cells showed a similar phenotype (fig. S5). Together these data emphasize the role of β TMD in polarizing the TCR within the IS and in inducing NF- κ B signals required to generate efficient memory T cells.

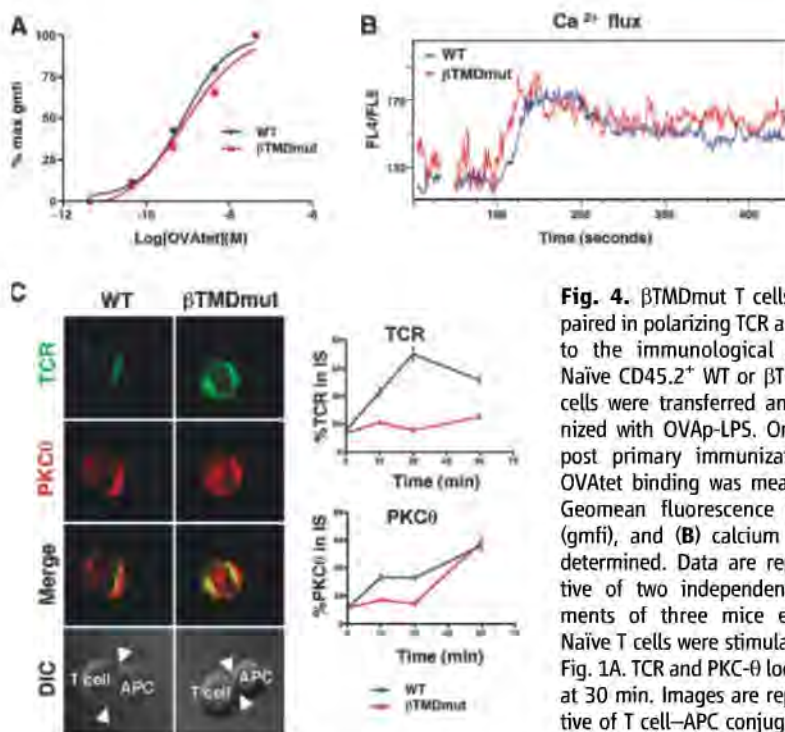


Fig. 4. β TMDmut T cells are impaired in polarizing TCR and PKC- θ to the immunological synapse. Naïve CD45.2⁺ WT or β TMDmut T cells were transferred and immunized with OVA₃₂₃₋₃₃₉-LPS. On day 80 post primary immunization, (A) OVA₃₂₃₋₃₃₉ binding was measured by Geomean fluorescence intensity (gmfi), and (B) calcium flux was determined. Data are representative of two independent experiments of three mice each. (C) Naïve T cells were stimulated as in Fig. 1A. TCR and PKC- θ localization at 30 min. Images are representative of T cell–APC conjugates ($n > 50$). DIC, differential interference

contrast; arrows indicate the IS. Graphs show the kinetics of TCR ($P = 0.0007$) or PKC- θ recruitment ($P = 0.04$) to the IS. Data represent the percentage of molecules in IS (means \pm SD) of 30 to 60 cells from five independent experiments.

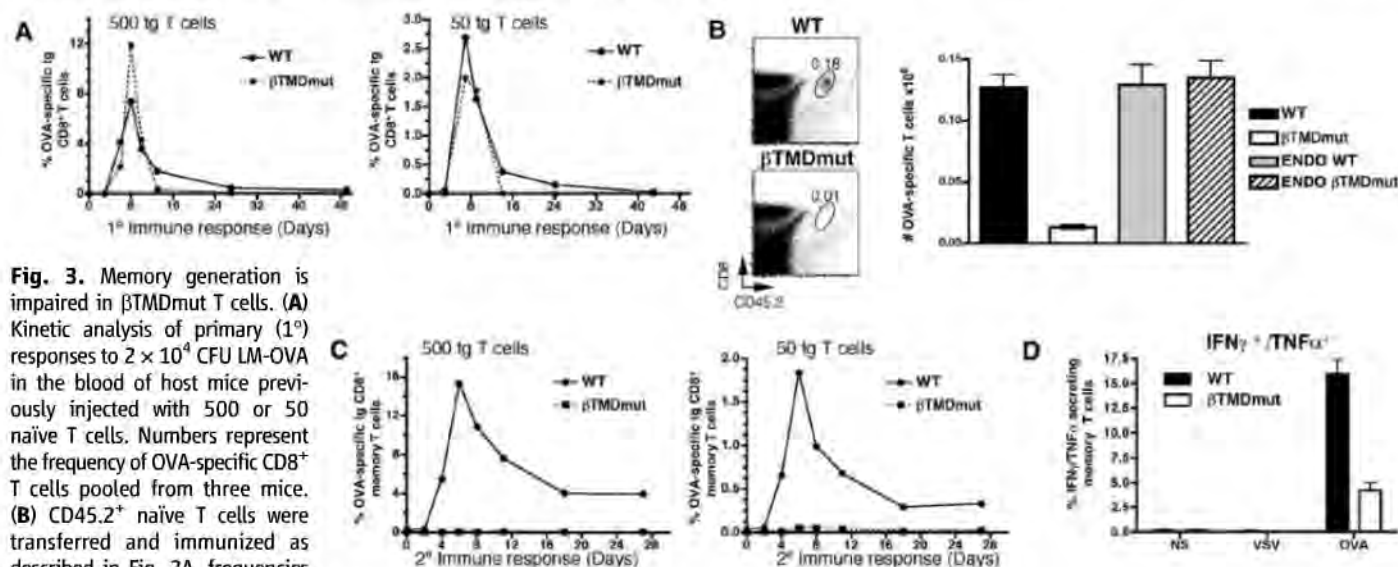


Fig. 3. Memory generation is impaired in β TMDmut T cells. (A) Kinetic analysis of primary (1^o) responses to 2×10^4 CFU LM-OVA in the blood of host mice previously injected with 500 or 50 naïve T cells. Numbers represent the frequency of OVA-specific CD8⁺ T cells pooled from three mice. (B) CD45.2⁺ naïve T cells were transferred and immunized as described in Fig. 2A. frequencies of T cells at day 46 p.i. from representative plots. Graph shows the numbers (means \pm SD) of representative data from four independent experiments; $n =$ three mice per group; for the mutant $P = 0.0005$. (C) CD45.2⁺ naïve T cells were treated as in (A). Kinetic analysis of the secondary (2^o) response in mice reinfected with 9×10^4 CFU

LM-OVA 46 days p.i. Numbers represent the frequency of OVA-specific CD8⁺ T cells pooled from three mice; $P < 0.0005$. (D) Memory T cells were restimulated and IFN- γ and TNF- α expression are shown; $P = 0.004$. (NS, nonstimulated.)

It has been unclear whether the TCR generates similar signals for the development of effector and memory T cells. Our results and others' (3–5) suggest that effector and memory differentiation require a different set of signals. Our data are consistent with a two-lineage model where memory or effector development is determined very early during the immune response by coordinating the recruitment of fate-determining proteins at the level of the IS.

Our studies suggest that different T cell programs are triggered by qualitatively distinct TCR signals, which implies that unique signaling pathways are important for T cell memory development. Several molecules, such as B cell lymphoma-6 (Bcl-6), the B and T lymphocyte attenuator (BTLA), and methyl-CpG binding domain protein 2 (MBD2), are selectively important for memory development but not for effector differentiation (21–23). Along the same lines, mutant T cells are uniquely defective in memory development and NF- κ B signaling. Several studies have reported a role for members of the NF- κ B signaling pathway in memory development (24, 25).

Our studies emphasize the importance of the TCR in regulating the NF- κ B signal required for memory development. We show here that effector and memory programming can be dissociated by the induction of a different arrangement of

TCR signals in CD8⁺ T cells. Studying how these TCR signals are modulated by inflammatory signals or CD4⁺ help will be important in the design of better vaccination regimes.

References and Notes

1. S. M. Kaech, S. Hemby, E. Kersh, R. Ahmed, *Cell* **111**, 837 (2002).
2. J. T. Opferman, B. T. Ober, P. G. Ashton-Rickardt, *Science* **283**, 1745 (1999).
3. G. Lauvau et al., *Science* **294**, 1735 (2001).
4. V. P. Badovinac, K. A. Messingham, A. Jabbari, J. S. Haring, J. T. Harty, *Nat. Med.* **11**, 748 (2005).
5. J. T. Chang et al., *Science* **315**, 1687 (2007).
6. N. S. Joshi et al., *Immunity* **27**, 281 (2007).
7. J. T. Harty, V. P. Badovinac, *Nat. Rev. Immunol.* **8**, 107 (2008).
8. A. Lanzavecchia, F. Sallusto, *Nat. Rev. Immunol.* **2**, 982 (2002).
9. M. J. van Stipdonk et al., *Nat. Immunol.* **4**, 361 (2003).
10. M. Prlic, G. Hernandez-Hoyos, M. J. Bevan, *J. Exp. Med.* **203**, 2135 (2006).
11. M. A. Williams, E. V. Ravkov, M. J. Bevan, *Immunity* **28**, 533 (2008).
12. T. R. Mempel, S. E. Henrickson, U. H. Von Andrian, *Nature* **427**, 154 (2004).
13. K. S. Campbell, B. T. Backstrom, G. Tiefenthaler, E. Palmer, *Semin. Immunol.* **6**, 393 (1994).
14. E. Teixeiro et al., *Immunity* **21**, 515 (2004).
15. E. Teixeiro, A. Garcia-Sahuquillo, B. Alarcon, R. Bragado, *Eur. J. Immunol.* **29**, 745 (1999).
16. Materials and methods are available as supporting material on Science Online.

17. Single-letter abbreviations for the amino acid residues are as follows: A, Ala; C, Cys; D, Asp; E, Glu; F, Phe; G, Gly; H, His; I, Ile; K, Lys; L, Leu; M, Met; N, Asn; P, Pro; Q, Gln; R, Arg; S, Ser; T, Thr; V, Val; W, Trp; and Y, Tyr.
18. K. A. Hogquist et al., *Cell* **76**, 17 (1994).
19. J. Hataye, J. J. Moon, A. Khoruts, C. Reilly, M. K. Jenkins, *Science* **312**, 114 (2006).
20. M. A. Williams, M. J. Bevan, *Annu. Rev. Immunol.* **25**, 171 (2007).
21. H. Ichii et al., *Nat. Immunol.* **3**, 558 (2002).
22. C. Krieg, O. Boyman, Y. X. Fu, J. Kaye, *Nat. Immunol.* **8**, 162 (2007).
23. E. N. Kersh, *J. Immunol.* **177**, 3821 (2006).
24. T. Hettmann, J. T. Opferman, J. M. Leiden, P. G. Ashton-Rickardt, *Immunol. Lett.* **85**, 297 (2003).
25. M. Schmidt-Suppran et al., *Immunity* **19**, 377 (2003).
26. We thank D. Roubaty, B. Hausmann, V. Jäggin, G. E. Fernandez, H. Karauzum, M. Schmalzer, and Z. Rajacic for technical assistance; R. Landmann-Suter for technical advice; and C. Pernas Pernas for helpful discussion. This work was supported by Mission Enhancement Program, University of Missouri (E.T. and M.A.D.) fellowships from the Fundación Ramón Areces, Spain (E.T.), the American Cancer Society (S.E.H.), the Cancer Research Institute (M.A.D.), the Spanish Ministry of Science and Education (MEC) (BFU 2005-02807) (R.B.), Novartis, Roche, Sybilla (EUPF7) and the Swiss National Science Foundation (E.P.).

Supporting Online Material

www.sciencemag.org/cgi/content/full/323/5913/502/DC1
Materials and Methods

Figs. S1 to S7

References

Movies S1 to S4

22 July 2008; accepted 26 November 2008

10.1126/science.1163612

Secondary Replicative Function of CD8⁺ T Cells That Had Developed an Effector Phenotype

Oliver Bannard, Matthew Kraman, Douglas T. Fearon*

Models of the differentiation of memory CD8⁺ T cells that replicate during secondary infections differ over whether such cells had acquired effector function during primary infections. We created a transgenic mouse line that permits mapping of the fate of granzyme B (gzmB)-expressing CD8⁺ T cells and their progeny by indelibly marking them with enhanced yellow fluorescent protein (EYFP). Virus-specific CD8⁺ T cells express gzmB within the first 2 days of a primary response to infection with influenza, without impairment of continued primary clonal expansion. On secondary infection, virus-specific CD8⁺ T cells that became EYFP⁺ during a primary infection clonally expand as well as all virus-specific CD8⁺ T cells. Thus, CD8⁺ T cells that have acquired an effector phenotype during primary infection may function as memory cells with replicative function.

During a primary immune response, naïve, pathogen-specific CD8⁺ T cells replicate and generate effector cells that control the primary infection, and “memory” cells that persist after resolution of the primary infection and respond to secondary infections. Two types of memory cells have been identified: a subset

that resides in the peripheral tissues and has immediate effector function, such as production of interferon- γ (IFN- γ) and cytolytic activity, but cannot replicate, and a subset that maintains a capacity for clonal expansion and generation of effector cells that are required for control of secondary or persistent infections (1). Because a single, antigen-specific CD8⁺ T cell can give rise to primary effector cells and both types of memory cells (2), only two models are possible for the development of memory cells with replicative potential: They arise directly from naïve CD8⁺ T cells and avoid effector differentiation

(3), perhaps by a process of asymmetrical division (4), or they come from proliferating cells that have acquired effector function but have not irreversibly lost replicative capability (5, 6). Determining which model is correct is necessary to guide experimental approaches to defining optimal vaccine strategies. We generated a mouse model that enables conditional, irreversible marking of CD8⁺ T cells that have acquired an effector function, the expression of the cytolytic granule protein, granzyme B (gzmB). In the asymmetrical division model, gzmB expression is considered to identify the daughter T cell that is committed to loss of secondary replicative function (4).

We created a transgenic mouse line using a bacterial artificial chromosome (BAC) containing the *gzmB* gene, which had been modified by inserting at the start codon the tamoxifen-inducible, site-specific recombinase, CreER^{T2} (fig. S1) (7, 8). We crossed this *gzmBCreER^{T2}* BAC transgenic line with the ROSA26EYFP reporter line in which enhanced yellow fluorescent protein (EYFP) is expressed following CreERT2-mediated excision of a loxP-flanked stop codon (9). Thus, in *gzmBER^{T2}/ROSAEYFP* mice, cells that transcribe the *gzmB* gene will express CreER^{T2}, but such cells may become EYFP⁺ only in the presence of tamoxifen. This enables the fate-mapping of such cells without the need for adoptive transfer, which may alter the dynamics of clonal expansion (10). Furthermore, a BAC transgene containing the *gzmB* gene for regulating expression of the

Wellcome Trust Immunology Unit, Department of Medicine, University of Cambridge, Medical Research Council Centre, Hills Road, Cambridge CB2 2QH, UK.

*To whom correspondence should be addressed. E-mail: dtf1000@cam.ac.uk

Cre recombinase circumvents the problem of earlier studies (11) using a truncated human *GzmB* promoter that did not accurately reflect expression of the endogenous *gzmB* gene (12).

A requirement for both *gzmB* transcription and tamoxifen to induce EYFP was assessed by culturing CD8⁺ T cells from *gzmBCreER^{T2}/ROSA26EYFP* mice in *gzmB*-inducing or noninducing conditions, with or without 4-hydroxytamoxifen (4-OHT). EYFP was observed only with culture conditions that induced *gzmB* synthesis by CD8⁺ T cells in the presence of 4-OHT (Fig. 1A). CD8⁺ T cells from the lungs of mice on day 10 of influenza infection were EYFP⁺ also only if tamoxifen had been present (Fig. 1B). EYFP was expressed only by antigen-experienced, CD44^{high} CD4⁺ and CD8⁺ T cells at day 10 and day 100 post infection (p.i.) (Fig. 1C), and by NK cells, but not by B cells, dendritic cells, or myelomonocytic cells (Fig. 1D). Therefore, induction of EYFP is stringently restricted to cells expressing *gzmB* in the presence of tamoxifen. The proportion of EYFP⁺ cells correlated with the magnitude of *gzmB* expression (fig. S2), which suggested that inefficient Cre-mediated recombination accounted for the occurrence of *gzmB*-expressing CD8⁺ T

cells that were EYFP⁺, despite the presence of tamoxifen.

To determine whether *gzmB* expression by CD8⁺ T cells early during a primary response impairs clonal expansion, mice were infected intranasally with influenza, pulsed with tamoxifen on days 1 and 2 or days 7 and 8 p.i., and assessed on day 10 p.i. for the presence in the lungs and mediastinal lymph nodes (MLNs) of EYFP⁺ CD8⁺ T cells that were specific for the H-2D^b/nucleoprotein (NP) peptide complex. D^b/NP-specific CD8⁺ T cells in the MLNs were EYFP⁺ even when tamoxifen was given only during the initial phase of clonal expansion, which indicated that *gzmB* is expressed by virus-specific CD8⁺ T cells in the first few cell cycles (13) and that such cells continue to proliferate and generate EYFP⁺ cells that migrate to the lungs (Fig. 2A). Their continued replication was confirmed by incorporation of 5-bromo-2'-deoxyuridine (BrdU) during days 5 to 9 (Fig. 2B). Administering tamoxifen on days 7 and 8 induced only slightly higher percentages of EYFP⁺ cells among the D^b/NP-specific populations, corroborating that early *gzmB* expression does not impair subsequent clonal expansion. Finally, the pulse characteristics of tamoxifen-mediated CreER^{T2} function were confirmed by the absence of EYFP⁺ D^b/NP-

specific CD8⁺ T cells in mice that had received tamoxifen on the 2 days preceding viral infection (Fig. 2A).

The capacity to mark irreversibly a cohort of cells that had expressed *gzmB* permitted an analysis of changes in their phenotypic characteristics over time. On day 10 of the primary response to influenza with tamoxifen administered on days 1 to 8, almost all EYFP⁺ CD8⁺ T cells in the lungs and spleen expressed *gzmB*, whereas a subset of EYFP⁺ cells in the MLNs had become *gzmB*⁺ (Fig. 3A). By day 49, most EYFP⁺ CD8⁺ T cells had lost expression of *gzmB* except for a small subpopulation in the lungs. A decrease in *gzmB* expression among virus-specific CD8⁺ T cells during the phase following clearance of a primary infection has been considered to exemplify a requirement for a "rest" period during which effector cells convert to memory cells (5). The present finding that CD8⁺ T cells have the capacity to switch *gzmB* expression on and off during the acute phase of the primary response suggests that decreased biosynthesis may be caused by diminished inducing signals, at least within the MLN. Consistent with this possibility, when tamoxifen was administered on days 1 to 4 p.i. and BrdU during the last 12 hours, before analysis on day 8 p.i., the EYFP⁺ CD8⁺

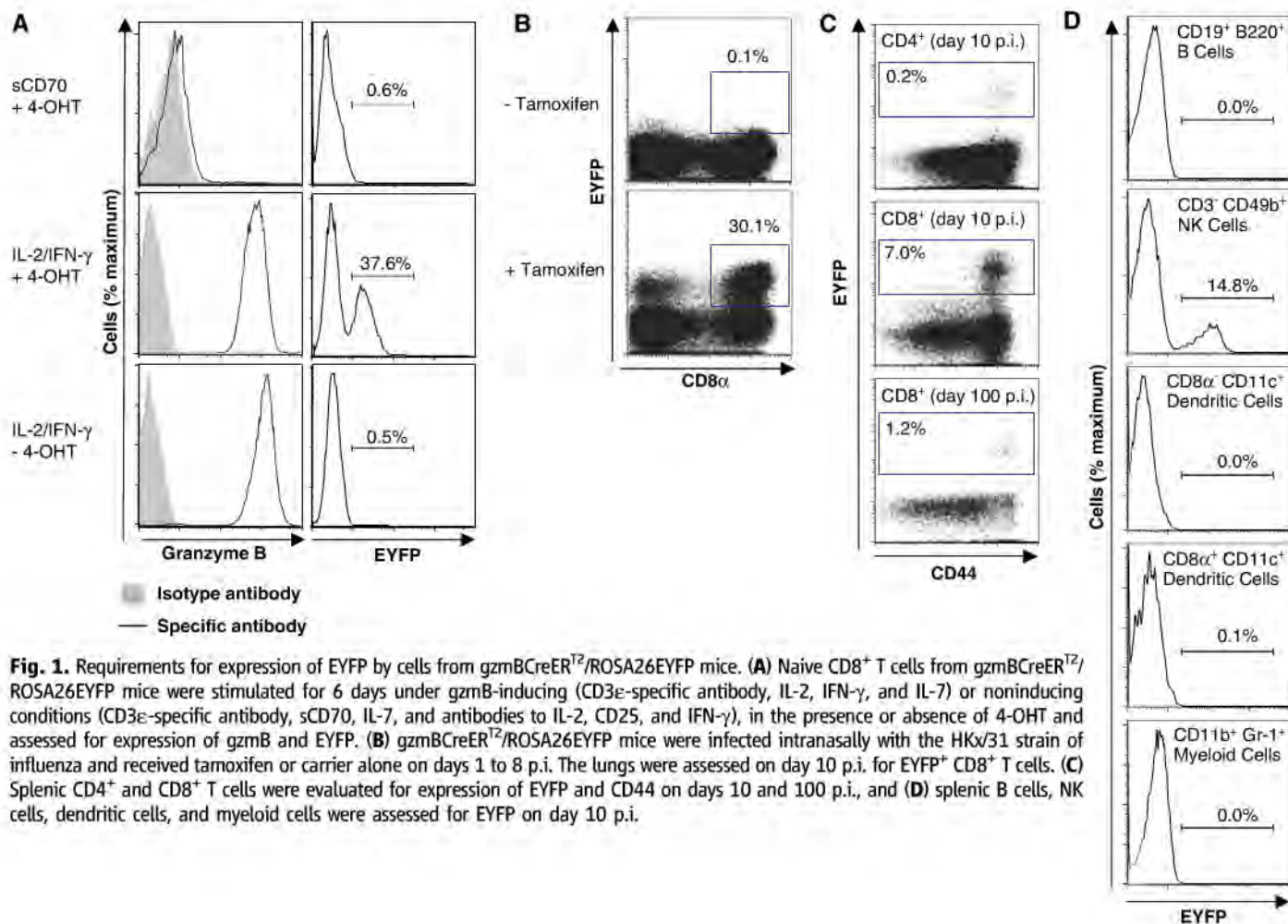


Fig. 1. Requirements for expression of EYFP by cells from *gzmBCreER^{T2}/ROSA26EYFP* mice. (A) Naive CD8⁺ T cells from *gzmBCreER^{T2}/ROSA26EYFP* mice were stimulated for 6 days under *gzmB*-inducing (CD3ε-specific antibody, IL-2, IFN-γ, and IL-7) or noninducing conditions (CD3ε-specific antibody, sCD70, IL-7, and antibodies to IL-2, CD25, and IFN-γ), in the presence or absence of 4-OHT and assessed for expression of *gzmB* and EYFP. (B) *gzmBCreER^{T2}/ROSA26EYFP* mice were infected intranasally with the HKx31 strain of influenza and received tamoxifen or carrier alone on days 1 to 8 p.i. The lungs were assessed on day 10 p.i. for EYFP⁺ CD8⁺ T cells. (C) Splenic CD4⁺ and CD8⁺ T cells were evaluated for expression of EYFP and CD44 on days 10 and 100 p.i., and (D) splenic B cells, NK cells, dendritic cells, and myeloid cells were assessed for EYFP on day 10 p.i.

T cells lacking expression of gzmB were mainly CD25⁻ and BrdU⁻, whereas the gzmB⁺ cells expressed high levels of CD25 and were BrdU⁺ (Fig. 3B). Thus, loss of gzmB expression may

reflect interrupted signaling through the interleukin 2 (IL-2) receptor.

The loss of expression of CD62L and IL-7R α by CD8⁺ T cells during the primary re-

sponse correlates with diminished survival and replicative capability in the memory phase of the response (5, 6). On day 10, EYFP⁺ CD8⁺ T cells in the MLNs, the site of clonal expansion, but not in the spleen or lungs, remained CD62L^{high} (Fig. 3A). Therefore, diminished expression of CD62L is not necessarily linked to expression of gzmB, as has been suggested (4). By day 49, CD62L^{high} EYFP⁺ CD8⁺ T cells were also present in the spleen, but not in the lung, which indicated either that, during the memory phase, CD62L^{high} cells from the MLNs migrate to the lymphoid areas of the spleen; that there is selective loss of CD62L^{low} cells in the spleen; or that both occur. Similarly, by day 42, EYFP⁺ CD8⁺ T cells expressing IL-7R α were present in the MLNs and spleen, but all EYFP⁺ cells in the lungs lacked this receptor (Fig. 3A). Therefore, the phenotype of CD62L^{high} and IL-7R α ⁺ of memory cells that have expressed gzmB correlates with their anatomic site and not with whether they have exhibited this differentiated function.

We examined whether EYFP⁺ D^b/NP-specific CD8⁺ T cells persisted into the memory phase and responded secondarily to influenza infection. The proportion of D^b/NP-specific CD8⁺ T cells in the lungs, MLNs, and spleen that were EYFP⁺ did not change between days 10 and

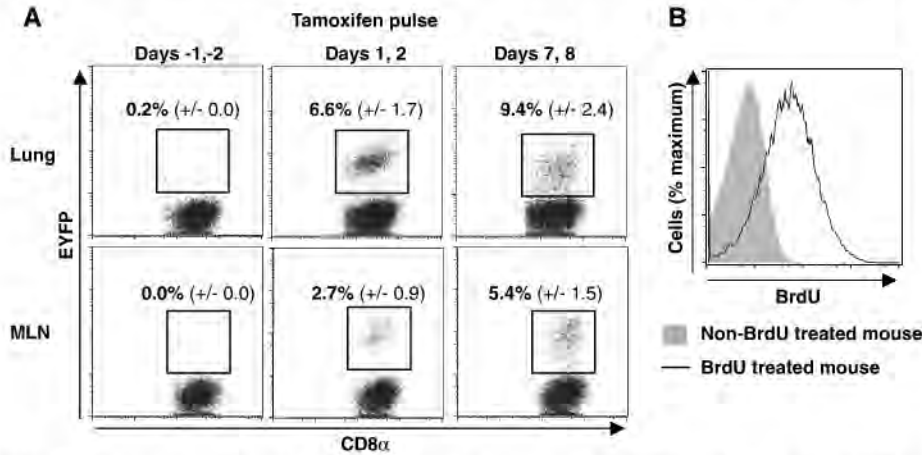


Fig. 2. Clonal expansion by CD8⁺ T cells that had expressed gzmB during the first days of influenza infection. (A) gzmBCreER¹²/ROSA26EYFP mice were infected intranasally with the HKx/31 strain of influenza and were given tamoxifen for 2 days before infection, on days 1 and 2 p.i., or on days 7 and 8 p.i. On day 10 p.i., we determined the proportion (mean \pm SEM) of D^b/NP-pentamer-binding CD8⁺ T cells that was EYFP⁺. (B) Influenza-infected mice that had received tamoxifen on days 1 and 2 were given BrdU on days 5 to 9 p.i., and EYFP⁺ CD8⁺ T cells from the lungs were assessed on day 10 p.i. for incorporation of BrdU.

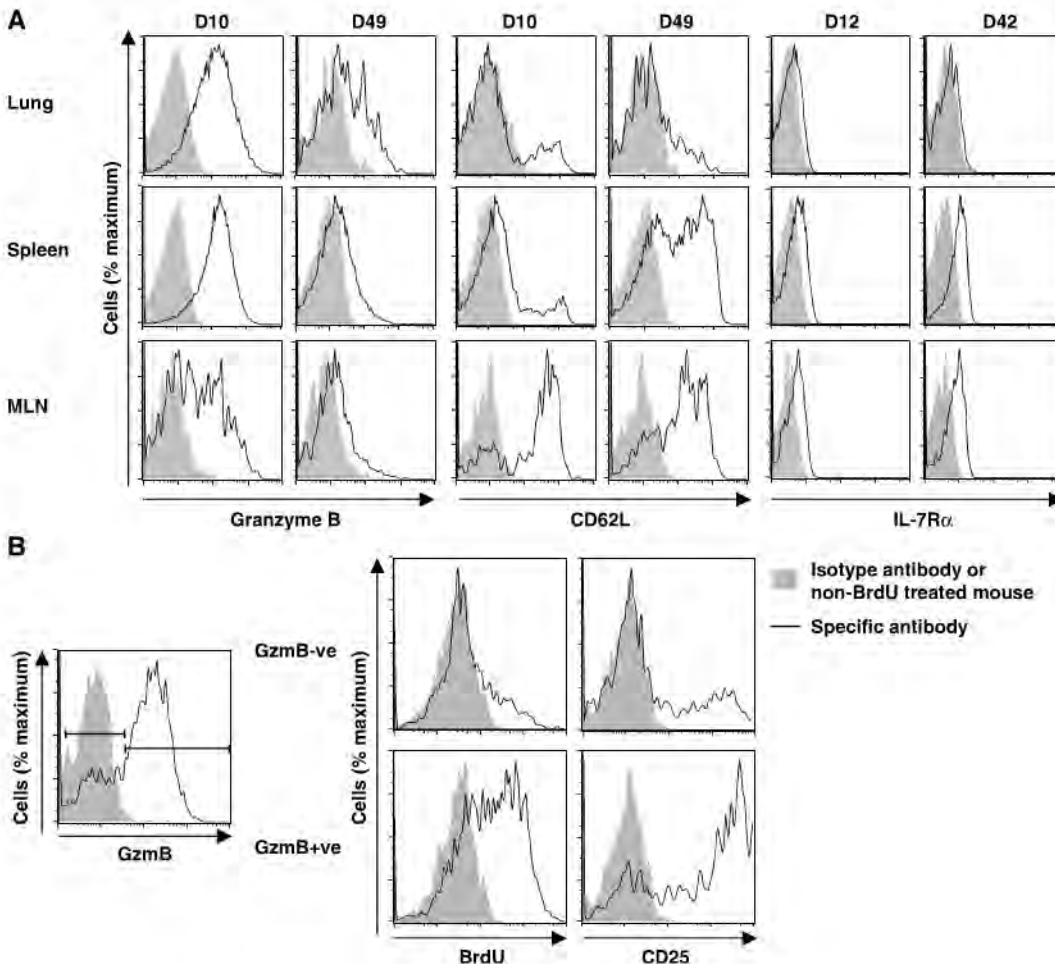


Fig. 3. Expression of gzmB, CD62L, IL-7R α , and CD25 by EYFP⁺ CD8⁺ T cells responding to influenza infection. (A) gzmBCreER¹²/ROSA26EYFP mice were infected intranasally with the HKx/31 strain of influenza and treated with tamoxifen on days 1 to 8 p.i. The EYFP⁺ CD8⁺ T cells from the lungs, MLNs, and spleen were analyzed for intracellular gzmB, CD62L, and IL-7R α at the peak of the primary response and during the memory phase (6 or 7 weeks p.i.). (B) Influenza-infected mice were given tamoxifen on days 1 to 4 p.i. and BrdU 12 hours before analysis on day 8 for BrdU incorporation and CD25 expression by EYFP⁺ CD8⁺ T cells from the MLNs.

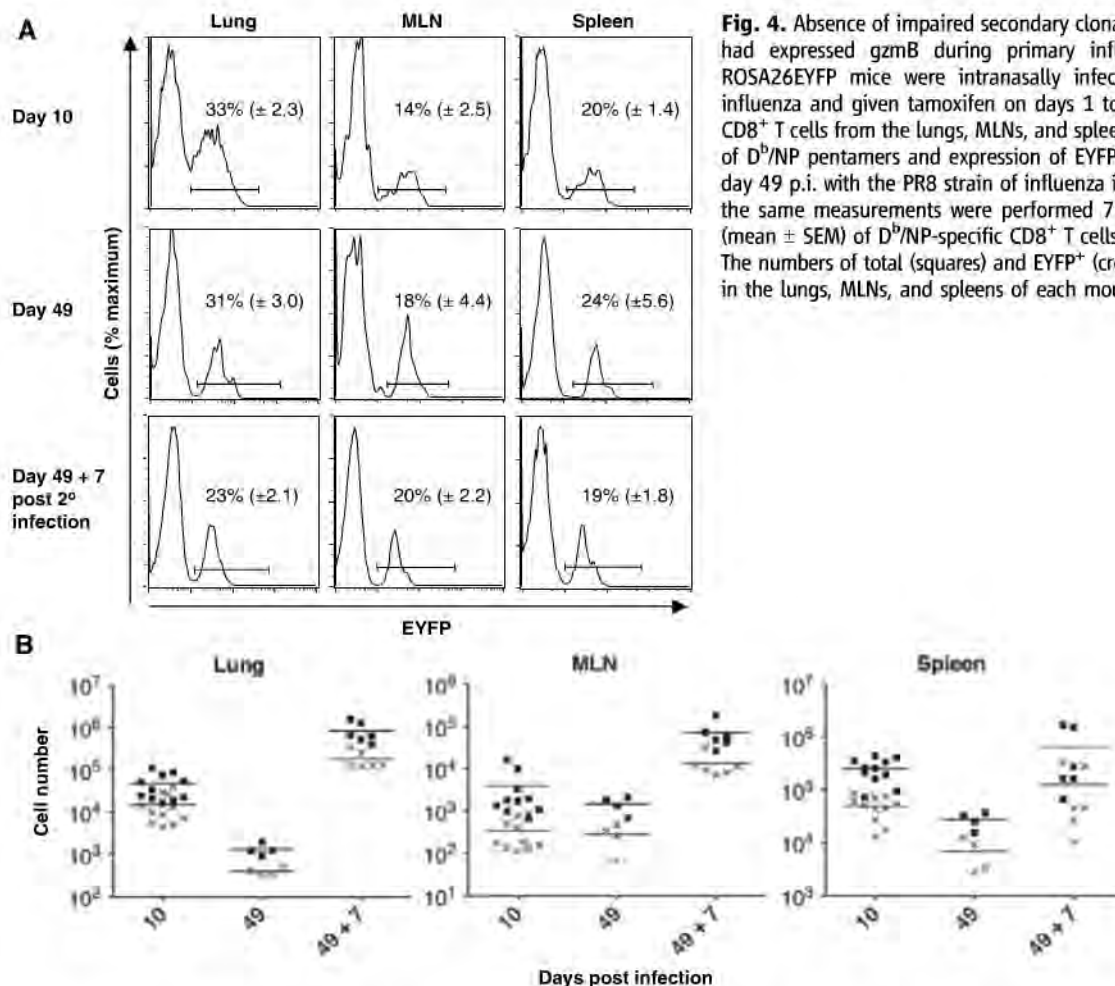


Fig. 4. Absence of impaired secondary clonal expansion by CD8⁺ T cells that had expressed gzmB during primary influenza infection. gzmBCreER^{T2}/ROSA26EYFP mice were intranasally infected with the HKx31 strain of influenza and given tamoxifen on days 1 to 8 p.i. On days 10 and 49 p.i., CD8⁺ T cells from the lungs, MLNs, and spleens were assessed for the binding of D^b/NP pentamers and expression of EYFP⁺. The mice were challenged on day 49 p.i. with the PR8 strain of influenza in the absence of tamoxifen, and the same measurements were performed 7 days later. **(A)** The proportions (mean \pm SEM) of D^b/NP-specific CD8⁺ T cells that were EYFP⁺ are shown. **(B)** The numbers of total (squares) and EYFP⁺ (crosses) D^b/NP-specific CD8⁺ T cells in the lungs, MLNs, and spleens of each mouse are shown.

49 p.i. ($P > 0.4$), which indicated that expression of gzmB during the primary response does not destine a cell for contraction (Fig. 4A). Furthermore, the proportion of EYFP⁺ D^b/NP-specific cells in the MLNs remained the same after secondary viral infection, which suggested that these cells replicated as well as all D^b/NP-specific memory CD8⁺ T cells. The modest decrease in the percentage of EYFP⁺ cells in the lungs after secondary expansion may reflect the presence at day 49 of cells that had been labeled at this peripheral site during the primary infection and were unable to replicate during the secondary infection.

Equivalent replicative capability of the EYFP⁺ and total D^b/NP-specific CD8⁺ T cells was confirmed by finding ~500-fold expansion of both populations in the lungs on day 7 post secondary infection (Fig. 4B). There were lower, although again comparable, increases in these two populations in the MLNs (Fig. 4B), where most new effector cells in the lungs are likely to be generated, and also in the spleen.

The capacity to replicate secondarily was also determined for EYFP⁺ D^b/NP-specific CD8⁺ T cells that had been marked by tamoxifen pulses on days 1 to 3 and days 7 to 9, respectively, during primary influenza infection. On day 7 post secondary infection, the EYFP⁺ D^b/NP-specific

CD8⁺ T cells in the two groups had similar fold increments in the MLNs, spleens, and lungs, and these were comparable to those of the total antigen-specific cells (fig. S3). This finding further excludes models of differentiation in which early expression of gzmB marks a CD8⁺ T cell that has lost a capacity for secondary replicative function.

In summary, the conditional and indelible marking of CD8⁺ T cells that had previously expressed gzmB permitted their identification among all subsets of CD8⁺ T cells in the primary and memory phases of an antiviral response, including the subset that mediates secondary clonal expansion. Combined with the observation that a CD8⁺ T cell may express gzmB early in the primary response without preventing continued expansion (Fig. 2A), one may conclude that such cells can self-renew and serve as progenitors of the more differentiated, senescent cells that have diminished expression of CD62L and IL-7R α (Fig. 3A). Although EYFP was not induced in all gzmB-expressing cells because of inefficient Cre-mediated recombination, the EYFP⁺ memory CD8⁺ T cell population was representative of the entire memory population with respect to survival and secondary expansion. Therefore, memory CD8⁺ T cells that proliferate during secondary infections can be

derived from cells that had acquired an effector phenotype during the primary response, as has been proposed (5, 6). This conclusion is consistent with the IL-2R-dependence of gzmB expression (Fig. 3B) and development of memory cells with replicative function (14) and with the secondary replication of IFN- γ -expressing memory CD4⁺ T cells (15). However, it does not support the asymmetrical division model in which the gzmB-expressing daughter cell of the first division of the activated naïve CD8⁺ T cell is restricted to a nonreplicative memory cell fate (4). Thus, as-yet-undefined signals, in addition to those leading to acquisition of gzmB-dependent effector functions and that cannot be defined in this experimental system, must account for terminal differentiation and senescence of the CD8⁺ T cell.

References and Notes

1. F. Sallusto, D. Lenig, R. Förster, M. Lipp, A. Lanzavecchia, *Nature* **401**, 708 (1999).
2. C. Stemberger et al., *Immunity* **27**, 985 (2007).
3. D. T. Fearon, P. Manders, S. D. Wagner, *Science* **293**, 248 (2001).
4. J. T. Chang et al., *Science* **315**, 1687 (2007).
5. E. J. Wherry et al., *Nat. Immunol.* **4**, 225 (2003).
6. N. S. Joshi et al., *Immunity* **27**, 281 (2007).
7. R. Feil, J. Wagner, D. Metzger, P. Chambon, *Biochem. Biophys. Res. Commun.* **237**, 752 (1997).

8. Materials and methods are available as supporting material on Science Online.
9. S. Srinivas *et al.*, *BMC Dev. Biol.* **1**, 4 (2001).
10. A. L. Marzo *et al.*, *Nat. Immunol.* **6**, 793 (2005).
11. J. Jacob, D. Baltimore, *Nature* **399**, 593 (1999).
12. R. D. Hanson, G. M. Sclar, O. Kanagawa, T. J. Ley, *J. Biol. Chem.* **266**, 24433 (1991).
13. M. R. Jenkins *et al.*, *J. Immunol.* **181**, 3818 (2008).
14. M. A. Williams, A. J. Tyznik, M. J. Bevan, *Nature* **441**, 890 (2006).
15. L. E. Harrington, K. M. Janowski, J. R. Oliver, A. J. Zajac, C. T. Weaver, *Nature* **452**, 356 (2008).
16. The authors thank D. Winton for ROSA26EYFP mice, B. Crombrughe for the CreER¹² construct, G. Eberl for the recombining shuttle vector, and P. Digard and E. Hutchinson for help with viruses. This work was funded by the Wellcome Trust.

Supporting Online Material

www.sciencemag.org/cgi/content/full/323/5913/505/DC1

Materials and Methods

Figs. S1 to S3

Table S1

References

6 October 2008; accepted 1 December 2008

10.1126/science.1166831

Electron Cryomicroscopy of *E. coli* Reveals Filament Bundles Involved in Plasmid DNA Segregation

Jeanne Salje,*† Benoît Zuber, Jan Löwe

Bipolar elongation of filaments of the bacterial actin homolog ParM drives movement of newly replicated plasmid DNA to opposite poles of a bacterial cell. We used a combination of vitreous sectioning and electron cryotomography to study this DNA partitioning system directly in native, frozen cells. The diffraction patterns from overexpressed ParM bundles in electron cryotomographic reconstructions were used to unambiguously identify ParM filaments in *Escherichia coli* cells. Using a low-copy number plasmid encoding components required for partitioning, we observed small bundles of three to five intracellular ParM filaments that were situated close to the edge of the nucleoid. We propose that this may indicate the capture of plasmid DNA within the periphery of this loosely defined, chromosome-containing region.

One of the simplest known mechanisms by which newly replicated DNA molecules are moved apart is encoded by the bacterial low-copy number plasmid R1. This type II plasmid partitioning system includes three components that are both necessary and sufficient to confer genetic stability and are encoded in a tight gene cluster (*1*). ParM is an actin-like adenosine triphosphatase (ATPase) protein that forms double-helical filaments (*2–4*) and exhibits dynamic instability from both ends in the presence of ATP (*5*). Upon addition of both the small DNA-binding protein ParR and the centromere-like DNA region, *parC*, a ParRC protein-DNA complex caps and stabilizes both ends of the ParM filament (*6–8*). Thus stabilized, the ParM filament elongates at both ends and drives the plasmid-attached ParRC complexes to opposite poles of the bacterial cell. This system has been extensively studied both in cells using light microscopy (*9–11*) and in vitro (*5, 6*), and here we turn to a direct characterization of ParMRC-driven DNA segregation in situ using vitreous sectioning (*12*) and electron cryotomography.

First, we set about characterizing ParM filaments directly in *Escherichia coli* cells that had been immobilized in a near-to-native vitreous state by high-pressure freezing (*13*). ParM was

overexpressed to very high concentrations in the absence of ParR or *parC*. ParM filaments form spontaneously at these high concentrations. Images of cryosections revealed that these cells contained a large volume of tightly packed bundles of filaments (Fig. 1A and fig. S1A). This packing is probably due to the crowded environment of the cell. A small amount of crowding agent is sufficient to induce bundling of purified ParM filaments (Fig. 1, B and C) (*14*). Unlike actin, no additional proteins that induce bundling by cross-linking along the filaments of ParM are known or required.

To verify the identity of the bundles of filaments as ParM protein, we compared the diffraction patterns from electron cryomicrographs of in vitro bundles with those extracted from in situ electron cryotomography reconstructions. The resulting lateral diffraction spacing corresponds to packing of the roughly 80 Å thick filaments and was determined to be 83 Å in the tomogram slice (Fig. 1, D and E) and smeared between 63 and 83 Å for the in vitro bundles (Fig. 1, E and F). This smear relates to the fact that in vitro bundles were several filaments thick, producing additional, smaller interfilament repeats in the diffraction pattern. The longitudinal repeat of filamentous ParM was measured to be 53 Å in the in vitro bundles (Fig. 1E), agreeing with previous measurements on single filaments (*2, 4*). We were able to measure the longitudinal repeat in tomographic slices, and this ranged from 41 to 53 Å, depending on the angle of rotation. The upper value confirmed the identity of these filaments. Bundles of filaments persisted in the presence of the MreB-depolymerizing drug

A22 (fig. S1B), ruling out the possibility that these filaments were composed of the chromosomally encoded bacterial actin MreB.

As a comparison, we performed electron cryotomography on whole, intact plunge-frozen cells containing bundles of ParM (Fig. 1G). These cells expressed an ATPase-deficient mutant form of ParM [Asp¹⁷⁰ → Ala¹⁷⁰ (D170A)] (*11*), which is unable to depolymerize, leading to strings of cells with blocked septa. Even here the sample was too thick to achieve resolutions comparable to those obtained using thin cryosections, and the longitudinal repeat in the diffraction pattern could not be detected (compare Fig. 1, E and G).

Having identified ParM filaments directly in cryo-immobilized cells, we next turned to studying intracellular ParM filaments that are actively involved in segregating plasmid DNA. We used three different systems, each moving closer to the situation of the original R1 low-copy plasmid system (Fig. 2A). The first system was T7-driven ParM overexpression (see above). Next, we put three copies of the ParMRC cluster on a high-copy number plasmid (pBR322 replicon). Finally, a low-copy number R1-derived plasmid stabilized by a single copy of the ParMRC partitioning complex was used (pKG491) (*1, 15*). A marked decrease in ParM levels was observed, moving from the overexpression system through the high-copy number plasmid to the low-copy number R1-derived plasmid (Fig. 2A). Cross sections through frozen cells overexpressing ParM protein clearly revealed tightly packed bundles of ParM (Fig. 2B, left, and fig. S1A). These images told us that ParM filaments would be best recognized in cross sections through the filaments (Fig. 2C). Cells carrying the ParMRC-containing high-copy number plasmid contained a combination of small bundles and single filaments within a single cell (Fig. 2B, middle, and fig. S2, A to C). Moving to even lower ParM concentrations using cells carrying the low-copy number R1 plasmid pKG491, we anticipated that observing filaments would be an extremely rare event. Previous studies have shown that pole-to-pole filaments of ParM can be observed in only ~40% of cells, with the others localizing in discrete clusters or diffuse throughout the cell (*11*). Furthermore, our ParM overexpression experiments told us that filaments could only be confidently recognized in those sections where the filament is exactly perpendicular to the imaging plane. Given that cells are frozen and sectioned in a semi-random orientation, we therefore imaged 300 to 400 cells.

Medical Research Council (MRC) Laboratory of Molecular Biology, Hills Road, Cambridge CB2 0QH, UK.

*To whom correspondence should be addressed. E-mail: jsalje@mrc-lmb.cam.ac.uk

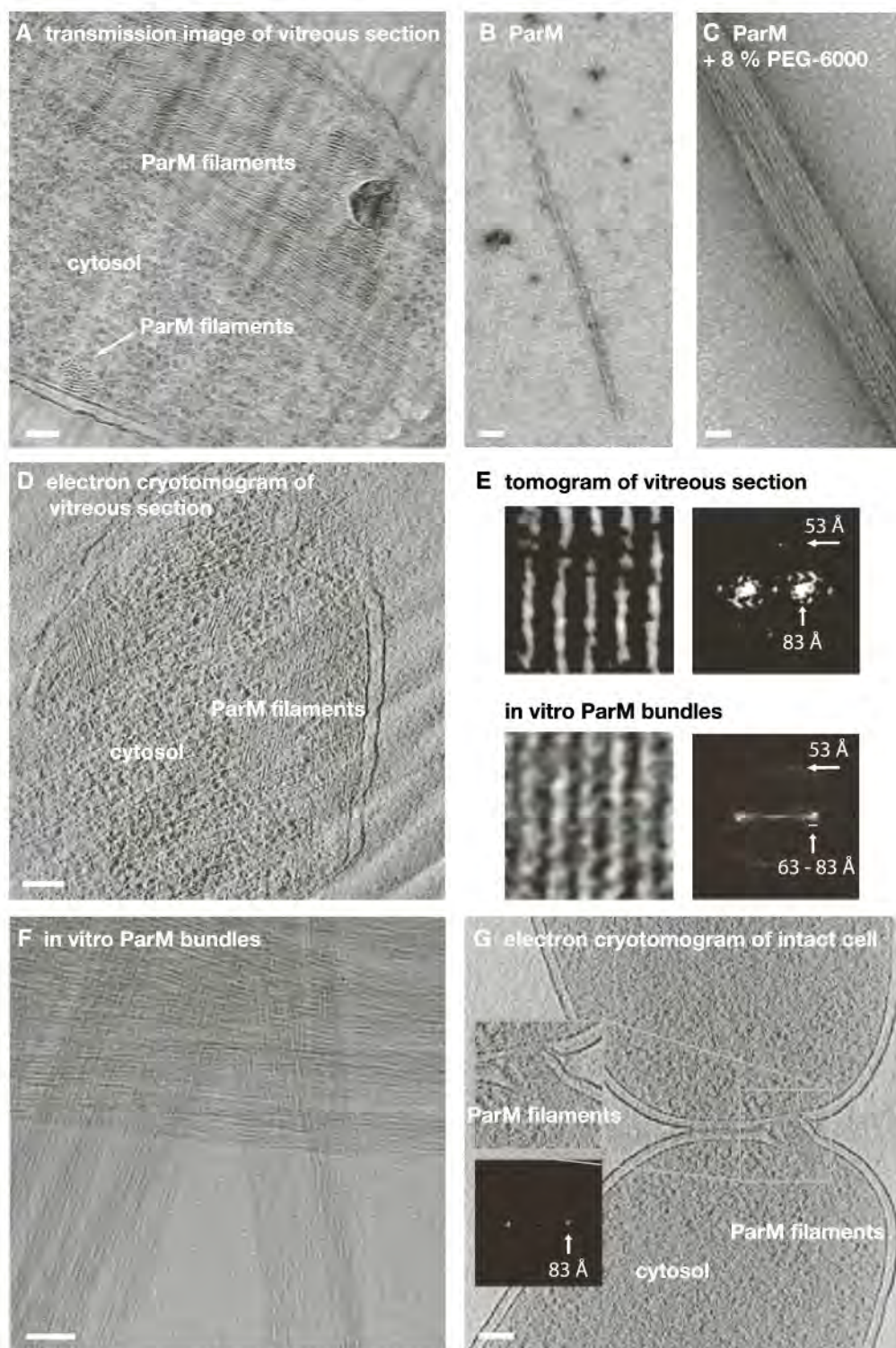
†Present address: Kyoto University, Department of Biophysics, Faculty of Science, Oiwake Kitashirakawa, Sakyo-Ku, Kyoto 606-8502, Japan.

In spite of these difficulties, we were able to identify small bundles of three to five filaments in cross sections of cells harboring the R1-derived low-copy plasmid (Fig. 2, B, right, and D). All filament bundles that we identified are shown in fig. S3, A to G. Similar structures were never observed in 385 images of plasmid-free cells (fig. S4, A to F). The packing of the bundles matched that observed in both the overexpression and high-copy number systems (Fig. 2B). We cannot for-

mally prove that the ParM bundles we observed were actively segregating attached plasmids and had not formed spontaneously because we cannot co-label the plasmid DNA and fully trace the filament through the cell. However, we find it highly probable that these bundles were in the process of segregating or anchoring plasmids for the following reasons. First, the high-copy number plasmid experiment showed that not all filaments bundle spontaneously at these low ParM concentrations

(Fig. 2B and fig. S2, A to C). Thus, a plasmid-related process, such as clustering, must have induced the bundles we observed in the R1 derivative. Second, ParM filaments only form in these cells in the presence of both ParR and *parC* (11), and plasmids localize to the ends of ParM filaments (10). Third, the plasmid copy number (4 to 6) (16) closely matches the number of filaments observed in our bundles (3 to 5), strongly supporting the current model for ParMRC DNA segregation (8).

Fig. 1. Direct observation of bundles of ParM filaments in frozen *E. coli* cells. **(A)** Transmission image of a vitreous cryosection of a cell containing overexpressed ParM filaments. **(B and C)** Negatively stained in vitro ParM filaments in the presence (C) and absence (B) of crowding agent (8% PEG-6000). **(D)** Slice through a three-dimensional (3D) tomographic reconstruction of a vitreous cryosection of a cell containing overexpressed ParM filaments. **(E)** Diffraction patterns from a 3D tomographic reconstruction slice [top, as shown in (D)] or in vitro bundles of ParM [bottom, as shown in (F)]. **(F)** Electron micrograph of bundles of frozen in vitro ParM filaments formed in the presence of 8% PEG-6000. **(G)** Slice through a 3D tomographic reconstruction of a whole, intact plunge-frozen cell containing D¹⁷⁰A (ATPase-defective) ParM filaments. The diffraction pattern from a small bundle extracted from the tomogram is shown. Scale bars are 100 nm [(A), (D), (E), and (G)] or 20 nm [(B) and (C)].



How are the filaments bundled in the cell? One possible explanation is that plasmids can be linked via the oligomeric ParRC complexes (17), and these linked complexes can bring together the ends of two ParM filaments (8). This may lead to bundling, as supported by the observation that covalently linked clusters of ParR-*parC* are sufficient to induce ParM bundling in vitro (18).

We next turned our attention to the subcellular localization of plasmid-segregating ParM bundles. Fluorescently labeled ParM from low-copy number plasmids forms curved pole-to-pole filaments running close to the edge of the bacterial cell (9–11) (Fig. 3E). Because of the small size of the cells (~0.8 to 1 μm thick), it has so far been impossible to distinguish whether the filaments are attached to the inner surface of the cell membrane or run through the cytosol, or where they lie relative to the bacterial nucleoid. Direct visualization of ParM bundles in cells using

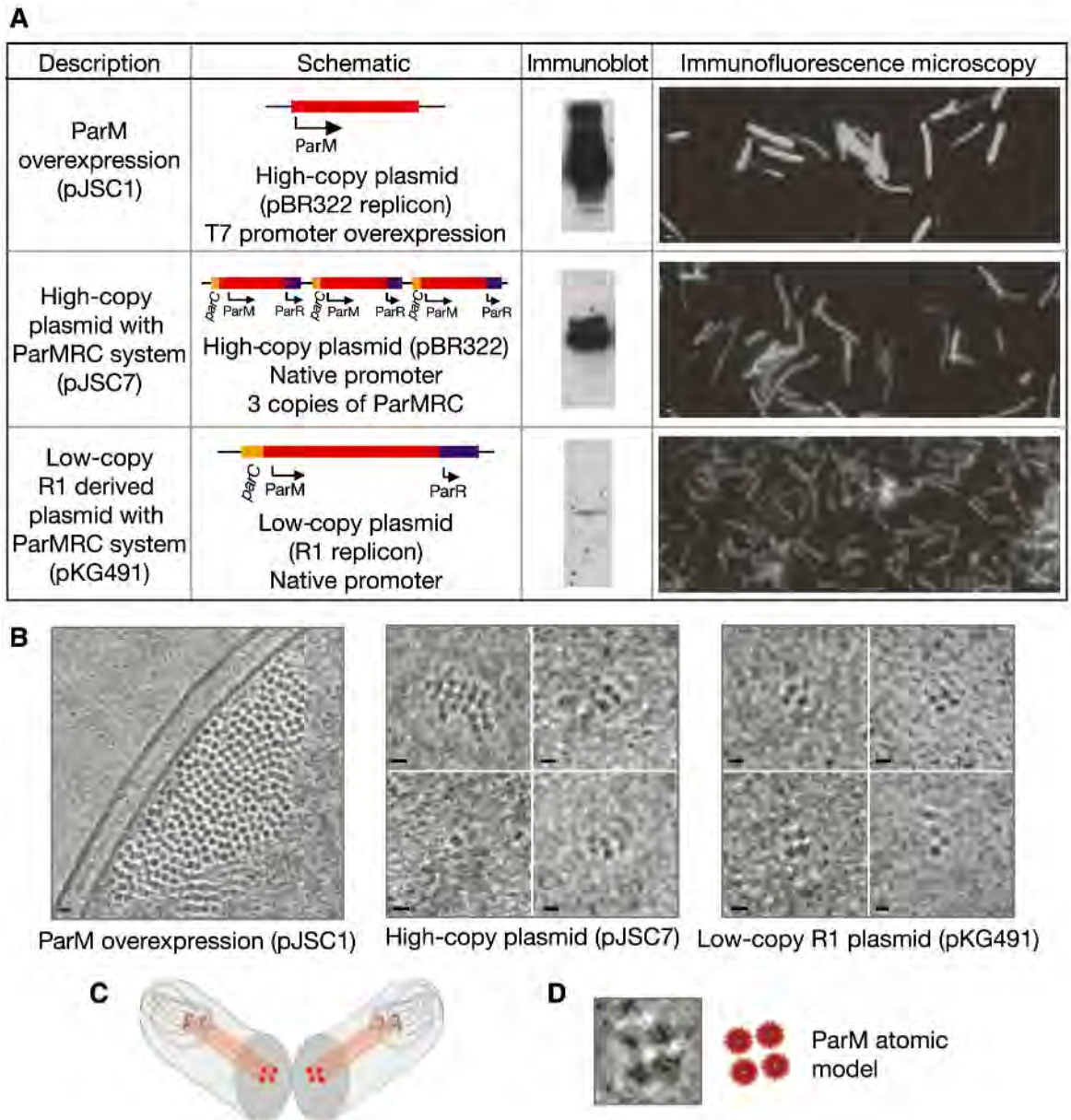
vitro sectioning offers the advantage that subcellular localization can be defined with high precision and that the nucleoid can easily be recognized as a region of low contrast (19).

We found that bundles of ParM filaments segregating the low-copy number R1 derivative were localized near the edge of the bacterial nucleoid (Fig. 3A and fig. S5). Out of seven good images of bundles, five were localized near the edge of the nucleoid, and the nucleoid was absent in the other two sections. This positioning suggests that the plasmids at the ends of the filaments are loosely captured within the nucleoid DNA region, and this gives the first high-resolution insight into intracellular plasmid localization (Fig. 3D). The prediction that these R1-derived ParM bundles point to plasmid localization within or near the nucleoid is supported by the observation that ParM filaments in cells carrying ParMRC-containing high-copy number plasmids also

cluster both in and around the nucleoid (Fig. 3B and fig. S2, A to C).

Our observations that plasmid-segregating ParM filaments are associated with the nucleoid and the ensuing prediction that plasmids are anchored therein immediately leads us to two further questions. First, where exactly do the ends of ParM filaments and the associated newly segregated plasmids lie in the cell? This relates to the question of how close the nucleoid extends into the poles of a bacterium. With the use of immunofluorescence microscopy, we found that ParM filaments extend close to the poles of the cells (Fig. 3E) in line with earlier experiments (10, 20, 21), but the resolution of these images is limited. The second question relates to the cause and nature of plasmid capture within or near the nucleoid. This association must be only weakly maintained because elongating ParM filaments push plasmids through the cell at a rate of 3.1 $\mu\text{m}/\text{min}$ (9).

Fig. 2. Small bundles of ParM filaments are involved in plasmid-DNA segregation. **(A)** Three different systems used to study ParM filaments in vitreous sections. **(B)** Vitreous cryosections of cells described in (A) showing end-on views of ParM filaments. **(C)** The plane of imaging is perpendicular to the filaments to achieve high contrast and recognize the characteristic packing. **(D)** To-scale atomic interpretation of the ParM bundles observed in (B). Scale bars are 1 μm (A) or 10 nm (B).



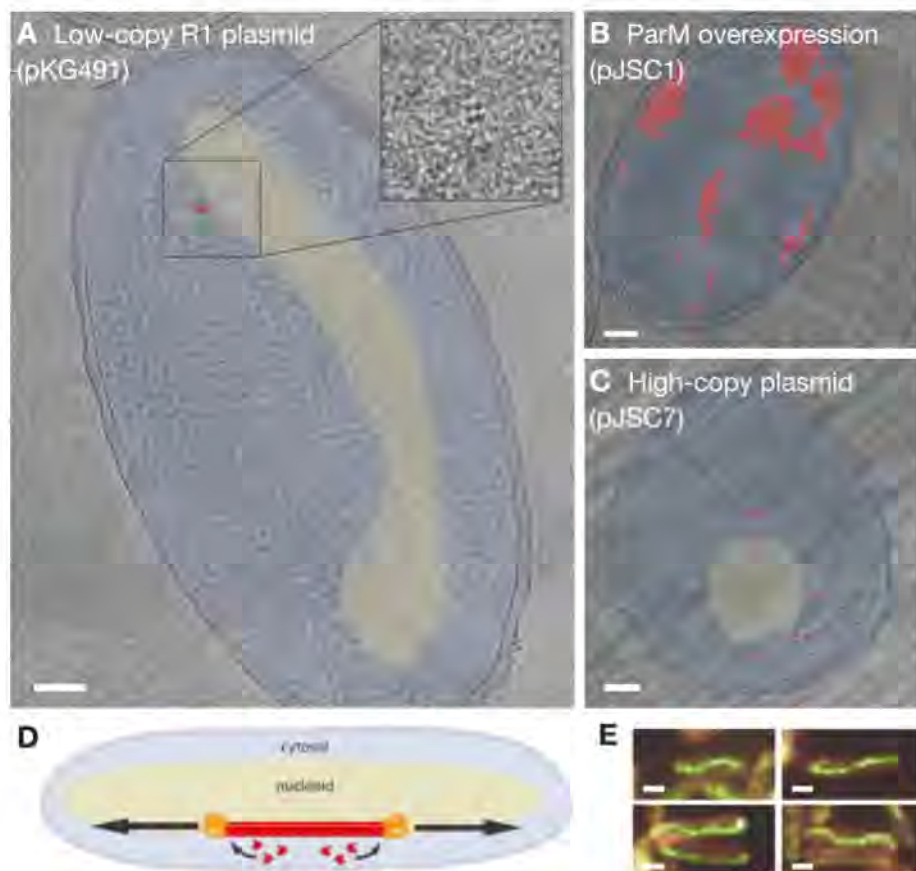


Fig. 3. Bundles of ParM filaments involved in R1 plasmid DNA segregation lie at the periphery of the nucleoid and may indicate plasmid capture therein. **(A to C)** Vitreous cryosections of cells carrying (A) pKG491 (low-copy), (B) pJSC1 (overexpression), and (C) pJSC7 (high-copy) plasmids. Dark blue, cell wall; light blue, cytosol; yellow, nucleoid; red, ParM filaments. Raw images are given in fig. S3, A to G. **(D)** A model for ParM-driven R1 plasmid DNA segregation. **(E)** Immunofluorescence microscopy showing ParM in cells carrying pKG491. ParM, green; membranes, red. Scale bars are 100 nm [(A) to (C)] or 1 μ m (E).

Such plasmid capture within the nucleoid may be achieved through association with host-encoded replication/transcription machinery or by linkage with bacterial condensins (21).

References and Notes

1. K. Gerdes, S. Molin, *J. Mol. Biol.* **190**, 269 (1986).
2. A. Orlova *et al.*, *Nat. Struct. Mol. Biol.* **14**, 921 (2007).
3. D. Popp *et al.*, *EMBO J.* **27**, 570 (2008).

4. F. van den Ent, J. Møller-Jensen, L. A. Amos, K. Gerdes, J. Löwe, *EMBO J.* **21**, 6935 (2002).
5. E. C. Garner, C. S. Campbell, R. D. Mullins, *Science* **306**, 1021 (2004).
6. E. C. Garner, C. S. Campbell, D. B. Weibel, R. D. Mullins, *Science* **315**, 1270 (2007).
7. R. B. Jensen, K. Gerdes, *J. Mol. Biol.* **269**, 505 (1997).
8. J. Salje, J. Löwe, *EMBO J.* **27**, 2230 (2008).
9. C. S. Campbell, R. D. Mullins, *J. Cell Biol.* **179**, 1059 (2007).
10. J. Møller-Jensen *et al.*, *Mol. Cell* **12**, 1477 (2003).
11. J. Møller-Jensen, R. B. Jensen, J. Löwe, K. Gerdes, *EMBO J.* **21**, 3119 (2002).
12. A. Al-Amoudi *et al.*, *EMBO J.* **23**, 3583 (2004).
13. Materials and methods are available as supporting material on Science Online.
14. D. Popp *et al.*, *Biochem. Biophys. Res. Commun.* **353**, 109 (2007).
15. M. Dam, K. Gerdes, *J. Mol. Biol.* **236**, 1289 (1994).
16. K. Nordström, S. Molin, H. Aagaard-Hansen, *Plasmid* **4**, 332 (1980).
17. R. B. Jensen, R. Lurz, K. Gerdes, *Proc. Natl. Acad. Sci. U.S.A.* **95**, 8550 (1998).
18. C. L. Choi, S. A. Claridge, E. C. Garner, A. P. Alivisatos, R. D. Mullins, *J. Biol. Chem.* **283**, 28081 (2008).
19. M. Eltsöv, B. Zuber, *J. Struct. Biol.* **156**, 246 (2006).
20. G. Ebersbach, D. J. Sherratt, K. Gerdes, *Mol. Microbiol.* **56**, 1430 (2005).
21. T. Weitao, S. Dasgupta, K. Nordström, *Mol. Microbiol.* **38**, 392 (2000).
22. We thank K. Gerdes (Newcastle, UK) and J. Møller-Jensen (Odense, Denmark) for kindly supplying plasmids and strains and W. Kühlbrandt and D. Mills (Frankfurt, Germany) for generously allowing us the use of their microscope. J.S. is supported by MRC and Leverhulme Trust studentships, and B.Z. is supported by a European Molecular Biology Organization long-term fellowship. J.S. performed all experiments and their analysis except the initial cryo-sectioning that was done with B.Z.

Supporting Online Material

www.sciencemag.org/cgi/content/full/1164346/DC1

Materials and Methods

Figs. S1 to S5

References

7 August 2008; accepted 24 November 2008

Published online 18 December 2008;

10.1126/science.1164346

Include this information when citing this paper.

Alternative Zippering as an On-Off Switch for SNARE-Mediated Fusion

Claudio G. Giraudo,^{1,†} Alejandro Garcia-Diaz,^{1,†} William S. Eng,^{1,2} Yuhang Chen,² Wayne A. Hendrickson,² Thomas J. Melia,^{1,†} James E. Rothman^{1,†}

Membrane fusion between vesicles and target membranes involves the zippering of a four-helix bundle generated by constituent helices derived from target- and vesicle-soluble *N*-ethylmaleimide-sensitive factor attachment protein receptors (SNAREs). In neurons, the protein complex clamps otherwise spontaneous fusion by SNARE proteins, allowing neurotransmitters and other mediators to be secreted when and where they are needed as this clamp is released. The membrane-proximal accessory helix of complexin is necessary for clamping, but its mechanism of action is unknown. Here, we present experiments using a reconstituted fusion system that suggest a simple model in which the complexin accessory helix forms an alternative four-helix bundle with the target-SNARE near the membrane, preventing the vesicle-SNARE from completing its zippering.

Intracellular membrane fusion is catalyzed by the assembly of SNARE complexes between membranes, forcing their bilayers together

(1, 2). Because SNARE complex assembly is strongly favored energetically (3), fusion will occur spontaneously in the absence of additional

proteins that may be provided to prevent this from happening. However, in synaptic transmission and hormone release, fusion does not occur until calcium enters the presynaptic cytoplasm when the action potential terminates at the nerve ending. Although synaptic vesicles are primed and ready with their SNAREs largely zippered (4), they are unable to complete fusion without calcium (5–7). Complexin (CPX) can function as a clamp (8) by binding the helical bundle of

¹Department of Physiology and Cellular Biophysics, Columbia University, College of Physicians and Surgeons, 1150 Saint Nicholas Avenue, Russ Berrie Building, Room 520, New York, NY 10032, USA. ²Department of Biochemistry and Molecular Biophysics, Columbia University, and Howard Hughes Medical Institute, New York, NY 10032, USA.

*To whom correspondence should be addressed. E-mail: james.rothman@yale.edu (J.E.R.); claudio.giraudo@yale.edu (C.G.G.)

†Present address: Department of Cell Biology, School of Medicine, Yale University, 333 Cedar Street, New Haven, CT 06520, USA.

SNAREs, which mediates neurotransmitter release (and related forms of exocytosis) (9–11), at a late stage of zippering but before fusion is completed (12). This, in turn, enables the primary calcium sensor for synaptic transmission, synaptotagmin [SYT (13–15)], to release the clamp and activate fusion when calcium appears (12).

How, at a molecular level, does CPX clamp SNARE proteins? CPX binds the cis-SNARE complex [the postfusion, fully assembled, four-helix bundle SNARE complex (16)] by a helical region near the middle of the CPX polypeptide chain (9, 10). This helix consists of distinct although contiguous domains (Fig. 1A) termed the central helix (residues 48 to 70 in the human sequence) and the accessory helix (residues 26 to 47). The central helix lies along the interface between the vesicle- (v-) and target- (t-) SNARE, making numerous contacts with both and positioning CPX about halfway along the bundle. The accessory helix (in the postfusion state) continues away from the bundle toward the membrane and is well defined in the crystal structure even though it lacks contacts with the SNARE proteins (9, 10). The location of the accessory helix before fusion is not known because of the lack of a structure of CPX with a trans-SNARE complex; however, it has been found to be required for clamping in vitro and in vivo (17–19) even though it is dispensable for CPX binding to the cis-SNARE complex (9, 11).

The arrangement of the accessory helix in the postfusion state suggests the simple idea that it might function as an on-off switch for fusion. In the on state (cis-SNARE complex) the accessory helix sticks out, and the membrane proximal region of the bundle zippers fully. And (hypothetically) in the off state (trans-SNARE complex) the accessory helix could potentially interact with the membrane-proximal region of the SNAREs to prevent them from zippering. To act as a clamp, the off state would have to be of lower energy in the context of all reactants. Fusion would be triggered from this state when the accessory helix is switched out by activators like SYT.

A clue came from the similarity of the sequence of the accessory helix of CPX to that of the membrane-proximal region of VAMP2 that is only evident when the sequence of the accessory helix is read backward, reflecting the overall antiparallel physical orientation of the accessory helix to the SNARE bundle (Fig. 1A). Certain key residues within the SNARE motif of VAMP2 [hydrophobic layer +3, +4, +7, K84, D63, and D64 (20)] were also found in the accessory helix of CPX-I when read backward (Fig. 1A). These residues are among the most conserved in all CPXs, and this pattern is not seen in attempted alignments of the inverted accessory helix with either syntaxins or soluble N-ethylmaleimide-sensitive factor attachment protein 25 (SNAP-25). Although weak, this homology made predictions confirmed in this work, all of which improved function of the clamp and which derive their strength from the fact that there are many

ways to cripple a protein but few ways to improve it.

The similarity between the accessory helix and VAMP2 suggested that the accessory helix assembles locally with the three-helix t-SNARE as an alternative partner to the v-SNARE VAMP2, forming an alternative nonfusogenic four-helix bundle and thereby clamping fusion. The other possible model, that the accessory helix binds up the v-SNARE, can be ruled out because VAMP remains accessible in the clamped state to a pro-

teolytic toxin [botulinum neurotoxin-B (BoNTB)], which recognizes and cleaves in this same region (4, 12).

Our hypothesis for the mechanism of action of the accessory helix in clamping makes several strong predictions: First, peptides from the aligning region of VAMP2 should functionally compete with CPX and prevent clamping. Second, mutations that “add back” the key hydrophobic residues in the sequence of VAMP2 to the CPX accessory helix should improve clamping, result-

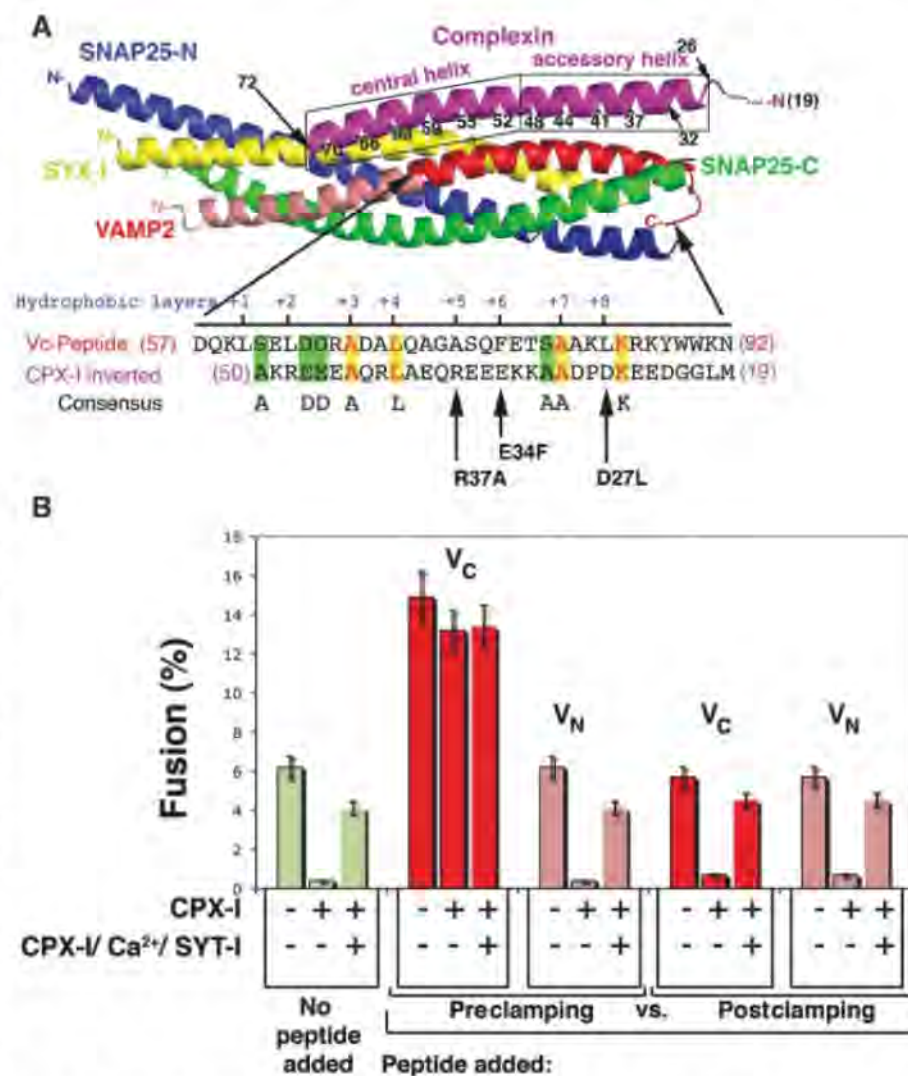


Fig. 1. CPX-I clamping mechanism. (A) (Top) Cartoon of the three-dimensional (3-D) structure of the CPX-SNARE complex (9). Actual structure of CPX-I spans from residues 32 to 72. CPX-I region 26 to 32 was modeled as an α helix according to secondary structure predictions. (Bottom) Amino acid sequence (20) alignment of the membrane proximal half of the VAMP2 SNARE motif and the inverted sequence of the accessory α -helical region highlighting identical residues in yellow, conserved residues in light blue, and similar residues in green. The hydrophobic layers are also indicated in blue. Arrows point to the missing hydrophobic layer on CPX-I sequence and the corresponding site-directed mutation performed. (B) Vc peptide but not Vn peptide competes with CPX-I-GPI. v-SNARE cells transfected with yellow fluorescent protein (YFP)-nuclear localization signal (nls) and CPX-I-GPI; YFP-nls, CPX-I-GPI, and SYT-I; or YFP-nls alone (control) were used for fusion experiments. We added 30 μ M of Vc peptide or Vn peptide to the reaction before the commencement of the reaction (preclamped) or added only during the fusion recovery with SYT-I and Ca (postclamped), and their corresponding effect was measured as a percentage of fusion. Results are mean \pm SEM of three independent experiments.

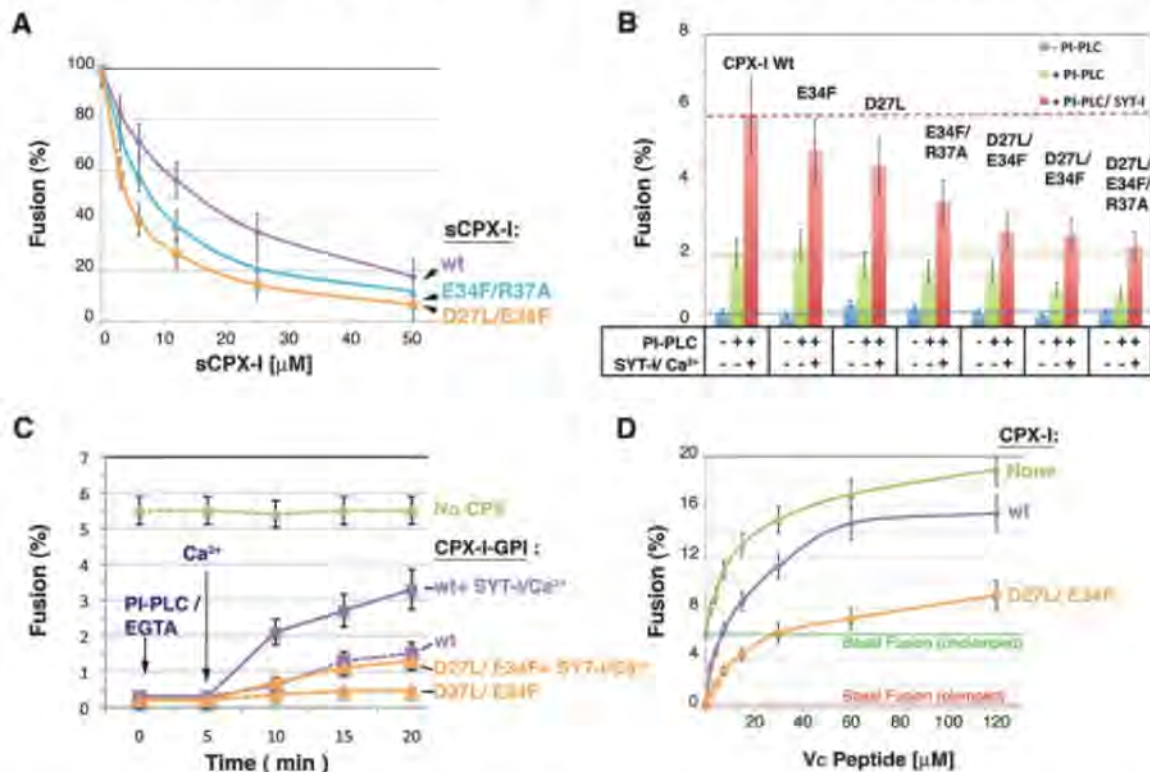
ing in “superclamp” CPXs that are more poorly released by Ca ion and SYT. Third, superclamp CPXs should compete better with the v-SNARE peptides than wild-type CPX. Fourth, CPXs harboring mutations in the accessory helix should be

found that bind to SNARE complexes but do not clamp, and these should dominantly interfere with clamping by CPXs.

To test the first prediction, we performed fusion experiments involving cells bearing

“flipped” exocytic or synaptic v- or t-SNAREs on their surfaces (21). Peptides coding for the N- or C-terminal half of the SNARE motif (helical region) of VAMP2 (Vn peptide and Vc peptide, respectively) were added to the flipped-SNARE

Fig. 2. Mutations on CPX-I designed to mimic hydrophobic layers on VAMP2 stabilize the clamp. **(A)** Dose-dependent inhibition of the cell fusion reaction using different sCPX-I mutants. Increasing concentration of each recombinant sCPX were added at the time the two cell populations were mixed. Cells were allowed to fuse overnight, and the fusion efficiency was determined as the percentage of fusion. Results are mean \pm SEM of three independent experiments. **(B)** Effect of different cell surface-expressed super-clamp CPX-I-GPI mutants on cell fusion (blue bars) and on the cell fusion recovery after addition of PI-PLC in the absence (green bars) or presence (red bars) of SYT-I and calcium. Experiments are the mean \pm SEM of three independent experiments. Dashed lines show the maximum cell fusion recovery in the absence (green) or presence (red) of Ca and SYT-I and the total overnight clamping (blue). **(C)** The SYT-I requirement of CPX-I^{D27L/E34F}-GPI was tested by performing a cell fusion experiment as described in Fig. 2B. In this case, the cell fusion recovery was carried out at 200 μ M free Ca²⁺, and samples were fixed at the indicated time every 5 min. The amount of fusion was determined as percentage of transfected v-cells that fused. Results are mean \pm



SEM of three independent experiments. **(D)** Differential Vc peptide sensitivity of CPX-I superclamp mutant constructs. Increasing concentrations of Vc peptide were added at the time the two cell populations were mixed. Cells were allowed to fuse overnight, and the fusion efficiency was determined as the percentage of fusion. Dashed lines correspond to the basal amount of overnight fusion in the absence of CPX-I (green) or in the presence of CPX-I (red). Results are mean \pm SEM of three independent experiments

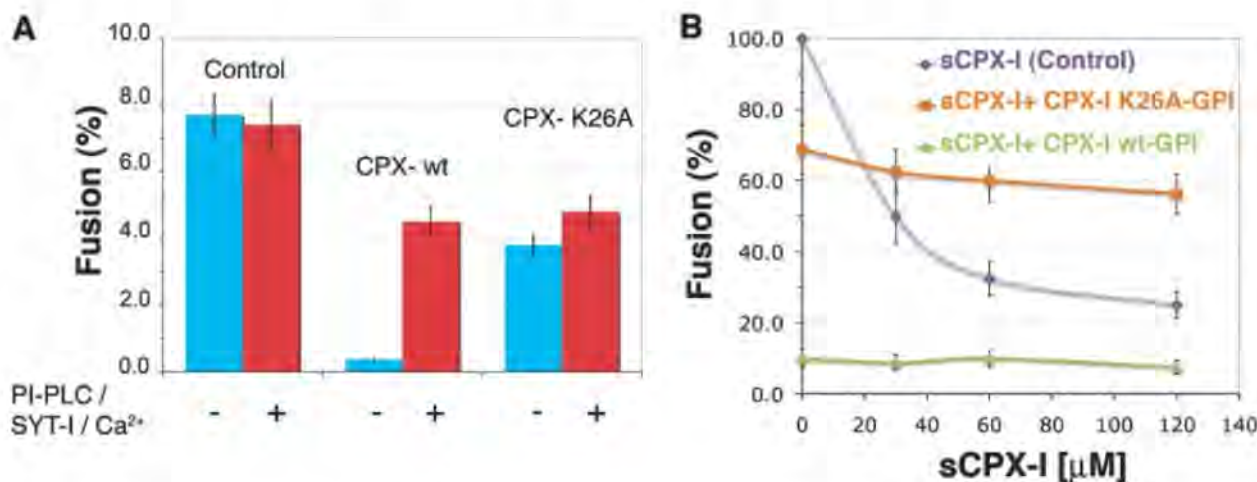


Fig. 3. Clamping role of the conserved amino acid, K26, in the accessory helix of CPX-I. **(A)** Effect of CPX-I^{K26A}-GPI mutant construct on cell fusion (blue) and on the efficiency of cell fusion recovery after addition of PI-PLC in the presence of SYT-I and calcium (red). **(B)** Dose-dependent

inhibition of the cell fusion reaction using ssCPX-I and flipped-SNARE expressing cells co-transfected with the indicated CPX-I-GPI mutant construct or mock-transfected (control). Experiments are the mean \pm SEM of three independent experiments.

cell fusion reaction before the commencement of the reaction (preclamping) or only during the fusion recovery by phosphatidylinositol-phospholipase C (PI-PLC) and SYT-I or Ca (post-clamping), and their corresponding effects were measured as the percentage of CPX-I-expressing cells that fused. Vc peptide forms a stable complex with t-SNARE by binding to the same region of t-SNARE as the corresponding region of VAMP2 because Vc and V_N peptides can simultaneously bind to t-SNARE (22). For liposome-liposome fusion, the Vc peptide (but not V_N peptide) binding preassembles the otherwise poorly stable membrane-proximal region of the t-SNARE and therefore increases the extent of fusion when added to reactions without CPX-I (2, 22). This same effect was observed with cell fusion mediated by flipped SNAREs (21, 23). When Vc peptide was added simultaneously with CPX-I at the beginning of the fusion reaction (preclamping, Fig. 1B), fusion was dramatically stimulated and became almost completely resistant to the CPX-I clamping effect. V_N peptide was without effect. When the Vc peptide was added only after cells were allowed to interact (postclamping), clamping was not reversed.

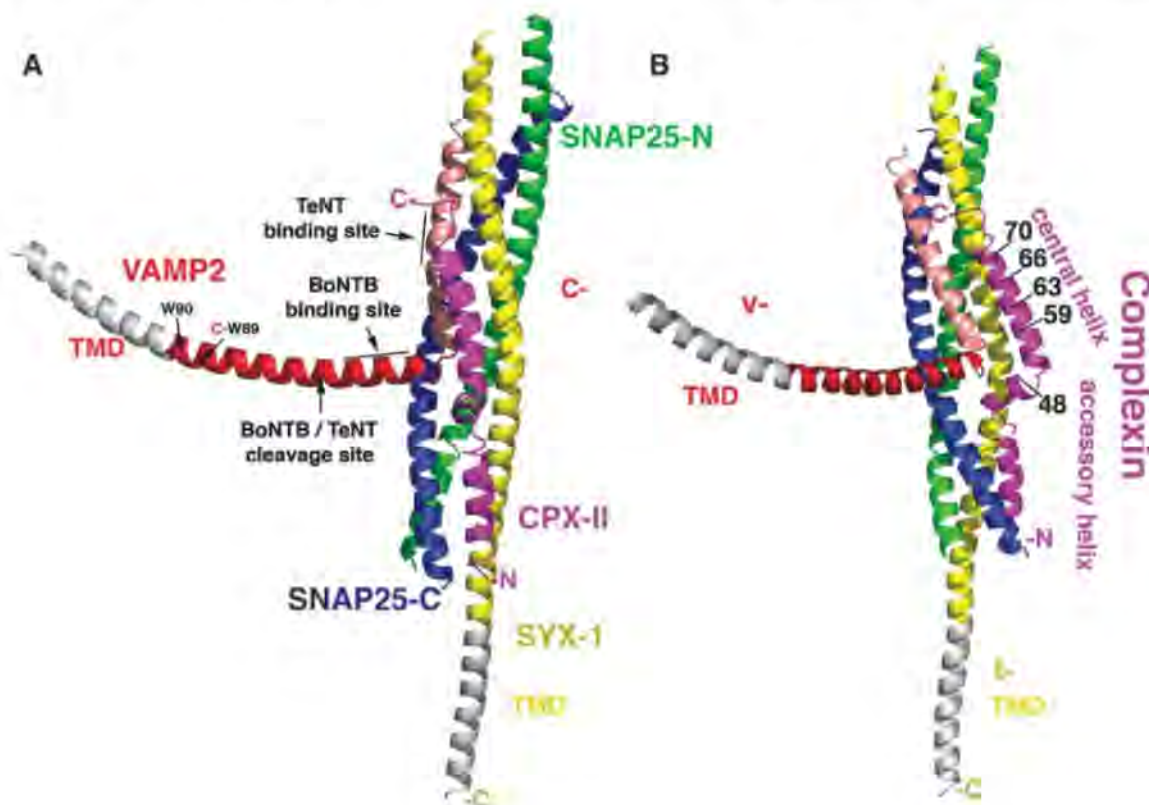
To test the second prediction, increased affinity of the CPX-I mutants for the t-SNARE complex, we introduced the missing hydrophobic layers on CPX-I by mutating the following residues: R37→A37 [R37A (20)] (layer +5), E34F (layer +6), and D27L (layer +8), alone or in combination. As predicted, each mutant super-clamp CPX clamped better as a soluble protein than wild type (Fig. 2A) with median inhibitory concentrations of 7, 9, and 17 μM, respectively, for soluble (s)CPX^{E34F/R37A}, sCPX^{D27L/E34F}, and wild type. We also tested the clamping ability of these and other designed superclamps when expressed as glycosylphosphatidylinositol (GPI)-anchored proteins on the surface of v-SNARE-expressing cells. Each of the mutants tested clamped the fusion reaction completely (as does wild-type CPX) (Fig. 2B). The superclamp CPXs were also poorly and differentially activated by SYT and calcium (Fig. 2C) but in every case was activated with the same calcium kinetics as wild-type CPX-I (fig. S1), indicating that the superclamping effect is due to a stronger SNARE-superclamp CPX-I interaction rather than a failure to interact with its calcium and SYT-I.

To test the third prediction, we performed titrations of Vc peptide on fusion assays clamped by CPX-I^{WT}-GPI or CPX-I^{D27L/E34F}-GPI or not clamped. The Vc peptide competed with the clamp in all cases (Fig. 3D), and clamping by the super-clamp CPX-I^{D27L/E34F}-GPI was more resistant to Vc peptide than to wild type.

Lastly, we tested the fourth prediction, dominant interference. The residues conserved among different CPX isoforms were identified and systematically and individually replaced by alanine or by serine when alanine was present (fig. S2). Mutation K26A produced a severe reduction in the clamping efficiency of CPX-I-GPI (Fig. 3A). Mutation A44S, which eliminated one of the conserved hydrophobic layer on CPX-I, partially inhibited the clamping activity (fig. S2C). The decrease in clamping activity of the CPX-I^{K26A}-GPI and CPX-I^{A44S}-GPI was not due to a lower binding affinity for cis-SNARE complexes (fig. S3). As predicted, CPX-I^{K26A}-GPI prevented clamping by soluble wild-type CPX-I (Fig. 3B).

This dominant-interfering mutant confirms the independent roles of the central helix (binding) and accessory helix (clamping). But, these

Fig. 4. (A and B) Model of the proposed mechanism of clamping of an exocytic SNAREpin by complexin, showing a hypothetical alternative 3D structure of the clamped state. The 3D structure of the CPX-cis-SNARE complex (9) was modified in accord with superclamping mutations analyzed in this study. The color code used to label each protein is as follows: CPX, magenta; VAMP2 V_C, red; VAMP2 V_N, pink; syntaxin1, yellow; SNAP25 N-terminal helix, green; and SNAP25 C-terminal helix, blue. Membrane anchors are shown as hypothetical helices (gray). The C-terminal end of VAMP2 was displaced from the CPX-cis-SNARE structure to accommodate the CPX accessory helix (residues 26 to 42), which was docked by superimposing CPX Cα positions 34 to 42 in inverted direction onto VAMP2 Cα positions 69 to 77. The clamped CPX linker segment (residues 43 to 52) was built using the Lego-loop feature and regularization in program O (25). To allow for this clamped CPX docking, we kinked the membrane-proximal segment of the VAMP2 helix (residues 60 to 85) away from the t-SNARE three-helix bundle after residue 58 by superimposing both this segment and the remaining N-terminal segment onto the AB helix juncture of lamprey hemoglobin [Protein Data Bank (PDB) code



2lhb]. Precise positioning of the C-terminal portion of VAMP2 (i.e., Vc) is arbitrary. The central and accessory helices of CPX-I and the residues involved in the binding with the SNAREs are labeled. The different recognition/binding regions for BoNTB (residues 62 to 71) and tetanus toxin (TeNT, 38 to 47) on VAMP2 are indicated as well as their common cleavage site [residue Q76 (20)], showing the accessibility of BoNTB but not of TeNT (12).

roles are also synergistic because the binding of CPX by its central helix strategically positions the accessory helix for clamping. The central helix binds to residues in both the v- and t-SNARE motifs present in the central and membrane-distal portions of the SNARE bundle (9, 10), ensuring that CPX can only begin to interfere with SNARE assembly after the SNAREpin has zippered at least halfway. The accessory helix then binds weakly and therefore reversibly to sequences in the membrane-proximal portion of the t-SNARE, ideal for a toggle switch.

We present a highly constrained but still speculative molecular model (Fig. 4) for the clamped state [details are in (24)] that establishes the structural feasibility of the proposed clamped state. The displaced sequences of VAMP2 include both the cleavage site and the protein recognition sequence for cleavage of VAMP2 by BoNTB toxin, which can still act on VAMP2 in the clamped state (4, 12), but the recognition sequence for tetanus toxin is assembled into the four-helix bundle in the model, explaining why the CPX-clamped intermediate was found to be resistant to this toxin. We note that, in addition to

its role as clamp, CPX is also positively required for fusion in an earlier step that requires the central helix and the N-terminal domain of 26 residues, but not the accessory helix (19). Ultimately, high-resolution structural studies will be needed to confirm the general outline of this model and provide intimate details, although the need for membrane insertion currently prevents this, necessitating less direct but, we believe, still forceful alternative approaches to central mechanistic problems in the control of membrane fusion.

References and Notes

1. T. Sollner et al., *Nature* **362**, 318 (1993).
2. T. Weber et al., *Cell* **92**, 759 (1998).
3. F. Li et al., *Nat. Struct. Mol. Biol.* **14**, 890 (2007).
4. S. Y. Hua, M. P. Charlton, *Nat. Neurosci.* **2**, 1078 (1999).
5. S. M. Wojcik, N. Brose, *Neuron* **55**, 11 (2007).
6. T. W. Koh, H. J. Bellen, *Trends Neurosci.* **26**, 413 (2003).
7. T. C. Südhof, *Annu. Rev. Neurosci.* **27**, 509 (2004).
8. J. Tang et al., *Cell* **126**, 1175 (2006).
9. X. Chen et al., *Neuron* **33**, 397 (2002).
10. A. Bracher, J. Kadlec, H. Betz, W. Weissenhorn, *J. Biol. Chem.* **277**, 26517 (2002).
11. S. Pabst et al., *J. Biol. Chem.* **275**, 19808 (2000).
12. C. G. Giraudo, W. S. Eng, T. J. Melia, J. E. Rothman, *Science* **313**, 676 (2006); published online 22 June 2006 (10.1126/science.1129450).

13. T. C. Südhof, *Nature* **375**, 645 (1995).
14. M. Geppert et al., *Cell* **79**, 717 (1994).
15. C. Li et al., *Nature* **375**, 594 (1995).
16. R. B. Sutton, D. Fasshauer, R. Jahn, A. T. Brunger, *Nature* **395**, 347 (1998).
17. M. Xue et al., *Nat. Struct. Mol. Biol.* **14**, 949 (2007).
18. C. G. Giraudo et al., *J. Biol. Chem.* **283**, 21211 (2008).
19. A. Maximov, J. Tang, X. Yang, Z. P. Pang, T. C. Südhof, *Science* **323**, 516 (2009).
20. Single-letter abbreviations for the amino acid residues are as follows: A, Ala; C, Cys; D, Asp; E, Glu; F, Phe; G, Gly; H, His; I, Ile; K, Lys; L, Leu; M, Met; N, Asn; P, Pro; Q, Gln; R, Arg; S, Ser; T, Thr; V, Val; W, Trp; and Y, Tyr.
21. C. Hu et al., *Science* **300**, 1745 (2003).
22. T. J. Melia et al., *J. Cell Biol.* **158**, 929 (2002).
23. C. G. Giraudo et al., *J. Cell Biol.* **170**, 249 (2005).
24. Materials and methods are available as supporting material on Science Online.
25. A. Jones, O. version 12.0 (2008), <http://xray.bm.bu.se/~alwyn/index.html>
26. This work was supported by an NIH grant to J.E.R.

Supporting Online Material

www.sciencemag.org/cgi/content/full/323/5913/512/DC1
Materials and Methods
Figs. S1 to S3
References

29 September 2008; accepted 5 December 2008
10.1126/science.1166500

Complexin Controls the Force Transfer from SNARE Complexes to Membranes in Fusion

Anton Maximov,^{1*} Jiong Tang,^{1†} Xiaofei Yang,^{1,2} Zhiping P. Pang,^{1,2} Thomas C. Südhof^{1,2,3,4,5,‡}

Trans-SNAP receptor (SNARE, where SNAP is defined as soluble NSF attachment protein, and NSF is defined as *N*-ethylmaleimide-sensitive factor) complexes catalyze synaptic vesicle fusion and bind complexin, but the function of complexin binding to SNARE complexes remains unclear. Here we show that in neuronal synapses, complexin simultaneously suppressed spontaneous fusion and activated fast calcium ion-evoked fusion. The dual function of complexin required SNARE binding and also involved distinct amino-terminal sequences of complexin that localize to the point where trans-SNARE complexes insert into the fusing membranes, suggesting that complexin controls the force that trans-SNARE complexes apply onto the fusing membranes. Consistent with this hypothesis, a mutation in the membrane insertion sequence of the v-SNARE synaptobrevin/vesicle-associated membrane protein (VAMP) phenocopied the complexin loss-of-function state without impairing complexin binding to SNARE complexes. Thus, complexin probably activates and clamps the force transfer from assembled trans-SNARE complexes onto fusing membranes.

Synaptic vesicle fusion is driven by assembly of trans-SNAP receptor (SNARE, where SNAP is defined as soluble NSF attachment protein, and NSF is defined as *N*-ethylmaleimide-sensitive factor) complexes (or SNAREpins) from syntaxin-1 and SNAP-25 on the plasma membrane and synaptobrevin/vesicle-associated membrane protein (VAMP) on the vesicle membrane (1–3). Ca²⁺ then triggers fast synchronous synaptic vesicle fusion by binding to the Ca²⁺-sensor synaptotagmin (4–6). Besides SNARE proteins and synaptotagmin, fast Ca²⁺-triggered fusion requires complexin (7). Complexin is composed of short N- and C-terminal sequences and two central α

helices. Complexin binds to SNARE complexes via its central α helix, which inserts in an antiparallel orientation into a groove formed by synaptobrevin/VAMP and syntaxin-1 (8, 9). Although multiple approaches have revealed an essential role of complexin in synaptic fusion (7, 10–15), the nature of this role remains unclear. In vertebrate autapses, the deletion of complexin selectively impairs fast synchronous neurotransmitter release without changing asynchronous or spontaneous release (7, 10). Conversely, in *in vitro* fusion assays, the addition of complexin causes a general block of SNARE-dependent fusion, indicating that complexin is a SNARE clamp

(11–14). In *Drosophila* neuromuscular synapses, the deletion of complexin produces a >20-fold increase in spontaneous release but only a small decrease in evoked release (15). Thus, the role of complexin in fusion is unclear. Moreover, even the importance of complexin SNARE-complex binding remains uncertain (16, 17). We addressed these questions with two complementary approaches: (i) RNA interference-mediated knockdown of complexin with rescue and (ii) replacing wild-type (WT) synaptobrevin with specific mutants using synaptobrevin knockout (KO) mice (18).

We knocked down complexin expression in cultured cortical neurons with the use of a short hairpin RNA (shRNA) that targets both complexin-1 and -2, the only complexin isoforms detectably expressed in these neurons (19). For this purpose, we used lentiviruses that simultaneously synthesize the complexin shRNA and either green fluorescent protein (GFP), WT complexin-1, or 4M-mutant complexin-1 that is unable to bind to SNARE complexes because it contains four amino acid substitutions [R48A/R59A/K69A/Y70A; for these substitutions and

¹Department of Neuroscience, University of Texas Southwestern Medical Center, Dallas, TX 75390, USA. ²Department of Cellular and Molecular Physiology, Stanford University, 1050 Arastradero Road, Palo Alto, CA 94304–5543, USA.

³Department of Molecular Genetics, University of Texas Southwestern Medical Center, Dallas TX 75390, USA. ⁴Howard Hughes Medical Institute, University of Texas Southwestern Medical Center, Dallas, TX 75390, USA. ⁵Howard Hughes Medical Institute, Stanford University, Palo Alto, CA 94304–5543, USA.

*Present address: Department of Cell Biology, The Scripps Research Institute, La Jolla, CA 92037, USA.

†Present address: Stanford University, Stanford, CA 94305, USA.

‡To whom correspondence should be addressed. E-mail: tcs1@stanford.edu

the synaptobrevin substitutions described below, amino acids are written in single-letter code (19); for example, R48A signifies the arginine-to-alanine substitution at position 48] (20, 21). Lentivirus expressing GFP without the shRNA served as a further control. This design enabled us to simultaneously analyze control neurons and complexin knock-down neurons expressing either GFP, WT complexin (as a rescue control), or 4M-mutant complexin. The shRNA strongly inhibited the expression of complexin-1 and -2, whereas the expression of other proteins (including SNARE proteins) was unchanged, and synapse numbers were unaltered (figs. S1 and S2).

The complexin knockdown increased by three- to fourfold the frequency of spontane-

ous miniature excitatory postsynaptic currents (mEPSCs), without altering the mEPSC amplitude (Fig. 1A). In contrast, the complexin knockdown decreased by three- to fourfold the amplitude of EPSCs evoked by isolated action potentials (Fig. 1B). Evoked EPSCs could not be restored by increasing the extracellular Ca^{2+} concentration, identifying complexin as a central component of the Ca^{2+} -triggering machinery (fig. S3). Both changes were rescued by WT, but not by 4M-mutant, complexin, confirming the specificity of the shRNA and the importance of SNARE binding. Finally, the complexin knockdown decreased the initial EPSCs during a 10-Hz stimulus train but did not alter the total synaptic charge transfer evoked by the train and even increased

the delayed EPSCs following the train (fig. S4). Thus, the complexin knockdown greatly impaired fast synchronous, but not asynchronous, synaptic vesicle fusion and increased spontaneous fusion, thereby reconciling the divergent phenotypes observed in vertebrate autapses, *Drosophila* neuromuscular junctions, and in vitro fusion assays (7, 10–15).

We next examined which complexin sequences mediate spontaneous and evoked fusion (Fig. 1C). An N-terminal deletion of 40 residues (Cpx^{41–134}) abolished all complexin function (Fig. 1, D and E). This abolishment was not due to an impairment in SNARE-complex binding in competition with synaptotagmin, because a complexin fragment containing only its central α -helical SNARE-binding

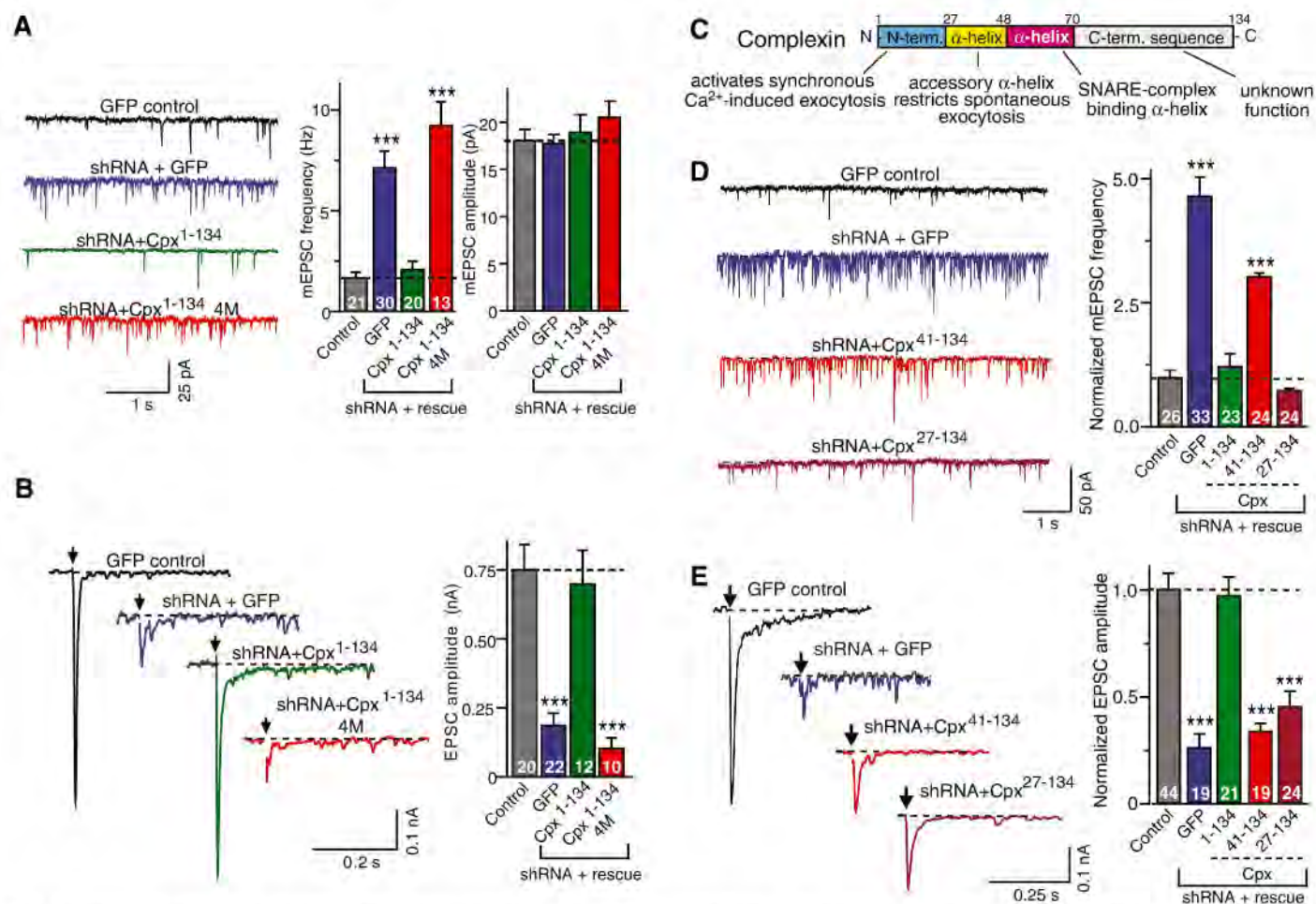


Fig. 1. Complexin knockdown increases spontaneous fusion but suppresses fast Ca^{2+} -evoked fusion. (A) Spontaneous fusion monitored as mEPSCs (left, representative traces; center and right, summary graphs of mEPSC frequencies and amplitudes, respectively). Recordings are from WT mouse neurons infected with lentiviruses expressing GFP only (control) or an shRNA that suppresses both complexin-1 and -2 and additionally expresses either GFP, WT rat complexin-1 (Cpx¹⁻¹³⁴), or mutant rat complexin-1 with inactivated SNARE-binding sites (Cpx¹⁻¹³⁴ 4M). For protein and synapse quantifications, see figs. S1 and S2; for calcium titrations of release, see fig. S3. (B) Ca^{2+} -evoked fusion monitored as EPSCs triggered by isolated action potentials at 0.1 Hz (left, representative traces; right, mean amplitudes). Neurons were infected with lentiviruses as described in (A). For responses elicited by 10-Hz stimulus trains, see fig. S4. (C) Domain structure of

complexin and assignment of domains based on the rescue analysis shown in (D) and (E). (D and E) Complexin sequences required for rescue of the dual complexin loss-of-function phenotype: the increase in mEPSC frequency (D) and the decrease in EPSC amplitudes (E). Left, representative traces; right, summary graphs of mEPSC frequency (D) and EPSC amplitude (E), both normalized to control. Recordings were from mouse neurons infected with a lentiviruses expressing GFP only (control) or the complexin shRNA and either GFP or the indicated rat complexin-1 fragments. Scale bars apply to all traces in a group. Summary graphs depict means \pm SEMs (see table S1 for numerical electrophysiology data). Statistical significance was evaluated by analysis of variance (ANOVA) in comparison to control neurons (triple asterisks denote $P < 0.001$); the total number of analyzed neurons in four to six independent cultures is shown in the bars.

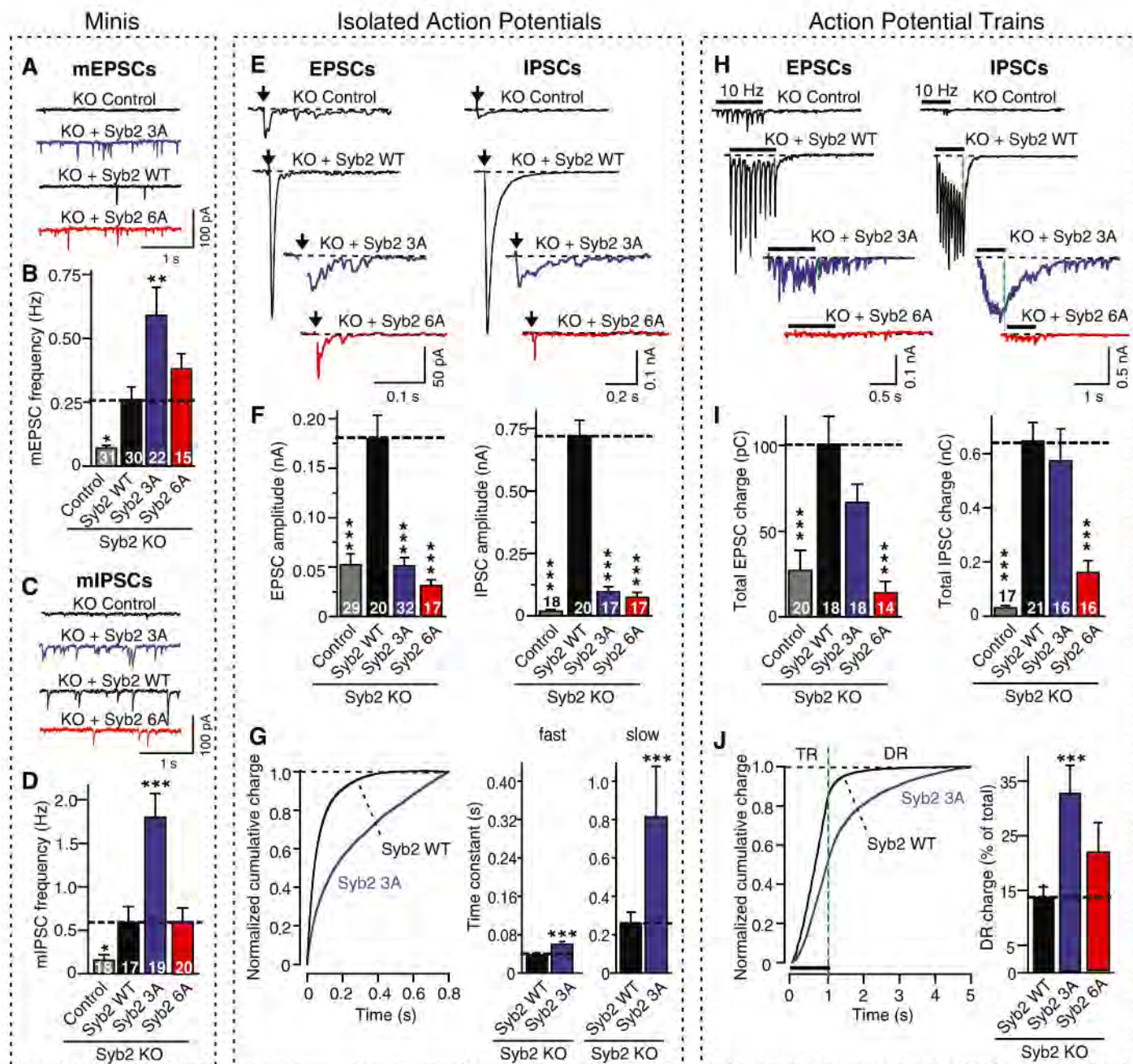


Fig. 2. Blocking complexin-binding to SNARE complexes increases spontaneous fusion but suppresses fast Ca^{2+} -evoked fusion. Synaptobrevin-2 KO neurons were infected with lentiviruses expressing GFP only (control) or WT (Syb2 WT), 3A-mutant (Syb2 3A), or 6A-mutant synaptobrevin-2 (Syb2 6A). The 3A-mutation in synaptobrevin selectively blocks complexin-binding to SNARE complexes, whereas the 6A-mutation additionally impairs SNARE-complex assembly (figs. S6 and S7). (A to D) Representative traces [(A) and (C)] and frequencies [(B) and (D)] of spontaneous mEPSCs [(A) and (B)] and miniature inhibitory postsynaptic currents (mIPSCs) [(C) and (D)]. For mini amplitudes, see fig. S8. (E and F) Representative traces (E) and mean amplitudes (F) of EPSCs (left) and IPSCs (right) evoked by isolated action potentials at 0.1 Hz. (G) Time course of isolated IPSCs monitored in synaptobrevin-2 KO neurons expressing WT (Syb2 WT) or 3A-mutant synaptobrevin-2 (Syb2 3A). The time course was analyzed as the cumulative normalized charge transfer (left) and fitted to a two-exponential equation yielding time constants of fast- and slow-release

phases (right) (see fig. S9 illustrating scaled superimposed IPSC traces). (H and I) Representative traces (H) or mean synaptic charge transfer (I) of EPSCs (left) and IPSCs (right) evoked by 10-Hz action potential trains (see fig. S10 for quantitations of charge transfers). (J) Time course of the cumulative IPSC charge transfer during the 10-Hz stimulus train. (Left) Plots of the cumulative normalized charge transfer allow quantitation of train release (TR) and delayed release (DR; shown only for neurons expressing WT or 3A-mutant synaptobrevin-2). (Right) Bar diagram of the contribution of delayed release to the total synaptic charge transfer in neurons expressing WT (Syb2 WT), 3A-mutant (Syb2 3A), and 6A-mutant synaptobrevin-2 (Syb2 6A). All scale bars apply to all traces in a series, and all bar diagrams depict means \pm SEMs. Statistical significance was evaluated by ANOVA in comparison to WT synaptobrevin-2: Single asterisks denote $P < 0.05$; double asterisks $P < 0.01$; and triple asterisks $P < 0.001$; the total number of analyzed neurons in five to six independent cultures is shown in the summary bars.

sequence (Cpx⁴¹⁻⁸⁶) still bound to SNARE complexes and potentially inhibited synaptotagmin-binding to SNARE complexes (fig. S5). Thus, SNARE-

complex binding in competition with synaptotagmin is necessary but not sufficient for complexin function, which also requires its N-terminal sequence.

Additional dissection of this N-terminal sequence revealed that the nonstructured N-terminal complexin sequence is essential for activating fast fu-

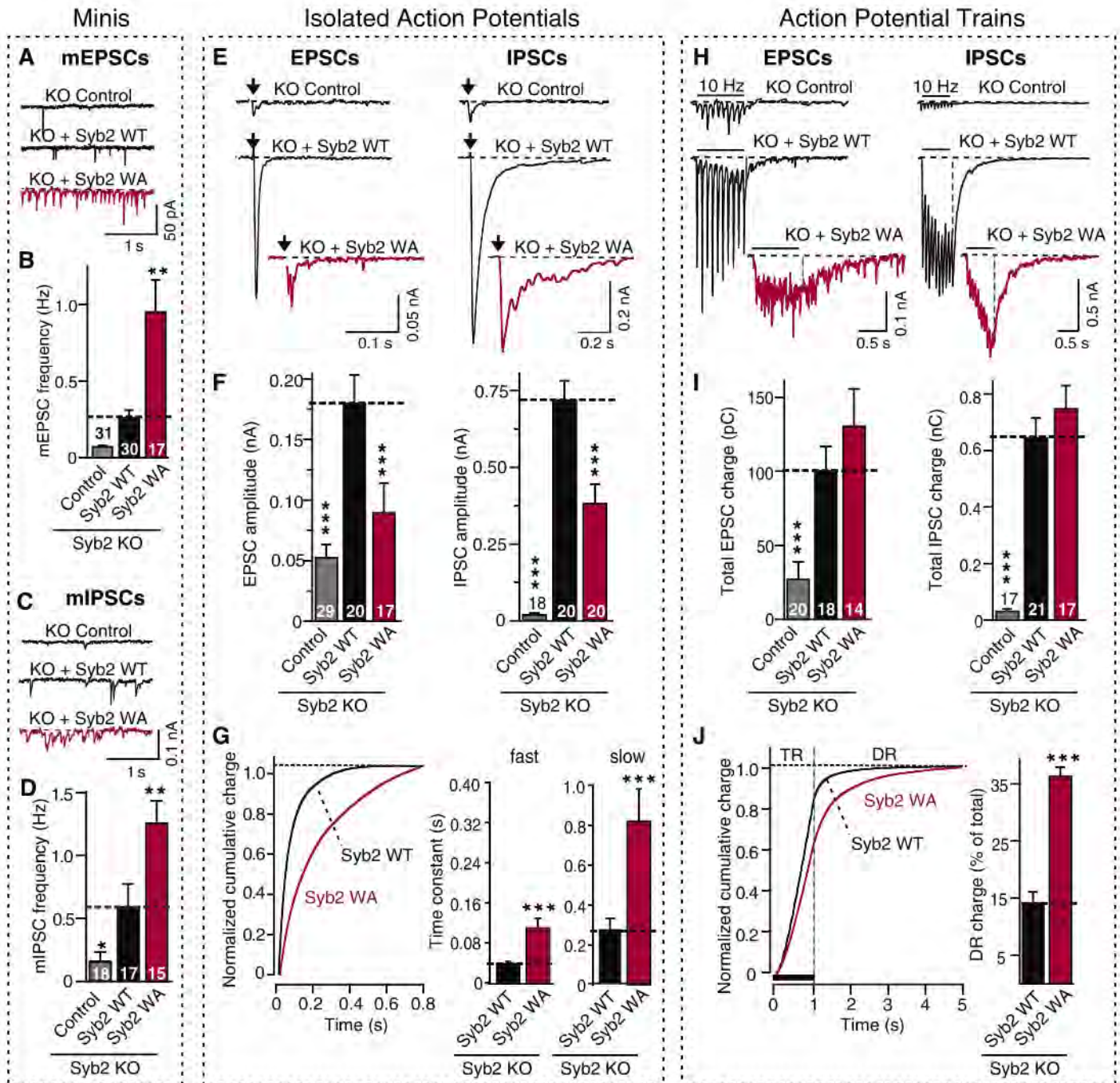


Fig. 3. A mutation in the membrane-insertion sequence of synaptobrevin (WA-mutation) phenocopies the complexin knockdown. Recordings were performed in synaptobrevin-2 KO neurons expressing either GFP only (control), WT (Syb2 WT), or WA-mutant (Syb2 WA; see figs. S6 and S7). (A to D) Representative traces [(A) and (C)] and mean frequencies [(B) and (D)] of spontaneous mEPSCs [(A) and (B)] and mIPSCs [(C) and (D)]. For synaptic targeting of WA-mutant synaptobrevin-2, see fig. S11; for mini amplitudes, see fig. S12. (E and F) Representative traces (E) and mean amplitudes (F) of EPSCs (left) and IPSCs (right) evoked by isolated action potentials at 0.1 Hz. (G) Time course of isolated IPSCs, analyzed as cumulative normalized charge transfer (left) and fitted to a two-exponential equation yielding time constants of fast and slow phases of release (right)

(see fig. S9 for scaled superimposed IPSC traces). (H and I) Representative traces (H) and mean synaptic charge transfer (I) of EPSCs (left) and IPSCs (right) evoked by 10-Hz action potential trains (see fig. S14 for quantifications of charge transfers). (J) Time course of the cumulative IPSC charge transfer during the 10-Hz stimulus train, analyzed as the cumulative normalized charge transfer and illustrated as the fraction of delayed release of the total synaptic charge transfer (right). All scale bars apply to all traces in a series, and all bar diagrams depict means \pm SEMs. Statistical significance was evaluated by ANOVA in comparison to WT synaptobrevin-2: Single asterisks denote $P < 0.05$; double asterisks $P < 0.01$; and triple asterisks $P < 0.001$; the total number of analyzed neurons in five to six independent cultures is shown in the bars in (B), (D), (F), and (I).

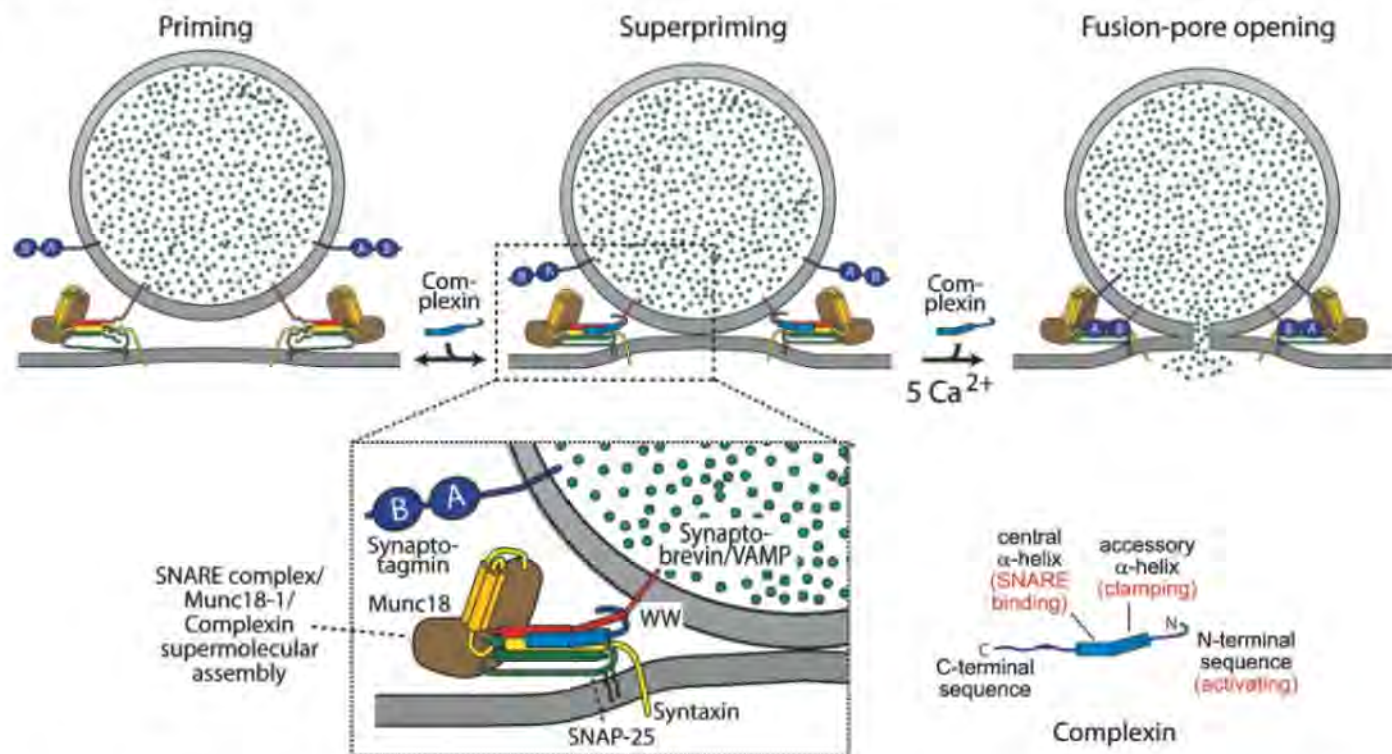


Fig. 4. Complexin action in SNARE-dependent fusion during fusion a vesicle goes through three stages: (i) priming, (ii) superpriming, and (iii) fusion pore opening (**top**). Complexin is proposed to suppress spontaneous fusion by inserting into the assembling trans-SNARE complex and to activate evoked fusion by directly or indirectly interacting with the membrane-insertion sequence of SNARE proteins in the trans-complex (**bottom**). Complexin binding to trans-SNARE complexes

simultaneously stabilizes SNARE complex assembly, blocks completion of assembly, and inhibits the transfer of the force generated by SNARE-complex assembly onto the fusing membranes. Synaptotagmin subsequently triggers fusion by reversing the complexin block on activated SNARE complexes in addition to its Ca^{2+} -dependent phospholipid-binding activity (21). Note that the C-terminal complexin sequence is not shown in the fusion diagrams to simplify the presentation.

sion but not for clamping spontaneous fusion (Fig. 1, D and E), indicating distinct sequence requirements for the dual activating/clamping functions of complexin.

To further analyze complexin function, we used synaptobrevin-deficient neurons that lack both spontaneous and evoked synaptic fusion (18). Expression of WT synaptobrevin rescued the loss of fusion in synaptobrevin-deficient neurons. In contrast, 3A-mutant synaptobrevin that forms SNARE-complexes normally but cannot support complexin binding to these SNARE complexes (figs. S6 and S7) not only rescued spontaneous fusion but increased it more than twofold above WT levels (Fig. 2, A to D). At the same time, 3A-mutant synaptobrevin decreased evoked fusion and decelerated and desynchronized its time course (Fig. 2, E to G, and figs. S8 and S9). Moreover, although fusion elicited by a 10-Hz stimulus train was initially decreased in synapses expressing 3A-mutant synaptobrevin, fusion quickly recovered, such that the total synaptic charge transfer evoked by the stimulus train was normal, and the amount of delayed fusion after the stimulus train was enhanced (Fig. 2, H to J, and fig. S10). A second synaptobrevin mutation (the 6A-mutation) that impaired both SNARE-complex formation and complexin binding to SNARE complexes did not rescue the decrease in evoked release induced by either isolated action poten-

tials or the stimulus train of action potentials (Fig. 2). Thus, the block of complexin binding by the 3A-mutation caused a selective loss of synchronous fast fusion, different from the impairment of all fusion caused by the inhibition of SNARE-complex assembly produced by the 6A-mutation.

The location of the N-terminal sequence of complexin at the point where SNARE complexes insert into the membrane suggests that the N-terminal complexin sequence may control the coupling of SNARE-complex assembly to membrane fusion. If so, complexin may act on SNARE sequences close to the membrane. We tested this hypothesis by mutating the juxta-membranous sequence of synaptobrevin/VAMP in three sets of alanine substitutions: K85A/R86A, R86A/K87A, and W89A/W90A, where W is Trp (referred to as the 85-, 86-, and WA-mutations, respectively) (figs. S6 and S7).

The WA-mutation had no effect on SNARE-complex stability, complexin- or synaptotagmin-binding to SNARE complexes, or synaptobrevin targeting to synapses (figs. S6, S7, and S11), but it caused a two- to threefold increase in mini frequency without a change in mini amplitude (Fig. 3, A to D, and fig. S12). Moreover, the WA-mutation produced an approximately twofold decrease in fast evoked fusion, with the remaining fusion being largely asynchronous because its kinetics were decelerated two- to threefold (fig. 3,

E to G, and fig. S9). Again, as observed for complexin knockdown neurons and neurons expressing 3A-mutant synaptobrevin that lacked complexin binding, synaptic vesicle fusion induced by a 10-Hz stimulus train was only impaired during the initial synchronous responses. Later responses during the train's asynchronous phase were normal, and delayed release was enhanced (Fig. 3, H to J, and fig. S13), thus rendering the WA-mutation a weaker phenocopy of the synaptotagmin-1 KO, the complexin KO, the complexin knockdown, and the synaptobrevin 3A-mutation phenotype (7, 15, 22) (Figs. 1 to 3). In contrast to the WA-mutation, the 85- and 86-mutations did not impair rescue of synaptic transmission by synaptobrevin in synaptobrevin-deficient neurons (fig. S14), thus confirming the specificity of the WA-rescue phenotype.

Here, we have shown that in neuronal synapses, complexin acted both as a clamp and as an activator of SNAREs. These functions required complexin binding to SNARE-complexes and depended on distinct N-terminal complexin sequences that localize to the point where trans-SNARE complexes insert into the two fusing membranes. A mutation in the juxta-membranous sequence of synaptobrevin phenocopies the complexin loss-of-function phenotype. Thus, the simultaneous control of spontaneous and evoked fusion by complexin appears to involve the translation of

the force generated by assembly of trans-SNARE complexes onto the two fusing membranes (Fig. 4), consistent with biochemical data (23). We postulate that after complexin binds to assembling SNARE complexes, its N-terminal sequence activates and clamps the force generated by SNARE-complex assembly. The N terminus of complexin might perform its activator function by pulling the complex closer to the membrane, possibly by binding to phospholipids, whereas the accessory N-terminal α -helix might clamp the complex by inserting into the space between the v- and t-SNAREs or even substituting for one of the SNAREs in the C-terminal segment of the trans-SNARE complex (24). Once anchored on the SNARE complex, the 40 N-terminal residues of complexin both activate and clamp SNARE complexes to control fast Ca^{2+} -triggered neurotransmitter release in a process that is conserved in all animals. Viewed in the broader picture, complexin and synaptotagmin therefore operate as interdependent clamp-activators of SNARE-dependent fusion, with synaptotagmin exploiting the activator effect of complexin and reversing its

clamping function (11, 21, 22). In this molecular pas-de-deux, the functions of both proteins are intimately linked: Their phenotypes are identical both as activators and as clamps, and one does not operate without the other.

References and Notes

1. J. B. Sørensen, *Trends Neurosci.* **28**, 453 (2005).
2. R. Jahn, R. H. Scheller, *Nat. Rev. Mol. Cell Biol.* **7**, 631 (2006).
3. M. Verhage, R. F. Toonen, *Curr. Opin. Cell Biol.* **19**, 402 (2007).
4. M. Geppert et al., *Cell* **79**, 717 (1994).
5. R. Fernandez-Chacon et al., *Nature* **410**, 41 (2001).
6. M. Yoshihara, J. T. Littleton, *Neuron* **36**, 897 (2002).
7. K. Reim et al., *Cell* **104**, 71 (2001).
8. X. Chen et al., *Neuron* **33**, 397 (2002).
9. A. Bracher, J. Kadlec, H. Betz, W. Weissenhorn, *J. Biol. Chem.* **277**, 26517 (2002).
10. M. Xue et al., *Nat. Struct. Mol. Biol.* **14**, 949 (2007).
11. C. G. Giraudo, W. S. Eng, T. J. Melia, J. E. Rothman, *Science* **313**, 676 (2006), published online 22 June 2006; 10.1126/science.1129450.
12. C. G. Giraudo et al., *J. Biol. Chem.* **283**, 21211 (2008).
13. J. R. Schaub, X. Lu, B. Doneske, Y. K. Shin, J. A. McNew, *Nat. Struct. Mol. Biol.* **13**, 748 (2006).
14. T. Y. Yoon et al., *Nat. Struct. Mol. Biol.* **15**, 707 (2008).
15. S. Huntwork, J. T. Littleton, *Nat. Neurosci.* **10**, 1235 (2007).

16. K. Weninger, M. E. Bowen, U. B. Choi, S. Chu, A. T. Brunger, *Structure* **16**, 308 (2008).
17. R. Guan, H. Dai, J. Rizo, *Biochemistry* **47**, 1474 (2008).
18. S. Schoch et al., *Science* **294**, 1117 (2001).
19. Single-letter abbreviations for the amino acid residues are as follows: A, Ala; C, Cys; D, Asp; E, Glu; F, Phe; G, Gly; H, His; I, Ile; K, Lys; L, Leu; M, Met; N, Asn; P, Pro; Q, Gln; R, Arg; S, Ser; T, Thr; V, Val; W, Trp; and Y, Tyr.
20. For a description of the experimental procedures, see the supporting online material.
21. J. Tang et al., *Cell* **126**, 1175 (2006).
22. A. Maximov, T. C. Südhof, *Neuron* **48**, 547 (2005).
23. K. Hu, J. Carroll, C. Rickman, B. Davletov, *J. Biol. Chem.* **277**, 41652 (2002).
24. C. G. Giraudo et al., *Science* **323**, 512 (2009).
25. We thank J. Rizo and L. Chen for advice and critical comments. This study was supported by an investigatorship to T.C.S. from the Howard Hughes Medical Institute.

Supporting Online Material

www.sciencemag.org/cgi/content/full/323/5913/516/DC1
SOM Text
Figs. S1 to S14
Table S1
References

29 September 2008; accepted 5 December 2008
10.1126/science.1166505

Widespread Increase of Tree Mortality Rates in the Western United States

Phillip J. van Mantgem,^{1*} Nathan L. Stephenson,^{1*†} John C. Byrne,² Lori D. Daniels,³ Jerry F. Franklin,⁴ Peter Z. Fulé,⁵ Mark E. Harmon,⁶ Andrew J. Larson,⁴ Jeremy M. Smith,⁷ Alan H. Taylor,⁸ Thomas T. Veblen⁷

Persistent changes in tree mortality rates can alter forest structure, composition, and ecosystem services such as carbon sequestration. Our analyses of longitudinal data from unmanaged old forests in the western United States showed that background (noncatastrophic) mortality rates have increased rapidly in recent decades, with doubling periods ranging from 17 to 29 years among regions. Increases were also pervasive across elevations, tree sizes, dominant genera, and past fire histories. Forest density and basal area declined slightly, which suggests that increasing mortality was not caused by endogenous increases in competition. Because mortality increased in small trees, the overall increase in mortality rates cannot be attributed solely to aging of large trees. Regional warming and consequent increases in water deficits are likely contributors to the increases in tree mortality rates.

A key regulators of global hydrologic and carbon cycles, forests are capable of contributing substantial feedbacks to global changes (1). Such feedbacks may already be under way; for example, forest carbon storage may be responding to environmentally driven changes in global patterns of tree growth and forest productivity (2–4). Recent warming has been implicated as contributing to episodes of forest dieback (pulses of greatly elevated tree mortality), such as those mediated by bark beetle outbreaks in western North America (5, 6). Yet little effort has gone toward determining whether environmental changes are contributing to chronic, long-term changes in tree demographic rates (mortality and recruitment). Changes in demographic rates, when compounded over time, can alter forest structure, composition, and function (7). For

example, a persistent doubling of background mortality rate (such as from 1 to 2% year⁻¹) ultimately would cause a >50% reduction in average tree age in a forest, and hence a potential reduction in average tree size. Additionally, changing demographic rates could indicate forests approaching thresholds for abrupt dieback. Yet spatially extensive analyses of long-term changes in tree demographic rates have been limited to tropical forests, where mortality and recruitment rates both have increased over the past several decades, perhaps in response to rising atmospheric CO₂ concentrations, nutrient deposition, or other environmental changes (2, 8). Comparably extensive analyses have not been conducted in temperate forests.

We sought to determine whether systematic changes in tree demographic rates have occurred

recently in coniferous forests of the western United States, and if so, to identify possible causes of those changes. Although the western United States has witnessed recent episodes of forest dieback related to bark beetle outbreaks or combinations of drought and outbreaks (5, 6), most forested land continues to support seemingly healthy forests that have not died back (9). To minimize transient dynamics associated with stand development and succession, we limited our analyses to data from repeated censuses in undisturbed forest stands more than 200 years old (10). Old forests contain trees of all ages and sizes (11, 12), and any large, persistent changes in demographic rates over a short period (such as a few decades) are likely to be consequences of exogenous environmental changes (2, 13). In contrast, in young forests rapid demographic changes can sometimes result largely from endogenous processes (such as self-thinning during stand development) (14), potentially obscuring environmentally driven changes.

¹U.S. Geological Survey, Western Ecological Research Center, Three Rivers, CA 93271, USA. ²USDA Forest Service, Rocky Mountain Research Station, Moscow, ID 83843, USA. ³Department of Geography, University of British Columbia, Vancouver, British Columbia V6T 1Z2, Canada. ⁴College of Forest Resources, University of Washington, Seattle, WA 98195, USA. ⁵School of Forestry and Ecological Restoration Institute, Northern Arizona University, Flagstaff, AZ 86011, USA. ⁶Department of Forest Science, Oregon State University, Corvallis, OR 97331, USA. ⁷Department of Geography, University of Colorado, Boulder, CO 80309, USA. ⁸Department of Geography, Pennsylvania State University, University Park, PA 16802, USA.

*These authors contributed equally to this work.
†To whom correspondence should be addressed. E-mail: pvanmantgem@usgs.gov (P.J.V.); nstephenson@usgs.gov (N.L.S.)

‡Present address: U.S. Geological Survey, Western Ecological Research Center, Arcata, CA 95521, USA.

Seventy-six long-term forest plots from three broad regions, spanning 14° of latitude and 18° of longitude and at elevations of 130 to 3353 m (Fig. 1 and table S1), met our criteria for analysis (10). Plots ranged from 0.25 to 15.75 ha (\bar{x} = 1.33 ha), collectively containing 58,736 living trees over the study period, of which 11,095 died. The plots were originally established for diverse purposes—such as to investigate different stages of forest development, document dynamics of certain forest types, explore forest dynamics along environmental gradients, or act as controls for silvicultural experiments [see references in (10)]—that are unlikely to produce bias relative to our study's goals. We analyzed data from 1955 and later; only five plots from one region had earlier censuses. For individual plots, the initial census year analyzed ranged from 1955 to 1994 (\bar{x} = 1981); the final census year ranged from 1998 to 2007 (\bar{x} = 2004). Plots were censused three to seven times (\bar{x} = 4.8). Our generally conservative estimates of forest ages at the time of initial censuses averaged ~450 years, with some plots exceeding 1000 years.

We used generalized nonlinear models to regress demographic rates on year; generalized nonlinear mixed models (GNMMs) were used when several plots were analyzed collectively (10). Demographic rates were estimated by annual compounding over the census interval length. All parameters were estimated by maximum likelihood.

Our models showed that mortality rates increased in 87% of plots (Fig. 1) ($P < 0.0001$, two-tailed binomial test). Mortality rate increased significantly for all plots combined and in each of the three regions (Fig. 2 and Table 1), with estimated doubling periods ranging from 17 years (Pacific Northwest) to 29 years (interior). Mortality rates also increased at low, middle, and high elevations (<1000 m, 1000 to 2000 m, and >2000 m, respectively) and for small, medium, and large trees (stem diameter <15 cm, 15 to 40 cm, and >40 cm, respectively) (Fig. 2 and Table 1). The three most abundant tree genera in our plots (comprising 77% of trees) are dominated by different life history traits (*Tsuga*, late successional; *Pinus*, generally shade-intolerant; *Abies*, generally shade-tolerant); all three showed increasing mortality rates (Fig. 2 and Table 1). An introduced fungal pathogen, *Cronartium ribicola*, is known to contribute to increasing mortality rates in five-needled species of *Pinus* (15). When all five-needled *Pinus* were removed from analysis, mortality rates among the remaining *Pinus* (those immune to the pathogen) still increased [$a = 0.027$, $P = 0.0011$, GNMM, $n = 22$, where a is the estimated annual fractional change in mortality rate; see (10)]. Finally, trees belonging to the remaining 16 genera (23% of all trees) collectively showed increasing mortality rates (Fig. 2 and Table 1).

In contrast to mortality rates, recruitment rates increased in only 52% of plots—a proportion indistinguishable from random ($P = 0.80$, two-tailed binomial test). There was no detectable

trend in recruitment for all plots combined, nor when regions were analyzed separately ($P \geq 0.20$, GNMM; table S2).

We examined three classes of possible causes of the increasing tree mortality rates: methodological artifacts, endogenous processes, and exogenous processes. We tested for and ruled out several obvious potential sources of methodological artifacts (10). Among endogenous processes, perhaps the best-known cause of increasing tree mortality rates is increasing competition resulting

from increasing forest density and basal area (11, 12). Such changes might especially be expected in the subset of old forests in the western United States that formerly experienced frequent surface fires; in these forests, fire exclusion (generally spanning the last century) often resulted in an initial increase in forest density and basal area (16, 17). However, consistent with our observations of increasing mortality without compensating increases in recruitment, forest density and basal area declined slightly during the study period

Fig. 1. Locations of the 76 forest plots in the western United States and southwestern British Columbia. Red and blue symbols indicate, respectively, plots with increasing or decreasing mortality rates. Symbol size corresponds to annual fractional change in mortality rate (smallest symbol, $<0.025 \text{ year}^{-1}$; largest symbol, $>0.100 \text{ year}^{-1}$; the three intermediate symbol sizes are scaled in increments of 0.025 year^{-1}). Numerals indicate groups of plots used in analyses by region: (1) Pacific Northwest, (2) California, and (3) interior. Forest cover is shown in green.

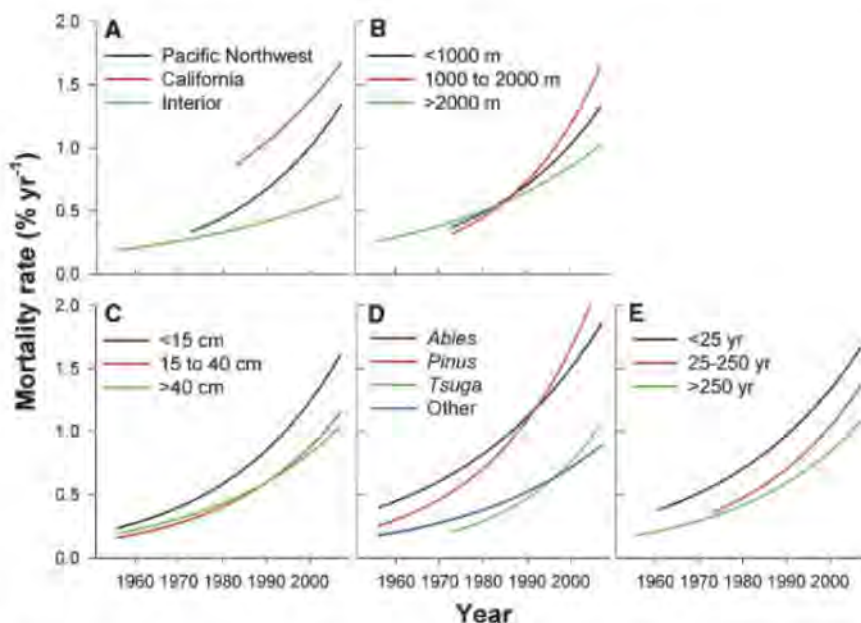


Fig. 2. Modeled trends in tree mortality rates for (A) regions, (B) elevational class, (C) stem diameter class, (D) genus, and (E) historical fire return interval class.

[$P \leq 0.028$, linear mixed model (LMM); fig. S1]. Thus, forest structural changes are consistent with a slight decline rather than an increase in potential for competition over the study period, which suggests that increasing mortality rates cannot be attributed to changes in forest structure.

Fire exclusion conceivably could affect mortality rates through mechanisms unrelated to forest structural changes, such as allowing increases in insects or pathogens that were formerly controlled by fire. We therefore classified plots by their pre-fire exclusion fire return intervals: short, intermediate, and long (<25 years, 25 to 250 years, and >250 years, respectively) (table S1). If fire exclusion ultimately were responsible for increasing tree mortality rates, we would expect to see increases in plots with historically short fire return intervals (which have experienced substantial recent changes in fire regime) and little or no change in mortality rates in plots with historically long return intervals (which have experienced little or no change in fire regime). However, mortality rates showed comparable increases in each of the three classes (Fig. 2 and Table 1); we therefore conclude that fire exclusion is an unlikely cause of the observed increases in mortality rates.

Mortality rates could increase if a cohort of old trees begins to die and fall, crushing smaller trees at an increasing rate [a mechanism related to the proposed "majestic forest" effect; see references in (8)]. If such a mechanism were responsible for the observed increase in tree mortality rates, we would expect to see no parallel increase in mortality rates of small trees that died standing (i.e., trees <15 cm in diameter that died of causes other than being crushed by falling trees from an aging cohort), because such deaths are independent of deaths in an aging cohort. However, the mortality rate of small trees that died standing increased rapidly in recent decades,

doubling in ~16 years ($P < 0.0001$, GNMM; table S3); thus, other mechanisms must be acting. Finally, mortality rates increased in all major genera rather than being limited to those dominated by a particular life history trait (such as shade intolerance), which suggests that successional dynamics are unlikely to be primary drivers of increasing mortality rates.

We conclude that endogenous processes are unlikely to be major contributors to the observed rapid, synchronous doubling of mortality rates in our heterogeneous sample of old forests at a sub-continental scale. Moreover, the available evidence is inconsistent with major roles for two possible exogenous causes: forest fragmentation and air pollution (10).

We suggest that regional warming may be the dominant contributor to the increases in tree mortality rates. From the 1970s to 2006 (the period including the bulk of our data; table S1), the mean annual temperature of the western United States increased at a rate of 0.3° to $0.4^\circ\text{C decade}^{-1}$, even approaching $0.5^\circ\text{C decade}^{-1}$ at the higher elevations typically occupied by forests (18). This regional warming has contributed to widespread hydrologic changes, such as declining fraction of precipitation falling as snow (19), declining snowpack water content (20), earlier spring snowmelt and runoff (21), and a consequent lengthening of the summer drought (22). Specific to our study sites, mean annual precipitation showed no directional trend over the study period ($P = 0.62$, LMM), whereas both mean annual temperature and climatic water deficit (annual evaporative demand that exceeds available water) increased significantly ($P < 0.0001$, LMM) (10). Furthermore, temperature and water deficit were positively correlated with tree mortality rates ($P \leq 0.0066$, GNMM; table S4).

Warming could contribute to increasing mortality rates by (i) increasing water deficits and thus

drought stress on trees, with possible direct and indirect contributions to tree mortality (13, 23); (ii) enhancing the growth and reproduction of insects and pathogens that attack trees (6); or (iii) both. A contribution from warming is consistent with both the apparent role of warming in episodes of recent forest dieback in western North America (5, 6) and the positive correlation between short-term fluctuations in background mortality rates and climatic water deficits observed in California and Colorado (13, 24).

The rapid and pervasive increases in tree mortality rates in old forests of the western United States are notable for several reasons. First, increasing mortality rates could presage substantial changes in forest structure, composition, and function (7, 25), and in some cases could be symptomatic of forests that are stressed and vulnerable to abrupt dieback (5). Indeed, since their most recent censuses, several of our plots in the interior region experienced greatly accelerated mortality due to bark beetle outbreaks, and in some cases nearly complete mortality of large trees (10). Second, the increasing mortality rates demonstrate that ongoing, subcontinental-scale changes in tree demographic rates are not limited to the tropics (8). Third, some of the changes in the western United States contrast sharply with those in the tropics, where increasing mortality rates have been paralleled by increasing recruitment rates and basal area (2, 8). In the western United States, recruitment rates have not changed while forest density and basal area have declined slightly. Fourth, our results are inconsistent with a major role for endogenous causes of increasing mortality rates. Instead, the evidence is consistent with contributions from exogenous causes, with regional warming and consequent drought stress being the most likely drivers.

References and Notes

- G. B. Bonan, *Science* **320**, 1444 (2008).
- S. L. Lewis et al., *Philos. Trans. R. Soc. London Ser. B* **359**, 421 (2004).
- A. S. Jump, J. M. Hunt, J. Peñuelas, *Glob. Change Biol.* **12**, 2163 (2006).
- K. J. Feeley, S. J. Wright, M. N. Nur Supardi, A. R. Kassim, S. J. Davies, *Ecol. Lett.* **10**, 461 (2007).
- D. D. Breshears et al., *Proc. Natl. Acad. Sci. U.S.A.* **102**, 15144 (2005).
- K. F. Raffa et al., *Bioscience* **58**, 501 (2008).
- R. K. Kobe, *Ecol. Monogr.* **66**, 181 (1996).
- O. L. Phillips et al., *Philos. Trans. R. Soc. London Ser. B* **359**, 381 (2004).
- J. A. Hicke, J. C. Jenkins, D. S. Ojima, M. Ducey, *Ecol. Appl.* **17**, 2387 (2007).
- See supporting material on Science Online.
- C. D. Oliver, B. C. Larson, *Forest Stand Dynamics* (McGraw-Hill, New York, 1990).
- J. F. Franklin et al., *For. Ecol. Manage.* **155**, 399 (2002).
- P. J. van Mantgem, N. L. Stephenson, *Ecol. Lett.* **10**, 909 (2007).
- J. A. Lutz, C. B. Halpern, *Ecol. Monogr.* **76**, 257 (2006).
- G. I. McDonald, R. J. Hoff, in *Whitebark Pine Communities*, D. F. Tomback, S. F. Arno, R. E. Keane, Eds. (Island Press, Washington, DC, 2001), pp. 193–220.
- R. T. Brown, J. K. Agee, J. F. Franklin, *Conserv. Biol.* **18**, 903 (2004).
- M. North, J. Innes, H. Zald, *Can. J. For. Res.* **37**, 331 (2007).
- H. F. Diaz, J. K. Eischeid, *Geophys. Res. Lett.* **34**, L18707 (2007).

Table 1. Fixed effects of generalized nonlinear mixed models describing mortality rate trends (10); a is the estimated annual fractional change in mortality rate (10) and n is the number of forest plots used in the model.

Model	Data	a	SE	P	n
Mortality trend	All plots	0.039	0.005	<0.0001	76
Mortality trend by region	Pacific Northwest	0.042	0.006	<0.0001	47
	California	0.028	0.009	0.0050	20
	Interior	0.024	0.009	0.0319	9
Mortality trend by elevation class	<1000 m	0.038	0.007	<0.0001	33
	1000 to 2000 m	0.050	0.010	<0.0001	20
	>2000 m	0.027	0.006	0.0003	23
Mortality trend by stem diameter class	<15 cm	0.039	0.006	<0.0001	61
	15 to 40 cm	0.040	0.006	<0.0001	76
	>40 cm	0.033	0.007	<0.0001	76
Mortality trend by genus	<i>Abies</i>	0.031	0.010	0.0025	62
	<i>Pinus</i>	0.044	0.010	<0.0001	37
	<i>Tsuga</i>	0.049	0.009	<0.0001	47
	All other genera	0.032	0.008	<0.0001	64
Mortality trend by fire return interval	<25 years	0.033	0.008	0.0009	15
	25 to 250 years	0.040	0.006	<0.0001	32
	>250 years	0.036	0.010	0.0008	29

19. N. Knowles, M. D. Dettinger, D. R. Cayan, *J. Clim.* **19**, 4545 (2006).
20. P. W. Mote, A. F. Hamlet, M. P. Clark, D. P. Lettenmaier, *Bull. Am. Meteorol. Soc.* **86**, 39 (2005).
21. I. T. Stewart, D. R. Cayan, M. D. Dettinger, *J. Clim.* **18**, 1136 (2005).
22. A. L. Westerling, H. G. Hidalgo, D. R. Cayan, T. W. Swetnam, *Science* **313**, 940 (2006); published online 5 July 2006 (10.1126/science.1128834).
23. N. McDowell *et al.*, *New Phytol.* **178**, 719 (2008).
24. C. Bigler, D. G. Gavin, C. Gunning, T. T. Veblen, *Oikos* **116**, 1983 (2007).
25. A. W. Fellows, M. L. Goulden, *Geophys. Res. Lett.* **35**, L12404 (2008).
26. We thank the many people involved in establishing and maintaining the permanent forest plots: C. Allen, A. Das, J. Halofsky, J. Hicke, J. Lutz, and four anonymous reviewers for helpful comments on the manuscript; and J. Yee for essential statistical advice. The forest plots were funded by NSF's Long-term Studies Program (DEB-0218088); the Wind River Canopy Crane Program through cooperative agreement PNW 08-DG-11261952-488 with the USDA Forest Service Pacific Northwest Research Station; various awards through the USDA Forest Service's Pacific Northwest, Pacific Southwest, and Rocky Mountain research stations and the McIntire-Stennis Cooperative Forestry Program; NSF awards DEB-0743498 and BCS-0825823; the Natural Science and Engineering Research Council of Canada;

and various awards through the U.S. National Park Service and U.S. Geological Survey (USGS). This work is a contribution of the Western Mountain Initiative (a USGS global change research project) and the Cordillera Forest Dynamics Network (CORFOR).

Supporting Online Material

www.sciencemag.org/cgi/content/full/323/5913/521/DC1

Materials and Methods

SOM Text

Figs. S1 to S6

Tables S1 to S4

References

22 August 2008; accepted 3 December 2008
10.1126/science.1165000

The Sphingolipid Transporter Spns2 Functions in Migration of Zebrafish Myocardial Precursors

Atsuo Kawahara,^{1,2*} Tsuyoshi Nishi,^{3,4} Yu Hisano,^{3,4} Hajime Fukui,¹ Akihito Yamaguchi,^{3,4} Naoki Mochizuki¹

Sphingosine-1-phosphate (S1P) is a secreted lipid mediator that functions in vascular development; however, it remains unclear how S1P secretion is regulated during embryogenesis. We identified a zebrafish mutant, *ko157*, that displays cardia bifida (two hearts) resembling that in the *S1P receptor-2* mutant. A migration defect of myocardial precursors in the *ko157* mutant is due to a mutation in a multipass transmembrane protein, *Spns2*, and can be rescued by S1P injection. We show that the export of S1P from cells requires *Spns2*. *spns2* is expressed in the extraembryonic tissue yolk syncytial layer (YSL), and the introduction of *spns2* mRNA in the YSL restored the cardiac defect in the *ko157* mutant. Thus, *Spns2* in the YSL functions as a S1P transporter in S1P secretion, thereby regulating myocardial precursor migration.

During the late stages of zebrafish segmentation characterized by the formation of the somites, the myocardial precursors from both sides of the anterior lateral plate mesoderm migrate toward the midline to form the heart tube (1, 2). Forward genetic analysis in zebrafish has helped to uncover genes involved in vertebrate heart formation (3). To identify additional regulators of heart development, we performed *N*-ethyl-*N*-nitrosourea (ENU) mutagenesis screening for mutations specifically affecting cardiac morphogenesis. We isolated a recessive *ko157* mutant that displayed two hearts, a condition known as cardia bifida with swollen pericardial sacs (Fig. 1, A, B, E, and F). The expression of myocardial markers [*nkx2.5* and *cardiac myosin light chain 2 (cmlc2)*] and chamber-specific markers [*atrial myosin heavy chain (amhc)* and *ventricular myosin heavy chain (vmhc)*] was de-

tected in two separated domains (Fig. 1, C and G, and fig. S2); this finding suggests that the myocardial precursors failed to migrate but differen-

tiated into two chambers at the bilateral positions.

The migration of several mesodermal derivatives examined by the expression pattern of a vascular marker (*fli1*), an erythroid marker (*gata1*), a pronephric marker (*pax2*), and a lateral plate mesoderm marker (*hand2*) was not impaired in *ko157* mutants (figs. S2 and S3), which suggests that the migration of myocardial precursors is dominantly affected. Besides cardia bifida, there were abnormal blisters at the tip of the tail in the mutant (Fig. 1, D and H). These two characteristic phenotypes (cardia bifida and tail blisters) in the *ko157* mutant were similar to those in the *miles apart (mil)/S1P receptor-2 (S1P2)* mutant (4). Sphingosine-1-phosphate (S1P) is a lipid mediator involved in cell growth, death, migration, and differentiation (5–8). Both cardia bifida and tail blisters were observed in embryos injected with an antisense morpholino for *mil/S1P2* (*mil* MO; 15 ng) (9) (fig. S4 and table S1), suggesting a genetic interaction between *ko157* and *mil/S1P2*.

Genetic mapping of the *ko157* mutation by means of simple sequence length polymorphism

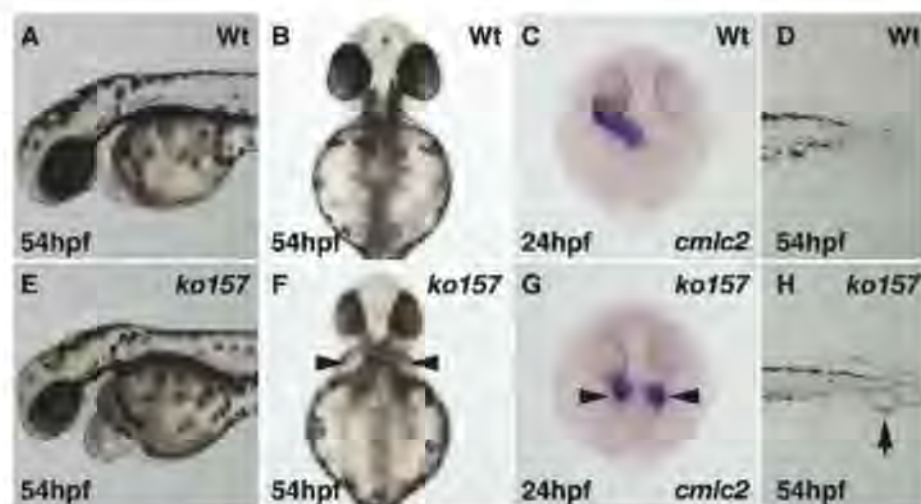


Fig. 1. Morphological phenotypes of *ko157* mutants. (A, B, D, E, F, and H) Stereomicroscopic views of wild-type (Wt) embryo [(A), (B), and (D)] and *ko157* mutant [(E), (F), and (H)]. Two swollen pericardial sacs (arrowheads) at 54 hours post-fertilization (hpf) were observed in *ko157* mutant [(E) and (F)] but not in Wt embryos [(A) and (B)]. (B) and (F) are ventral views. (C and G) Two hearts (arrowheads) in *ko157* mutants at 24 hpf were visualized (dorsal view) by whole-mount in situ hybridization with antisense *cmlc2* probe. *ko157* mutant (H), but not Wt embryos (D), exhibited tail blisters (arrow).

¹Department of Structural Analysis, National Cardiovascular Center Research Institute, Fujishirodai 5-7-1, Suita, Osaka 565-8565, Japan. ²HMRO, Kyoto University Faculty of Medicine, Yoshida, Sakyo-Ku, Kyoto 606-8501, Japan. ³Department of Cell Membrane Biology, Institute of Scientific and Industrial Research, Osaka University, 8-1 Mihogaoka, Ibaraki-shi, Osaka 567-0047, Japan. ⁴Graduate School of Pharmaceutical Sciences, Osaka University, Suita-shi, Osaka 565-0871, Japan.

*To whom correspondence should be addressed. E-mail: atsuo@ri.ncvc.go.jp

(SSLP) markers revealed that the locus of *ko157* was very close to z9419 and z63525 on linkage group 5 (Fig. 2A). We found that the *ko157* mutant allele contained a point mutation in the *spns2* gene with a substitution of arginine to serine at amino acid position 153 (R153S). This arginine is conserved between zebrafish *Spns2* and mammalian homologs of *Spns2* (fig. S5). *Spns1*

is a member of the *Spns* protein family (10, 11), but injection of *spns1* MO (8 ng) into wild-type embryos did not induce cardia bifida, and injection into *ko157* embryos did not worsen the phenotype (fig. S6). Hence, *Spns2*, but not *Spns1*, is involved in cardiac morphogenesis.

To examine whether the mutation in *Spns2* caused the functional impairment in *ko157* mu-

tants, we performed knockdown analysis with antisense morpholino (*spns2* MO). The *spns2* MO injection, but not control morpholino, (5-base mismatched control morpholino for *spns2* MO; 5-mis MO), suppressed the production of the mature form of *spns2* mRNA (fig. S7). Injection of *spns2* MO resulted in cardia bifida (table S1; 86%, $n = 69$) with bilateral expression of *cmhc2* (Fig. 2, B to D), with no cardia bifida in control 5-mis MO-injected embryos (table S1; 0%, $n = 68$). To evaluate whether *spns2* could rescue the *ko157* mutant phenotype, we injected *spns2* or *spns2*(R153S) (*spns2* mutant) mRNA (250 pg) into the embryos derived from *spns2*^{*ko157*} heterozygous carriers. Using more than 250 pg caused severe defects in the trunk and the tail as well as observation of one beating heart (fig. S8). Injection of *spns2* mRNA, but not mutant *spns2*(R153S) mRNA, effectively restored both the migration of myocardial precursors and the tail blisters (Fig. 2, E to G, fig. S9, and table S2). Injection of human *Spns2* (*hSpns2*) mRNA also rescued the cardia bifida phenotype in the *spns2*^{*ko157*} mutant, whereas injection of the corresponding *hSpns2* mutant, *hSpns2*(R199S), did not (fig. S10 and table S3). The *spns2*^{*ko157*} mutant phenotype was not restored by injection of a construct in which human *Spns1* is fused to enhanced green fluorescent protein (EGFP), *hSpns1*-EGFP (fig. S10 and table S3). These results show that *Spns2* function is conserved from fish to mammals and that *Spns1* cannot compensate for the loss of *Spns2*.

Because the cardia bifida phenotype in the *spns2*^{*ko157*} mutant was similar to that in the *mil*/*SIP2* mutant, we investigated a possible genetic interaction between *spns2* and *mil*/*SIP2*. Injection of *mil* MO induced cardia bifida in embryos derived from a wild-type-*Tg(cmhc2:mRFP)* cross in a dose-dependent manner (table S1, *mil* MO 15-ng injection; 90%, $n = 49$; table S4, *mil* MO

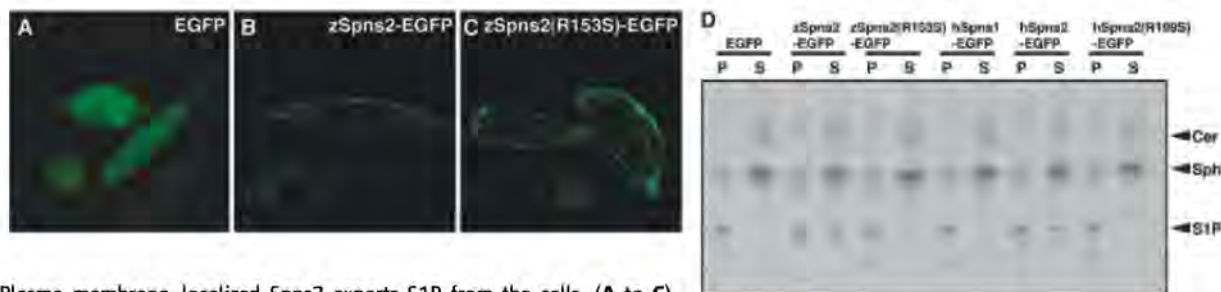
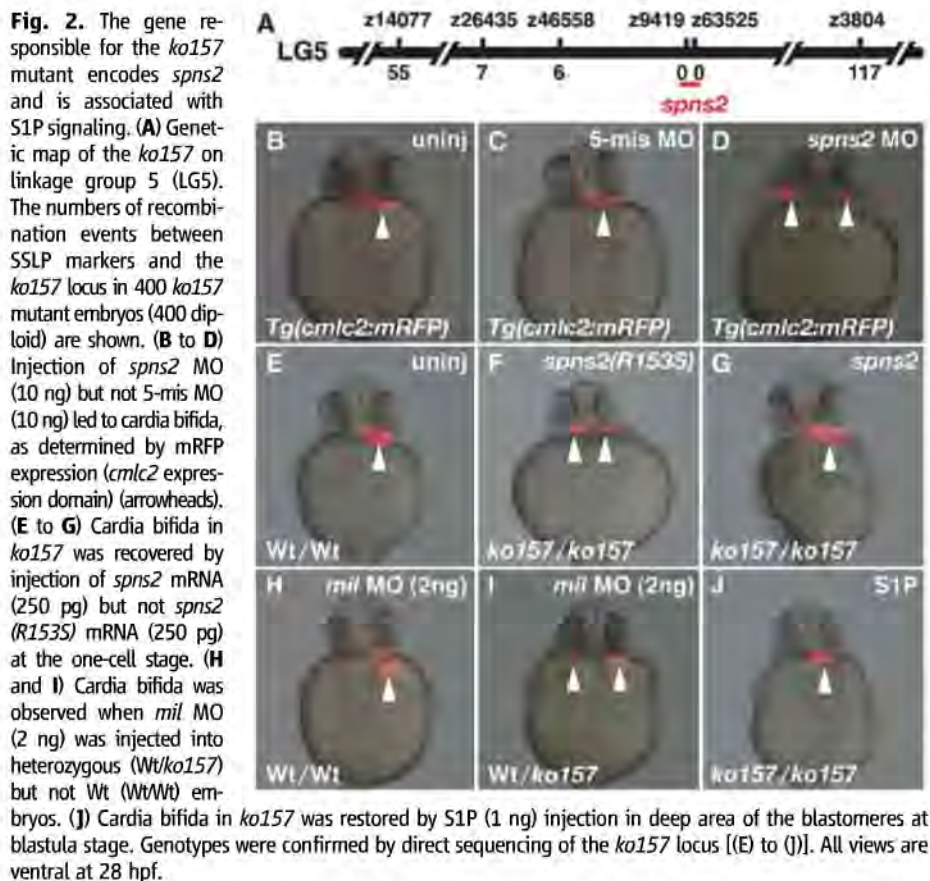


Fig. 3. Plasma membrane-localized *Spns2* exports S1P from the cells. (A to C) Confocal fluorescence microscopy images of CHO cells expressing mouse SphK1 transfected with the plasmids indicated. (D) [³H]S1P converted from [³H]sphingosine in the lipids extracted from medium (S, supernatant) and cells (P, pellet) was separated on a thin-layer chromatography plate. Cer, Sph, and S1P indicate the positions of [³H]ceramide, [³H]sphingosine, and [³H]S1P, respectively. (E) Relative amount of secreted S1P indicates the percentage of total [³H]S1P (P + S). Data are expressed as means \pm SD of more than three independent experiments of (D).

2-ng injection; 7%, $n = 55$). Low-dose *mil* MO (2 ng) injections in *spns2*^{ko157} heterozygous embryos resulted in a higher frequency of cardia bifida relative to wild-type embryos (table S4; 44%, $n = 18$). Genotyping revealed that most cardia bifida embryos were wild-type/*ko157* (Fig. 2, H and I, and table S4). The severity of the cardiac defect was comparable between *mil* MO (15 ng)-injected wild-type and *mil* MO-injected *ko157* embryos (fig. S11). These data suggest that *spns2* genetically interacts with *mil/SIP2*.

To further examine the functional interaction of Spns2 and SIP signaling, we performed a rescue experiment of the *spns2*^{ko157} mutant by SIP injection. When SIP (1 ng) was injected deep into an area of the blastomeres of blastula-stage embryos derived from *spns2*^{ko157} heterozygous carriers, cardia bifida was effectively restored (Fig. 2J and table S2). In addition, the cardia bifida phenotype induced by *mil* MO (15 ng) injection into the yolk was not rescued by subsequent injection of *spns2* mRNA (250 pg) into the blastomere of one- to two-cell-stage embryos (fig. S12), which suggests that Spns2 functions upstream of *Mil/SIP2* (fig. S1).

The putative 12-transmembrane domains, together with the predicted structural similarity between zebrafish Spns2 (zSpns2) and the bacterial glycerol-3-phosphate transporter (12) and the genetic interaction of Spns2 and the SIP-mediated signaling, suggested that Spns2 might function as a SIP transporter. To test this, we used Chinese hamster ovary (CHO) cells expressing a sphingosine kinase, *mSphK1*, essential for SIP synthesis (CHO-SphK cells) (fig. S1). Although [³H]sphingosine was taken up by the cells and effectively converted to [³H]SIP, it was not secreted because of the absence of an SIP export activity. We examined whether the expression of zSpns2-EGFP or zSpns2(R153S)-EGFP was able to induce SIP export. Both zSpns2-EGFP and zSpns2(R153S)-EGFP were predominantly localized within the plasma membrane and in the endosomes of transfected CHO-SphK cells (Fig. 3, A to C), consistent with a role in membrane trafficking. Expression of zSpns2-EGFP resulted in a time-dependent export of [³H]SIP that was not seen in either the EGFP- or zSpns2(R153S)-EGFP-transfected cells (Fig. 3, D and E, and fig. S13). Moreover, endogenous SIP release was also detected only in the medium from the zSpns2-EGFP-expressing cells (fig. S14) without altering the content of cellular sphingolipids (fig. S15). Overexpression of hSpns2-EGFP enhanced SIP export to a similar extent as zSpns2-EGFP, whereas that of hSpns2(R199S)-EGFP and hSpns1-EGFP did not (Fig. 3, D and E). SIP release was not due to cell death induced by Spns2-EGFP expression (fig. S16), and the activity of sphingosine kinase in the medium was not affected by Spns2-EGFP expression (fig. S17).

Recently it was proposed that ABC transporters including ABCC1 and ABCA1 are required for SIP transport (13–15). The cellular distribution of Spns2-EGFP is similar to that of ABCA1

(16). Therefore, the net SIP release to the outside of the cells would depend on the amount of Spns2 and other SIP transporters expressed on the plasma membrane. The contribution of ABC transporters in the SIP transport is still controversial in vivo because the quantity of plasma SIP is not altered in mice deficient for ABCC1 or ABCA1 (17). We propose that Spns2 is a SIP transporter essential for the SIP-mediated signaling pathway in vivo (fig. S1).

To further understand where and how Spns2 functions in vivo, we examined *spns2* expression during early embryogenesis by whole-mount in situ hybridization. The expression of *spns2* was induced at the marginal cells of the blastoderm at dome stage (fig. S18). During gastrulation stages, *spns2* was predominantly expressed in the extraembryonic yolk syncytial layer (YSL) with a dorsal-to-ventral gradient (Fig. 4A and fig. S18). *spns2* expression in the YSL was strongly detected just below the developing myocardial precursors and was maintained throughout the segmentation period (Fig. 4, B to D). Recent evidence demonstrated that both endoderm and YSL regulate cardiac morphogenesis (18–20). Expression of the endoderm markers *sox17* and *foxa2* was not affected in *spns2*^{ko157} mutant em-

bryos (fig. S3). In addition, *spns2* expression was not affected in endoderm-defective *casanova/sox32* morphants (fig. S18), which suggests that *spns2* expression in the YSL is regulated independently of the endoderm. *spns2* expression was detected in somites and in the tip of the tail at the 15-somite stage (fig. S18). We observed *spns2* expression in the myocardial precursors and in the intermediate cell mass (fig. S18). Thus, the expression of *spns2* is complex and dynamic. Although the overall morphology of the head and trunk appeared to be normal in the *spns2*^{ko157} mutant, we observed substantially increased apoptotic cells in the tail but not in the heart, head, and anterior trunk of the *spns2*^{ko157} mutant (fig. S19). These results suggest the involvement of Spns2 in the regulation of multiple organogenesis processes.

Because *spns2* was strongly expressed in the YSL below the developing myocardial precursors, we further examined whether Spns2 in the YSL contributes to the migration of myocardial precursors. When *spns2* MO (10 ng) was injected into the YSL at shield stage, cardia bifida was observed (Fig. 4, E and F, and table S5). In contrast, *mil* MO (15 ng) injection in the YSL at shield stage did not induce cardia bifida (Fig. 4,

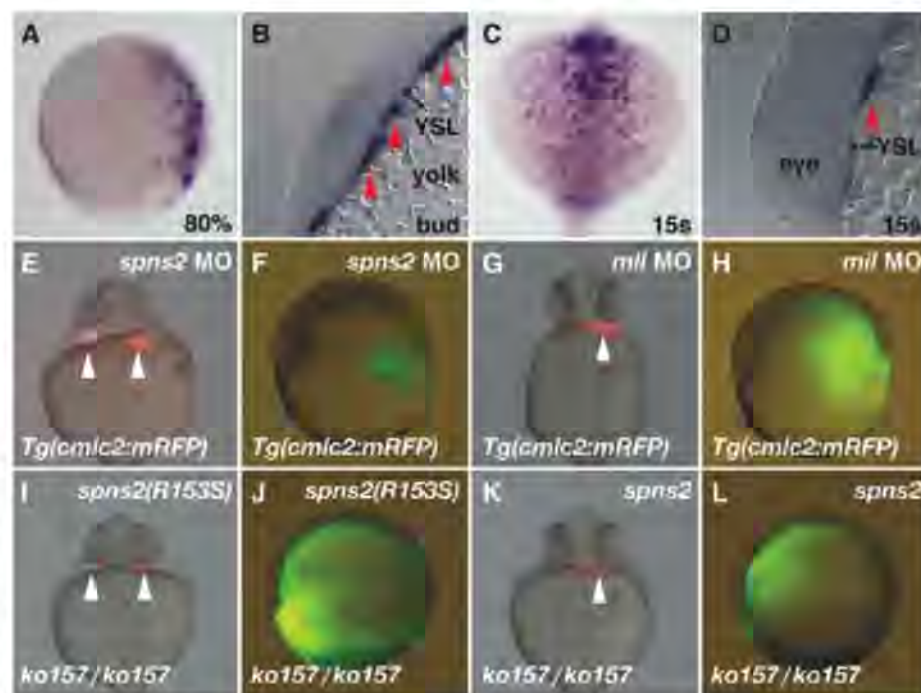


Fig. 4. Spns2 in the YSL is required for the migration of myocardial precursors. (A to D) Whole-mount in situ hybridization with antisense *spns2* probe at different stages of development. (B) and (D) show transverse sections of *spns2*-stained embryos. *spns2* was expressed in the YSL with a dorsal-to-ventral gradient at 80% epiboly stage [(A); dorsal right, lateral view]. *spns2* expression was maintained in the YSL at bud and 15s stages [(B) and (D); red arrowheads] and detected under the anterior midline [(C); dorsal up, anterior view]. (E to H) Injection of *spns2* MO (10 ng) with fluorescein isothiocyanate (FITC)-dextran into the YSL of shield-stage embryos led to cardia bifida, whereas injection of *mil* MO (15 ng) did not. (I to L) Cardia bifida in *spns2*^{ko157/ko157} mutant was recovered by mRNA injection of *spns2* (250 pg) with FITC-dextran into the YSL of shield-stage embryos but not by mRNA injection of *spns2*(R153S) (250 pg). Genotypes were confirmed by direct sequencing of the *ko157* locus. Injection into the YSL was confirmed by the distribution of FITC-dextran in the YSL at gastrulation stages [(F), (H), (J), and (L)]. White arrowheads indicate the positions of *cmlc2* expression domain [(E), (G), (I), and (K)].

G and H, and table S5). Because *mil/SIP2* is expressed in the mesoderm just lateral to the midline (4), *mil/SIP2* is proposed to function in mesoderm over the YSL. Further, cardia bifida in the *spns2^{ko157}* mutant was restored by the injection of *spns2* mRNA but not *spns2(R153S)* mRNA into the YSL at shield stage (Fig. 4, I to L, and table S6).

The rescue frequency by injection of *spns2* mRNA into the YSL was slightly lower than for injection into the blastomere (tables S2 and S6). One explanation is that *spns2* mRNA injected into the blastomere at the one-cell stage is widely distributed in the YSL because the YSL is constituted by marginal blastomeres collapsing onto the yolk around the 1000-cell stage. Another explanation is that the function of Spns2 in embryonic tissues as well as in the YSL may be partly required for the migration of myocardial precursors. Furthermore, transplantation analysis showed that Spns2 at least functions in a cell-nonautonomous manner, because *ko157*-derived donor cells were incorporated into single beating hearts of wild-type recipients, and wild type-derived donor cells were incorporated into one of two beating hearts of *ko157* recipients (movies S1 to S3). One attractive interpretation is that Spns2 in the YSL regulates the SIP export from the yolk to the embryonic body, leading to the activation of Mil/SIP₂ in mesoderm just lateral to the midline (fig. S1). Recent reports have pointed out the importance of *ferroportin1* (*fpn1*) as a transporter of iron from the yolk to the embryonic body (21) and the clinical relevance to hypochromic anemia and hemochromatosis in humans (22, 23).

By investigating characteristic features of the zebrafish *spns2^{ko157}* mutant and analyzing the biological activity of Spns2, we have demonstrated that Spns2 functions as a SIP transporter and that Spns2 in the extraembryonic YSL is a prerequisite for the migration of myocardial precursors, presumably mediated by the SIP-Mil/SIP₂ pathway. The identification of Spns2 not only contributes to our understanding of the molecular mechanism of biological SIP delivery, but may also elucidate the physiological importance of Spns2 in autoimmune disease (24), cardiovascular diseases, and cancer (25) in which SIP plays a central role.

References and Notes

1. D. Y. Stainier, *Nat. Rev. Genet.* **2**, 39 (2001).
2. J. J. Schoenebeck, D. Yelon, *Semin. Cell Dev. Biol.* **18**, 27 (2007).
3. J. N. Chen, M. C. Fishman, *Trends Genet.* **16**, 383 (2000).
4. E. Kupperman, S. An, N. Osborne, S. Waldron, D. Y. Stainier, *Nature* **406**, 192 (2000).
5. M. J. Lee et al., *Science* **279**, 1552 (1998).
6. T. Hla, *Pharmacol. Res.* **47**, 401 (2003).
7. S. Spiegel, S. Milstien, *Nat. Rev. Mol. Cell Biol.* **4**, 397 (2003).
8. Y. A. Hannun, L. M. Obeid, *Nat. Rev. Mol. Cell Biol.* **9**, 139 (2008).
9. T. Matsui et al., *Nat. Clin. Pract. Cardiovasc. Med.* **4** (suppl. 1), S77 (2007).
10. Y. Nakano et al., *Mol. Cell. Biol.* **21**, 3775 (2001).
11. R. M. Young et al., *Dev. Dyn.* **223**, 298 (2002).
12. Y. Huang, M. J. Lemieux, J. Song, M. Auer, D. N. Wang, *Science* **301**, 616 (2003).
13. N. Kobayashi et al., *J. Lipid Res.* **47**, 614 (2006).
14. P. Mitra et al., *Proc. Natl. Acad. Sci. U.S.A.* **103**, 16394 (2006).
15. K. Sato et al., *J. Neurochem.* **103**, 2610 (2007).
16. E. B. Neufeld et al., *J. Biol. Chem.* **276**, 27584 (2001).
17. Y. M. Lee, K. Venkataraman, S. I. Hwang, D. K. Han, T. Hla, *Prostaglandins Other Lipid Mediat.* **84**, 154 (2007).

18. Y. Kikuchi et al., *Genes Dev.* **15**, 1493 (2001).
19. T. Dickmeis et al., *Genes Dev.* **15**, 1487 (2001).
20. T. Sakaguchi, Y. Kikuchi, A. Kuroiwa, H. Takeda, D. Y. Stainier, *Development* **133**, 4063 (2006).
21. A. Donovan et al., *Nature* **403**, 776 (2000).
22. O. T. Njajou et al., *Nat. Genet.* **28**, 213 (2001).
23. G. Montosi et al., *J. Clin. Invest.* **108**, 619 (2001).
24. M. Sekiguchi et al., *J. Immunol.* **180**, 1921 (2008).
25. S. Milstien, S. Spiegel, *Cancer Cell* **9**, 148 (2006).
26. We thank M. Sone and M. Minamimoto for technical assistance; S. Endo and R. Hanaoka for the mutagenesis screening; T. Kitaguchi for the establishment of *cmlc2:mRFP*; M. Masuda, Y. Igarashi, A. Kihara, S. Mitsutake, K. Shioya, I. B. Dawid, and Y. Kaziro for support and suggestions; M. Hibi, J. S. Gutkind, and M. Tsang for critical reading and valuable suggestions; D. Y. Stainier for discussions and sharing of unpublished data; and H. Okamoto, K. Kawakami, Y. Kikuchi, H. Yanagisawa, D. Yamamoto, R. Y. Tsien, and H.-J. Tsai for fish and reagents. Supported by grants from the Ministry of Education, Culture, Sports, Science and Technology of Japan; the National BioResource Project of Japan; the Japan Society for the Promotion of Science; the Program for the Promotion of Fundamental Studies in Health Sciences of the National Institute of Biomedical Innovation; the Ministry of Health, Labor and Welfare of Japan; and the Takeda Science Foundation. The sequences of zebrafish *spns2*, human *Spns2*, and mouse *Spns2* have been deposited in the DNA Data Bank of Japan [accession numbers: AB441164 (zebrafish), AB441165 (human), AB441166 (mouse)]. The authors are filing a patent based on the results reported in this paper.

Supporting Online Material

www.sciencemag.org/cgi/content/full/1167449/DC1

Materials and Methods

Figs. S1 to S19

Tables S1 to S6

Movies S1 to S3

References

20 October 2008; accepted 3 December 2008

Published online 11 December 2008;

10.1126/science.1167449

Include this information when citing this paper.

The Peopling of the Pacific from a Bacterial Perspective

Yoshan Moodley,^{1*†} Bodo Linz,^{1*‡} Yoshio Yamaoka,^{2*} Helen M. Windsor,³ Sebastien Breurec,^{4,5} Jeng-Yih Wu,⁶ Ayas Maady,⁷ Steffie Bernhöft,¹ Jean-Michel Thiberge,⁸ Suparat Phanukoonnon,⁹ Gangolf Jobb,¹⁰ Peter Siba,⁹ David Y. Graham,² Barry J. Marshall,³ Mark Achtman^{1,11§}

Two prehistoric migrations peopled the Pacific. One reached New Guinea and Australia, and a second, more recent, migration extended through Melanesia and from there to the Polynesian islands. These migrations were accompanied by two distinct populations of the specific human pathogen *Helicobacter pylori*, called hpSahul and hspMaori, respectively. hpSahul split from Asian populations of *H. pylori* 31,000 to 37,000 years ago, in concordance with archaeological history. The hpSahul populations in New Guinea and Australia have diverged sufficiently to indicate that they have remained isolated for the past 23,000 to 32,000 years. The second human expansion from Taiwan 5000 years ago dispersed one of several subgroups of the Austronesian language family along with one of several hspMaori clades into Melanesia and Polynesia, where both language and parasite have continued to diverge.

After modern humans dispersed “out of Africa” about 60,000 years ago (60 ka) (1), they reached Asia via a southern coastal route (2). That route extended along the Pleistocene landmass, known as Sundaland (i.e., the Malay peninsula, Sumatra, Java, Borneo, and

Bali), that was joined to the Asian mainland as a result of low sea levels during the last ice age (12 to 43 ka) (3). Low sea levels also meant that Australia, New Guinea, and Tasmania were connected in a continent called Sahul, separated from Sundaland by a few narrow deep-sea channels. It

seems Sahul was colonized only once, ~40 to 50 ka (3, 4), although backed-blade stone tool technology and the dingo appear to have been introduced from India at a later date (5, 6).

¹Max-Planck-Institut für Infektionsbiologie, Department of Molecular Biology, Charitéplatz 1, 10117 Berlin, Germany.

²Department of Medicine-Gastroenterology, Baylor College of Medicine and Michael E. DeBakey VA Medical Center, Houston, TX 77030, USA.

³Microbiology and Immunology M502, School of Biomedical, Biomolecular and Chemical Sciences, University of Western Australia, Australia 6009.

⁴Institut Pasteur, BP 220, Dakar, Sénégal.

⁵Institut Pasteur de Nouvelle-Calédonie, BP61, 98845 Noumea, New Caledonia.

⁶Department of Gastroenterology, Kaohsiung Medical University, 100 Shih-Chuan 1st Road, Kaohsiung 80708, Taiwan.

⁷Department of Endoscopy, Republic Hospital No. 1, Kyzyl City 667003, Republic of Tuva, Russia.

⁸Institut Pasteur, Genotyping of Pathogens and Public Health, 28 rue du Dr Roux, 75724 Paris, France.

⁹Papua New Guinea Institute of Medical Research, Post Office Box 60, Goroka, EHP, 441 Papua New Guinea.

¹⁰Fritz-Kortner-Bogen 36, 81739 Munich, Germany.

¹¹Environmental Research Institute and Department of Microbiology, University College Cork, Cork, Ireland.

*These authors contributed equally to this work.

†Present address: Austrian Academy of Sciences, Konrad Lorenz Institute for Ethology, Savoyenstrasse 1A, A-1160, Vienna, Austria.

‡Present address: Department of Biochemistry and Molecular Biology, Pennsylvania State University, University Park, PA 16802, USA.

§To whom correspondence should be addressed. E-mail: m.achtman@ucc.ie

Human genetic data are compatible with these interpretations, but have not provided the details. Redd and Stoneking identified multiple mitochondrial DNA (mtDNA) lineages among New Guinea peoples with coalescence times of 80,000 to 122,000 years (80 to 122 ky), predating the out-of-Africa migrations (5). In subsequent analyses, Australian aboriginals and Melanesians fell into multiple, distinct mtDNA haplogroups interdispersed among lineages from East Asia and India (4), with one exception: haplogroup Q, which had a coalescent estimate of 32 ka and contained both Australian and Melanesian lineages. Y-chromosome markers yielded one lineage for Australians and a second one for Melanesians (4). Australia and New Guinea remained connected by a land bridge until sea levels rose ~8 to 12 ka, and it is surprising that the native inhabitants of Sahul are not genetically associated except for haplogroup Q.

Subsequent prehistoric migrations to island East Asia and the Pacific have been designated differently depending on whether they were traced by language, archaeological remains, or genetic studies. Most of the native Pacific languages from near the African coast (Madagascar) through to Polynesia are Malayo-Polynesian, a subgroup of the Austronesian language family (7). The nine other subgroups of Austronesian are only spoken in Taiwan, suggesting that Taiwan is the origin of Austronesian (7). In support of this interpretation, agriculturists spread from Taiwan via insular and coastal Melanesia into the Pacific, as marked by the Lapita cultural complex, including red-slipped pottery, Neolithic tools, chickens, pigs, and farm-

ing (8). A human genetic marker of this route of spread is the "Polynesian" mtDNA HV1 motif of lineage B4a1a, which is found at high frequency among native Taiwanese (9), Melanesians, and Polynesians (10, 11).

We attempted to trace human prehistory in the Pacific by analyzing the distribution of a bacterial parasite of humans, *Helicobacter pylori*. *H. pylori* accompanied modern humans during their migrations out of Africa (12). Subsequent founder effects, plus geographic separation, have resulted in populations of bacterial strains specific for large continental areas. Thus, Africans are infected by the *H. pylori* populations hpAfrica1 and hpAfrica2, Asians are infected by hpAsia2 and hpEastAsia, and Europeans are infected by hpEurope (12, 13). It seemed possible that the distribution of *H. pylori* genotypes among native inhabitants might provide insights into migrations throughout the Pacific. We cultivated 212 bacterial isolates from gastric biopsies or mucus obtained from aboriginals in Taiwan and Australia, highlanders in New Guinea, as well as Melanesians and Polynesians in New Caledonia (table S1). Concatenated sequences of seven gene fragments (3406 base pairs, of which half are polymorphic) from these isolates yielded 196 unique haplotypes. These were compared with 99 unique haplotypes from 100 Europeans in Australia and 222 other unique haplotypes from Asia and the Pacific, including 15 haplotypes from Chinese inhabitants of Taiwan, as well as ~1700 haplotypes from other sources.

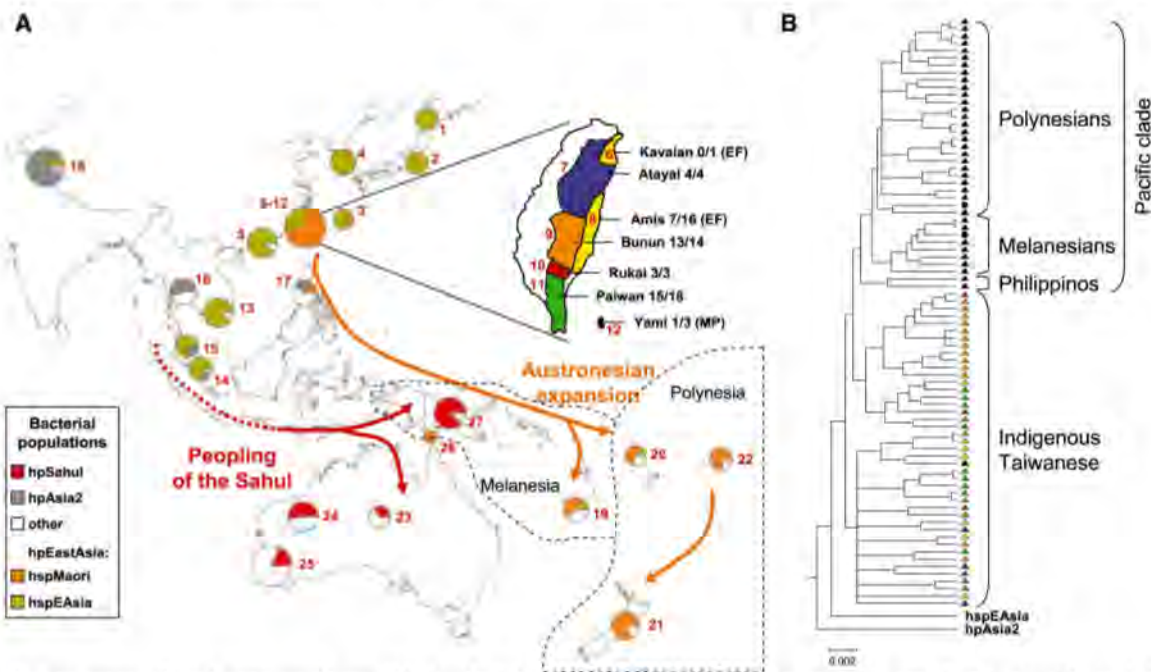
According to Bayesian assignment analysis, our samples from native inhabitants yielded 50

unique haplotypes that formed a distinct biogeographic group called hpSahul (14). Twenty-eight percent (26 of 92) of the haplotypes from aboriginals in Australia and 89% (24 of 27) of the haplotypes from highlanders in New Guinea were hpSahul (Fig. 1A). One hpSahul haplotype was found among 99 haplotypes from Europeans in Australia and none among the other haplotypes from elsewhere.

hspMaori is a subpopulation of hpEastAsia, isolated from Polynesians (Maoris, Tongans, and Samoans) in New Zealand (13) and three individuals in the Philippines and Japan. hspMaori isolates have not previously been isolated from other individuals, including the 15 Chinese inhabitants of Taiwan (12). Fifty-four of the 196 unique haplotypes from native inhabitants were hspMaori (14), and all came from Austronesian sources. These included native Taiwanese (43 of 59, 73%), Melanesians (6 of 13, 46%), and Polynesians (3 of 5, 60%) in New Caledonia, and two inhabitants of the Torres Straits islands that lie between Australia and New Guinea and which have been visited extensively by Polynesians (Fig. 1A and table S1). These observations suggest that hspMaori is a marker for the entire Austronesian expansions rather than only for Polynesians. The remaining unique haplotypes from native inhabitants were hpEurope, hspEAsia, and hpAfrica1, which can be attributed to very recent human travels.

If Taiwan were the source of the Austronesian expansions, hspMaori haplotypes would be expected to be widespread among aboriginal Taiwanese tribes. Indeed, hspMaori was isolated

Fig. 1. (A) The distribution of *H. pylori* populations in Asia and the Pacific. The proportions of haplotypes at each sampling location (red numbers; table S1) that were assigned to different bacterial populations are displayed as pie charts whose sizes indicate the numbers of haplotypes. The geographic location of Melanesia and Polynesia is depicted. The term "Austronesia" refers to the entire region inhabited by Austronesian-speaking people from Madagascar through to the Easter Islands. **(Inset)** A detailed map of Taiwan showing the distribution of aboriginal tribes. The names of the tribes plus the proportion of hspMaori haplotypes among all haplotypes are shown in black at the right. The language-family designations are the same as the tribal names except where indicated by parentheses (EF, East Formosan; MP, Malayo-Polynesian). **(B)** Phylogenetic relationships among hspMaori strains (80% consensus of 100 ClonalFrame analyses). One haplotype each of



hpAsia2 and hspEAsia was used to root the tree. Strains are color-coded according to Austronesian language family in (A). Two black circles within the Pacific clade indicate haplotypes isolated from the Torres Strait islands, and a black triangle among indigenous Taiwanese indicates an hspMaori haplotype from Yami.

frequently (44 to 100%) from five of the six tribes sampled (Fig. 1A). Taiwan should also harbor the greatest diversity, and the branching order within a phylogenetic tree should reflect the direction of subsequent migrations. The phylogenetic analyses showed that genetic diversity was significantly higher in Taiwanese hspMaori ($\Pi_{95} = 1.79$ to 1.82%) than in non-Taiwanese hspMaori ($\Pi_{95} = 1.58$ to 1.62%). All non-Taiwanese hspMaori haplotypes form a single clade, the Pacific clade, which originates from one of several clades among indigenous Taiwanese haplotypes (Fig. 1B). The sequence of branching events within the Pacific clade is consistent with sequential migrations from Taiwan via the Philippines and island Melanesia to Polynesia (Fig. 1B). These results

also support an association between language and haplotype group. The indigenous Taiwanese haplotypes were isolated from tribes that speak 5 of the 10 subgroups of the Austronesian family of languages, whereas the Pacific clade was isolated from individuals that speak variants of Malayo-Polynesian. The sole exception to these generalizations was one haplotype from the Yami of Lanyu, a small island off the coast of Taiwan, where the language is a variant of Malayo-Polynesian but the haplotype clustered with the indigenous Taiwanese haplotypes. Together, these observations provide support for a Taiwanese source of the Austronesian expansions.

Using the isolation with migration model (IMa), we calculated the magnitude of migrations

in both directions after the initial split between the Taiwan and Pacific clades of hspMaori (15). IMa uses sequence data within a probabilistic framework to simulate a model of initial geographic separation between two populations followed by occasional migration in both directions. Because homologous recombination is frequent within *H. pylori* (13, 16), we excluded blocks of sequences that had a high likelihood of recombination (14). The calculations indicated that migrations subsequent to the initial split were unidirectional, from Taiwan to the Pacific (Fig. 2A).

Other splits between pairs of *H. pylori* populations were also unidirectional: for example, the Amerind colonization over the Bering Strait and the subsequent colonization of South

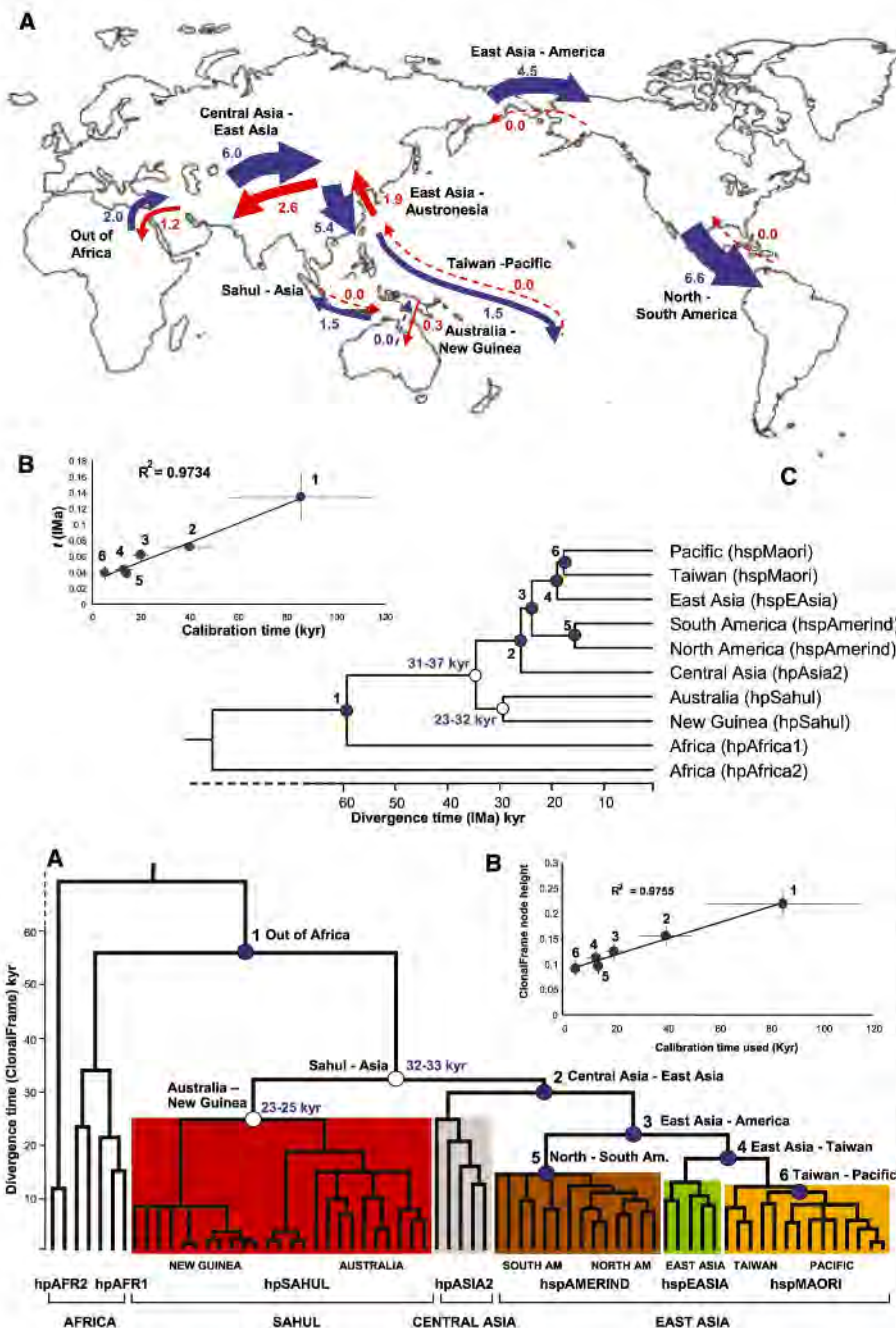


Fig. 2. Global patterns of migration between eight pairs of *H. pylori* populations as calculated by the isolation with migration model (IMa). (A) Map. The magnitudes of migration are denoted by numbers and arrow thickness and their direction is indicated in blue or red. (B) Graph showing a linear relation between the calibration time (table S2) of six events (filled blue circles) that are dated by archaeological estimates and the estimated time (t). (C) Population tree reconstructed from a consensus of 1000 bootstrap samples from the range of calculated t values to determine the ages of nodes (thousands of years, kyr) associated with the peopling of the Sahul (unfilled circles). Ages (in light blue) are the 95% confidence limits of estimated coalescence times obtained by applying global rate minimum deformation (GRMD) rate-smoothing, as implemented in Treefinder, to the range of t values within the limits of calibration dates.

Fig. 3. Global phylogeny of *H. pylori* as calculated by a haplotype approach based on the 80% consensus of 100 ClonalFrame analyses. (A) Phylogenetic tree of divergence time, as indicated by node height versus geographic sources (bottom line) and population assignments (second line). Detailed sources of clades within populations are indicated in the third line from the bottom. Node heights were used to date the two hpSahul nodes (unfilled circles) based on six calibration times (filled blue circles, table S2). Age ranges (light blue numbers) are the 95% confidence limits of estimated coalescence times obtained with GRMD rate-smoothing over the range of node height values and calibration time limits. hpAFR2, hpAfrica2; hpAFR1, hpAfrica1; AM, America. (B) Graph showing a linear relation of calibration time with the range of heights for each node.

America from North America. However, migrations out of Africa, from Central to East Asia, and from East Asia to Taiwan were followed by appreciable levels of return migration (Fig. 2A).

Molecular mutation rates are unknown for most bacteria, so we cannot directly use IMA data to calculate the dates of initial splits. Instead, we calibrated against known dates for splits among human populations. The archaeologically attributed split between Taiwan and the Pacific Clade is 5 ka (8). Five other calibration dates are presented in table S2. The time when populations split (t) calculated by IMA varied linearly with the calibration dates (Fig. 2B). We used random values within the range of five t values that were calculated for each split between all pairs of populations (table S2) to construct 1000 bootstrap trees using Treefinder (17). These trees were then used to calculate the age of the Sahulian migration by rate-smoothing within the limits of the six calibration dates (14).

The dates and numbers of migrations to the Sahul are controversial. According to our IMA calculations, the population split leading to hpSahul postdated the out-of-Africa migrations but predated the splits that resulted in hpAsia2 (found in Central Asia) and hpEastAsia [East Asia (hspEAsia); the Pacific (hspMaori); the Americas (hspAmerind)]. The 95% confidence limits of the date of the split between hpSahul and the Asian populations were estimated as 31 to 37 ka and the split between hpSahul in New Guinea and Australia as 23 to 32 ka. The combined data presented here indicate that hpSahul migrated only once from Asia toward Sahul, and once between New Guinea and Australia, and subsequent migration did not occur from Australia to New Guinea (Fig. 2A).

To verify the use of IMA for dating of population splits in a bacterial species like *H. pylori*, we also used a haplotype-based coalescent approach, which accounts for recombination with unrelated sources of DNA, as implemented in the program ClonalFrame (18). ClonalFrame generated a haplotype tree whose branch order agreed with the population tree generated by IMA (Fig. 3A). It also assigned individual haplotypes to clades that are congruent with the population assignments, including the separation between hpSahul and other populations. The observation that all hpSahul strains clustered in a monophyletic clade verifies a single colonization event and confirms that modern Asians and the inhabitants of the Sahul have undergone independent evolutionary trajectories since they first split. The two hpSahul clades in New Guinea and Australia are also distinct, confirming a lack of migration between the two areas.

Similarly to the IMA analyses, we observed a linear relation between the calibration dates and time of splitting calculated by ClonalFrame as node heights (Fig. 3B). Applying the same rate-smoothing calibration method as above, we estimated that hpSahul split from the Asian population 32 to 33 ka. Subsequently, hpSahul

from New Guinea and Australia split 23 to 25 ka. Both estimates overlap with the range of IMA estimates (31 to 37 ka and 23 to 32 ka, respectively). The date of origin of hpSahul is comparable to the estimated age of 32 ka for the Q mtDNA haplogroup (4), but less than the 40 to 50 ky associated with the oldest archaeological finding of human artefacts in Australia (3).

Our results lend support for two distinct waves of migrations into the Pacific. First, early migrations to New Guinea and Australia accompanied by hpSahul and second, a much later dispersal of hspMaori from Taiwan through the Pacific by the Malayo-Polynesian-speaking Lapita culture. Each sampling area yielded either hpSahul or hspMaori haplotypes, but not both. The lack of overlap between these populations may reflect differential fitness of the parasite, as has been inferred for the modern replacement of hspAmerind haplotypes by European and African *H. pylori* in South America (19, 20). Alternatively, hpSahul and hspMaori may still coexist in unsampled islands of East Asia, Melanesia, and coastal New Guinea, where their identification might help to unravel the details of human history in those areas.

References and Notes

1. H. Liu, F. Prugnolle, A. Manica, F. Balloux, *Am. J. Hum. Genet.* **79**, 230 (2006).
2. V. Macaulay et al., *Science* **308**, 1034 (2005).
3. K. O. Pope, J. E. Terrell, *J. Biogeography* **35**, 1 (2008).
4. G. Hudjashov et al., *Proc. Natl. Acad. Sci. U.S.A.* **104**, 8726 (2007).
5. A. J. Redd, M. Stoneking, *Am. J. Hum. Genet.* **65**, 808 (1999).
6. P. Savolainen, T. Leitner, A. N. Wilton, E. Matisoo-Smith, J. Lundberg, *Proc. Natl. Acad. Sci. U.S.A.* **101**, 12387 (2004).
7. R. D. Gray, F. M. Jordan, *Nature* **405**, 1052 (2000).

8. M. J. T. Spriggs, in *Prehistoric Mongoloid Dispersals*, T. Akazawa, E. Szathmari, Eds. (Oxford Univ. Press, Oxford, 1996), pp. 322–346.
9. J. A. Trejaut et al., *PLoS Biol.* **3**, e247 (2005).
10. T. Melton et al., *Am. J. Hum. Genet.* **57**, 403 (1995).
11. B. Sykes, A. Leifoff, J. Low-Beer, S. Tetzner, M. Richards, *Am. J. Hum. Genet.* **57**, 1463 (1995).
12. B. Linz et al., *Nature* **445**, 915 (2007).
13. D. Falush et al., *Science* **299**, 1582 (2003).
14. Materials and methods and supplementary tables, figures, and scripts are available on Science Online.
15. J. Hey, R. Nielsen, *Proc. Natl. Acad. Sci. U.S.A.* **104**, 2785 (2007).
16. D. Falush et al., *Proc. Natl. Acad. Sci. U.S.A.* **98**, 15056 (2001).
17. G. Jobb, A. von Haeseler, K. Strimmer, *BMC Evol. Biol.* **4**, 18 (2004).
18. X. Didelot, D. Falush, *Genetics* **175**, 1251 (2007).
19. Y. Yamaoka et al., *FEBS Lett.* **517**, 180 (2002).
20. C. Ghose et al., *Proc. Natl. Acad. Sci. U.S.A.* **99**, 15107 (2002).
21. We gratefully acknowledge C. Stamer for technical assistance, F. Balloux and D. Falush for helpful discussions, and J. Hey for advice on IMA. Support was provided by grants from the ERA-NET PathoGenoMics (project HELDIVNET) to M.A. and S.B., the Science Foundation of Ireland (05/FE1/B882) to M.A., the NIH (grant R01 DK62813) to Y.Y., and the Institut Pasteur and the Institut de Veille Sanitaire to J.-M.T. This publication made use of the *Helicobacter pylori* Multi Locus Sequence Typing Web site (<http://pubmlst.org/helicobacter/>) developed by K. Jolley and sited at the University of Oxford. Each strain has an ID number, and the strains newly isolated here have the continuous block of IDs from 930 to 1242. The development of this site has been funded by the Wellcome Trust and European Union.

Supporting Online Material

www.sciencemag.org/cgi/content/full/323/5913/527/DC1
Methods
Fig. S1
Tables S1 and S2
References

18 September 2008; accepted 11 December 2008
10.1126/science.1166083

Rapid Membrane Disruption by a Perforin-Like Protein Facilitates Parasite Exit from Host Cells

Björn F. C. Kafsack,^{1,2} Janethe D. O. Pena,³ Isabelle Coppens,² Sandeep Ravindran,⁴ John C. Boothroyd,⁴ Vern B. Carruthers^{1*}

Perforin-like proteins are expressed by many bacterial and protozoan pathogens, yet little is known about their function or mode of action. Here, we describe *Toxoplasma* perforin-like protein 1 (TgPLP1), a secreted perforin-like protein of the intracellular protozoan pathogen *Toxoplasma gondii* that displays structural features necessary for pore formation. After intracellular growth, TgPLP1-deficient parasites failed to exit normally, resulting in entrapment within host cells. We show that this defect is due to an inability to rapidly permeabilize the parasitophorous vacuole membrane and host plasma membrane during exit. TgPLP1 ablation had little effect on growth in culture but resulted in a reduction greater than five orders of magnitude of acute virulence in mice. Perforin-like proteins from other intracellular pathogens may play a similar role in microbial egress and virulence.

Perforin (PF) and members of the membrane attack complex (MAC) (complement proteins C6 to C9) are pore-forming proteins of the innate and adaptive immune re-

sponse that constitute the founding members of the MACPF domain family (1). Recent studies (2, 3) have suggested a shared mechanism of pore formation between the MACPF domain and

cholesterol-dependent cytolysins, which are important virulence factors of many pathogenic bacteria (4).

Perforin-like proteins (PLPs) are found in the genomes of bacterial (5, 6) and protozoan pathogens (fig. S1) (7), including the intracellular parasite *Toxoplasma gondii*. *Toxoplasma* causes congenital birth defects, ocular disease, and life-threatening encephalitis in immunocompromised individuals (8). It also serves as a model of other parasites in the phylum Apicomplexa (9) that cause important human diseases, such as malaria. Despite their expression by many pathogens, no mode of action or pore-forming activity has been demonstrated for any microbial PLP. Here, we show that *Toxoplasma* perforin-like protein 1 (TgPLP1) aids parasite egress by rapidly compromising the integrity of membranes encasing the parasite.

MACPF-domain proteins of the mammalian immune system induce cell death by oligomerizing on the surface of target cells and inserting to form large (~100 Å in diameter) pores (10). The MACPF domain of TgPLP1 exhibits the core sequence elements that are important for pore formation, including a high degree of similarity to mammalian, bacterial, and protozoan MACPF domains and the signature (Y/W)-X₆-(F/Y)GTH (F/Y)-X₆-GG motif (fig. S2). Also, structural homology modeling of the TgPLP1 MACPF domain predicts an exquisite preservation of the MACPF-domain fold (fig. S3A). Furthermore, the clusters of helices 1 (CH1) and CH2 (helices C to E and I to J) (fig. S3B) have alternating hydrophilic and hydrophobic residues, which is consistent with the ability to convert into amphipathic membrane-spanning β hairpins during pore insertion (11, 12). Finally, a β sheet-rich domain occupies the TgPLP1 C terminus, reminiscent of C-terminal β-rich domains in other MACPF proteins (2, 13) that play critical roles in membrane binding (11, 14).

TgPLP1 localizes to micronemes (Fig. 1A), which are apical secretory organelles important for parasites' gliding motility and invasion, and is secreted in a calcium-dependent manner similar to other microneme proteins (Fig. 1B). Deletion of the *plp1* gene by homologous recombination resulted in the loss of TgPLP1 expression in *plp1ko* (Fig. 1, A and C) (15). TgPLP1 expression was restored, albeit to slightly below normal, in *plp1ko/PLP1myc* by transfection with PLP1myc cDNA (Fig. 1C). Although a second MACPF gene (*plp2*) is present in the genome, no expression of the encoded protein was detected in

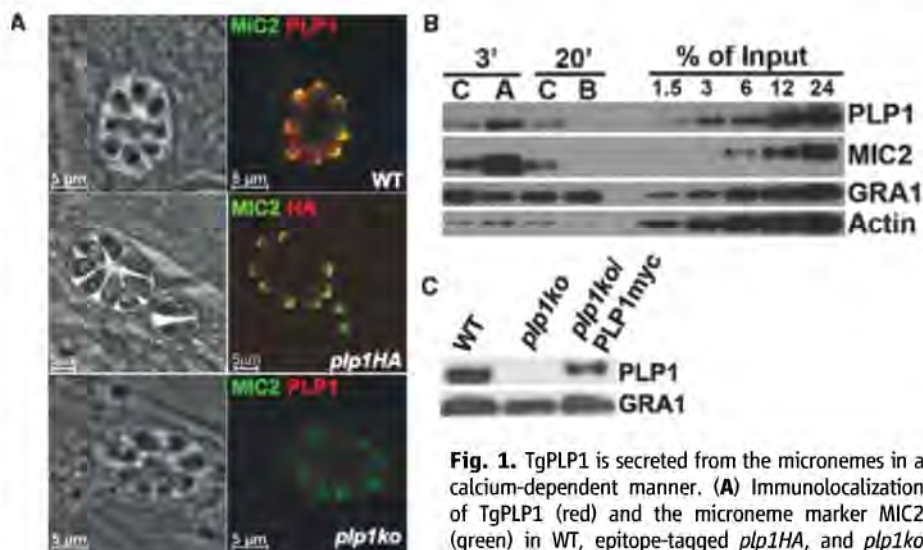


Fig. 1. TgPLP1 is secreted from the micronemes in a calcium-dependent manner. (A) Immunolocalization of TgPLP1 (red) and the microneme marker MIC2 (green) in WT, epitope-tagged *plp1HA*, and *plp1ko* strains. (B) Secretion of TgPLP1, MIC2, and constitutively secreted GRA1 in response to a 3-min treatment with the calcium ionophore A23187 (A), 20 min with the calcium chelator BAPTA-AM (B), or appropriate solvent control (C). Actin included as control for inadvertent lysis. (C) Immunoblot of TgPLP1 in WT, *plp1ko*, and *plp1ko/PLP1myc* strains.

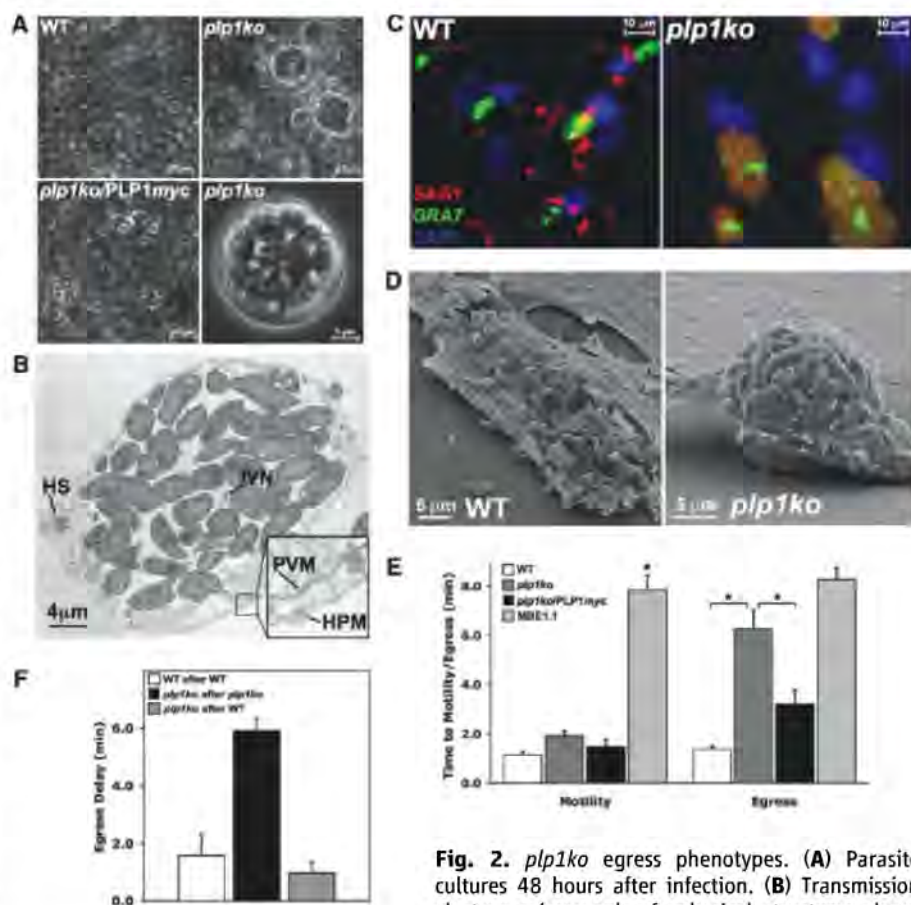


Fig. 2. *plp1ko* egress phenotypes. (A) Parasite cultures 48 hours after infection. (B) Transmission electron micrograph of spherical structures shows remnants of host cell structures (HS), the intra-vacuolar network (IVN), and numerous tachyzoites encased by the PVM and HPM. (C and D) Ionophore-induced egress from WT or *plp1ko* vacuoles. Immunofluorescence colors are red, parasites; green, PVM; and blue, host nuclei. (E) Time to motility activation or egress after addition of calcium ionophore in WT, *plp1ko*, *plp1ko/PLP1myc*, and MBE1.1. Error bars are SEM ($n \geq 30$ vacuoles; * $P < 0.05$, Student's *t* test). (F) Egress delay of secondary vacuoles after egress of an initial vacuole from cells that are multiply infected with WT, *plp1ko*, or both.

¹Department of Microbiology and Immunology, University of Michigan Medical School, Ann Arbor, MI 48109, USA.

²Department of Molecular Microbiology and Immunology, Johns Hopkins Bloomberg School of Public Health, Baltimore, MD 21205, USA. ³Department of Immunology, Universidade Federal de Uberlândia, Uberlândia, Brazil. ⁴Department of Microbiology and Immunology, Stanford University School of Medicine, Stanford, CA 94305, USA.

*To whom correspondence should be addressed. E-mail: vcarruth@umich.edu

proteomic studies (16) or in parasites containing an epitope or fluorescent tag inserted at the endogenous *plp2* locus.

In malaria parasites, PLP proteins play a role in the traversal of the mosquito midgut epithelium by ookinetes (17, 18) and the mammalian

hepatic sinusoids by sporozoites (19), but their mode of action remains unclear. Cell traversal by sporozoites results in the characteristic wounding of the plasma membrane. However, similar to previous findings (20), no cell wounding by *Toxoplasma* tachyzoites was observed, even at a

very high (>75:1) multiplicity of infection (fig. S4). Thus, TgPLP1 plays a role distinct from the characterized malarial PLPs.

After 48 hours of growth when parasites normally egress, we noticed spherical structures in *plp1ko* cultures that were absent from the wild

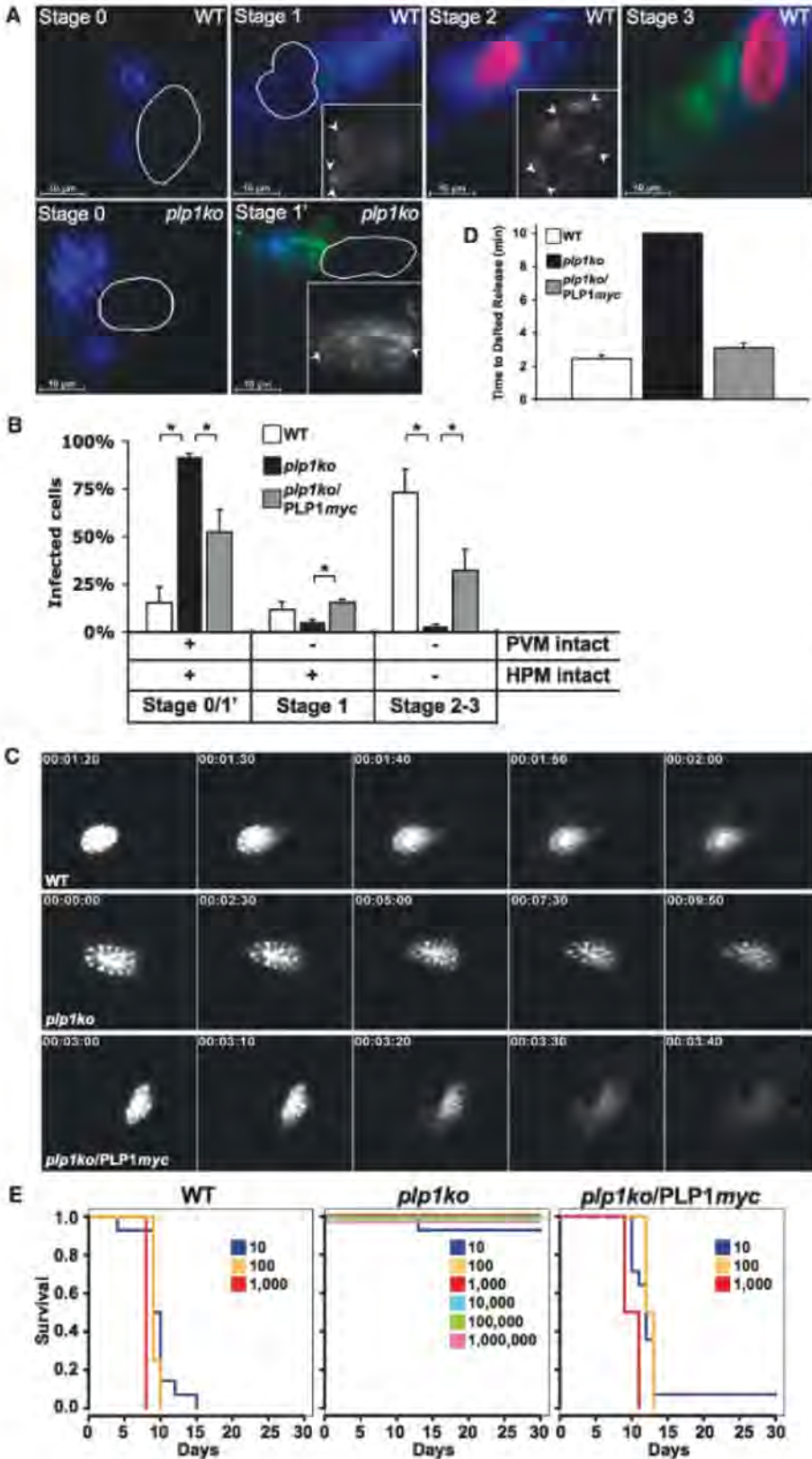


Fig. 3. Evidence of pore formation by TgPLP1. (A) Ionophore-induced permeabilization by immobilized WT or *plp1ko* tachyzoites. In stage 0, the PV marker (GRA1, blue) remains contained within the PVM, with no microneme release (SUB1, green) and no labeling of the host-cell nucleus by PI (red or outlined when unlabeled). In stage 1, microneme contents have been secreted onto the parasite surface (green) (inset, arrowhead indicates parasite apex); PV markers have diffused throughout the host cell but the host-cell nucleus remains unlabeled. In stage 2, the host nucleus is now PI positive, which indicates permeabilization of the HPM. In stage 3, microneme proteins have diffused throughout the host cytoplasm. Cells infected by *plp1ko* remain in stage 0 or display microneme secretion without PV marker release (stage 1'). (B) Quantification of induced PVM and HPM permeabilization for WT, *plp1ko*, or *plp1ko/PLP1myc*. Error bars are SEM ($n = 6$ experiments; $*P < 0.05$, Student's t test). (C) Rapid release of DsRed from the vacuole in WT (top) and *plp1ko/PLP1myc* (bottom) but not *plp1ko* (middle). Time stamp (hours:min:sec) indicates time after calcium ionophore addition. (D) Average time to DsRed release within a 10-min observation period. Error bars are SEM ($n \geq 30$ vacuoles). (E) Virulence in outbred mice following inoculation of escalating tachyzoite numbers.

type (WT) or *plp1ko*/PLP1myc and appeared to contain multiple parasites (Fig. 2A). Parasites were often encased by both the parasitophorous vacuolar membrane (PVM) and the host cell plasma membrane (HPM) (Fig. 2B), suggesting an egress defect.

Indeed, following a 2-min treatment with the calcium ionophore A23187, virtually all WT parasites had egressed from infected host cells, whereas *plp1ko* parasites remained inside their vacuoles (Fig. 2, C and D). For a more detailed view of this egress, we determined the kinetics of ionophore-induced exit from infected host cells with video microscopy (Fig. 2E). Thirty hours after infection, WT parasites responded rapidly to ionophore addition by initiating gliding motility (average 1.1 ± 0.7 min SD) and exiting from the parasitophorous vacuole (PV) shortly thereafter (1.4 ± 0.7 min). In contrast, *plp1ko* displayed a substantially delayed and temporally heterogeneous egress (6.3 ± 4.3 min), with many failing to egress within the 10-min observation time. This defect is not due to a failure to respond to ionophore because *plp1ko* parasites activated calcium-dependent motility within the PV at approximately the same time (1.9 ± 1.3 min) as WT parasites. Although WT tachyzoites registered little resistance in crossing the PVM during egress (movie S1), *plp1ko* parasites often demonstrated vigorous movement within the vacuole, prodding and deforming the limiting membrane (movie S2). Eventual escape appears to be the result of persistent gliding motility. Additionally, during attempted egress, some *plp1ko* vacuoles rounded up into spherical structures that resembled those seen following 48 hours of culture (movie S3). The complemented *plp1ko*/PLP1myc strain displayed an intermediate phenotype with motility activation (1.5 ± 1.7 min) similar to both WT and *plp1ko* and egress timing (3.2 ± 3.3 min) slower than WT yet significantly faster than *plp1ko*. The failure to fully restore the WT phenotype might be due to the subnormal TgPLP1 protein levels (Fig. 1B) or possible interference by the C-terminal epitope tag. This *plp1ko* egress phenotype was clearly distinct from the previously described calcium ionophore-response mutant MBE1.1 (21), which displayed a marked delay in motility activation (7.9 ± 2.8 min) but exited the vacuole shortly after becoming motile (8.3 ± 3.4 min).

Coinfection of host cells with *plp1ko* and WT parasites also restored normal egress of *plp1ko* (Fig. 2F and movie S4). After egress of an initial WT vacuole, *plp1ko* parasites egressed from the same infected host cell with a delay indistinguishable from parasites that were from an additional WT vacuole. No such complementation was seen in adjacent infected cells, which suggests the effect is local (fig. S5). This transfer of egress competency in coinfecting cells implies that TgPLP1 can act on both the luminal side of the PVM and the cytoplasmic side of a second vacuole. A specific role of TgPLP1 in this process is supported by the persistent egress delay in cells infected with multiple *plp1ko* vacuoles, even after parasites leaving

an initial *plp1ko* vacuole had released micronemal and PV contents into the host cytoplasm.

If TgPLP1 indeed facilitates egress by pore formation, then its secretion should result in permeabilization of the PVM and possibly the HPM. To test this, we treated cells at 30 hours after infection with cytochalasin D to disable parasite motility and then induced microneme secretion with ionophore treatment. To detect disruption of the HPM, we added the membrane-impermeant nuclear dye propidium iodide (PI) to the medium. After fixation and selective detergent permeabilization of the HPM and PVM, we stained for a soluble PV marker [*T. gondii* dense granule protein 1 (GRA1)] to monitor PVM permeabilization and a microneme protein [*T. gondii* subtilisin-like protease 1 (SUB1)] to detect microneme secretion. These three markers (PI, GRA1, and SUB1) enabled us to discern four distinct permeabilization stages in cells infected by WT parasites.

In stage 0, PI remained excluded from the host cell, GRA1 remained contained within the PV, and no SUB1 staining was observed, indicating that both the HPM and PVM were intact and that micronemes were not secreted (Fig. 3A). Progression to stage 1 was marked by the release of microneme proteins onto the parasite surface (Fig. 3A, inset) and disruption of the PVM as indicated by GRA1 staining diffusely throughout the host cell, yet the HPM remained intact and continued to exclude PI. By stage 2, the HPM became permeable to PI, as indicated by labeling of the host-cell nucleus. Nuclear labeling only occurred after GRA1 diffusion from the PV, never before, which suggests an inside-out disruption of the PVM first and the HPM second. The final stage (stage 3) was characterized by diffusion of SUB1 into the host-cell cytoplasm. Although PVM permeabilization was often (84.7%) observed in WT-infected cells, it was rarely (8.2%) seen in *plp1ko*-infected cells (Fig. 3B). Similarly, HPM permeabilization occurred in 73.0% of WT-infected cells and only 3.0% of *plp1ko*-infected cells. The *plp1ko*/PLP1myc complementation strain showed partial restoration of both GRA1 release from the PV (47.4%) and nuclear labeling (32.2%). Additionally, cells infected with *plp1ko* displayed a distinct labeling pattern (Fig. 3A, bottom row, second panel) not observed in either WT or *plp1ko*/PLP1myc, marked by microneme secretion without the concomitant release of the vacuolar contents (stage 1'), which again suggests that TgPLP1 is critical for PVM permeabilization, even when other microneme contents have been secreted.

By expressing the soluble fluorescent marker DsRed in the PV, we monitored PVM permeabilization in real time. After calcium ionophore addition, we observed a rapid redistribution of fluorescence from cytochalasin D-immobilized WT and *plp1ko*/PLP1myc vacuoles to the host-cell cytoplasm (Fig. 3, C and D, and movies S5 and S6). No such fluorescence release was ever observed from *plp1ko* vacuoles (Fig. 3, C and D, and movie S7) within the 10-min observation

window. These findings demonstrate that TgPLP1 is necessary to permit the escape of macromolecules from the PV, and also suggest that mechanical disruption of the PVM by gliding motility rather than a second pore-forming activity (for example, TgPLP2) is responsible for the residual egress of *plp1ko*.

Although deletion of *plp1* had no apparent effect on in vitro intracellular growth (fig. S6), in vivo studies revealed an attenuation of virulence greater than five orders of magnitude (Fig. 3E). Mice injected with 10 or more tachyzoites of WT or *plp1ko*/PLP1myc generally died within 15 days, but mice infected with up to 1 million *plp1ko* tachyzoites survived to the endpoint.

We propose that pore formation in the PVM weakens this membranous barrier to permit parasite escape and/or acts as a conduit for additional effector proteins that aid in egress. Also, an uncharacterized PLP expressed in malaria blood-stage parasites (22) may play a role analogous to TgPLP1 in parasite egress from infected erythrocytes.

References and Notes

1. I. Voskoboinik, M. J. Smyth, J. A. Trapani, *Nat. Rev. Immunol.* **6**, 940 (2006).
2. C. J. Rosado et al., *Science* **317**, 1548 (2007).
3. M. A. Haddad, D. X. Beringer, P. Gros, *Science* **317**, 1552 (2007).
4. R. K. Tweten, *Infect. Immun.* **73**, 6199 (2005).
5. C. P. Ponting, *Curr. Biol.* **9**, R911 (1999).
6. C. J. Rosado et al., *Cell. Microbiol.* **10**, 1765 (2008).
7. K. Kaiser et al., *Mol. Biochem. Parasitol.* **133**, 15 (2004).
8. J. G. Montoya, O. Liesenfeld, *Lancet* **363**, 1965 (2004).
9. K. Kim, L. M. Weiss, *Int. J. Parasitol.* **34**, 423 (2004).
10. M. E. Pipkin, J. Lieberman, *Curr. Opin. Immunol.* **19**, 301 (2007).
11. O. Shatursky et al., *Cell* **99**, 293 (1999).
12. S. J. Tilley, H. R. Saibil, *Curr. Opin. Struct. Biol.* **16**, 230 (2006).
13. R. B. Sutton et al., *Cell* **80**, 929 (1995).
14. J. D. Li, J. Carroll, D. J. Ellar, *Nature* **353**, 815 (1991).
15. Materials and methods are available as supporting material on Science Online.
16. See http://toxodb.org/toxo/showRecord.do?name=GeneRecordClasses.GeneRecordClass&project_id=ToxoDB&primary_key=59.m03629.
17. T. Ishino, Y. Chinzei, M. Yuda, *Cell. Microbiol.* **7**, 199 (2005).
18. A. Ecker et al., *Exp. Parasitol.* **116**, 504 (2007).
19. K. Kadota et al., *Proc. Natl. Acad. Sci. U.S.A.* **101**, 16310 (2004).
20. M. M. Mota et al., *Science* **291**, 141 (2001).
21. M. Black, G. Arrizabalaga, J. Boothroyd, *Mol. Cell. Biol.* **20**, 9399 (2000).
22. L. Florens et al., *Nature* **419**, 520 (2002).
23. We thank T. Schultz, S. Meshinchi, A. Silva, E. Mastrantonio, and C. Pereira for technical assistance; D. Roos and F. Dzierszinski for reagents; G. Zeiner for help with the HA-tagging; and M.-H. Huynh, L.D. Sibley, J. Swanson, and M. O'Riordan for valuable discussion and input. This work was supported by NIH grant R01 AI46675 and a predoctoral fellowship by the American Heart Association. TgPLP1 GenBank accession number is EF102772.

Supporting Online Material

www.sciencemag.org/cgi/content/full/1165740/DC1
Materials and Methods
Figs. S1 to S6
Movies S1 to S7
References

10 September 2008; accepted 17 November 2008
Published online 18 December 2008;
10.1126/science.1165740
Include this information when citing this paper.

New Products

**X-Ray Area Detectors**

The High Efficiency (HE) series X-ray area detectors feature back-illuminated charge-coupled devices (CCD) permanently bonded to the fiber optic tapers. They produce high-resolution, low-noise images over a wide range of X-ray energies, but with higher electrooptical gain due to the backlit CCD technology. A baseline stabilization option is standard. X-rays are converted to light by a scintillator layer at the front of the fiber optic taper array, which travels through the fiber optic tapers to the back-thinned CCD devices.

Rayonix

For information 877-627-9729

www.rayonix.com

SAM Methyltransferase Assay

The SAM510: SAM Methyltransferase Assay is a colorimetric, continuous enzyme-coupled assay for the kinetic analysis of protein S-adenosylmethionine (SAM) methyltransferase enzymes with no radioactive labels. The assay involves the removal of the methyl group from SAM-generating S-adenosylhomocysteine, which is rapidly converted to S-ribosylhomocysteine and adenine by the included adenosylhomocysteine nucleosidase. Finally, the adenine is converted to hypoxanthine by adenine deaminase, which in turn is converted to urate and hydrogen peroxide. The rate of production is measured with a colorimetric assay by an increase in absorbance at 510 nm.

G-Biosciences/Genotech

For information 314-991-6034

www.GBiosciences.com

Syringe Filters

The 33-mm Millex syringe filters with Millipore Express Plus membranes are now available in 0.22- μ m and 0.45- μ m pore sizes. They deliver fast filtration rates with low protein-binding properties. With 20 percent more surface area than standard 25-mm devices, the new filters offer a high process volume (200 ml) and burst strength (150 psig), allowing for high operating pressure. Without the risk of filters bursting or clogging, researchers need not use multiple filters per sample or worry about incomplete filtration. Because 33-mm filters have a low hold-up volume, there is minimal sample loss during filtration. The low-protein-binding membrane allows maximum recovery of soluble proteins, such as serum components typically added to cell culture media, for reproducible cell growth and better downstream results.

Millipore

For information 800-548-7853

www.millipore.com

Absorbent Protective Paper

BenchGuard is a highly absorbent paper for protecting benches and surfaces against liquid spills. It has a strong polyethylene coating on one side and when placed paper side up it quickly absorbs hazardous spills, protecting the benchtop and reducing contamination risks. BenchGuard is available in two absorbencies: 400 ml per cubic meter and 800 ml per cubic meter. It is offered in packs of 50 or 100 sheets and in roll form. It is applicable for use in various laboratories, includ-

ing life sciences, microbiology, radiochemistry, and animal research. Sterilin

For information +44-(0)-844-844-3737

www.sterilin.co.uk

Liquid Handling Robot

The Cavro Omni Robot is a general-purpose, original-equipment-manufacturing liquid-handling robot for a wide range of applications in clinical diagnostics, life sciences, and analytical chemistry. Easy to install and operate, the Omni Robot features a modular design that allows it to be configured for many different uses. Its closed-loop positioning system provides the assurance of knowing exactly where the pipetting probe is located at all times, while its high payload opens up a broad range of capabilities. All working parts are hidden to provide a finished appearance. Using the Cavro Integration Kit, any Tecan Cavro pump or robot can be set up for evaluation in a matter of minutes.

Tecan

For information +41-44-922-8111

www.tecan.com

Imaging Microscope

The Nicolet iN10 MX infrared imaging microscope enables analysts to quickly determine the identity and distribution of chemical species within complex structures and random mixtures on a microscopic scale. It performs rapid and accurate analysis of materials ranging from forensic evidence to high-tech polymer composites. The instrument's software guides the operator through the entire analytical process, from sample loading to final reporting, in a few mouse clicks. It combines machine vision and spectral identification technology to greatly facilitate data acquisition and sample analysis. Its optical efficiency allows chemical images to be generated from highly scattering samples. The system can be equipped with up to three detectors. A room-temperature detector allows point-and-shoot analysis to be performed without liquid nitrogen. This detector can be combined with an efficient slide-on attenuated-total-reflectance sampling device to make the Nicolet iN10 MX as quick and easy to use as a basic infrared spectrometer.

Thermo Fisher Scientific

For information 800-532-4752

www.thermo.com/FT-IR

Electronically submit your new product description or product literature information! Go to www.sciencemag.org/products/newproducts.dtl for more information.

Newly offered instrumentation, apparatus, and laboratory materials of interest to researchers in all disciplines in academic, industrial, and governmental organizations are featured in this space. Emphasis is given to purpose, chief characteristics, and availability of products and materials. Endorsement by *Science* or AAAS of any products or materials mentioned is not implied. Additional information may be obtained from the manufacturer or supplier.

Connecting you
to the world of...
Science

Science Careers
Classified Advertising

For full advertising details, go to ScienceCareers.org and click **For Advertisers**, or call one of our representatives.

UNITED STATES & CANADA

E-mail: advertise@sciencecareers.org
Fax: 202-289-6742

Joribah Able
Industry - US & Canada
Phone: 202-326-6572

Alexis Fleming
Northeast Academic
Phone: 202-326-6578

Tina Burks
Southeast Academic
Phone: 202-326-6577

Daryl Anderson
Midwest/Canada Academic
Phone: 202-326-6543

Nicholas Hintibidze
West Academic
Phone: 202-326-6533

EUROPE & INTERNATIONAL

E-mail: ads@science-int.co.uk
Fax: +44 (0) 1223 326532

Tracy Holmes
Associate Director, Science Careers
Phone: +44 (0) 1223 326525

Alex Palmer
Phone: +44 (0) 1223 326527

Dan Pennington
Phone: +44 (0) 1223 326517

Susanne Kharraz Tavakol
Phone: +44 (0) 1223 326529

Louise Moore
Phone: +44 (0) 1223 326528

JAPAN

Mashy Yoshikawa
Phone: +81 (0) 3 3235 5961
E-mail: myoshikawa@aaas.org

To subscribe to *Science*:
In US/Canada call 202-326-6417 or 1-800-731-4939.
In the rest of the world call +44 (0) 1223 326515.

Science makes every effort to screen its ads for offensive and/or discriminatory language in accordance with US and non-US law. Since we are an international journal, you may see ads from non-US countries that request applications from specific demographic groups. Since US law does not apply to other countries we try to accommodate recruiting practices of other countries. However, we encourage our readers to alert us to any ads that they feel are discriminatory or offensive.

Science Careers

From the journal *Science* 

POSITIONS OPEN

**MOLECULAR GENETICS RESEARCH
ASSOCIATE/INSTRUCTOR POSITION**
Functional Genetics at Brigham and Women's Hospital

A Research Associate or Instructor position in functional genetics is available beginning March 1, 2009, at the Channing Laboratory and the Pulmonary Division and the Respiratory Genetics Research Center of the Brigham and Women's Hospital. The Research Associate/Instructor will be responsible for functional evaluation of disease-associated sequence variants identified from integrative genomic and genome-wide association studies in asthma, chronic obstructive pulmonary disease (COPD), and other disorders of the respiratory system. Specific responsibilities will include design and execution of studies to characterize the functional properties of disease-related variants, to supervise laboratory technicians assisting with these studies, and to assist faculty in the training of doctoral and postdoctoral researchers in these methods.

Requirements: (1.) Applicants must have a Ph.D. degree or the equivalent in hand and be eligible for employment in the United States (citizenship, residency, or work visa). (2.) At least two years of full-time postdoctoral training. (3.) Laboratory skills and prior work experience must include proficiency with molecular and cellular biology techniques, including cell culture, overexpression studies (including reporter assay construction and viral transfection and transduction studies), nuclear protein extraction and gel retardation assays, gene cloning, siRNA gene silencing, and characterization of differential splicing patterns.

Preference will be given to candidates with additional experience with allelic imbalance assays.

Interested applicants are instructed to provide curriculum vitae via e-mail, and arrange two letters of reference, which should be addressed to the following:

Scott T. Weiss, M.D., M.S.
Professor of Medicine
Channing Laboratory
Brigham and Women's Hospital
181 Longwood Avenue
Boston, MA 02115
Telephone: 617-525-2278; fax: 617-525-0958
E-mail: scott.weiss@channing.harvard.edu

Augustine M. Choi, M.D.
Parker Francis Professor
Chief, Pulmonary and Critical Care Medicine
Brigham and Women's Hospital
75 Francis Street
Boston, MA 02115

Edwin K. Silverman, M.D., Ph.D.
Associate Professor of Medicine
Channing Laboratory
Brigham and Women's Hospital
181 Longwood Avenue
Boston, MA 02115

Brigham and Women's Hospital and Harvard Medical School are Equal Opportunity Employers and strongly encourage application from women and minority candidates.

**POSTDOCTORAL NEUROIMMUNOLOGY
RESEARCH FELLOWSHIP**
University of California, San Francisco

A Research Fellowship opportunity is available in a neuroimmunology laboratory to work on human T cell and B cell immune responses to central nervous system (CNS) autoantigens in neuromyelitis optica (NMO), a CNS demyelinating disease. Studies involve cellular immunology and molecular biology. Fellow will work under the direct guidance of **Dr. Zamvil** and his team. Salary support is available for two years, although applicant will be supported in obtaining competitive three-year fellowship funding. Send curriculum vitae and statement of research interests by e-mail or mail to:

Scott S. Zamvil, M.D., Ph.D.
Department of Neurology
University of California, San Francisco
513 Parnassus Avenue, S-268
San Francisco, CA 94143
E-mail: zamvil@ucsf.neuroimmunol.org

POSITIONS OPEN



The U.S. Department of Agriculture, Agricultural Research Service, Pacific Basin Agriculture Research Center, Hilo, Hawaii, invites applications for an **INTERDISCIPLINARY RESEARCH SCIENTIST** position (**GENETICIST/ENTOMOLOGIST/MOLECULAR BIOLOGIST, GENOMICS**) GS-12/13/14 (\$59,383.00 to \$108,483.00 plus 18 percent cost of living allowance per annum). A scientist is needed to conduct research to identify, develop, and implement environmentally acceptable and sustainable strategies for management of tropical insect pests in support of Hawaii, the Pacific Basin, and U.S. agriculture. You will develop and lead fundamental research on the genomics of fruit flies, in particular the oriental fruit fly. (Announcement ARS-X9W-0054.) The ideal candidate has experience in initiating, organizing, and leading an insect genome project. This is a competitive, permanent appointment and U.S. citizenship is required. Vacancy announcements and where to apply can be found at website: <http://www.afm.ars.usda.gov/hrd/jobs/index.htm#vacancy>. Closing date for applications is February 20, 2009. For more detailed information on this listing, please contact **Dr. Eric Jang**, telephone: 808-959-4340 or e-mail: eric.jang@ars.usda.gov. The USDA is an Equal Opportunity Provider and Employer.

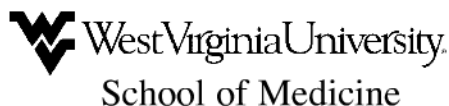
**POSTDOCTORAL POSITIONS in
BIOMOLECULAR NETWORKS**

Two NIH-funded Postdoctoral positions are immediately available for recent graduates holding a Ph.D. in the biological sciences to work on the role of G protein-coupled receptor (GPCR)-associated proteins on GPCR signaling and trafficking. For examples of recent projects, see: *J. Biol. Chem.* **282**:5085-99, 2007 and **281**:33537-53, 2006. One position is open to candidates with experience in cell biological techniques including confocal/fluorescence resonance energy transfer microscopy, immunohistochemistry, intracellular trafficking, and co-immunoprecipitation. The second position is for candidates with expertise in myocardial cell biology of rats or transgenic mice including culture of neonatal heart cells, transgene analyses by real time polymerase chain reaction, transfection with adeno and lentiviral vectors, and other relevant cardiovascular techniques. Please forward a cover letter, curriculum vitae, and the names of three references to: **Suleiman Bahouth, Ph.D., The University of Tennessee Health Science Center, Department of Pharmacology, 874 Union Avenue, Memphis, TN 38163**, or via e-mail: sbahouth@utmem.edu.

The University of Tennessee is an Affirmative Action, Equal Opportunity Employer.

The Biology Department at Missouri State University anticipates an August 2009 opening for an **ASSISTANT PROFESSOR** with a specialty in animal physiology. For a full position description and to apply online go to website: <http://www.missouristate.edu/academicopenings>. Letter of application, curriculum vitae, statement of teaching experience and interests, research plan, transcript copies, and names and addresses for three to five references can be uploaded electronically. For additional information contact: **Paul Durham, Department of Biology, Missouri State University, Springfield, MO 65897**. Employment will require a criminal background check at University expense. Equal Opportunity/Affirmative Action.

Employment Opportunities



Open Rank Faculty Research Positions

The Department of Pediatrics of the West Virginia University School of Medicine is experiencing considerable expansion and in summer of 2009 will open the **WVU Pediatric Research Institute**. This new center of excellence will focus on childhood obesity, diabetes and asthma, with emphasis on perinatal exposures that relate to the early origins of disease. Within this context, investigators with interest and expertise in the following areas are particularly encouraged to apply for faculty appointments: 1. Genomics and epigenomics of environmental diseases; 2. Lung development and organogenesis; 3. Stem cell approaches in cardiovascular and respiratory diseases; 4. Pediatric clinical and translational research; and 5. Epidemiology of cardiovascular, respiratory and environmental diseases.

In addition to holding a Ph.D. and/or MD degree, ideal candidates should have outstanding research credentials, keen interest in mentoring graduate students and postdoctoral fellows, genuine desire to participate in collaborative research efforts, and strong motivation for an academic career. Faculty appointed at the Assistant Professor level are expected to achieve NIH funding within 3-4 years. Faculty appointed at the Associate or Full Professor level are expected to have current NIH funding. Starting funds are available from over \$12 million in new endowments and will be used primarily to hire research scholars, who along with the existing team of investigators will create an integrated infrastructure where interactions among the varied research teams can be encouraged and supported. Currently, about 60% of the WVU Department of Pediatrics faculty are actively engaged in research using more than 16,500 sq. ft. of space, and grant dollars awarded to pediatric research at WVU has doubled in the past 2 years. The new Institute will occupy a 3-floor classroom and laboratory building on the Health Sciences Campus.

WVU is a comprehensive, land grant, Carnegie-designated Doctoral Research/Extensive public institution, with approximately 22,000 undergraduates plus 5,500 graduate and professional students. If interested, submit curriculum vitae with list of references to the Chair of the Search Committee:

Laura F. Gibson, Ph.D.

**Vice-Chair of Research, Department of Pediatrics
c/o Laura Blake, Director, Professional Recruitment
Phone: (304) 293-6135, Fax: (304) 293-0230
Email: blakel@wvuh.com**

Additional information about research and graduate education at the WVU Health Sciences Center is available online at

www.hsc.wvu.edu/som/resoff/index.asp

WVU is an AA/EOE Employer. Minorities, persons with disabilities and women are encouraged to apply.



UCL Research Department of Structural and Molecular Biology

Lectureship in Biomolecular NMR Spectroscopy

The Institute for Structural and Molecular Biology (ISMB) is seeking applications to fill a lectureship in the field of biomolecular nuclear magnetic resonance spectroscopy.

We particularly want to recruit an outstanding individual who is capable of developing world-class, interdisciplinary research in the structural molecular biology of cell signalling, metabolic regulation, molecular cell biology and molecular microbiology. The successful applicant will also be expected to make an appropriate contribution to the affiliated departmental portfolios of graduate and undergraduate teaching. A PhD and postdoctoral experience in the field of Structural and Molecular Biology is essential.

The ISMB (www.ismb.lon.ac.uk) is a centre of excellence, which jointly consists of the School of Crystallography at Birkbeck College and the Research Department of Structural & Molecular Biology at University College London (UCL). It was established to foster closer links between the two departments and also to provide a bridge with the Department of Chemistry at UCL. The Institute provides a scientific environment conducive to world-class research in the field of biomolecular science. Work at the Institute seeks to integrate the chemical and physical sciences to reveal the molecular basis of protein function. The ISMB also seeks to exploit the knowledge of protein function to further our understanding of human diseases.

The salary that is offered for this appointment will be within either the University Lecturer A range (£35,239 – £38,250 pa, inclusive of £2,781 pa London Allowance) or Lecturer B range (£39,313 – £46,403 pa, inclusive of £2,781 pa London Allowance), according to experience. Further details can be found at www.ismb.lon.ac.uk/JD1NMR.html and at the respective departmental web sites (<http://www.biochem.ucl.ac.uk/> and <http://www.cryst.bbk.ac.uk/>).

Applicants should send their CV and names and addresses of three referees to Ms Emily Bellshaw, Executive Officer, Research Department of Structural & Molecular Biology, Division of Biosciences, University College London, Gower Street, London, WC1E 6BT, UK. CVs should contain an account of the applicant's current research activities together with a plan of future research intentions. Please also provide details requested at http://www.ucl.ac.uk/hr/docs/download_forms/recruitment_selection_1.doc (Information Sheet and Equal Opportunities Information).

The Head of the ISMB, the UCL Research Department of Structural and Molecular Biology and of the Birkbeck School of Crystallography is Professor Gabriel Waksman. He can be contacted informally for general information (email: g.waksman@ucl.ac.uk or g.waksman@bbk.ac.uk).

Closing date: 15th March 2009.

UCL Taking Action for Equality.



**Department of Health and Human Services
National Institutes of Health
National Institute on Alcohol Abuse and Alcoholism**

Tenure-Track Investigator Position Available

The National Institute on Alcohol Abuse and Alcoholism (NIAAA), a major research component of the National Institutes of Health (NIH) and the Department of Health and Human Services (DHHS), is recruiting for a tenure-track Investigator to establish and direct an independent research program in the area of comparative behavioral genomics in the Laboratory of Neurogenetics (LNG), Division of Intramural Clinical and Biological Research (DICBR), NIAAA.

The selected candidate will be expected to establish an independent research program that examines how genetic and environmental factors relate to intra- and inter-specific variation in traits that, in humans, are known risk factors for alcohol use disorders (i.e., stress reactivity, behavioral dyscontrol, reward seeking/sensitivity). Candidates must hold a Ph.D., M.D. or equivalent degree. Criteria for selection will include: a strong publication record in the field of genetics/genomics, demonstrated experience using animal models of human psychiatric disorders or addictions, demonstrated success in establishing and maintaining collaborations and demonstrated success in leading and mentoring research staff at various levels (i.e., postdoctoral fellows, research associates, and/or technicians).

Resources provided to the selected candidate include laboratory and core laboratory facilities, office space, personnel and an operating budget sufficient to develop this independent research program.

Interested candidates wishing to be considered for this position may submit a curriculum vitae, bibliography, the names and addresses of three references, and a brief proposal that reflects the applicant's research interests/goals and an approach for establishing an independent research program, by the closing date to Ms. Patricia Scullion at address below. *Note – we encourage you to submit your complete application electronically so that we may confirm receipt of your materials. **Chair, Search Committee, c/o Ms. Patricia Scullion, National Institute on Alcohol Abuse & Alcoholism (NIAAA), NIH, c/o Ms. Patricia Scullion, 5635 Fishers Lane, Room 2023, Bethesda, MD 20892*, *For Federal Express delivery, Rockville, MD 20852, or Submit Via Secure Email to: LNGRecruit@mail.nih.gov. *NOTE – This is a re-advertisement due to technical problems experienced with receipt of applications**

The closing date for receipt of applications is February 27, 2009

The NIH encourages the application and nomination of qualified women, minorities and individuals with disabilities. DHHS and NIH are Equal Opportunity Employers.



**DEPARTMENT OF HEALTH AND HUMAN SERVICES
NATIONAL INSTITUTES OF HEALTH (NIH)
Director, Division of Extramural Activities
National Institute of Nursing Research (NINR)**

The Department of Health and Human Services (DHHS) and the National Institutes of Health (NIH) are seeking exceptional, creative candidates for the position of Director, Division of Extramural Activities (DEA), National Institute of Nursing Research (NINR), to advance the Institute's complex mission.

The NINR fosters, conducts, supports, and administers research and research training programs directed at promoting the growth and quality of research related to nursing, health care, and the related biomedical and behavioral sciences, as well as expanding the pool of scientists needed to conduct research related to the mission of NINR through research grants, contracts, cooperative agreements, and individual and institutional research training awards.

The Division of Extramural Activities is responsible for the development of proposals for new research initiatives and for the management and oversight of research grants, contracts, training, and fellowship awards that support nursing research activities and ensure effective utilization of available resources to attain program objectives.

The Extramural Division Director is the principal advisor to the NINR Director on all extramural research and program activities within the Division, which is the largest organizational component with the highest percentage of the budget. The Extramural Director is responsible for the development, implementation, and oversight of a broad research portfolio, both nationally and internationally. These responsibilities include exercising scientific and managerial leadership in planning, organizing, implementing, coordinating, directing, reviewing, and evaluating NINR's extramural research programs, such as project grants, center grants, training grants, small business awards, and other mechanisms. Applying a broad strategic vision, the Extramural Director advances the NINR's goals and objectives by leading the development of new research priorities and seeking opportunities for research partnerships with other federal and non-federal organizations.

The Extramural Director is responsible for the overall management of the extramural scientific programs, the grants management staff, and the scientific merit review system. This individual maintains a productive work environment, fosters workplace diversity and serves as one of the top five senior staff on the Institute. The Extramural Director is involved in strategic planning, priority setting and plays an integral role in shaping the vision and direction of the NINR. For information on NINR's programs, applicants may browse the NINR Home Page: <http://ninr.nih.gov/>

Applicants must possess a Ph.D. or doctoral degree equivalent in health or allied sciences relevant to the position, senior level research experience, and expertise in scientific, clinical or public health research administration that includes grants and contract development, as well as budget formulation and managerial skills. Applicants must be able to plan, implement and direct research programs of national and international importance; have the ability to communicate with, and obtain cooperation from outside organizations and individuals who represent wide-ranging views and competing priorities. Salary is commensurate with qualifications and experience. Full Federal benefits include leave, health and life insurance, long-term care insurance, retirement, and a savings plan (401K equivalent). Qualified individuals are encouraged to e-mail a CV, bibliography, a list of three references, and a cover letter outlining their relevant experience to: **Ms. Ana M. Ferreira, ferreim@mail.gov, NINR/DEA Search Committee. Application Deadline: March 31, 2009.** E-mail receipt of applications and inquiries is preferred however, candidates needing reasonable accommodation may fax the application materials to 301-480-4969. The NIH encourages applications and nominations from women, minorities, and individuals with disabilities.



**The National Human Genome Research Institute
National Institutes of Health
Department of Health and Human Services**

DIRECTOR

The Office of the Director, National Institutes of Health (NIH), is seeking exceptional candidates for the position of Director, National Human Genome Research Institute (NHGRI). The incumbent serves as the leader to an organization which conducts and supports pioneering approaches to biomedical and behavioral research in genetics and genomics to advance scientific understanding of diseases affecting public health today. The organization plays an additional role in the dissemination of genomic research findings to health professionals and the public; the study of the ethical, legal and social implications of genome research and the support of training programs for young investigators. The Director, NHGRI, provides overall leadership for the research portfolio; sets Institute policies; develops scientific, fiscal, and management strategies to oversee the research portfolio; and coordinates genomics research initiatives for the NIH with other Federal, private, and international programs. In addition, the Institute supports international meetings, workshops, and other activities essential to the efficient international coordination and exchange of genomics data within the global research community.

Applicants must possess an M.D., Ph.D., or a comparable degree in the health sciences field, plus senior-level experience and outstanding scientific knowledge of research programs in one or more scientific areas related to genetics or molecular biology and demonstrated expertise in policy development regarding genetic research and the ethical, legal, and social implications of such research. Salary is commensurate with experience, and a full package of benefits (including retirement, health and life insurance, long-term care insurance, Thrift Savings Plan participation, etc.) is available. A detailed vacancy announcement, along with mandatory qualifications and application procedures, can be obtained via NIH's Executive Jobs website: <http://www.jobs.nih.gov/vacancies/executive.htm>. Questions on application procedures may be addressed to Regina Reiter at (301) 402-1130. CV, bibliography, and a statement addressing the qualifications requirements must be received by close of business **April 16, 2009**.

DHHS and NIH are Equal Opportunity Employers



The University of Maryland School of Medicine Institute of Human Virology, in conjunction with the Marlene and Stewart Greenbaum Cancer Center, is recruiting a highly qualified **tenure track assistant or associate professor** in the field of viral oncology and AIDS-related malignancies, including investigators interested in the search for novel, human tumor viruses. The new laboratory will be a component in the growing program on HIV and Cancer and will interact with ongoing efforts in our clinical and epidemiology divisions, including the study of cancers from developing countries.

The Institute of Human Virology offers excellent laboratory facilities, competitive salary and startup packages, and access to numerous core facilities including state-of-the-art BSL3 and ABSL3 facilities in a strong academic environment. Preference will be given to candidates with established research programs and current NIH funding. The level of appointment will be commensurate with the candidate's experience.

Please submit a letter of interest, CV and three references to:

Viral Oncology Faculty Search Committee
c/o Beth Peterson
Institute of Human Virology
725 West Lombard Street, S307
Baltimore, MD 21201
bpeterson@ihv.umaryland.edu

*The University of Maryland, Baltimore is an
Equal Opportunity, Affirmative Action Employer.*

**Faculty Position in
Microbial Pathogenesis
and Immunity**



**Department of Microbiology and Immunology
Tulane University School of Medicine**

The Department of Microbiology and Immunology, Tulane University School of Medicine is recruiting a tenure-track faculty member at the rank of Assistant, Associate or Full Professor. We are primarily interested in investigators whose research complements existing strengths in host-pathogen interaction and vaccine development. The successful candidate will join a multidisciplinary department focusing on molecular, cellular, and genetic aspects of infectious disease and host-pathogen interactions. He/she will be expected to maintain an independent and dynamic, funded research program and to contribute to the teaching of medical and graduate students.

The Department of Microbiology and Immunology offers a competitive salary, attractive start-up packages, renovated laboratory space, BSL-3 and select agent laboratories, and an interactive environment. For further information about the Department and Tulane University School of Medicine visit our website at <http://www.microbiology.tulane.edu>.

Applicants should submit a curriculum vitae, a statement of research interests, and the names, addresses, email addresses, and telephone numbers of three qualified references to: **Faculty Search Committee, Department of Microbiology and Immunology, Tulane University School of Medicine, 1430 Tulane Avenue SL-38, New Orleans, LA 70112** or email to **Ms. Amy Pick (aepick@tulane.edu)**. Review of applications will begin immediately and continue until the position is filled.

*Tulane University is an Equal Opportunity, Affirmative Action
Employer. Women, Minorities and Veterans are encouraged to apply.*

TUFTS UNIVERSITY SCHOOL OF MEDICINE

**Chair - Department of Molecular
Biology and Microbiology**

Tufts University School of Medicine invites applications for Professor and Chair of the Department of Molecular Biology and Microbiology. The candidate should have a Ph.D. or an M.D. and be an internationally recognized scientist in microbiology with an outstanding and well-funded research program. The candidate should also have a track record of institutional service, group leadership and participation in the mentorship of junior faculty.


Tufts University School of Medicine has a distinguished record of training some of the leading physicians and scientists in the U.S. The Department of Molecular Biology and Microbiology has a particularly outstanding and distinguished history of excellence in research and training. A notable strength of the Department is the atmosphere of cooperation and collegiality that prevails at all levels. Faculty members are well funded by both federal and private sources, including Gates Foundation awards and Howard Hughes Medical Institute investigatorships. The Department occupies contiguous space in the recently built Jaharis Center for Biomedical Sciences and the adjoining buildings of the M&V Research Complex. A variety of core facilities serve to greatly enhance the research environment. The Molecular Microbiology Graduate Program based in the Department is vigorous and is funded by two training grants. This Chair position provides an exciting opportunity to lead and further build an already distinguished department.

Please send a curriculum vitae, statement of research funding, and the names of at least three references to:

Henry H. Wortis, M.D., Chair, Search Committee,
c/o Mary Broderick, Medical Deans Office, Tufts University
School of Medicine, 136 Harrison Ave., Boston, MA 02111

Tufts University is an AA/EEO employer and actively seeks candidates from diverse backgrounds.





How can you translate Oncology Research into life-changing drug discovery?

As a part of Pfizer's newly formed Oncology Research team, you have the distinct opportunity to help enhance our ability to achieve the key strategies important in the discovery and development of novel oncology therapeutics.

Located in La Jolla, CA, the Research Unit is the very center of Pfizer's research and development strategies in oncology. Our core philosophy is simple: to establish and maintain expertise in cancer drug discovery. With this mindset, we create focused groups that specialize in specific cancer indications, such as lung and colon, and we are dedicated to becoming experts in the utilization of "omic" technologies to drive our target discovery, drug discovery, translational research and development strategies.

We now have open positions in our Oncology Research Unit that will enhance our ability to perform translational research on a broad and extensive portfolio, to integrate clinical genomics into our drug discovery and development efforts, and to get the right drug to the right patient at the right time. Openings range from Director and Senior Group Leader to Associate Scientist level. Candidates with cancer biology expertise and one or more of the following skill sets are being sought: molecular classification of cancer subtypes, cancer genetics, functional genomics, integrative omics, genetically engineered mouse models, development of specialized cancer cell models, cancer stem cells, molecular pathology, biomarker discovery/validation, target identification/validation, novel therapeutic modalities, translational research. All these skills are considered an integral part of advancing our mission and shaping the future of oncology research.

Join our leading cancer biologists and help us continue in our quest to revolutionize drug discovery.

To view all of our positions and to apply, visit www.pfizer.com/careers and **search keyword Oncology**.

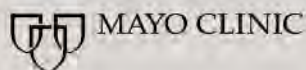
We are proud to be an equal opportunity employer and welcome applications from people with different experiences, backgrounds and ethnic origins.



Encompassing approximately 5,718 acres along the western edge of the north coastal region of the City of San Diego, La Jolla's idyllic beauty and stunning scenery is physically defined by a rugged coastline of ocean bluffs and beaches together with steep canyons and hillsides that culminate at Mount Soledad. And right in the center of it all is **Pfizer La Jolla**.



Working together for a healthier world™



Heal the sick, advance the science, share the knowledge.

Molecular Imaging in Psychiatry

Mayo Clinic in Rochester, MN, seeks an exceptional mid-career or senior investigator to join psychiatric researchers at Mayo Clinic and the University of Minnesota. The Mayo Clinic and University of Minnesota have created a partnership that has been designed to provide a unique opportunity to establish a clinical neuroscience corridor linking the two institutions. The Mayo Clinic Department of Psychiatry has developed a major program in genomics that is supported by the NIGMS Pharmacogenomics Research network. The University of Minnesota Department of Psychiatry, in partnership with others, has developed a world-class psychiatric brain-imaging program. We are seeking an established investigator who will be able to promote the scientific collaboration between the two programs.

Focusing on understanding the biological basis of psychiatric disease, the incumbent will lead development of ground-breaking molecular techniques that can be evaluated in preclinical and early clinical trials for their potential in diagnosis and treatment. This position has access to cutting-edge molecular technology facilities, plus a clinical patient population primarily being treated for schizophrenia, bipolar disorder and substance abuse. Candidates must have a PhD, MD/PhD or MD degree with national or international recognition, rank of associate professor or full professor, and a track record of NIH or similar grant funding. At Mayo Clinic, you'll enjoy highly competitive pay and benefits, and impressive resources for your research, as well as ample opportunity for multidisciplinary collaboration.

To learn more about Mayo Clinic and Rochester, visit www.mayoclinic.org/scientist-jobs

Please direct inquiries and CV with letter of interest to:
David Mrazek, MD, Chair
Department of Psychiatry and Psychology
Mayo Clinic
200 First Street SW • Rochester, MN 55905

Mayo Foundation is an affirmative action and equal opportunity employer and educator. Post-offer/pre-employment drug screening is required.



Eidgenössische Technische Hochschule Zürich
Swiss Federal Institute of Technology Zurich

Professor of Translational Nutrition Biology

The Department of Agricultural and Food Sciences (www.agrl.ethz.ch) at ETH Zurich invites applications for the position of a professor in Translational Nutrition Biology. The professor will be responsible for developing a leading research and teaching program in translational nutrition biology, using an integrative approach to investigate the complex effects of nutrients on the organism, from the genetic and molecular through the cellular to the systemic levels. Candidates with interest in molecular nutrition are especially encouraged to apply. The professorship's main research topics may include:

- Nutrient-gene interactions
- Nutrition and metabolomics
- Nutrient neuroendocrine interactions
- Nutrition and health
- Nutritional factors in the development of obesity and its co-morbidities (e.g., type II diabetes and cardiovascular diseases)

The professorship comes with several salary lines for academic and technical assistants, as well as access to excellent experimental animal facilities and to the Functional Genomics Centre of ETH and the University of Zurich. Moreover, the position is expected to be an integral part of the emerging research focus «Food, Nutrition, and Health» at ETH Zurich. The successful candidate will be expected to teach undergraduate level courses (German or English) and graduate level courses (English) covering basic and advanced nutrition physiology.

Please submit your application together with a curriculum vitae and a list of publications and projects to the **President of ETH Zurich, Prof. Dr. R. Eichler, ETH Zurich, Raemistrasse 101, 8092 Zurich, Switzerland, no later than March 31, 2009**. With a view toward increasing the number of female professors, ETH Zurich specifically encourages qualified female candidates to apply.



www.ox.ac.uk/jobs

University Lecturer in Zoology

Mathematical, Physical and Life Sciences Division

Department of Zoology in association with
St John's College

Reference Number AT09004

The Department of Zoology proposes to appoint a University Lecturer with effect from 1 September 2009 or as soon as possible thereafter. The successful candidate will be offered an Official Fellowship at St John's College, under arrangements described in the further particulars. The combined University and College salary will be on a scale up to £56,917 per annum.

Preference will be given to applicants working on an aspect of vertebrate diversity. The appointee will be required to engage in research, which will contribute to the Department's research reputation; to teach, supervise and examine undergraduate and graduate students; and to contribute to administration in the College and Department.

Further particulars, containing details of the application procedure and of the duties, may be obtained from Mrs Sally Burton, University of Oxford, Department of Zoology, Tinbergen Building, South Parks Road, Oxford OX1 3PS, email: Sally.Burton@zoo.ox.ac.uk quoting reference AT09004 or by visiting <http://www.zoo.ox.ac.uk/jobs/adverts/at09004pdf>. The closing date for applications is midday on Friday 27 February 2009.

Committed to equality and valuing diversity

MEETINGS

- Biosphere 09

The International Conference on Biodiversity Informatics
1-3 June, 2009 London, England

Two Challenges to the Biodiversity Community

- How much faster can taxonomists describe the millions of undiscovered species? Can a new species be formally described and documented during a three-day conference?
- What will users of biodiversity information need in the coming years? What new databases and analytical capabilities should be developed?

The organizers of e-Biosphere 09 have organized an online collaboration system at www.e-biosphere09.org for the communities of biodiversity researchers and users of biodiversity information. In the months leading up to the conference, we challenge you to:

- Form online communities of biodiversity researchers, database and software developers, and users
- Explore these questions and develop Position Papers
- Develop plans to describe, document, publish a new species and related data, and create an Encyclopedia of Life species page during the conference
- Select Discussion Group leaders for the conference
- Develop plans to demonstrate databases and software during the conference, and
- Organize side-events that will take place during the conference

Registration now open!

Visit www.e-Biosphere09.org for more information

Senior Staff Scientist – Ref: 80276

The Wellcome Trust Sanger Institute is a world leader in genomic research, with an expanding scientific programme dedicated to understanding gene function in health & disease.

The Cancer Genome Project at the Wellcome Trust Sanger Institute has led the way in the systematic analysis of cancer genomes by using the human genome sequence and high throughput mutation detection techniques to identify somatically acquired sequence variants/mutations and hence identify genes critical in the development of human cancers. We are seeking to appoint a Senior Staff Scientist to lead a new project, funded in the first instance for five years, in the discovery of drug sensitising genotypes in human cancers. This will be a major collaboration between the Wellcome Trust Sanger Institute and Massachusetts General Hospital, Boston which aims to expose 1000 cancer cell lines to several hundred potential anti-cancer drugs, with the goal of identifying genetic and genomic determinants of anti-cancer drug response that will inform clinical trials and patient treatment. The Senior Staff Scientist, who will lead a team of approximately eight people, should be a dynamic, highly experienced postdoctoral scientist, capable of managing both the staff and the project with a high degree of independence.

Essential Skills: Experience of liquid handling robotics, tracking/sample databases and large-scale data handling/analyses are required. The successful applicant will be expected to establish and maintain key collaborations with Massachusetts General Hospital in order to achieve the objectives of the project and as such have excellent written, verbal, people management and problem solving skills.

Ideal Skills: Expertise in running high-throughput assays and high-throughput tissue culture would be ideal.

Benefits: We offer a comprehensive range of benefits including a final salary pension scheme and excellent on-site facilities. Further details can be found on our website <https://jobs.sanger.ac.uk>

Other information: Clinical responses to anticancer therapeutics are often restricted to a subset of cases treated. Accumulating evidence indicates that clinical responses may correlate with specific tumor genotypes. Such findings suggest that response rates may be substantially improved by directing treatment towards genetically defined subsets of patients that are most likely to benefit from a particular therapy. Toward this goal, we have formed scientific strategic alliance between investigators at Massachusetts General Hospital (MGH) and the Wellcome Trust Sanger Institute (WTSI) to "personalize" cancer therapy by identifying in vitro, prior to clinical trial, tumor cell genotypes that predict sensitivity to anticancer agents. We will expose approximately 1,000 cell lines derived from a broad spectrum of cancer classes to several hundred known and potential anticancer therapeutic agents in order to characterize the variation in response to these agents and correlate response to genomic copy number information, cancer gene mutation data and expression data. The detection of correlations between genotype or expression and response will then be validated in clinical specimens and will subsequently inform the design of clinical studies in which patients are stratified on the basis of a tumor genotype prior to treatment in order to maximize the frequency of clinical response. The collaboration will develop and share the experience in automated high throughput exposure of cancer cell lines to small molecules at MGH and the background in large scale genotyping, sequencing and informatics that exists at WTSI. References and other information: Cancer Research 68, 3389-3395, May 1, 2008. Methods Enzymol. 2008;438:331-41 Proc Natl Acad Sci U S A. 2007 Dec 11;104(50):19936-41. <http://www.sanger.ac.uk/genetics/CGP/CellLines/>. Salary from £36,772 per annum, however the successful candidate will receive a salary commensurate with their skills & experience.

To submit your CV and apply for this job please go to <https://jobs.sanger.ac.uk> to register and apply on line. The closing date for applications is 13th February 2009.



Working towards diversity through equality

Genome Research Limited is a Registered Charity No.102145

GRADUATE PROGRAM



Discover the formula
for **business success**



Master in Biotechnology Management

Recent advances in life sciences have brought about a revolution in the biotechnology industry. To face these challenges and meet the business opportunities, IE Business School offers an innovative and challenging Master's program in Biotechnology Management, which combines essential business knowledge with specialized industry know-how.

The program is aimed at professionals from either a scientific or management background looking to jump-start or further their careers within the biotech industry.

Our online program methodology reflects today's international business environment, where cross-cultural teams work on global projects regardless of their geographic location. You will not have to leave your residence or work place for extended periods of time to pursue this career-advancing degree.

For details of this program, please visit: www.ie.edu/biotech
For admissions, contact: biotech@ie.edu

Science Careers is the catalyst for your ambition.

Visit our
**ENHANCED
WEBSITE!**



Promoting your ambition is what we do. We're your catalyst for connecting with the industry's top employers. We're the experts and source for accessing the latest and most relevant career information across the globe.

Our newly designed website offers a set of tools that help you discover career opportunities and your personal potential. Whether you're seeking a new job, career advancement in your chosen field, or ways to stay current on industry trends, *Science Careers* is your catalyst for an accelerated future.

Improved Website Features:

- » Relevant Job E-mail Alerts
- » Improved Resume Uploading
- » Content Specific Multimedia Section
- » Facebook Profile

Job Search Functionality:

- » Save and Sort Jobs
- » Track Your Activity
- » Search by Geography
- » Enhanced Job Sorting



Your Future Awaits.

Science Careers

From the journal *Science*



ScienceCareers.org



Northeastern University

Professor and Chair Department of Biology

(Job Requisition: 111150; Position Number: 04001514)

Applications are invited for the position of Chair of the Department of Biology at Northeastern University (<http://www.biology.neu.edu/index.html>). The successful candidate will lead a dynamic department that plays a key role in the research and educational missions of the University.

The Biology Department includes 27 tenured and tenure track faculty. Approximately 1000 undergraduates are enrolled in the Biology, the Biochemistry, and the Behavioral Neuroscience majors. Our graduate programs serve 50 PhD students, and the Biology department participates in Professional MS programs in Bioinformatics, Biology, Biotechnology, and Marine Biology.

We are searching for a scholar who will lead the continued development of our department and complement and expand our research programs both intramurally and externally. Research interests in the department are diverse and interdisciplinary and span the spectrum from organismal to molecular biology. Important assets of the Biology Department are the Marine Science Center, an internationally recognized research and educational institution dedicated to the study of marine systems, the Antimicrobial Discovery Center and the New England Inflammation and Tissue Protection Institute. Existing interdisciplinary initiatives include Biotechnology, Neuroscience, Sensing and Imaging, and Nanotechnology, with participants from Chemistry and Chemical Biology, Physics, Engineering and the College of Health Sciences.

List of responsibilities. The chair will provide effective oversight of a dynamic department with major potential for growth and development; leadership in expansion of research and teaching activities including interdisciplinary programs; mentoring of faculty; an active role in University development efforts; and effective advocacy for the Department at the highest levels of the University.

Qualifications. PhD in Biology or related field. Nationally recognized scientific leader who has an on-going record of competitive research funding. Candidates must have excellent leadership skills.

Northeastern University occupies a vibrant 67-acre campus in the heart of Boston, surrounded by other leading educational, health care, technological, and research institutions, as well as world-renowned venues for art and music. The campus has received an American Institute of Architects award for "most beautiful new or renovated exterior space."

A competitive startup package will be provided. Please send a letter of application, curriculum vitae, the names and contact information for five references, and a brief description of research interests to biojobs@neu.edu. Candidate must have experience in, or a demonstrated commitment to, working with diverse student populations and/or in a culturally diverse work and educational environment.

The earliest anticipated start date is July 1, 2009. Review of applications will begin **March 1, 2009** and continue until the position is filled.

How to Apply

Applications should be submitted electronically to biojobs@neu.edu. For informal discussions regarding the post, candidates may contact **Professor Geoffrey Trussell**, g.trussell@neu.edu.

Northeastern University is an Equal Opportunity, Affirmative Action Educational Institution and Employer. Title IX University and particularly welcomes applications from minorities, women and persons with disabilities. Candidates from groups underrepresented in science are especially encouraged to apply.

AWARDS



Federal Ministry
of Education
and Research



"Bernstein Award" 2009

Young Scientists Research Award in Computational Neuroscience

The German Federal Ministry of Education and Research (BMBF) has established the "National Network for Computational Neuroscience" with four high-performing "Bernstein Centers for Computational Neuroscience" as the major structural elements.

The "Bernstein Award" is equipped with up to 1.25 Mio Euros in the form of a grant over a period of five years. It will be awarded to a highly qualified young researcher, considering the candidates' verifiable research profile in the field of Computational Neuroscience and the scientific concept for a future young research group. Young researchers can apply for their own position and group. The group funded by the "Bernstein Award" will become an integral part of the National Network for Computational Neuroscience. Future announcements of the "Bernstein-Award" are in the scope of the Ministry's planning.

The grant is provided for a scientific project of a young research group headed by a postdoc regardless of nationality. The project will be conducted at a German university or research institution – within or outside the Bernstein Centers. It is a prerequisite for funding that the university or research institution concerned employs the young researcher during the funding period and supports him/her with the basic equipment in terms of laboratory space and other infrastructure. A statement made to that effect by the receiving institution must be included with the project outline to be submitted.

Deadline for applications is May 25th, 2009.

For more detailed information about the "Bernstein-Award" including application conditions please visit

<http://www.nncn.de>
or

<http://www.gesundheitsforschung-bmbf.de/en/1834.php>

Science Careers is the key that opens doors.

Visit our
ENHANCED
WEBSITE!



Opening doors is what we do. We're the key to connecting with the industry's top employers. We're the experts and source for accessing the latest and most relevant career information across the globe.

Our newly designed website offers a set of tools that help you unlock career opportunities and your personal potential. Whether you're seeking a new job, career advancement in your chosen field, or ways to stay current on industry trends, *Science Careers* is your key to a brighter future.

Improved Website Features:

- » Relevant Job E-mail Alerts
- » Improved Resume Uploading
- » Content Specific Multimedia Section
- » Facebook Profile

Job Search Functionality:

- » Save and Sort Jobs
- » Track Your Activity
- » Search by Geography
- » Enhanced Job Sorting



Your Future Awaits.

Science Careers

From the journal *Science*



ScienceCareers.org

Renewable Energy Laboratory

Battelle Science & Technology Malaysia (BSTM) is the Malaysian subsidiary of Battelle, the world's leader in science and technology research, with over 20,000 employees in more than 120 locations including seven national laboratories that Battelle manages or co-manages. BSTM is in the process of establishing a Renewable Energy Laboratory (REL) for a private client in Malaysia. The REL will be a showcase laboratory known for performing world-class research and development within modern facilities to provide innovative solutions to the world's energy needs as well as address the challenge of climate change. The laboratory will be located in Malaysia near Kuala Lumpur, the capital and largest city. Kuala Lumpur is home to 1.8 million diverse inhabitants, most of whom speak English as a second language. Malaysia is situated in the midst of Southeast Asia with easy access to Singapore, Thailand, Vietnam, and Indonesia, as well as China, Japan, and Korea. The REL will feature a unique environment combining attractive and functional physical spaces, effective support systems, strategic focus, and a commitment to the highest standards of excellence that will empower exceptional researchers to make important contributions to the science and technology of renewable energy and sustainability.

We are inviting applications (CV and references) from highly qualified and accomplished researchers to fill the following Senior Leadership positions:

Director of Product Innovation

This function is key to ensuring that results of REL research and development activities are appropriately applied to achieve timely translation into high-value products made from renewable sources. Applicants should have a strong record of technical accomplishments as well as impact in the marketplace. We are looking for individuals with at least 10 years' experience.

Science and Technology Leaders

- Biomass Production and Sustainability
- Systems Biology
- Process Engineering
- Computational Science and Informatics
- Chemical Catalysis
- Polymer Science

Successful applicants have doctorate degrees in relevant science and engineering disciplines, an internationally respected strong record of accomplishments in science and engineering, and the proven ability to lead cross-disciplinary teams of researchers to the highest levels of performance. REL leaders will be expected to work horizontally across the organization in order to perform world-leading R&D and to accomplish ambitious critical outcomes for the laboratory.



John Pender, Human Resources Director
Battelle Science & Technology Malaysia Sdn. Bhd. (809178-W)
<http://www.battelle-malaysia.com>
E-mail: resumes@battelle-malaysia.com

Battelle Science & Technology Malaysia is an Affirmative Action/ Equal Employment Opportunity M/F/D/V

Do what
you love.

Love what
you do.

www.sciencecareers.org

Science Careers

From the journal *Science*



THE UNIVERSITY of York

DEPARTMENT OF BIOLOGY

Two Lectureships: Evolutionary Biology and Ecology

The Department of Biology at the University of York represents a thriving research community of the highest international calibre. York Biology ranks first-equal among UK broad-spectrum biology departments for the percentage of its research judged "world-leading" by the 2008 UK Research Assessment Exercise. York was also top in the UK for citations per research paper published between 2001 and 2005 in the field of Plant and Animal Science (Thomson Scientific UK).

As part of major developments in the Department, we wish to appoint two new Lecturers. We are seeking outstanding and dynamic scientists with proven track records of high quality research. You will be expected to develop a research programme of international standing and develop teaching in the same field. Applications are encouraged in the following fields:

Lecturer in Evolutionary Biology

Ref: UoY00220

Any area of evolutionary biology, including adaptation, phylogenetics, population genetics and environmental genomics. Informal contact: Professor Peter Young, email: jpy1@york.ac.uk or tel: 01904 328630.

Lecturer in Ecology

Ref: UoY00221

Any area of ecology, including environmental change, ecosystem ecology and global change biology. Informal contact: Professor Chris Thomas, email: cdt2@york.ac.uk or tel: 01904 328646.

For informal enquiries contact the above people or the Head of Department, Professor Dale Sanders, email: biohod@york.ac.uk or tel: 01904 328555.

Salary will be within range: £35,469 to £43,622 per annum.

For further information and to apply on-line, please visit our website: <http://www.york.ac.uk/jobs/> Alternatively contact HR Services on 01904 434835 quoting the appropriate reference number.

Closing date: Friday 27 February 2009.

The University of York is committed to diversity and has policies and developmental programmes in place to promote equality of opportunity.

www.york.ac.uk



Your career is our cause.

Get help from the experts.

www.sciencecareers.org

- Job Postings
- Job Alerts
- Resume/CV Database
- Career Advice
- Career Forum
- Graduate Programs
- Meetings and Announcements

Science Careers
From the journal Science 

POSITIONS OPEN

FACULTY OPENING PROFESSOR (ASSISTANT, ASSOCIATE, FULL) Purdue University

Purdue University's College of Engineering and the School of Pharmacy and Pharmaceutical Sciences are seeking applications to a position in the general area of engineering and physical sciences applied to pharmaceutical products and processes. The selected individual will be expected to develop and sustain an extramurally funded research program, as well as to contribute to professional and graduate education.

The position is for a full-time, tenure-track Assistant, Associate, or Full Professor, where specific rank will be determined as appropriate for the record of accomplishment of the candidate. This position is intended to support the work of the new multi-university National Science Foundation Engineering Research Center on Structured Organic Particulate Systems and the interdisciplinary Pharmaceutical Technology and Education Center. The academic home of the candidate will be within one or more of the engineering schools with a potential joint appointment in the Department of Industrial and Physical Pharmacy.

Candidates should have expertise in fundamental and applied research related to the development, design and manufacturing of pharmaceutical products. Representative areas of interest include: material science of pharmaceutical solids and compacts; pharmaceutical product performance modeling; crystal engineering; fundamentals of operations associated with drug substance and drug product manufacture; down-stream processing of biologics; stability of nanoparticles; dynamics and automatic control of pharmaceutical processes; sensing and imaging in pharmaceutical systems; and statistical modeling and analysis relevant to this domain.

Qualifications. Candidates must hold a Ph.D. degree in a relevant discipline; have a strong academic record, exceptional potential for world-class research and a commitment to both undergraduate and graduate education.

Application. For consideration, please complete the online form at website: <https://engineering.purdue.edu/Engr/AboutUs/Employment/Applications>, and submit in electronic form your curriculum vitae, statement of research and teaching interest, and the names and contact information for at least three references. In case of difficulties in submitting an application to this website, please contact Ms. Marion Ragland at e-mail: ragland@purdue.edu. Review of applications will begin January 5, 2009, and will continue until filled.

Purdue University is an Equal Opportunity/Equal Access/Affirmative Action Employer fully committed to achieving a diverse workforce.

POSTDOCTORAL FELLOW POSITIONS

available to study the molecular mechanisms underlying leukocyte trafficking through three-dimensional extracellular matrix barriers in vitro and in vivo (e.g., *Trends in Cell Biol.* 18:560, 2008). Strong background in cell/molecular biology and/or intravital microscopy will be required. Send curriculum vitae and letters of reference to: Stephen J. Weiss, M.D., Upjohn Professor of Medicine, Life Sciences Institute, University of Michigan, 5000 LSI, 210 Washtenaw, Ann Arbor, MI 48109-0640. The University of Michigan is an Equal Opportunity Employer.

Shantou University Medical College, a dynamic and innovative school in Guangdong province, China, jointly funded by the Chinese government and the Li Ka-shing Foundation, is seeking M.D.s and/or Ph.D.s with outstanding credentials to teach medical students in English. Retired or on sabbatical leave Professors are also welcome. We provide a competitive package. Please send letter of intent and curriculum vitae to e-mail: karenmai@stu.edu.cn.

POSITIONS OPEN

Help employers find you. Post your resume/cv.

Science Careers

From the journal Science



www.ScienceCareers.org

Stop searching for a job; start your career.

Science Careers

From the journal Science



www.ScienceCareers.org

MARKETPLACE

Promab Biotechnologies Inc.
Custom Monoclonal Antibody \$4,200

>3,000 CLONES WILL BE SCREENED

1-866-339-0871

www.promab.com info@promab.com

Oligo Synthesis Columns

- ✦ Columns For All Synthesizers
- ✦ Bulk Column Pricing Available
- ✦ Call for Free Column Samples

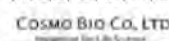
 **BIOSEARCH TECHNOLOGIES**
Advancing Molecular Biology

+1.800.GENOME.1
www.bticolumns.com

For COLLAGEN Detection... Connect with Cosmo Bio

ELISAs to measure COLLAGENs: Type 1 (hu); Type 2 (hu, ms, rt, +). ELISAs to measure ANTI-COLLAGEN ANTIBODIES: Type 1 (hu); Type 2 (hu, ms, rt, +). **SPECIFIC ANTIBODIES:** Types 1, 2, 3, 4, 5, 6, 7, 8, 9, 10, 11, 12, 14.

Research Products from Japan
www.cosmobio.com

 **COSMO BIO CO., LTD.**
Immunological Research & Science



Spain: Science Business Class

Spain ranks 9th in world scientific output. Between 2003 and 2007, the government budget allocated to R&D grew at the second highest rate. Spain: a country of cultural and scientific talent.

GOBIERNO
DE ESPAÑA

MINISTERIO
DE CIENCIA
E INNOVACIÓN

You Will Love Them!



Thousands
of scientists
have discovered
the power and
performance of
PCR ARRAYS.
Join them on the
path to success.

Offer Ends March 2nd 2009

www.SABiosciences.com